Modelling Species Invasions in Heterogeneous Landscapes

Mark A. Gilbert

Brasenose College

University of Oxford

A thesis submitted for the degree of

Doctor of Philosophy

Trinity 2016

I dedicate this thesis to:

God - Father, Son and Holy Spirit;

My parents, Susan and Eric;

My wife, Katie.

How many are your works, Lord!

In wisdom you made them all;

the Earth is full of your creatures.

- Psalm 108:24

Acknowledgements

Studying for a DPhil has been a challenging and exciting four years, both intellectually and emotionally. This thesis owes its existence to a very large number of friends, family and colleagues. First, I would like to thank my supervisors, Eamonn Gaffney, Steven White and James Bullock. Thank you for all your advice, guidance, support and comments over the last four years.

I thank my DPhil examiners, Christina Cobbold and Philip Maini, as well as Radek Erban (Transfer of Status examiner), and Thomas Woolley (Confirmation of Status examiner), for their insightful comments, corrections and suggestions.

I'd like to thank everyone associated with the Wolfson Centre for Mathematical Biology (WCMB). It's been a pleasure to work there. In particular I'd like to thank my fellow graduate students: Jake Taylor-King, Jody Reimer, Debbie Markham, Lucie Bowden, Jake Scott, Paul Taylor, Shuohao Liao, Jochen Kursawe, Aaron Lim, Linus Schumacher, Laurence Hutton-Smith, Lucy Hutchinson, Chris Lester, Robert Ross, Fergus Cooper, Heidi Dritschel, Daniel Humphries, Andrew Parker, Tomislav Plesa, Citlali Solis Salas, Casper Beentjes, Liam Brown, Jonathan Harrison, Bernadette Stolz, Samara Pillay and Joshua Bull.

The peer reviewers of the Journal of Theoretical Biology (JTB) and Methods in Ecology and Evolution (MEE) are also gratefully thanked for their comments on the published manuscripts that have helped hone the quality of the work presented here. I'd also like to thank several colleagues and mentors and the wider theoretical ecology community. In particular: Mark Lewis, Tal Avgar, Devin Goodsman and Frithjof Lutscher.

Completing a DPhil is the culmination of many years of education, and I am grateful to all my school teachers and undergraduate tutors. In particular, I'd like to thank Richard Cook, David Worden, Nigel Oates, Zhongmin Qian, Cornelia Drutu and Brian Stewart. Finally, I've been extremely lucky to have the support of my friends and family. Above all, I'm particularly grateful for the love and support of my wife, Katie, my parents, Susan and Eric and my siblings, Erica and Edward.

Abstract

Biological invasions are devastating ecosystems and economies world-wide, while many native species' survival depends on their ability to track climate change. Characterising the spread of biological populations is therefore of utmost importance, and can be studied with spatially explicit, discrete-time integrodifference equations (IDEs), which reflect numerous species' processes of demography and dispersal. While spatial variation has often been ignored when implementing IDE models, real landscapes are rarely spatially uniform and environmental variation is crucial in determining biological spread.

To address this, we use novel methods to characterise population spread in heterogeneous landscapes. Asymptotic analysis is used for highly fragmented landscapes, where habitat patches are isolated and smaller than the dispersal scale, and in landscapes with low environmental variation, where the ecological parameters vary by no more than a small factor from their mean values. We find that the choice of dispersal kernel determines the effect of landscape structure on spreading speed, indicating that accurately fitting a kernel to data is important in accurately predicting speed. For the low-variation case, the spreading speeds in the heterogeneous and homogeneous landscapes differ by ϵ^2, where ϵ governs the degree of variation, suggesting that in many cases, a simpler homogeneous model gives similar spread rates.

For irregular landscapes, analytical methods become intractable and numerical simulation is needed to predict spread. Accurate simulation requires high spatial resolution, which, using existing techniques, requires prohibitive amounts of computational resources (RAM, CPU etc). We overcome this by developing and implement-

ing a novel algorithm that uses *adaptive mesh refinement*. The approximations and simulation algorithm produce accurate results, with the adaptive algorithm providing large improvements in efficiency without significant losses of accuracy compared to non-adaptive simulations. Hence, the adaptive algorithm enables faster simulation at previously unfeasible scales and resolutions, permitting novel areas of scientific research in species spread modelling.

Contents

Chapter 1

Introduction

The spread of species' populations through space is a major area of interest in applied and fundamental ecology. Two main foci and applications of such work are on the invasion of non-native (invasive) species and, conversely, the ability of native species to spread to track climate change. Invasive species threaten the stability of the world's ecosystems, causing ecosystem degradation, loss of biodiversity (Vilà et al., 2011; Katsanevakis et al., 2014), have detrimental impacts on human health (Conn, 2014) and well-being (Pejchar and Mooney, 2009), increase the rate of extinctions (Sax and Gaines, 2008; Murray et al., 2014), cost nations hundreds of billions of US dollars per year (Pimentel, 2011) and damage developing economies (Binimelis et al., 2008). At the same time, a wide range of species need to be able to spread poleward or to higher elevations if they are to keep pace with climate change (Chen et al., 2011; Virkkala and Lehikoinen, 2014; Santini et al., 2016). Using mathematical models of spread allows us to extend ecological theory to understand species invasions, to make efficient and effective predictions about spread to inform management strategies and risk assessment (Guisan et al., 2013; Matlaga and Davis, 2013; Phillips and Kot, 2015) and to understand the sensitivity of population spread to different ecological parameters such as fecundity, survival rates and dispersal distances (Neubert and Caswell, 2000).

1.1 Population Spread

Population spread is the process by which population distributions change in space with species colonizing and persisting in previously uninhabited regions. This definition includes both invasive species and range expansion to track changing environmental conditions (e.g. under climate change). We consider both types of spreading species throughout this thesis.

1.1.1 Invasive Species

Invasive species are populations that have been introduced into and spread in a region that is geographically distinct from their original distribution. The term *invasive species* is usually associated with detrimental impacts to human activity or to other species native to that region (Pejchar and Mooney, 2009), although not all non-native species that become established are pests (Altieri et al., 2010). Invasive species include mammals, birds, insects, plants and fungi and have affected every continent (Pyšek et al., 2012). However the extent to which different regions suffer is not uniform. Small islands host a greater number of invasive species (Vilà et al., 2011) and have been found to be worse affected by invasives than larger landmasses (Pyšek et al., 2012). Several biological factors promote and exacerbate the effects of invasive species including habitat degradation (Perrings et al., 2010) and the loss of apex consumers (top predators) (Carlsson et al., 2009; Estes et al., 2011).

Invasive species are transported across geographic boundaries by humans, with Hulme et al. (2008) categorising the human aided means of introduction as intentional release, escape from captivity, contaminant and stowaway. Some species are transported across boundaries by natural (non-human) means, for example the spread of species after the emergence of a land bridge between North and South America around two million years ago (Woodburne, 2010). Over the past few hundred years, humans have become the principal cause of introductions, with the number of invasions increasing by orders of magnitude (see for example Figure 1.1a and Mack et al.,

2000).

Invasions by introduced species can have profound economic and ecological effects and, together with overexploitation, habitat destruction and the spread of diseases by invasive species, were described by Wilson (1999) as one of the four "mindless horsemen of the environmental apocalypse". Invasive species have huge impacts on ecoystems and biodiversity. Invasives reduce native populations (McCleery et al., 2015) and transform entire ecosystems by changing fuel properties and fire regimes (Balch et al., 2013), altering carbon (Clark et al., 2010; Flower et al., 2013) and nitrogen (Vargas et al., 2015) cycles, altering ecological interactions and disrupting seed dispersal (Rodriguez-Cabal et al., 2012) and pollination (Spellman et al., 2015). Invasive species increase the risk of extinctions (Murray et al., 2014) and are a major threat to endangered species (Wagner and Van Driesche, 2010; Wilcove et al., 1998). They are one of the largest threats to biodiversity (Hulme et al., 2015; Pyšek and Richardson, 2010) and species richness (Gaertner et al., 2009), and cause biotic homogenisation, reducing the distinctiveness of biological communities (Pauchard et al., 2013).

Invasive species can have detrimental impacts on human health and well-being. They cause and carry human diseases, act as a host to livestock parasites, cause injuries and allergies, cause the accumulation of toxins, and contaminate soil and water (Pyšek and Richardson, 2010). Invasions also impair ecosystem services that benefit humans, including the provision of water, food and fibre, the regulation of erosion, flooding and the spread of diseases; and impair aesthetic, recreational, and cultural value (Kettunen et al., 2009; Walsh et al., 2016). These impacts are associated with huge economic consequences in many sectors, including agriculture (Oliveira et al., 2013), forestry, fisheries (Oreska and Aldridge, 2011) and nature conservation, with damage estimated at $\sim$ 5% of global GDP, and effects on individual nations estimated to be in the hundreds of billions of US dollars per year (Pimentel, 2011). Not all introduced species have significant ecological or economic impacts (Manchester and Bullock, 2000); many become established in a location without adversely affecting

native species (Colautti and MacIsaac, 2004). These non-natives have been found to be associated with different values of certain physiological traits (fitness, size etc) to invasive species (Van Kleunen et al., 2010). However, the methods presented in this thesis are as applicable to them as to harmful invasive species.

1.1.2 Range Expansion

As the Earth's climate changes due to anthropogenic global warming, climatic regimes and environmental variables such as wind-speed, temperature and precipitation at individual locations are changing. This affects resident species' ability to persist at these locations as the new conditions may be outside their physiological thresholds of temperature and precipitation tolerance (Smale and Wernberg, 2013).

Overall, species' optimal climatic conditions are shifting towards the poles or to higher elevation (Yamano et al., 2011), but due to the spatial and temporal heterogeneity of climate change (Burrows et al., 2011), this process has itself been heterogeneous, with larger shifts in certain regions or between certain years. Chen et al. (2011) estimates the recent median shift to higher elevations at 11.0 metres per decade, and towards the poles at 16.9 kilometres per decade, and identifies a high degree of correlation between average local changes and the size of the shift. Loarie et al. (2009) defined the *velocity of climate change* at each location as the instantaneous horizontal velocity of temperature change ($\mathrm{km\,yr^{-1}}$), which is given by the ratio of temporal ($^{\mathrm{o}}\mathrm{C\,yr^{-1}}$) and spatial ($^{\mathrm{o}}\mathrm{C\,km^{-1}}$) temperature gradients.

For populations to survive and avoid extinction, they must be able to extend their ranges at an equal or greater rate than that at which their optimal climatic conditions shift (Bullock et al., 2012). Santini et al. (2016) estimates that 30% of mammal species will fail to keep pace with the velocity of climate change. In addition, this may be complicated by other impacts of climate change, such as on community structure (Walther, 2010), community richness (Shi et al., 2015), and dispersal (Travis et al., 2013), which may help or hinder species in their ability to track habitat shifts.

(a)

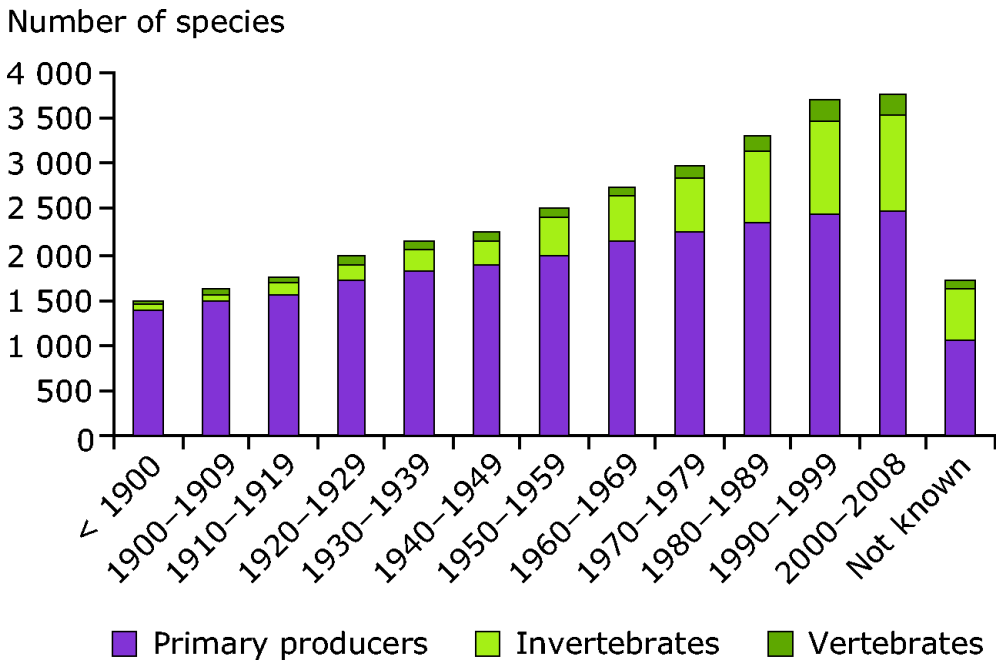

(b)

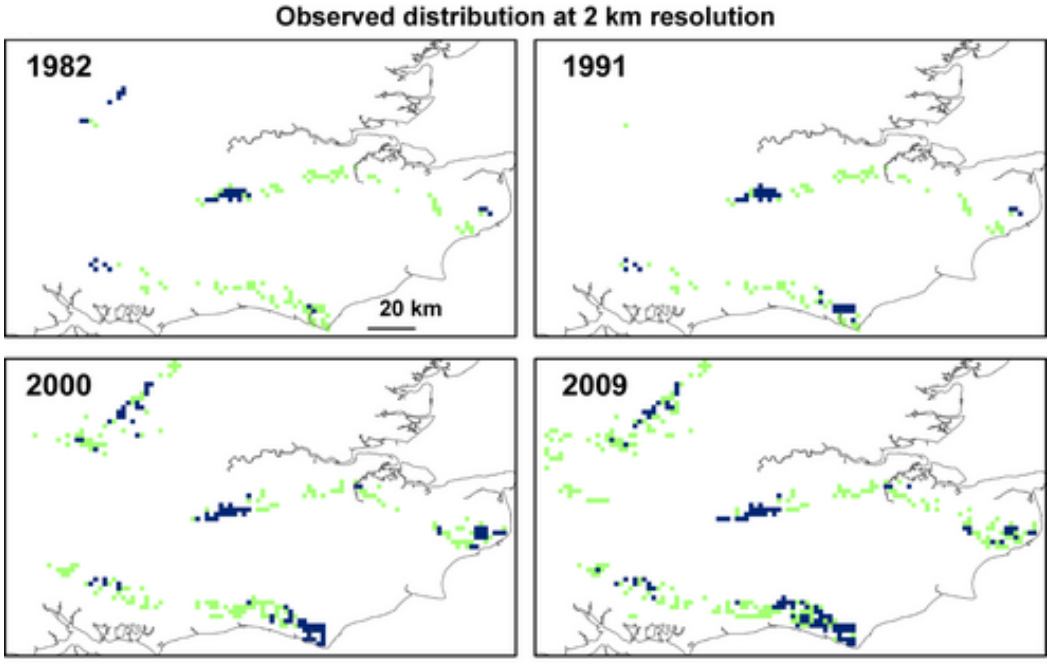

Figure 1.1: (a) Cumulative number of alien species established in terrestrial environments in Denmark, Estonia, Finland, Germany, Iceland, Latvia, Lithuania, Poland, Norway, Russia and Sweden, reproduced from Condé et al. (2010) with permission. (b) Observed distribution (dark blue) of the silver spotted skipper (*H. comma*) between 1982 and 2009 in South East England, as it expanded its range due to warmer temperatures. Reproduced from Bennie et al. (2013) under the Creative Commons Attribution 3.0 Unported license.

1.1.3 Examples

With such large numbers of invasive species and species affected by climate change driven habitat shifts, there is no shortage of candidates to be used as examples. We briefly outline two invasive and one range expanding species.

The golden apple snail (*Pomacea canaliculata*), see Figure 1.2c, is native to South America (Halwart, 1994) and was introduced to Taiwan from Argentina (Hayes et al., 2008) by private entrepreneurs as an additional source of food and income for rice farmers (Vitousek et al., 1996). The snail populations grew rapidly, consumed large numbers of young rice plants and spread through irrigation canals. Although the snail failed as a source of income for farmers, additional populations were introduced to other south east Asian countries by the same entrepreneurs. The snail has devastating economic and ecological effects, causing between 28 and 45 million US dollars in damage to the rice farming industry in the Phillipines in 1990 (Naylor, 1996), and forcing farmers to use highly toxic pesticides to control the snail (Halwart, 1994). The snail invasion has also affected the function and community structure of wetland ecosystems (Fang et al., 2010; Carlsson et al., 2004; Horgan et al., 2014) and facilitates the spread of the human infection angiostrongyliasis in China (Lv et al., 2011).

Corsican pine (*Pinus nigra* subsp. *laricio*), see Figure 1.2b, is a subspecies of black pine (*Pinus nigra*) that is native to Mediterranean Europe and is invasive in New Zealand (Caplat et al., 2012). It was introduced throughout New Zealand in the 1880s to control erosion (Gous et al., 2014) and produce timber (Buckley et al., 2005). It has spread beyond its introduction sites, due to its ability to disperse long distances (Richardson et al., 1994). It primarily threatens natural grasslands, shrublands and abandoned pastures, is a threat to biodiversity (Buckley et al., 2005) and has a significant effect on many ecosystem processes (Richardson et al., 1994). Further spread would result in "a significant loss of natural landscape value and biodiversity" (Gous et al., 2014).

The silver-spotted skipper (*Hesperia comma*), see Figure 1.2a, is a butterfly that

is distributed throughout mainland Europe, with its range extending from North Africa to Scandanavia, and attaining the north-western limit of its European range in south-east England. Due to agricultural intensification and reduced grazing by the European rabbit following the myxamatosis outbreaks in the late 20th century, the *H. comma* population suffered a drastic decline in Britain, with fewer than 70 populations remaining in 1982. Since then, the species has expanded its range (see Figure 1.1b). This is due in part to climate change, and "a series of exceptionally warm summers compared with 20th Century norms" (Bennie et al., 2013).

1.1.4 Usefulness of Modelling

A population's ability to spread in a new region depends on a complex set of factors that determine the region's suitability as habitat for the species and the species' ability to disperse in the new region and colonise it. In order to disentangle these factors and their interactions, models can be used to represent the biological processes in a logical and objective way. Biological models can be formulated in a variety of ways (Evans et al., 2013), such as mathematical, computational, conceptual or statistical models, and use species specific data to predict outputs such as spread rates, persistence, future distributions, geographical extent etc. Using models to study invasions develops our understanding of the underlying relationship between species' traits and spreading ability, allows potential ranges to be determined (Reshetnikov and Ficetola, 2011), facilitates better informed conservation decisions and control (Lee et al., 2013) and mitigation strategies, enables more accurate risk assessment (Robinet et al., 2012), and may enable better scanning for future threats (Roy et al., 2014).

Modelling has been applied to many species, including the examples in Subsection 1.1.3. Models of the golden apple snail have been used to estimate invasion risk (Jerde et al., 2009). For Corsican pine, modelling has been used to determine the relative effects of different traits on spread (Caplat et al., 2012), to inform man-

(a)

(b)

(c)

Figure 1.2: Photographs of (a) silver-spotted skipper (*Hesperia comma*), (b) corsican pine (*Pinus nigra* subsp. *laricio*), and (c) golden apple snail (*Pomacea canaliculata*), reproduced from wikipedia.

agement strategies (Buckley et al., 2005), and to compare the invasion success of Corsican pine (*Pinus nigra* subsp. *laricio*) with other *Pinus* species (Nuñez and Medley, 2011). Modelling has enabled researchers to determine the factors leading to colonisation (Lawson et al., 2012) and to predict future distributions of the silver spotted skipper (Bennie et al., 2013).

1.2 Species Invasions in Heterogeneous Landscapes

Population dynamics and spread rates are determined by a range of factors, including demography, dispersal, species interactions, evolution, environment and physiology (Urban et al., 2016). In addition, each of these factors may vary spatially, such as the distributions of other species, or depend on other factors (e.g. topography, drainage) that vary across landscapes. This results in members of the same species exhibiting different behaviour at different locations. In particular, some locations may be more suitable for the species than others. This spatial distribution of suitable habitat, or *landscape structure*, affects both dispersal and demographic processes, and is a decisive factor in determining a species' ability to spread and its spreading speed (King and With, 2002). Both localised, fine-scale variation in habitat quality (Bennie et al., 2013) and large scale variation have been found to determine the rate and extent of range expansion.

From the perspective of a specific species, landscape heterogeneity encompasses any variation in individuals' behaviour and habitat suitability determined by spatial location. Heterogeneity occurs across spatial scales (Stein et al., 2014), manifesting itself through mosaics of habitat patches (Hansson et al., 2012) and in continuous variation in relevant parameters within habitat patches (e.g. Jurena and Archer, 2003; Miller et al., 1995). The precise effects on a particular species will depend on the species movement and dispersal patterns (Baguette et al., 2013). For example, roads and rivers block the movement of some terrestrial mammals, but may not impact the transport of wind dispersed seeds.

1.2.1 Causes of Heterogeneity

Landscape heterogeneity is caused by a range of different interacting abiotic and biotic processes. These processes can be broadly classified as: environmental variation, population and community processes, ecological disturbance and anthropogenic habitat fragmentation (Turner, 2005).

Environmental Variation

Abiotic environmental variation is determined by underlying variation in the region's topography, geology and climate (Turner, 2005). These processes are not independent, for example the topography and climate interact to determine micro-climate. Environmental factors that vary throughout landscapes and affect species behaviour include sediment composition (Wang et al., 2009), water quality (Leps et al., 2015), elevation/altitude (Boyce et al., 2003), temperature (Graham et al., 2012), precipitation (Puri et al., 2015) and light levels (Buckland-Nicks et al., 2016). These variables affect individuals' behaviour in a number of ways. For example, within a particular range of temperatures, trees form thick forests. However, at higher altitudes, lower temperatures result in stunted growth with lower tree density. Eventually, at sufficiently high elevation, the temperatures are too low for the trees to be able to grow (Hoch and Körner, 2012).

Specific species behave differently in particular environmental conditions and levels of precipitation, altitude, soil pH, light levels etc. Under some conditions, survival rates and fecundity are sufficiently high for the species to persist, whereas under others, the species is unable to survive. Given the spatial heterogeneity of the environmental variables, different locations in the landscape will be more or less suitable for the species.

Population and Community Processes

As well as abiotic environmental factors, biotic factors also vary throughout landscapes and affect the suitability of locations as habitat for different species. These biotic factors include competition, herbivory, predation and the presence of ecosystem engineers (Turner, 2005). For example, trees give shade which generates temperature heterogeneity in alpine habitat (Graham et al., 2012), heterogeneous herbivore grazing patterns provide varied habitat that sustains diverse arthropods (van Klink et al., 2015), and natural variation between host organisms provides a heterogeneous environment for parasites (Fleming-Davies et al., 2015).

Disturbance

An ecological disturbance is a process or event that has significant impacts (either a perturbation or stress) on ecosystems (Rykiel, 1985). The effects are not spatially uniform, so act as a driver of spatial heterogeneity (Pickett and White, 1985). Disturbances that drive heterogeneity include hurricanes (Weishampel et al., 2007), fire (Fuhlendorf et al., 2009), flooding (Ward et al., 1999), insect outbreaks (Kayes and Tinker, 2012), landslides (Walker et al., 1996), earthquakes (Chou et al., 2009) and volcanoes (García-Romero et al., 2015). For example localised fire in the southwestern USA helps maintain the heterogeneity in grasslands (Fuhlendorf et al., 2009).

Habitat Fragmentation

Fragmentation is the removal and resulting disruption of contiguous natural or semi-natural habitat, and results in a number of smaller patches isolated from each other by a matrix of habitat that is different from the original (Villard and Metzger, 2014). It is a global phenomenon (Fischer and Lindenmayer, 2007) which reduces biodiversity (Pardini et al., 2010; Fahrig, 2003), makes species more vulnerable to extinction (Schnell et al., 2013; Fahrig, 2002) and affects species richness (Krauss et al., 2010), genetic variation (Aguilar et al., 2008; Vranckx et al., 2012) and predator-prey inter-

actions (Ryall and Fahrig, 2006; Cooper et al., 2012).

Fragmentation comprises several processes (Fahrig, 2003): the loss of suitable habitat, an increase in the number of habitat patches, the increased isolation of remaining habitat patches, and the decreased size of the remaining patches (see Figure 1.3 for an example of the fragmentation of forest habitat in Wisconsin, USA). Several authors have tried to disentangle the effects of habitat loss and the other aspects of habitat fragmentation, or habitat fragmentation *per se*, with Hooftman et al. (2015) finding connectivity loss to be the strongest driver of extinctions, Cooper et al. (2012) finding intermediate fragmentation to provide the greatest stability in predator-prey dynamics, and Mortelliti et al. (2011) observing connectivity loss to have different effects on different species. However, ambiguity in the precise definition of fragmentation is still an issue (Lindenmayer and Fischer, 2013).

1.2.2 Effects of Heterogeneity on Population Spread

A wide range of differing results have been published on the relationship between spatial heterogeneity and the spread of species. Some studies demonstrate that heterogeneous landscapes are more resilient to species invasions, and may reduce species' ability to track regions of suitable climate as these regions shift (Hodgson et al., 2012; Renton et al., 2012), while others suggest that heterogeneity increases the vulnerability of landscapes to invasive species (Doherty et al., 2015; Knops et al., 1995; Urban et al., 2008).

Tamburello and Côté (2015) found that patchy and continuous coral reef habitat structures led to different invasion behaviour, and Mosher et al. (2009) found that past environmental disturbance affected invasive species' spread rates. Habitat fragmentation and destruction have been found to favour invasions by generalists (Marvier et al., 2004), with edge habitat (which accounts for a high proportion of fragments) found to favour invasive species in forests due to its proximity to other (non-forest) habitats (Bustamante et al., 2003). Disturbance and livestock grazing

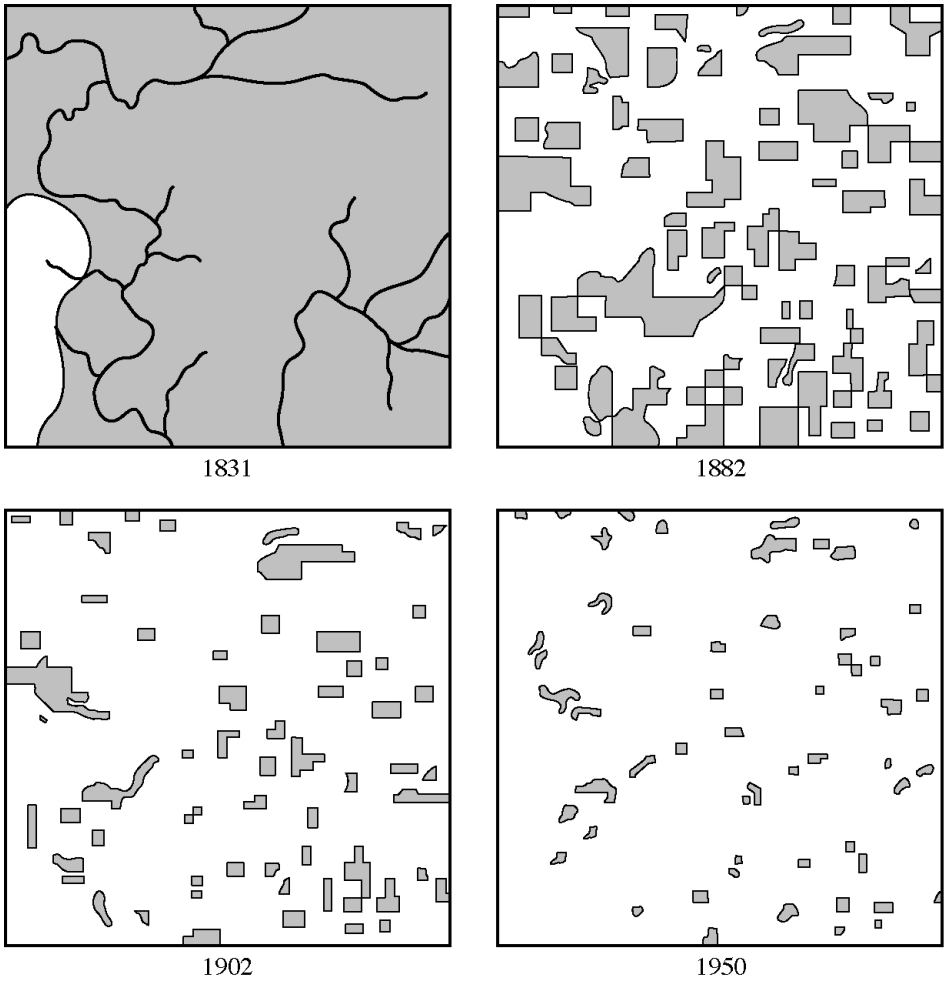

Figure 1.3: Fragmentation of forest habitat in Cadiz township, Wisconsin, USA between 1831 and 1950. Reprinted with permission from Curtis (1956). Copyright ©1956 by the University of Chicago

(which often accompany fragmentation where land is being converted to agricultural use) have also been found to favour invasive mammals (Hobbs, 2001).

1.2.3 Modelling Invasions in Heterogeneous Landscapes

Since landscape heterogeneity has such a large effect on the dynamics of biological invasions, incorporating spatial heterogeneity into models allows them to more accurately reflect the dynamics of real species invasions and to gain more insight into the biological processes and make better informed predictions. Classically, mathematical models have been concerned with homogeneous landscapes as they allow analytical estimates of invasion speed (Murray, 2003), persistence (Cantrell and Cosner, 2004), and sensitivity to different ecological parameters (Neubert and Caswell, 2000). Unlike simulation techniques (which are applicable to all landscapes), these analytical expressions are relatively simple, do not require significant computational resources to calculate and can provide insight into the relationships between different parameters and spread. Incorporating heterogeneity in mathematical models prevents us from using these analytical techniques, and necessitates the development of appropriate analytical or numerical techniques.

1.3 Knowledge Gaps

Given the adverse effects of invasive species and the extinction risk for species failing to extend their ranges to track climate change, being able to predict and explain population spread is of utmost importance (Williamson, 1999).

In particular, the ways in which populations interact with the structure of heterogeneous landscapes are not fully understood. Predicting the spread of species over heterogeneous landscapes, and understanding the relationship between demographic and dispersal parameters, landscape scale and spread rate, would better inform landscape management and risk assessment. Understanding when heterogeneity needs to be incorporated into models, or whether there are cases where it can be ignored,

would provide further justification for existing approaches. Using spatially explicit mathematical models that can incorporate landscape heterogeneity enables us to explore these relationships. However, modelling heterogeneous landscapes has been inherently more difficult as heterogeneous models are generally amenable only to numerical simulation, rather than analytics. Simulating mathematical models over large or spatially complex landscapes is difficult as it can require vast computational resources in RAM or CPU-time.

1.4 Mathematical Models

Since species invasions happen over spatial scales ranging from small islands to entire continents, understanding the interaction between biological invasions and the complex structure of real and heterogeneous landscapes is of utmost importance to ecologists. Spatially explicit mathematical and computational models can help achieve this by representing the relevant biological processes mathematically and enabling the prediction of spreading speed, persistence, changes in population distributions and future ranges. These models have been very useful to ecologists and are widely used (Shigesada and Kawasaki, 1997). We will now outline some of the dominant modelling frameworks used to model population distributions and their spread.

1.4.1 Species Distribution Models

Species distribution models (SDMs), or environmental niche models, are statistical methods that create a map showing geographic variation in site suitability for a single species (Elith and Leathwick, 2009a). An SDM relates species distribution data, usually in the form of occurrence or abundance at known locations, with information on the environmental and/or spatial characteristics of those locations (Elith and Leathwick, 2009b).

SDMs do this by combining observation data with environmental data. The observation (abundance, occurrence or occurrence-absence) data of a species on a landscape

$X \subset \mathbb{R}^2$ are taken at a set of N points $\{x_i\}_{i=1}^N \subset X$. The environmental data can be thought of as a real vector valued function $\mathbf{f} : X \to \mathbb{R}^n$ between the landscape X and the environmental state space $\mathbb{R}^n$, where each dimension of the environmental state space and each component f_j of $\mathbf{f}$ corresponds to one of the n specific environmental variables (e.g. humidity, temperature, soil pH etc).

The task is then to use the values of the environmental variables at the observation sites $\{\mathbf{f}(x_i)\}_{i=1}^N$ to estimate the suitability $\lambda : \mathbb{R}^n \to \mathbb{R}$ of all points in the environmental state space. The composition of the suitability function λ and the spatial environmental data $\mathbf{f}$ can then be taken to get the suitability $\lambda(\mathbf{f}(x))$ of each point in the landscape.

There are a range of methods and approaches for using the $\{\mathbf{f}(x_i)\}_{i=1}^N$ to estimate λ including generalised linear models, artificial neural networks, multivariate adaptive regression splines, classification and regression trees, genetic algorithms, support vector machines and maximum entropy methods (Elith and Leathwick, 2009b).

SDMs have been successfully used to investigate a range of ecological problems (Guisan and Thuiller, 2005) including species invasions (Peterson, 2003). SDMs can be generalised to incorporate competition, predator-prey and other species interactions (Wisz et al., 2013). However, SDMs are not mechanistic and trained only on data from locations and conditions experienced by the species. Predictions outside of these ranges may be unrealistic as they are beyond the scope of the data, making predictions at range limits or the testing of different scenarios (e.g. the addition of another species or biological control) unreasonable. An additional weakness of using SDMs to model species invasions is that they model the suitability of habitat for a species (its potential range) rather than the realised distribution, which will be different if a species is still spreading through its potential range. This means that SDMs assume that all population dynamics are at equilibrium (Dormann, 2007) and do not model the dynamics of spread. Therefore, SDMs are restricted to predicting the potential ranges of species invasions rather than the dynamics of spread or the realised range. Potential ranges have been found for invasive plants (Gallien et al.,

2012; Rouget et al., 2004; Beaumont et al., 2009), insects (Roura-Pascual et al., 2004) and fish (Reshetnikov and Ficetola, 2011), and the effects of climate change on ranges have been explored (Hanewinkel et al., 2013). However, many species do not fill their potential ranges (Svenning and Skov, 2004), are observed outside their ranges due to migration (Pulliam, 2000), or are unable to track shifting ranges (Zhu et al., 2012), so potential ranges may be of limited use in predicting the spread of species invasions.

There have been attempts to overcome this shortcoming by incorporating mechanistic processes into the model. These models exist on a continuum between purely mechanistic models and purely statistical/correlative models (Dormann et al., 2012). These have taken the form of hybrid models in which dynamic models are run over the suitable habitat found by the SDM (e.g. Smolik et al., 2010; Schurr et al., 2012) and process-based models parameterised with experimental data (e.g. Chapman et al., 2014), but in general, a weakness of these models is over-fitting, caused by the large number of parameters that need to be empirically estimated or assumed (Wisz et al., 2013).

1.4.2 Partial Differential Equations

Partial differential equations (PDEs) model the spread of a spatially and temporally varying continuum population $u(t, \mathbf{x})$ as the simultaneous processes of dispersal and population growth (Shigesada and Kawasaki, 1997). Dispersal is typically modelled by diffusion and population growth as a density dependent deterministic process. PDEs were first used in population modelling by R. A. Fisher to model the spread of genes through a population (Fisher, 1937), and were subsequently used to model muskrats (*Ondrata zibethicus*) by Skellam (1951). Fisher's equation (also known as the Kolmogorov-Petrovsky-Piscounov equation) is given by

$$\frac{\partial u}{\partial t}(t, \mathbf{x}) = D\,\nabla^2 u(t, \mathbf{x}) + (r - \mu\, u(t, \mathbf{x}))\, u(t, \mathbf{x}) \tag{1.1}$$

where D is the diffusion coefficient, r is the intrinsic growth rate and μ represents

the effects of intraspecific competition on the growth rate. Equation (1.1) models population growth using the logistic equation, with the rate of population growth $f(u)$ at each $(t, \mathbf{x})$ related to the population density $u(t, \mathbf{x})$ by

$$f(u) = (r - \mu\, u(t, \mathbf{x})) \ . \tag{1.2}$$

In some cases, the logistic equation may not be an accurate model for population growth, so a different growth function $f(u)$ may be used, giving the more general reaction-diffusion equation

$$\frac{\partial u}{\partial t}(t, \mathbf{x}) = D\, \nabla^2 u(t, \mathbf{x}) + f(u(t, \mathbf{x}))\, u(t, \mathbf{x}) \ . \tag{1.3}$$

This equation assumes that an individual's behaviour is independent of their location in the landscape. However, given the extent to which demographic and dispersal behaviour depend on habitat and location, it may be more reasonable to allow the diffusion coefficient and growth function to be spatially heterogeneous and to depend on $\mathbf{x}$. Assuming that movement is non-myopic, i.e. some non-local sensing of the environment occurs (Belmonte-Beitia et al., 2013), then Fickian diffusion can be assumed (Cantrell and Cosner, 2004), with the heterogeneous reaction-diffusion equation given by

$$\frac{\partial u}{\partial t}(t, \mathbf{x}) = \nabla \cdot (D(\mathbf{x}) \nabla u(t, \mathbf{x})) + f(u(t, \mathbf{x}), \mathbf{x})\, u(t, \mathbf{x}) \ . \tag{1.4}$$

This allows the incorporation of landscape structure in the dispersal and demographic behaviour, enabling the modelling of spread over heterogeneous landscapes. In addition, the reaction-diffusion model can be generalised to incorporate multiple species, alleles or life-stages by using coupled systems of PDEs.

PDEs assume that the changes in population distribution depend only on the current population. While this may be appropriate in some cases, there are situations where the population dynamics are determined by behaviour at some time in the past

(e.g. the previous generation). Delay PDEs have been developed to incorporate these effects. For example Lee et al. (2013) used a delayed PDE with a delay of time T of the form

$$\frac{\partial \mathbf{u}}{\partial t}(\mathbf{x}, t) = D\nabla^2 \mathbf{u}(\mathbf{x}, t) + \mathbf{f}(\mathbf{u}(\mathbf{x}, t - T)) + \mathbf{g}(\mathbf{u}(\mathbf{x}, t)) \tag{1.5}$$

to model the spatial interactions of two *Aedes aegypti* mosquito alleles represented by the population vector $\mathbf{u}(x, t)$.

PDEs have been used extensively to model population spread (Shigesada and Kawasaki, 1997), and in the homogeneous case, have analytically tractable solutions and simple expressions for persistence thresholds (Cantrell and Cosner, 2004) and spreading speeds (Murray, 2003), and have a small number of parameters. However, PDEs make some strong assumptions about individuals' behaviour which may not be appropriate if dispersal is not local or diffusive, or if the species exhibits strong seasonality. In PDEs, dispersal is assumed to be spatially localised and diffusive, which is not an accurate model of many dispersal mechanisms (Nathan, 2006) and may lead to underestimates of spreading speed (Kot et al., 1996). In addition, dispersal and demographic change (birth, maturation etc) are assumed to be simultaneous and continuous processes, and ignore differences between seasons, annual cycles and, with the exception of delay PDEs, maturation times.

1.4.3 Integrodifferential Equations

Integrodifferential equations are another deterministic and mechanistic framework that has been employed in ecology. The integrodifferential equation models that have been used fall into two categories: (1) temporally continuous non-spatial models with an integral representing a time delay introduced by Volterra (1936) used to model age-structure, and (2) spatially and temporally continuous models with an integral representing long distance dispersal. Since the former does not model spatial spread, only the latter is explored here.

Like PDEs, this type of integrodifferential equation models the spread of a continuum population $u(t, \mathbf{x})$ as the simultaneous processes of dispersal and localised population growth, with growth given by the population growth function $f(u)$. However, unlike PDEs, dispersal is conceived as a position jump process where individuals jump with a particular rate μ and jumpers originating at a location $\mathbf{y}$ in the domain Ω arrive at location $\mathbf{x}$ with probability given by the dispersal kernel $\kappa(\mathbf{x}, \mathbf{y})$. The evolution equation for the population density is then given by

$$\frac{\partial u}{\partial t}(t, \mathbf{x}) = f(u(t, \mathbf{x})) - \mu\, u(t, \mathbf{x}) + \mu \int_{\Omega} \kappa(\mathbf{x}, \mathbf{y}) u(t, y) \mathrm{d}\mathbf{y} \ . \tag{1.6}$$

This equation has been used by Medlock and Kot (2003) to model the spread of individuals infected by an epidemic, by Hutson et al. (2003) to model competition between alleles with different dispersal behaviour, and by Lutscher et al. (2005) to model populations in a stream. Medlock and Kot (2003) derived analytical expressions for spreading speeds of populations governed by (1.6) and Lutscher et al. (2005) derived expressions for the persistence of populations on bounded domains with advection (directional flow). Integrodifferential equations allow greater flexibility than PDEs in the choice of dispersal pattern via the kernel $\kappa(\mathbf{x}, \mathbf{y})$, but do not incorporate annual cycles or demographic structure.

1.4.4 Metapopulation Models

Metapopulation models model landscapes as a collection of sites that can host a population, with the dynamics governed by local extinctions and colonisation by neighbouring populations. Several types of models fall under this category, including coupled ordinary differential equation models (Metz and Gyllenberg, 2001) and models where each site has a population of individuals (Schreiber and Lloyd-Smith, 2009).

The simplest metapopulation model is the Levins model (Levins, 1969) where there are T identical sites that can host the population, which are equally connected to

each other (Nicholson and Ovaskainen, 2009). This is a spatially implicit population model, and the fraction $N(t)$ of sites occupied by the species is governed by the differential equation and initial condition,

$$\frac{\mathrm{d}N(t)}{\mathrm{d}t} = m\,N(t)\left(1 - \frac{N(t)}{T}\right) - E\,N(t) \qquad \text{and} \qquad N(0) = N_0 \ , \tag{1.7}$$

where N_0 is the fraction of sites occupied at $t = 0$, m is the migration/colonisation rate, T is the total number of sites, and E is the rate of local extinctions.

If the Levins model's simplifying assumptions of identical sites and equal connections between all sites are relaxed, then the model becomes spatially explicit, with each patch corresponding to a different region of habitat in space. If there are n sites in which a population can be either present or absent, then the model has 2^n possible states. Numbering these $j \in \{1, ..., 2^n\}$, one can define a vector $\mathbf{p}(t)$, where the j^{th} element is the probability of being in state j at time t. The change in each p_j will depend on the colonisation and extinction probabilities as well as (linearly) on the other elements of $\mathbf{p}$, so the evolution equation can be written

$$\frac{\mathrm{d}\mathbf{p}}{\mathrm{d}t}(t) = \mathbf{T}_n\,\mathbf{p}(t) \ , \tag{1.8}$$

where $\mathbf{T}_n$ is the 2^n by 2^n matrix of transition probabilities between the states of the model. In practice, these heterogeneous metapopulation models are typically solved either using numerical simulation or approximation by adding additional assumptions such as independence or moment-closure.

Levins type metapopulation models have been used to model the spread of invasive insects (Morris et al., 2005), the spread of a fungicide resistant crop pathogen (Parnell et al., 2006) and to evaluate management strategies for invasive species (Marvier et al., 2004). Other types of metapopulation models, including discrete time models, have been applied to model the spread of butterflies (Hanski and Thomas, 1994) and the persistence of herring populations (Secor et al., 2009). However, these models ignore spatial structure within patches, which may be unrealistic for spreading populations

and lead to inaccurate predictions of spread.

1.4.5 Individual Based Models

Individual based models (IBMs), or agent based models (ABMs), are models where each individual is modelled as a collection of one or more state variables (e.g. location, age, height, weight, dispersal ability). Events (e.g. birth, death, movement, feeding, maturation) happen to individuals following a scheduling pattern defined in the model. These processes affect the individual's state variables or lead to the generation of state variables for new individuals, and can incorporate evolutionary processes (Travis and Dytham, 1998). IBMs are described by computational algorithms and are implemented and studied using computational simulation (Grimm and Railsback, 2013). They can be used to study the emergence of population level behaviours (e.g. persistence, resilience and spread) from the behaviour of individuals and have been applied to a range of problems (Botkin et al., 1972; DeAngelis et al., 1980) including invasive species (Buckley et al., 2003) and the range expansion of species tracking climate change (Travis et al., 2011, 2013). IBMs can be easily used by non-experts by using programmes such as NetLogo (Tisue and Wilensky, 2004). IBMs can incorporate multiple biological processes, including a range of dispersal patterns and demography, as well as intrinsic stochasticity and genetics. However, implementing complex IBMs can require very large amounts of computational resources which may become prohibitive if the model is to be run over longer time-scales or large spatial scales or if it is run multiple times in an ensemble of simulation runs.

1.4.6 Merits of Different Modelling Approaches

Each of the model frameworks described above has been used to model a wide variety of species. The approaches differ in terms of the biological processes they incorporate, SDMs are concerned with the relationships between ecological variables and fitness; PDEs with representing population growth and dispersal as simultaneous processes;

metapopulation models with local extinctions and colonizations; and IBMs with the effect of individuals' behaviour.

In terms of modelling the spread of populations, the purely statistical SDMs are appropriate for the prediction of potential ranges (where the species could persist) rather than realised ranges. The remaining population models are mechanistic in that they explicitly incorporate biological processes such as birth, maturation, dispersal etc, so can generate predictions of spread from the results of ecological experiments. Metapopulation models such as (1.7) are spatially implicit and do not describe invasions in the same way as spatially explicit models but may be appropriate for studying the relationship between local colonisations and extinctions, and spread. Spatially explicit metapopulations such as (1.8) are appropriate for patch type systems, particularly where individuals seek habitat patches (e.g. nesting sites). PDEs are more suitable for modelling invasions with local diffusion-type dispersal (e.g. animal movement or dispersal by water), but are less suitable for discrete events, for example the annual dispersal of pine seeds over large distances. IBMs are suitable for incorporating a large number of biological processes, but are less suitable for modelling large numbers of individuals due to the high cost in computational resources.

Ultimately, the choice of model depends on the species and scenario being studied and the desired output. If the goal is to determine the potential range of an invasion, then SDMs may be appropriate, whereas deterministic spatial models are more suitable for finding spread rates. Where the relationships between the (re-)establishment and extinction of local popuations and the general patterns of spread are important, metapopulation models may be an appropriate choice. If the precise locations of individuals in a landscape are relevant then a spatially continuous model (e.g. PDE or IBM) may be most appropriate. In other cases, none of the models presented in this section will be satisfactory in modelling the processes relevant to the dynamics and desired output. In these cases, other frameworks (including hybrid models) will be more suitable. For example, a species may have dynamics that are highly seasonal (and so require a discrete time model), are driven by long-distance dispersal (rather

than local diffusive dynamics) and have sufficiently large populations that individual dynamics can be approximated by a continuous population distribution. In such cases, none of the models in this section fulfil all of these criteria, and a different approach is required.

1.5 Integrodifference Equations (IDEs)

IDEs (Kot and Schaffer, 1986) are a spatially explicit, mechanistic modelling framework that reflects the seasonal growth and dispersal of many species, by modelling the demography and dispersal of populations as two separate sequential phases. IDEs have been used to model population spread in a range of species (see Table 1.2), have been applied to critical patch size problems (Reimer et al., 2016), and have been used to model continuously structured populations (Rees et al., 2014). In the context of spread modelling, they have several major advantages over other mechanistic modelling approaches:

1. IDEs treat time as a discrete quantity, so more accurately reflect the behaviour of many populations (Wright and Hastings, 2007), including seasonal growth and dispersal. They are also able to incorporate stage-structured matrix population models (Neubert and Caswell, 2000; Caswell, 2000).

2. IDEs can incorpate any pattern of dispersal that can be formulated as a *dispersal kernel*, the distribution of displacements of individuals from their original position, or (for juveniles) the position of their parent.

3. IDEs have a relatively small number of free parameters, enabling them to be parameterised by available distribution data.

4. IDEs can be studied analytically, enabling the calculation of invasion potential, local spreading speeds, persistence and elasticities for model parameters and facilitating ecological risk assessment (see Table 1.1).

5. IDEs can represent populations in real landscapes through spatially heterogeneous demographic and dispersal parameters, and can be simulated numerically (Andersen, 1991), although this can become computationally expensive over large scales and at high resolutions.

IDEs have generated extensive theoretical work (Table 1.1), and have been used to model the spread of a wide range of species (Table 1.2). Theoretical work includes the study of population dynamics, such as analytical and numerical exploration of population spreading speeds, persistence, the sensitivities of spread to the model parameters and pattern formation; data fitting methods; optimal control theory; the relevance of intrinisic (individual) stochasticity to the population dynamics; and extensions of IDEs to include effects such as density dependence and extrinisic (environmental) stochasticity.

IDEs have been applied to a range of species, including crustaceans (Kanary et al., 2014; Marculis and Lui, 2016), mammals (Krkošek et al., 2007; Smith et al., 2009; Hurford et al., 2006), birds (Veit and Lewis, 1996), insects (Coutinho et al., 2012; Mistro et al., 2005; Zhou and Kot, 2013; Stokes et al., 2006), trees (Clark, 1998; Neupane and Powell, 2015; Buckley et al., 2005; Harsch et al., 2014; Caplat et al., 2012; Harsch et al., 2014), grasses (Jacquemyn et al., 2005; Pittman et al., 2015; Lamoureaux et al., 2015; Matlaga and Davis, 2013), thistles (Marchetto et al., 2010; Skarpaas and Shea, 2007; Jongejans et al., 2008), seaweed (Britton-Simmons and Abbott, 2008), lupin (Fagan et al., 2005), shrubs (Travis et al., 2011), pathogens (Skelsey et al., 2010; Leung and Kot, 2015) and parasites (Legaspi Jr et al., 1998). In addition, IDEs have also been used to model the spread of the use of agricultural tools by humans during the neolithic transition (Fort et al., 2007).

Under certain simplifying conditions, the solutions to IDEs can be studied analytically, either exactly or by using approximations, to determine outputs such as spreading speeds, persistence and sensitivities to ecological parameters. These simplifying assumptions and the resulting outputs ignore the complex geometry of real

landscapes, and instead use a homogeneous or a periodic landscape. This simplification enables the calculation of simple quantitative outputs (spreading speeds, persistence etc), which can improve the understanding of species' qualitative behaviour and provide useful indications of the level of risk posed by an invasive species (e.g. Neubert and Caswell, 2000) or the ability of a species to keep pace with climate change (e.g. Harsch et al., 2014). Analytical methods are also less computationally expensive (than simulation), and so allow for efficient parameter sweeps, which allows different scenarios (e.g. management strategies, climate scenarios) to be tested and uncertainties in parameters to be incorporated into spread forecasts (Higgins et al., 2003).

In other cases, it is useful to predict the exact dynamics of a species invasion. To do this, the assumption of landscape homogeneity or periodicity needs to be relaxed, and real landscapes incorporated into spread models. Incorporating real landscape structure is crucial in many cases, as many landscapes exhibit strong variation across large spatial scales, making homogeneous or periodic approximations invalid (Svenning et al., 2014; Miller and Tenhumberg, 2010). Unfortunately, introducing real landscapes generally makes the solutions analytically intractable. Instead, to make predictions on complex landscapes, numerical simulations of the models are required (Andersen, 1991).

Over thirty papers have been published which apply IDE theory and simulation techniques to estimate the rate of spread of species (see Table 1.2). Of these, most have made assumptions that enable the use of analytics. Others (e.g. Veit and Lewis, 1996) have used simulation on homogeneous landscapes, either to explore the two-dimensional structure of spread or due to the incorporation of other effects that preclude the use of analytics (e.g. interspecies competition, a stable zero population steady state or Allee Effect). As of April 2016, the archive "Web of Science" held only four papers under the topics "integrodifference" or "integro-difference" that used IDEs with a realistic landscape to model a specific spread problem. Of these, three used randomly generated neutral landscapes, while only one (Lamoureaux et al.,

2015) used real mapping data to make conclusions about the future distribution of the weedy grass, *Nassella trichotoma*, in New Zealand. The lack of simulation studies on heterogeneous landscapes may be due to the lack of usable implementations of algorithms for modelling IDEs over real landscapes, or to a greater interest in analytics than in simulation.

Theory	**References**
Introduced	Weinberger (1982); Kot and Schaffer (1986); Andersen (1991); Kot (1992)
Review Papers	Hastings et al. (2005)
Spreading Speeds	Allen et al. (1996); Kot et al. (1996); Hart and Gardner (1997); Neubert and Caswell (2000); Wang et al. (2002); Lutscher (2007); Kawasaki and Shigesada (2007); Kot and Neubert (2008); Samia and Lutscher (2010); Weinberger and Zhao (2010); Miller et al. (2011); Li (2012); Wang and Castillo-Chavez (2012); Ding et al. (2013); Gilbert et al. (2014a,b); Bateman et al. (2015); Musgrave et al. (2015)
Persistence	Van Kirk and Lewis (1997); Latore et al. (1998, 1999); Etienne et al. (2002); Lutscher and Lewis (2004); Cobbold et al. (2005); Fagan et al. (2007); Carrillo et al. (2009); Lutscher et al. (2010); Zhou and Kot (2011); Hastings (2014); Musgrave and Lutscher (2014); Fuller et al. (2015); Jacobsen et al. (2015); Kot and Phillips (2015); Phillips and Kot (2015); Reimer et al. (2016)
Mathematical Analysis	Weinberger (1982); Lin (1995); Lutscher and Lewis (2004); Kachurivs kyi (2010); Lin and Li (2010); Pan and Lin (2011); Pan and Zhang (2011); Yu and Yuan (2012); Lutscher and Van Minh (2013); Miller and Zeng (2013); Pan and Lin (2014)
Landscape Heterogeneity	Kawasaki and Shigesada (2007); Dewhirst and Lutscher (2009); Samia and Lutscher (2010); Gilbert et al. (2014a,b); Musgrave and Lutscher (2014); Li et al. (2015); Musgrave et al. (2015)
Simulation	Andersen (1991); Legaspi Jr et al. (1998)
Sensitivity/Elasticity	Neubert and Caswell (2000); Caswell et al. (2003)
Intrinsic Stochasticity	Lewis (2000); Snyder (2003); Kot et al. (2004)
Model Fitting	Wikle (2002); Fujiwara et al. (2006); Heavilin and Powell (2008); Dewar et al. (2009); Scerri et al. (2009); Wikle and Hooten (2010); Aram and Freestone (2016)
Optimal Control	Joshi et al. (2006, 2007); Gaff et al. (2007); Gordillo (2014); Martinez et al. (2015)
Pattern Formation	Neubert et al. (1995, 2002); Wright and Hastings (2007)
Wave-back behaviour	Sherratt et al. (1997)
Temporal Variation	Neubert et al. (2000); Caswell et al. (2011); Schreiber and Ryan (2011)
Climate Change	Bullock et al. (2012); Santini et al. (2016)

Table 1.1: Survey of papers exploring the theory of integrodifference equations grouped by theme.

	Homogeneous	Heterogeneous
Invasive Species	Kanary et al. (2014); Marculis and Lui (2016); Jacquemyn et al. (2005); Neupane and Powell (2015); Buckley et al. (2005); Marchetto et al. (2010); Skarpaas and Shea (2007); Leung and Kot (2015); Skelsey et al. (2005); Matlaga and Davis (2013); Caplat et al. (2012); Travis et al. (2011); Stokes et al. (2006); Jongejans et al. (2008); Cuddington and Hastings (2004); Veit and Lewis (1996); Legaspi Jr et al. (1998); Fagan et al. (2005); Coutinho et al. (2012); Horvitz et al. (2015); Marculis and Lui (2016); Schofield (2002)	*1D Periodic:* Mistro et al. (2005). *2D Randomly Generated:* Britton-Simmons and Abbott (2008); Skelsey et al. (2010); Pittman et al. (2015). *2D Real Landscape:* Lamoureaux et al. (2015)
Range Shifting	Clark (1998); Penz et al. (2015); Zhou and Kot (2013); Harsch et al. (2014); Santini et al. (2016)	
Reintroduction	Krkošek et al. (2007); Smith et al. (2009); Hurford et al. (2006); Bullock et al. (2008)	*1D:* Tinker et al. (2008)
Other (e.g. Anthropology)	Fort et al. (2007, 2008)	

Table 1.2: Survey of papers using IDEs to predict the behaviour of a particular species or scenario, classified by whether the paper investigates invasive species, range-shifting species, reintroductions and whether the landscape used in the model was homogeneous or heterogeneous.

1.5.1 The Model

A general non-stage-structured IDE on a one- or two-dimensional domain $\Omega \subseteq \mathbb{R}^j$ where $j \in \{1, 2\}$ relates the continuous population distribution $u^{t+1}(\mathbf{x})$ at time $t+1$, with the scalar distribution $u^t(x)$ at integer time t, where $\mathbf{x} \in \Omega$ is a location in the domain, via

$$u^{t+1}(\mathbf{x}) = \int_\Omega k(\mathbf{x}-\mathbf{y}, \mathbf{y})\, r(u^t(\mathbf{y}), \mathbf{y})\, u^t(\mathbf{y})\, \mathrm{d}\mathbf{y} \ . \tag{1.9}$$

In the growth phase, the population distribution is multiplied by the density and location dependent *growth rate* $r(u^t(\mathbf{y}), \mathbf{y})$ (Neubert and Caswell, 2000; Caswell et al., 2003; Coutinho et al., 2012; Zhou and Kot, 2011). For the dispersal phase, the value of the post-dispersal population distribution at $\mathbf{x}$ is obtained by taking the spatial integral of the product of the pre-dispersal population, $r(u^t(\mathbf{y}), \mathbf{y})u^t(\mathbf{y})$ and the *dispersal kernel* $k(\mathbf{x} - \mathbf{y}, \mathbf{y})$, the relative density of dispersal from $\mathbf{y}$ to $\mathbf{x}$ (Kot et al., 1996). In other words, the population abundance at spatial location $\mathbf{x}$ at the next generation is simply the contribution from the birth/death processes of the current generation that move to location $\mathbf{x}$ according to the redistribution kernel, k. Hence, the spatio-temporal population dynamics fundamentally depend on the growth and dispersal functions.

1.5.2 Stage-Structured IDEs

One complication in modelling species invasions is that spreading populations are composed of individuals that are at different points in their life cycle, and will therefore exhibit different characteristics at any given time (Caswell, 2000). The differences between individuals of the same species at different levels of development has been an important area of study for ecologists. Initially, it led to the classification of individuals by age and sex by Lewis (1942) and (independently) by Leslie (1945), and later to classification by more general factors such as developmental level and size by Lefkovitch (1965) and Usher (1966), respectively. Classification into developmental/size stages has several advantages over age-classification: experimentally, an individual's current demographic stage may be easily recognised (Hartshorn, 1975), may tell us much more about an individual's demographic properties (Caswell, 2000), and stage-classification is easily incorporated into spatially explicit population models.

The simplest type of discrete time stage-structured model (of which stage-structured IDEs are a spatially explicit extension) is a matrix model. Individuals in each demo-

graphic stage have a specific probability of (1) remaining in the same demographic stage, (2) transitioning to another demographic stage, e.g. through maturation, (3) reproducing and generating new individuals in the first/juvenile stage, and (4) dying and being removed from the population. These rates may be density dependent due to factors such as intraspecific competition, but depend only on the numbers of individuals in each stage at the current time-step (i.e. the population is assumed to have the Markov property).

Mathematically, these rates can be represented as an $M \times M$ population projection matrix, where M is the number of demographic stages, which relates the populations in each demographic stage at time $t+1$ with time t. Each demographic stage is assigned a number between 1 and M, with the first being the juvenile (new-born) stage. The (i, j)-th element of the matrix thus relates the j and i-th demographic stages. If $i = j$ or $i \neq 1$, then the (i, j)-th element is the proportion of individuals in the j-th demographic stage at time t that will be in the i-th stage at time $t+1$. For elements on the diagonal, where $j = i$, then this is just the proportion of individuals that remain in this stage. On the other hand, if $i = 1$ and $j > 1$, then the $(1, j)$-th element is the rate at which new juveniles are born to individuals in the j-th demographic stage.

For example, pea aphids (*Acythosiphon pisum*, see Figure 1.4a), can be divided into five demographic stages (Tenhumberg, 2010). There are four juvenile instars (stages), corresponding to different developmental milestones and one adult stage. Between spring and autumn, pea aphids give birth to live young (Tenhumberg et al., 2009) and spend an average of around two days in each of the juvenile instars. For small populations, the daily transition rates between the stages can be represented with a life cycle diagram (top of Figure 1.4b) with the arrows showing the transition rates. For example, members of the adult stage (A) each generate an average of 1.7 new offspring in the first instar (L1) over 24 hours and 0.95 of the current adults will still be in the population after 24 hours (the other 5% will be dead). The life-cycle diagram is a useful illustration of individuals' behaviour and can be used to generate

the mathematically useful linear population projection matrix $\mathbf{A}$ (bottom of Figure 1.4b) with the (i, j)-th element corresponding to the arrow between the j-th and i-th stages in the life-cycle diagram. The $(1, 5)$-th element of $\mathbf{A}$ corresponds to the arrow between the 5th stage (A) and the 1st stage (L1) which represents the birth of new individuals.

To incorporate stage-structure into the IDE framework, the growth rate r is replaced with a *population projection matrix* $\mathbf{B}\left(\mathbf{u}^t(y), y\right)$, where the (i, j)-th element is the ratio of the number of individuals in stage j after the growth phase and the number of individuals in stage i at time t (at location y). Similarly, the dispersal kernel k is replaced by a matrix of dispersal kernels $\mathbf{K}(x - y, y)$, where the (i, j)-th element $K_{i,j}(x - y, y)$ is the dispersal kernel for individuals which transitioned from stage i to stage j in the growth phase. It is necessary to consider the dispersal pattern of individuals transitioning between each (permitted) pair of demographic stages separately, as the stage of the individual or, in the case of juveniles, its parent before the growth phase will often affect the individual's dispersal behaviour. For example, for plants with wind dispersed seeds, the mean dispersal distance of a seed/new juvenile will depend on the seed release height of its parent and therefore on its parent's demographic stage (Katul et al., 2005; Travis et al., 2011). The general stage-structured IDE, of which the non-stage-structured IDE (1.9) is a specific case, is then given by

$$\mathbf{u}^{t+1}(\mathbf{x}) = \int_{\Omega} \left[\mathbf{K}(\mathbf{x} - \mathbf{y}, \mathbf{y}) \circ \mathbf{B}\left(\mathbf{u}^t(\mathbf{y}), \mathbf{y}\right)\right] \mathbf{u}^t(\mathbf{y}) \mathrm{d}\mathbf{y} \ , \tag{1.10}$$

where $\circ$ denotes the Hadamard (elementwise) product of two matrices (Neubert and Caswell, 2000). This relation is non-dimensional in that no scales or units are given to length, population density or time, with the analysis applicable to all choices of non-dimensionalising length and time scales.

The reader is referred to the following key papers which develop the theory of non-stage-structured IDEs: Kot and Schaffer (1986); Kot et al. (1996); Weinberger (1982), stage-structured IDEs: Neubert and Caswell (2000); Neubert and Parker

(a)

(b)

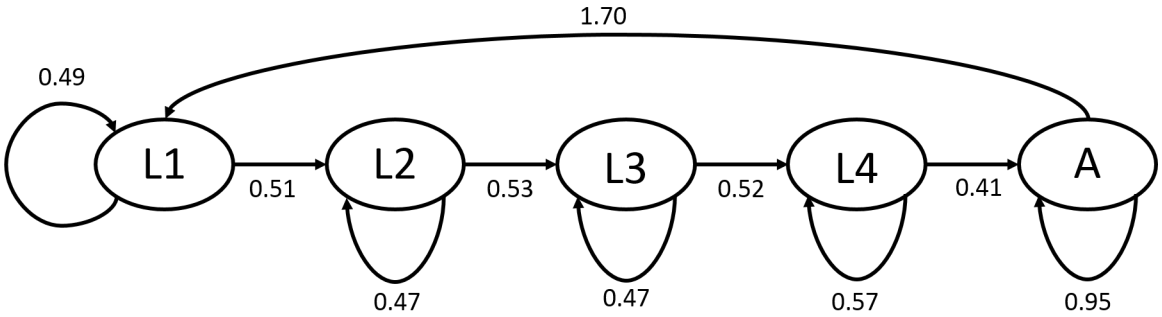

(c)

$$\mathbf{A} = \begin{pmatrix} 0.49 & 0 & 0 & 0 & 1.70 \\ 0.51 & 0.47 & 0 & 0 & 0 \\ 0 & 0.53 & 0.47 & 0 & 0 \\ 0 & 0 & 0.52 & 0.57 & 0 \\ 0 & 0 & 0 & 0.41 & 0.95 \end{pmatrix}$$

Figure 1.4: (a) Photograph of pea-aphids (*Acythosiphonp pisum*), pea-aphid (b) life-cycle and (c) population projection matrix with the numerical values indicating transition and birth rates for small populations. Reproduced from Tenhumberg (2010) with permission.

(2004); Garnier and Lecomte (2006), spatially heterogeneous IDEs: Dewhirst and Lutscher (2009); Weinberger (2002); Weinberger et al. (2008).

Several methods exist for studying the spreading behaviour of IDE models. For spatially homogeneous models, exact analytical expressions for the spreading speed can be calculated under certain conditions. For the spatially periodic case, the spreading speed problem can be converted into the problem of calculating the principal eigenvalue of an integral operator. In general this is analytically intractable, but enables asymptotic approximations to the spreading speed to be derived. For IDEs with landscapes that are not homogeneous or periodic, it is generally necessary to simulate. In Chapters 2 and 3 of this thesis, we will develop novel analytical methods for studying spatially periodic IDEs and in Chapter 4, will develop an efficient algorithm for the simulation of IDEs over large complex landscapes. To set the scene for Chapters 2-4, we now examine the most relevant methodological developments in analytics and simulation of IDEs.

1.5.3 Asymptotic Spreading Speeds for Homogeneous IDEs

The parameters in homogeneous IDEs do not depend on the spatial location, with the domain assumed to be infinite and equal to $\mathbb{R}$ or $\mathbb{R}^2$ for one and two-dimensional IDEs, respectively. For an homogeneous IDE, the form of the dispersal kernel $\mathbf{K}(\mathbf{x}-\mathbf{y},\mathbf{y})$ depends only on the displacement $\mathbf{x}-\mathbf{y}$ between the dispersal origin and destination and not explicitly on the origin $\mathbf{y}$, allowing us to write it as $\mathbf{K}(\mathbf{x}-\mathbf{y})$. Similarly, the scalar growth rate $r(u(\mathbf{y}),\mathbf{y})$ (for non-stage-structured populations) or population projection matrix $\mathbf{B}(\mathbf{u}(\mathbf{y}),\mathbf{y})$ (for stage-structured populations) depends only on the local population density, so can be written as $r(u(\mathbf{y}))$ or $\mathbf{B}(\mathbf{u}(\mathbf{y}))$. For the general stage-structured case, a homogeneous IDE is any IDE of the form

$$\mathbf{u}^{t+1}(\mathbf{x}) = \int_{\Omega} \left[\mathbf{K}(\mathbf{x}-\mathbf{y}) \circ \mathbf{B}\left(\mathbf{u}^t(\mathbf{y})\right)\right] \mathbf{u}^t(\mathbf{y})\, \mathrm{d}\mathbf{y} \ . \tag{1.11}$$

where $\Omega = \mathbb{R}^j$ with $j \in \{1,2\}$. In the non-stage-structured case, the population

density, dispersal kernel and population projection matrix are scalar, and we have

$$u^{t+1}(\mathbf{x}) = \int_{\Omega} k(\mathbf{x}-\mathbf{y})\, r\left(u^t(\mathbf{y})\right) u^t(\mathbf{y})\, \mathrm{d}\mathbf{y} \ . \tag{1.12}$$

The asymptotic ($t \to \infty$) behaviour of a population distribution with compact initial support modelled by (1.11) or (1.12) in one spatial dimension ($\Omega = \mathbb{R}$) depends on the details of the dispersal kernel $\mathbf{K}(\mathbf{x}-\mathbf{y})$ and the population projection matrix $\mathbf{B}\left(\mathbf{u}^t(\mathbf{y})\right)$. If the zero population state is unstable (i.e. the population projection matrix has no *Allee effect*) and the dispersal kernel $\mathbf{K}(z)$ has moments of all orders, or is *exponentially bounded*, then the asymptotic ($t \to \infty$) behaviour of solutions with compact initial support is a propagating front with exponential decay in the wave-front (Kot, 1992), see for example Figure 1.5a.

The spreading behaviour of these propagating fronts is governed by the behaviour of the solution's wave-front, where the population density is small (van den Bosch et al., 1990). This is often referred to as the *Linear Conjecture* (Mollison, 1991), and allows us to approximate the IDE by its linearisation, where the growth rate $r\left(u^t(\mathbf{y})\right)$ or population projection matrix $\mathbf{B}\left(\mathbf{u}^t(\mathbf{y})\right)$ is replaced by its linearisation around the zero steady state, $r\left(0\right)$ and $\mathbf{B}\left(\mathbf{0}\right)$, which for simplicity, are denoted r_0 and $\mathbf{A}$ respectively. The linearised stage-structured IDE in one spatial dimension is given by

$$\mathbf{u}^{t+1}(x) = \int_{-\infty}^{\infty} \left[\mathbf{K}(x-y) \circ \mathbf{A}\right] \mathbf{u}^t(y)\, \mathrm{d}y \ , \tag{1.13}$$

and the linearised non-stage-structured IDE in one spatial dimension by

$$u^{t+1}(x) = \int_{-\infty}^{\infty} k(x-y)\, r_0\, u^t(y)\, \mathrm{d}y \ . \tag{1.14}$$

Linearised IDEs with an exponentially bounded dispersal kernel have exponential *travelling wave* solutions, of the form

$$\mathbf{u}^t(x) = \mathbf{v}\exp(s(x - c(s)t)) \ ,$$

which have decay rate s and wave-speed $c(s)$. Weinberger (1982) showed that the asymptotic wave-speed for travelling wave solutions of a homogeneous IDE of the form (1.9) with no Allee effect, an exponentially bounded dispersal kernel and bounded initial support is given by the speed of the slowest travelling wave solution

$$c^* = \min_{s>0} c(s) \ , \tag{1.15}$$

where the wave-speed of the travelling wave for non-stage-structured populations is given by the *dispersion relation*,

$$c(s) = \frac{1}{s}\log\left(r_0\, M(s)\right) \ .$$

Here $M(s)$ is the moment generating function (MGF) of the dispersal kernel $k(x-y)$, $M(s) = \int_{-\infty}^{\infty} k(z)\mathrm{e}^{sz}\mathrm{d}z$. Neubert and Caswell (2000) incorporated stage structure into homogeneous IDEs, with the speed of the travelling wave with decay rate s given by

$$c(s) = \frac{1}{s}\log\left(\rho(s)\right) \tag{1.16}$$

where $\rho(s)$ is the principal eigenvalue of the operator

$$\mathbf{H}(s) = \mathbf{A} \circ \mathbf{M}(s) = \mathbf{A} \circ \int_{-\infty}^{\infty} \mathbf{K}(z)\mathrm{e}^{sz}\mathrm{d}z \ , \tag{1.17}$$

where $\circ$ denotes the Hadamard (elementwise) product of two matrices, $\mathbf{K}(z)$ denotes the stage-structured dispersal kernel, $\mathbf{M}$ is the (matrix) moment generating function of $\mathbf{K}(z)$ and $\mathbf{A}$ is the stage-structured population projection matrix linearised around the zero population state.

Equation 1.15 gives a simple expression for the asymptotic spreading speed of an IDE in one spatial dimension in terms of the moment generating function of the

dispersal kernel and the linearisation of the growth rate or population projection matrix at zero. This means that the wave-speed depends only on the behaviour of small populations and not on the precise shape of the growth function.

1.5.4 Asymptotic Spreading Speeds for Periodic IDEs

An IDE with one spatial dimension is spatially periodic if the dispersal kernel and population projection matrix (or growth function) are spatially periodic. For example, regular banded patterning of vegetation is observed on semi-arid regions of Burkina Faso (Müller, 2013). For a stage-structured IDE to be L-periodic, i.e. periodic with period L, the location and density dependent population projection matrix $\mathbf{B}(\cdot,\cdot)$ must have periodic location dependence with period L and the spatially heterogeneous dispersal kernel matrix $\mathbf{K}(\cdot,\cdot)$ must be periodic in the dispersal origin y with period L, with

$$\mathbf{B}\left(\mathbf{v}, y+L\right) = \mathbf{B}\left(\mathbf{v}, y\right) \tag{1.18}$$

$$\mathbf{K}(x-y, y+L) = \mathbf{K}(x-y, y) \ . \tag{1.19}$$

for all $x, y \in \mathbb{R}$ and for all vectors $\mathbf{v}$ with non-negative elements. For periodic IDEs without an Allee effect and with compact initial support, the asymptotic spreading speed of populations with initial compact support is given by the slowest *periodic travelling wave* solution to the linearised IDE. Periodic, or pulsating, travelling wave solutions are of the form

$$\mathbf{u}^t(x) = \exp\left(s(c(s)t - x)\right)\boldsymbol{\phi}(x) \ , \tag{1.20}$$

where $\boldsymbol{\phi}$ is L-periodic,

$$\boldsymbol{\phi}(x+L) = \boldsymbol{\phi}(x) \ , \tag{1.21}$$

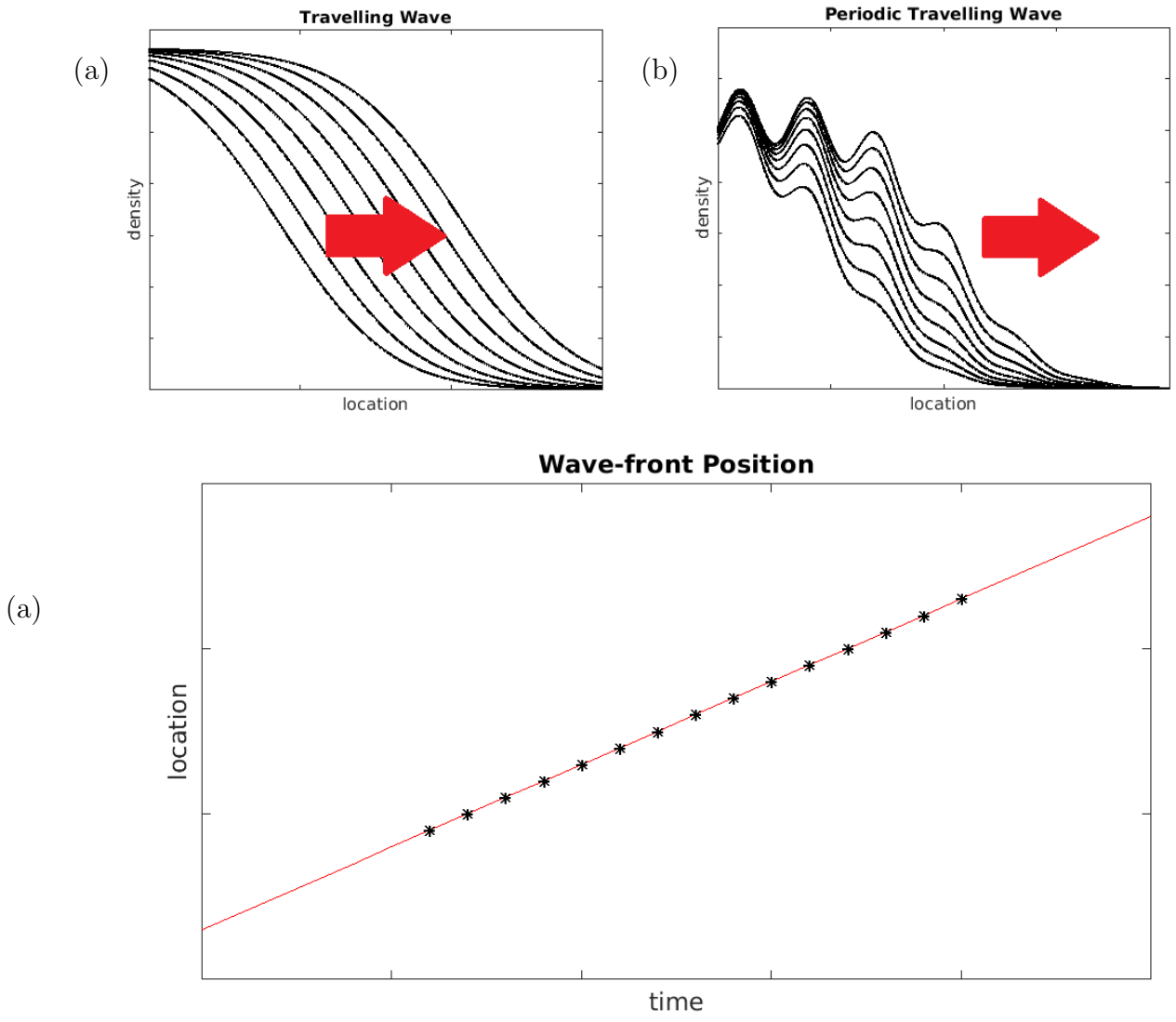

Figure 1.5: Solutions to (a) a homogeneous IDE and (b) a heterogeneous IDE, with the arrow showing the direction of spread. (c) The position of the wave-front (where the density crosses a threshold) of a homogeneous IDE for a range of times, with a line of best fit (red) with gradient equal to the spreading speed.

for all $x \in \mathbb{R}$. The asymptotic spreading speed is given by (1.16), but with $\rho(s)$ as the principal eigenvalue of the operator

$$F_s\left[\boldsymbol{\phi}\right](x) = \int_{-\infty}^{\infty} \left[\mathbf{K}(x-y,y) \circ \mathbf{A}\left(y\right)\right] \mathrm{e}^{s(x-y)} \boldsymbol{\phi}(y) \mathrm{d}y \ . \tag{1.22}$$

In general, this is analytically intractable, but the eigenvalue can either be found numerically, or under certain conditions, by using asymptotic analysis (Dewhirst and Lutscher, 2009).

1.5.5 Example

We now consider a hypothetical example of a spreading species and demonstrate how to calculate its spread rate c^* in a one-dimensional homogeneous landscape.

Suppose that we are interested in the spread of a particular species. The species has been studied in field experiments, and the parameters governing its demography and dispersal have been inferred. Individuals exhibit seasonal behaviour (over annual cycles) with the species categorised into three demographic stages. Members of the second and third stages reproduce, generating new individuals in the first demographic stage (juveniles), and only new juveniles disperse.

Demography

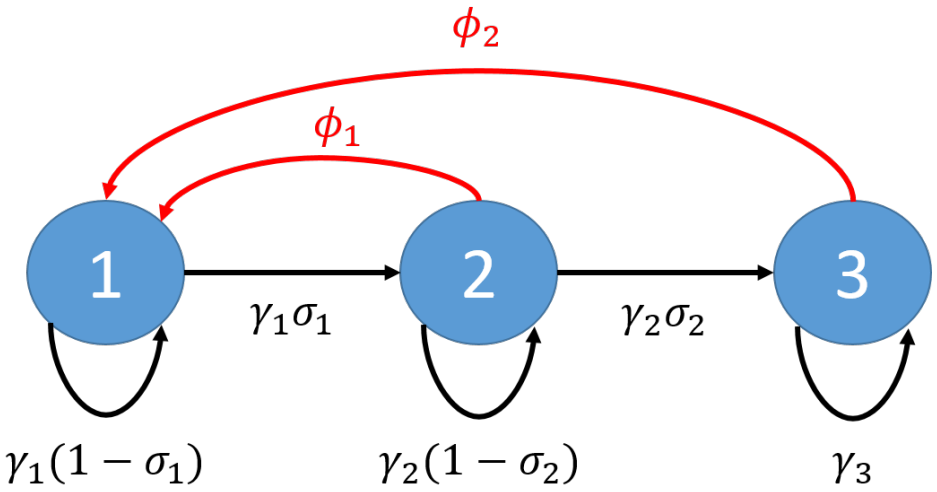

Figure 1.6: Life-cycle of a hypothetical species with three demographic stages (labelled 1,2 and 3). The arrows denote the transitions between the stages, with the accompanying values (given in terms of the maturation rates, σ_n, survival rates, γ_n and birth rates ϕ_n) giving the transition rates for small populations. Transitions occurring within the life-history of the same individual are denoted by black arrows and reproduction is denoted by red arrows.
F

Each year during the growth phase, individuals have a survival probability of γ_n (where n is the individual's demographic stage). Individuals in stages 1 and 2 mature to stages 2 and 3 with probabilities σ_1 and σ_2 respectively. This means that individuals mature from stages $n \in \{1, 2\}$ to the stage $n+1$ at rate $\gamma_n\sigma_n$ and remain in the same stage with rate $\gamma_n(1-\sigma_n)$. When the population is small (i.e. the effects of intra-specific competition are absent), individuals in stages 2 and 3 produce offspring at rates ϕ_1 and ϕ_2 respectively. We suppose that in this example, each of the parameters $\gamma_1, \gamma_2, \gamma_2, \sigma_1, \sigma_2, \phi_1$ and ϕ_2 have been determined experimentally. This information is sufficient to label the life-cycle diagram (Figure 1.6).

Suppose also that while the survival and maturation rates are not affected by population density, the birth rates are density dependent and decay exponentially as the population increases. Hence, the birth rate for individuals in the n-th ($n \in \{2, 3\}$) demographic stage at location x and time t is given by $\phi_{n-1}\exp(\mathbf{q}\cdot\mathbf{u}^t(x))$, where $\mathbf{u}^t(x)$ is the stage-structured population density at location x and time t and the

vector $\mathbf{q}$ determines the weights of the different demographic stages in their effects on competition.

This allows us to determine the population projection matrix $\mathbf{B}(\mathbf{u}^t(x))$, which is given by

$$\mathbf{B}(\mathbf{u}^t(x)) = \begin{bmatrix} \gamma_1(1-\sigma_1) & \phi_1\, \mathrm{e}^{\mathbf{q}\cdot\mathbf{u}^t(x)} & \phi_2\, \mathrm{e}^{\mathbf{q}\cdot\mathbf{u}^t(x)} \\ \gamma_1\sigma_1 & \gamma_2(1-\sigma_2) & 0 \\ 0 & \gamma_2\sigma_2 & \gamma_3 \end{bmatrix}. \tag{1.23}$$

Dispersal

For our hypothetical species, dispersal is associated with reproduction, and occurs only from demographic stages 2 and 3 to stage 1. Transition between the other pairs of demographic stages is not associated with dispersal, and so the dispersal kernels for these pairs of stages is the Dirac delta function $\delta(x)$. Dispersal from stages 2 and 3 to stage 1 is governed by the Laplace (double-exponential) kernel with parameter α_{n-1} for dispersal from the n-th ($n \in \{2, 3\}$) stage to the 1st stage. The stage-structured dispersal kernel is given by

$$\mathbf{K}(z) = \begin{bmatrix} \delta(x) & \frac{1}{2\,\alpha_1} \exp\left(\frac{|z|}{\alpha_1}\right) & \frac{1}{2\,\alpha_2} \exp\left(\frac{|z|}{\alpha_2}\right) \\ \delta(x) & \delta(x) & \delta(x) \\ \delta(x) & \delta(x) & \delta(x) \end{bmatrix}. \tag{1.24}$$

Calculation of the spreading speed

In Section 1.5.3, we derived the spreading speed of an IDE with no Allee Effect and an exponentially-bounded dispersal kernel in a homogeneous landscape. We will now use the expressions for the spreading speed in (1.16) and (1.17) to categorise the spreading speed for the hypothetical species. This expression depends only on the

linearised population projection matrix $\mathbf{A}$ which is given by the population projection matrix evaluated at $\mathbf{u}^t(x) = \mathbf{0}$,

$$\mathbf{A} = \mathbf{B}(\mathbf{0}) = \begin{bmatrix} \gamma_1(1-\sigma_1) & \phi_1 & \phi_2 \\ \gamma_1\sigma_1 & \gamma_2(1-\sigma_2) & 0 \\ 0 & \gamma_2\sigma_2 & \gamma_3 \end{bmatrix} , \tag{1.25}$$

and the moment generating function $\mathbf{M}(s)$,

$$\mathbf{M}(s) = \int_{-\infty}^{\infty} \mathbf{K}(z)\mathrm{e}^{s\,z}\mathrm{d}z = \begin{bmatrix} 1 & (1-\alpha_1^2 s^2)^{-1} & (1-\alpha_2^2 s^2)^{-1} \\ 1 & 1 & 1 \\ 1 & 1 & 1 \end{bmatrix} . \tag{1.26}$$

where s is the wave-number and determines the steepness of the travelling wave. For our hypothetical species, the matrix $\mathbf{H}(s)$ defined in (1.17) is then given by

$$\mathbf{H}(s) = \begin{bmatrix} \gamma_1(1-\sigma_1) & \phi_1\,(1-\alpha_1^2 s^2)^{-1} & \phi_2\,(1-\alpha_2^2 s^2)^{-1} \\ \gamma_1\sigma_1 & \gamma_2(1-\sigma_2) & 0 \\ 0 & \gamma_2\sigma_2 & \gamma_3 \end{bmatrix} , \tag{1.27}$$

and its principal eigenvalue $\rho(s)$ determines the spreading speed

$$c^* = \min_{s>0} \frac{1}{s} \log\left[\rho(s)\right] \quad . \tag{1.28}$$

Simplifying (1.28) to a closed form expression for c^* is in general, not possible. However, for given parameter values, one may calculate the wave-speed numerically (by calculating $\rho(s)$ for a range of s and taking the minimum, for example see Figure 1.7).

Thus, we can calculate the spreading speed of our hypothetical species as a minimum of a function of the eigenvalues of a family of matrices $\mathbf{H}(s)$, which are given in terms of the species' demographic and dispersal parameters.

1.5.6 Sensitivity and Elasticity for Homogeneous IDEs

In homogeneous landscapes, it is also possible to calculate analytical formulae for the sensitivity and elasticity of the asymptotic spreading speed to the elements of the linearised population projection matrix $\mathbf{A}$ (or scalar growth rate) and on dispersal parameters. Sensitivity and elasticity were introduced for stage-structured IDEs by Neubert and Caswell (2000) and quantify the relationship between the spreading speed c^* and dispersal and demographic parameters. The sensitivity is the rate of change of the spreading speed c^* as a parameter is varied, and the elasticity is the ratio of the relative change in spreading speed with respect to the relative change in a parameter. Both sensitivity and elasticity are useful in analysing the relevance of each part of the life-cycle for spread, and can thus facilitate conservation decisions (Jacquemyn et al., 2005).

The sensitivity of the asymptotic wave-speed c^* to the (i,j)-th element of $\mathbf{A}$, $a_{i,j}$ is the ratio between the sizes of a change in c^* resulting from an infinitesimal change in $a_{i,j}$ and the size of the infinitesimal change in $a_{i,j}$. Ecologically, it characterises the relationships between changes in parameters and the absolute change in c^*. It is given by

$$\frac{\partial c^*}{\partial a_{i,j}} = \frac{m_{i,j}(s^*)}{s^*\rho(s^*)} \frac{\partial \rho_1}{\partial h_{i,j}}(s^*) \tag{1.29}$$

where s^* is the value of s at which $c(s)$ attains its minimum and is equal to c^*, where $\rho(s^*)$ is the principal eigenvalue of matrix $\mathbf{H}(s^*)$ from (1.17) evaluated at s^*, and where $a_{i,j}$, $h_{i,j}$ and $m_{i,j}$ are the (i,j)-th elements of the linearised population projection matrix $\mathbf{A}$, and matrices $\mathbf{H}(s^*)$ and the moment generating function $\mathbf{M}(s^*)$ of $\mathbf{K}$, where

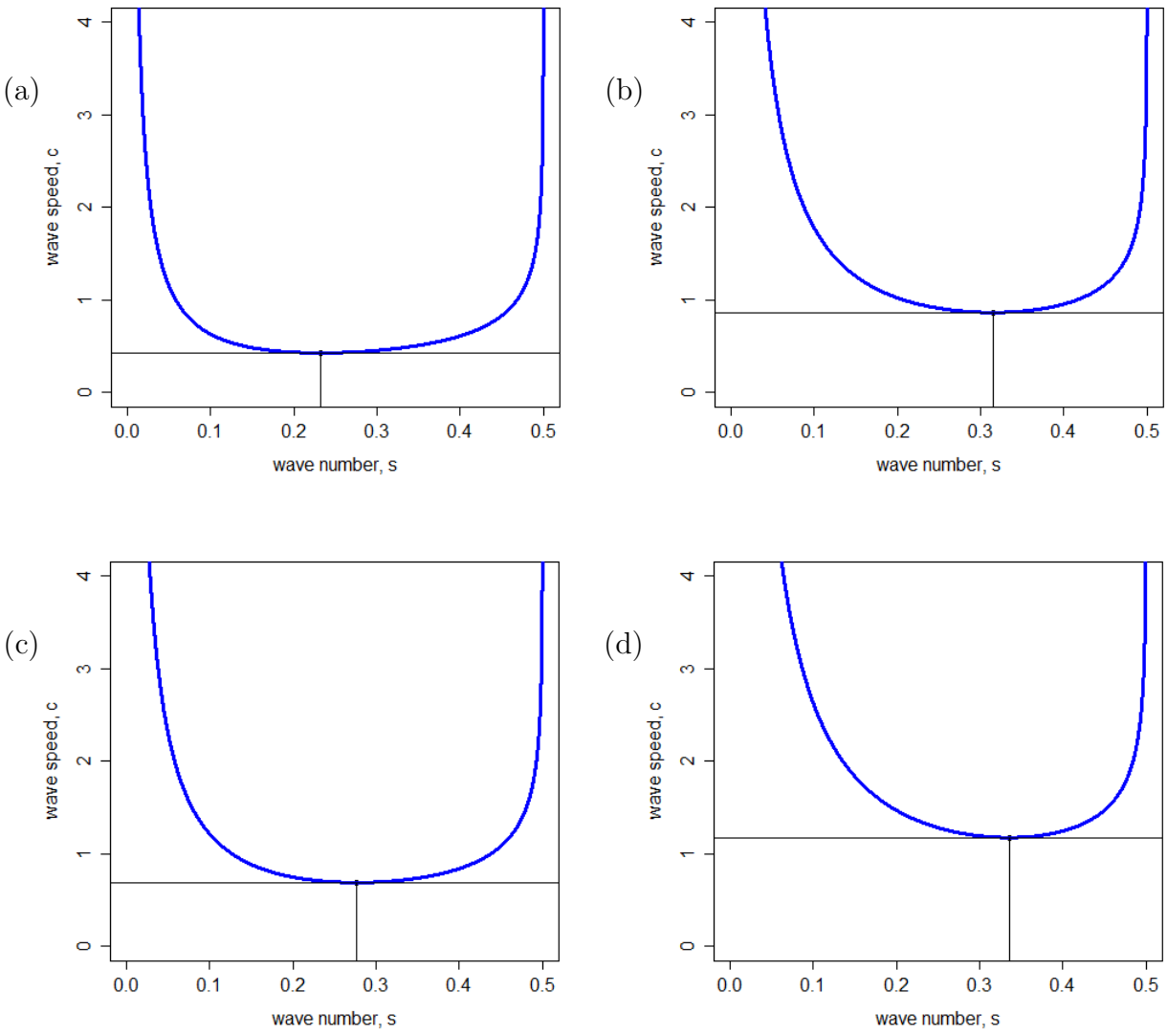

Figure 1.7: Plots of the relationship between the wave-number s and the spreading speed c (thick blue line) for (a) $\sigma_2 = 0.4$, $\phi_2 = 3$, (b) $\sigma_2 = 0.4$, $\phi_2 = 6$, (c) $\sigma_2 = 0.8$, $\phi_2 = 3$, (d) $\sigma_2 = 0.8$, $\phi_2 = 6$. The other parameters were given by $\gamma_1 = 0.4$, $\gamma_2 = 0.5$, $\gamma_3 = 0.6$, $\sigma_1 = 0.8$, $\phi_1 = 1$, $\alpha_1 = 1$ and $\alpha_2 = 2$. The asymptotic spreading speed of populations with compact initial support is given by the minimum of c, and is shown by the thin black line.

$$\mathbf{M}(s) = \int_{-\infty}^{\infty} \mathbf{K}(z) \mathrm{e}^{sz} \mathrm{d}z \ . \tag{1.30}$$

The elasticity of c^* with respect to $a_{i,j}$ characterises the relationship between the relative change in a parameter and the relative change in c^*. Mathematically, it is the ratio of the proportional change in c^* resulting from an infinitiesimal change in $a_{i,j}$ divided by the proportional change in $a_{i,j}$. It is given by

$$\frac{a_{i,j}}{c^*} \frac{\partial c^*}{\partial a_{i,j}} = \frac{h_{i,j}(s^*)}{\rho_1(s^*) \log\left[\rho_1(s^*)\right]} \frac{\partial \rho_1}{\partial h_{i,j}}(s^*) \ . \tag{1.31}$$

We can also calculate the sensitivity and elasticity of c^* to dispersal parameters. If the (i,j)-th element of the matrix of dispersal kernels $\mathbf{K}(z)$, $k_{i,j}(z)$ depends on a dispersal parameter $\alpha_{i,j}$, then the sensitivity of c^* to $\alpha_{i,j}$ is

$$\frac{\partial c^*}{\partial \alpha_{i,j}} = \frac{a_{i,j}}{s^* \rho_1(s^*)} \frac{\partial m_{i,j}}{\partial \alpha_{i,j}}(s^*) \frac{\partial \rho_1}{\partial h_{i,j}}(s^*) \ , \tag{1.32}$$

and the elasticity of c^* to $\alpha_{i,j}$ is given by

$$\frac{\alpha_{i,j}}{c^*} \frac{\partial c^*}{\partial \alpha_{i,j}} = \frac{a_{i,j}\alpha_{i,j}}{\rho_1(s^*) \log\left[\rho_1(s^*)\right]} \frac{\partial \rho_1}{\partial h_{i,j}}(s^*) \ . \tag{1.33}$$

The expressions for sensitivity and elasticity in equations (1.29)-(1.33) are all products of (1) a function of known demographic and dispersal parameters, the moment generating functions of the dispersal kernels, and the principal eigenvalue of $\mathbf{M}(s^*)$; and (2) the derivative of the principal eigenvalue $\rho_1(s^*)$ with respect to the (i,j)-th element of $\mathbf{H}(s^*)$. This derivative can be calculated using the left $\mathbf{v}$ and right $\mathbf{w}$ eigenvectors of $\mathbf{H}(s^*)$ corresponding to $\rho_1(s^*)$ by using the formula

$$\frac{\partial \rho_1}{\partial h_{i,j}}(s^*) = \frac{v_i w_j}{\mathbf{v} \cdot \mathbf{w}} \tag{1.34}$$

where v_i and w_j are the i-th and j-th elements of $\mathbf{v}$ and $\mathbf{w}$ respectively.

The analytical expressions for sensitivity and elasticity of the wave-speed in equa-

tions (1.29)-(1.33) are useful as they allow the parameters and processes that have the greatest effect on spread to be identified. These insights can then be used to inform conservation decisions (e.g. Caplat et al., 2012).

1.5.7 Simulation of IDEs

To predict the dynamics of species invasions in real (heterogeneous) landscapes, IDEs must be simulated numerically. To be suitable for numerical simulation, spatially continuous models such as IDEs must be discretised in space. In particular, the continuous population density function $\mathbf{u}^t(\mathbf{y})$ is approximated by a density vector $\mathbf{v}^t$ with N elements each representing an equal region of space (Powell et al., 1998). A finer discretisation reduces the error of the approximation, but uses more computational resources.

If the IDE is over one-dimensional space, then this is equivalent to dividing the domain into N equal line segments, or into N equal squares if the domain is two-dimensional. How the IDE is simulated depends on how the dispersal kernel varies with space. If the elements of the dispersal kernel matrix $\mathbf{K}(\mathbf{x}-\mathbf{y}, \mathbf{y})$ vary continuously with $\mathbf{y}$, then the integral should be evaluated by standard quadrature. This means multiplying the discretised post-growth phase population $\mathbf{w}^t$ by an $N \times N$ matrix $\mathbf{H}$, with the density vector after the growth phase given by $\mathbf{v}^{t+1} = \mathbf{H}\mathbf{w}^t$. This requires $\mathrm{O}(N^2)$ computational complexity. If, on the other hand, the dispersal kernels do not depend on $\mathbf{y}$ (the matrix of dispersal kernels can be written as $\mathbf{K}(\mathbf{x}-\mathbf{y})$) and Ω is a rectangular domain, then (1) can be written as a convolution of $\mathbf{K}(\mathbf{x})$ and $f\left(\mathbf{u}^t(\mathbf{x}), \mathbf{x}\right)$. The convolution can be computed using fast-Fourier transforms (FFTs), see Andersen (1991), and has $\mathrm{O}(N \log N)$ computational complexity, i.e. floating point operations. However to avoid the effects of wrapping, since FFTs are cyclical, the population distribution must be padded, multiplying its size by four. To simulate population dynamics over a large area with sufficiently high resolution, these methods become extremely computationally expensive. For example, the CEH UK Land Cover Map

2007 (LCM2007) provides maps with over a billion cells, so in a non-stage-structured model, where each point is represented by a 32-bit floating point number, 300 GB of RAM are required to run a simulation. To refine the model to include demographic stage-structure or use larger or higher resolution maps would require even further increases in the CPU-time and RAM.

1.6 Motivation

In the preceding sections, we have outlined the usefulness of modelling species invasions, introduced IDEs as an appropriate framework for modelling invasions, and explored some of the existing approaches used to quantify spread rates and spreading behaviour. While these approaches provide useful techniques for management and risk assessment, there are opportunities to extend these approaches further by developing the analytical theory and developing more efficient algorithms for numerical simulation.

Exact explicit analytical expressions for the asymptotic spreading speed of travelling wave solutions to IDEs exist for homogeneous landscapes (Kot et al., 1996). These analytical expressions are useful in that they help understand qualitative behaviour and dependencies on particular parameters, and provide a less computationally expensive way to study the dynamics of solutions than numerical simulation. For IDEs with spatially heterogeneous growth or dispersal parameters, the analysis is much less straightforward. However, via small parameters implicit within the model, at least in distinguished limits, it is possible to derive analytical approximations to the spreading-speed (e.g. Shigesada et al. (1986); Dewhirst and Lutscher (2009)). By considering other limiting cases of the deterministic models, there is an opportunity to derive further approximations.

Despite the usefulness of analytical approximations, the numerical simulation of spread on landscapes generated from real geographic data (e.g. Kadoya and Washitani, 2012; Pergl et al., 2011) is very useful when analysing specific ecological threats.

However, IDE models are rarely simulated for real species (see Table 1.2), possibly due to the computational requirements of running the models over real landscapes. The simulation of PDE models is well understood and well-developed numerical methods exist to solve them (e.g. Brenner and Scott, 2008). In IDEs, time is discrete, and the stage-structured population distribution $\mathbf{u}^{t+1}(x)$ at time $t+1$ at x is given by a definite integral over the entire landscape. Therefore, only space needs to be discretised for simulation. There is clearly room for better schemes for discretising landscapes and numerically evaluating the integral. Additionally, incorporating real GIS (Geographic Information System) data into an IDE model and simulating the spread of invasive species over a real landscape (e.g. part or all of the UK) would be helpful in predicting species spread. GIS data of habitat types are publicly available from several sources, including United States Geological Survey (USGS) and the European Environment Agency, and (on request from `http://www.ceh.ac.uk/data-request-form?ref_nid=16315&node_title=land cover map 2007`) from the Centre for Ecology & Hydrology. Developing simulation methods to incorporate this type of data into an IDE model would be very useful for incorporating large scale land map data into predictive modelling.

1.7 Thesis Summary

In this thesis, we will address several issues in the modelling of species invasions in heterogeneous landscapes using IDEs. In Chapters 2 and 3, we will use asymptotic analysis to derive approximations to the asymptotic spreading speeds of solutions to integrodifference equations in landscapes with different types of heterogeneity. We consider landscapes with a high degree of fragmentation (Chapter 2) and landscapes which exhibit low variation (Chapter 3). In Chapter 4, we will introduce a novel adaptive algorithm to enable more efficient simulation of IDEs without a significant loss of accuracy, as detailed below.

1.7.1 Sparse Fragmented Landscapes

In Chapter 2, we investigate landscapes comprised of small isolated patches of suitable habitat surrounded by a matrix of less suitable habitat or non-habitat. We represent these landscapes in one spatial dimension by periodic landscapes of alternating good and bad patches, where the dispersal scale is greater than the extent of each good patch and where the ratio of the demographic rates in the good and bad patches is given by a small parameter, denoted ϵ.

We propose an analytical approximation to the wave-speeds of the solutions to IDEs on these landscapes. The approximation is derived for the general case of stage-structured IDEs with exponentially bounded dispersal kernels and no Allee effect. We apply this approximation for the Gaussian and Laplace dispersal kernels and for stage-structured and non-stage-structured populations, and compare the results against numerical simulations. The analytical approximation is found to be accurate for the landscapes considered, and that the type of dispersal kernel affects the relationship between landscape structure, as classified by landscape period and good patch size, and the spreading speed. This indicates that accurately fitting a kernel to data is important in determining the relationship between landscape structure and spreading speed. The approximations developed in this chapter were published in the Journal of Theoretical Biology (Gilbert et al., 2014b).

1.7.2 Landscapes with Low Variation

In Chapter 3, we consider landscapes where the spatial variation in demographic and dispersal parameters from the mean is small. In these landscapes, the spatial scales of environmental variation are arbitrarily large, but the maximum change in environmental parameters is $\mathrm{O}(\epsilon)$, where $\epsilon \ll 1$. The difference between the wave-speeds of populations spreading in a spatially structured periodic landscape and its homogenisation is found to be, in general, proportional to ϵ^2, where ϵ governs the degree of environmental variation. For stochastically generated landscapes we numerically

demonstrate that the error decays faster than ϵ. In both cases, this means that for sufficiently small ϵ, the homogeneous approximation is a suitable approximation for the spreading speed in the heterogeneous model. To deal with the loss of accuracy as ϵ increases, we formulate a second order approximation to the wave-speed for periodic landscapes and compare both approximations against the results of numerical simulation and show that they are both accurate for the range of landscapes considered. We have published the approximations and results in this chapter in the Journal of Theoretical Biology (Gilbert et al., 2014a).

1.7.3 Speeding up Simulation

In Chapter 4, we develop and implement a novel algorithm for the simulation of IDEs using *adaptive mesh refinement* techniques that have been applied to PDEs. We measured the accuracy of the adaptive algorithm, by comparing the results of simulations using the adaptive and a standard non-adaptive algorithm. The relative error of the population's spatial extent was low (< 0.05) for a range of parameter values. Comparing efficiency, the adaptive algorithm used up to ten times less CPU-time and RAM than the non-adaptive algorithm. The adaptive approach provides large improvements in efficiency without significant loss of accuracy, so enables faster simulation of IDEs and simulation at scales and at resolutions that have not been previously feasible. This is useful for running large scale simulations and we provide the example of the simulation of the spread of a hypothetical species over the UK at a resolution of 25m $\times$ 25m. The implementation of the algorithm is provided as a user-friendly executable application. A paper outlining the algorithm has been accepted for publication in Methods in Ecology and Evolution, and an implementation of the algorithm is available from GitHub (Gilbert et al., 2016).

Chapter 2

Sparse Fragmented Landscapes

This chapter is based on the paper *Spreading Speeds for Stage Structured Plant Populations in Sparse Fragmented Landscapes* by Gilbert, White, Bullock and Gaffney, which has been published in the Journal of Theoretical Biology (Gilbert et al., 2014b).

2.1 Introduction

Fragmented habitats (Fahrig, 2003) such as calcareous grassland in Dorset, UK (Hooftman and Bullock, 2012) and woodland in Wisconsin (Curtis, 1956) are often composed of small habitat fragments separated by distances which have sufficient length to make inter-patch dispersal rare. Fragmented landscapes are a specific type of heterogeneous landscape and generally exhibit heterogeneity at larger scales than the scale of dispersal, making the analytical expressions for spreading speed in landscapes that are homogeneous (Kot et al., 1996) or heterogeneous only on small spatial scales (Dewhirst and Lutscher, 2009) inappropriate. Given the usefulness of analytical approximations to invasion speeds, there is a need for analytical approximations of spreading speeds which can incorporate a wide range of dispersal scales and kernels, stage structure and landscape heterogeneity, and are appropriate to fragmented landscapes.

In this chapter, we address this important gap for fragmented landscape, and derive analytical approximations for the asymptotic invasion speeds of stage-structured populations in one-dimensional landscapes where (i) the spatial extent of the suitable habitat patches is smaller than the scale of dispersal and (ii) the matrix of demographic rates in the non habitat matrix habitat patches are much lower than the matrix of demographic rates in the habitat patches (see Figure 2.1b). These approximations are not restricted to particular choices of landscape period, or to particular dispersal kernels and so extend the work of previous studies. They also incorporate the important role of the non-habitat *matrix* (Driscoll et al., 2013; Fahrig, 2001) in determining invasion success/speed. To derive this approximation, we will exploit (i) the difference in scale between dispersal and the spatial extent of the suitable habitat patches to treat the population in each habitat patch as a population at a single point, and (ii) the much smaller growth rate in the non-habitat matrix to find the wave speed in terms of an asymptotic expansion in the ratio of the growth rates. In Section 2.2, we will present the derivation of an approximation to the asymptotic wave-speed of solutions to IDEs satisfying these conditions with compact initial sup-

(a) (b)

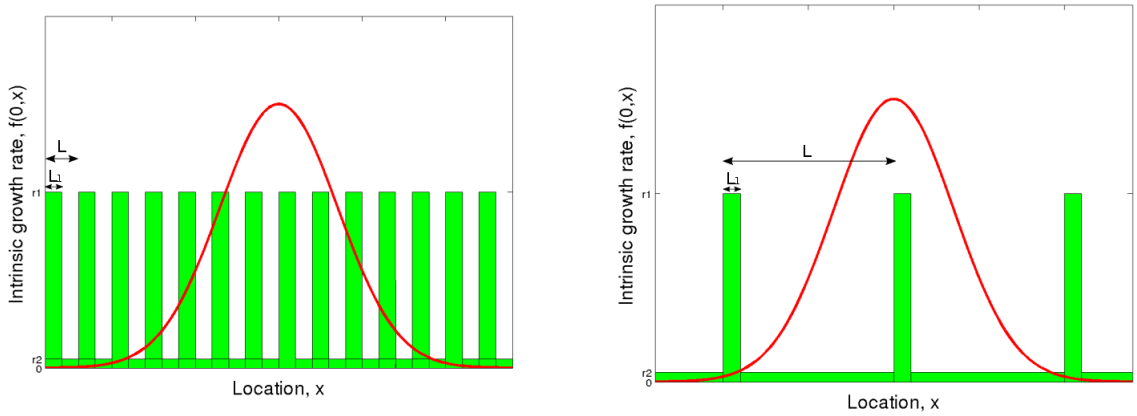

Figure 2.1: Intrinsic growth rates $r(0, x)$ for a non-stage-structured population in two periodic landscapes plotted alongside a dispersal kernel. In both landscapes, the growth rate in the bad patches are much lower than that in the good patches. In (a) the ratio of the landscape period to the mean dispersal distance is small (see Dewhirst and Lutscher (2009)), and in (b), the ratio of the length of the good patches and the mean dispersal distance is small (considered here).

port. In Section 2.3, we will derive particular approximations for IDEs with Gaussian and Laplace dispersal kernels, and will compare the approximations with the results of numerical simulation. The chapter concludes with a discussion of the results in Section 2.4.

2.2 Method

The analysis presented in this chapter is applicable to IDEs of the form (1.10) in one spatial dimension on a bi-infinite landscape, and is applicable to all choices of length and time scale (provided that the scale of dispersal is much larger than the extent of the suitable habitat patches). We consider non-dimensional IDEs (in the sense that scales or units are not given to length, population density or time), as they correspond to the greatest variety of possible ecological scales.

In Sections 2.2.1-2, the IDE model for a fragmented landscape is introduced, in Section 2.2.3, conditions for an analytical approximation of the wave-speed are given, in Sections 2.2.4-7, these conditions are used to derive the wave-speed approximations,

Parameter	**Symbol**	**Range**
Time	t	[1 100]
Spatial Variables	x, y	
Population density at x at t	$\mathbf{u}^t(x)$	
Landscape Period	L	[0.25 10]
Good Patch size	L_1	[0.01 0.2]
Proportion of Good Habitat, $p = L_1/L$	p	[0.001 0.8]
Ratio of Demographic Parameters in Good and Bad Patches	ϵ	0, 0.05, 0.25
Non-stage-structured zero-population growth rate in Good patches	r	10
Gaussian Dispersal Parameter	σ	0.3, 1
Laplace Dispersal Parameter	α	0.3, 1
Wave-number	s	
Wave-speed	$c(s)$	
Principal Eigenvalue of (2.11)	ρ_s	
Approximation to ρ_s using Point-Source Approx.	ρ_s^{app}	
n-th order term in asymptotic expansion of ρ_s^{app} in ϵ	$\rho_{s,n}^{\text{app}}$	
Asymptotic wave-speed	c^*	
Simulated asymptotic wave-speed	c^{sim}	
Analytical approximation of c^*	c^{app}	
Numerical density threshold for invasion	μ	0.0005
(Stage-Structured Example) Birth rate	ϕ	30
(Stage-Structured Example) Juvenile survival Rate	ν	0.8
(Stage-Structured Example) Maturation rate	γ	0.625
(Stage-Structured Example) Adult survival Rate	θ	0.2

Table 2.1: Parameter Table - A table of non-dimensional variables and parameters used in the analytical approximation, its derivation and examples in Chapter 2. These are not species specific, but are chosen to illustrate the range of model behaviours that correspond to the analysis.

and a summary of the approximation is presented in Sections 2.2.8-9.

2.2.1 Heterogeneous Stage-Structured Integrodifference Equations

The general heterogeneous stage-structured IDE in one dimension on a bi-infinite landscape (Neubert and Caswell, 2000) is given by

$$\mathbf{u}^{t+1}(x) = \int_{-\infty}^{\infty} \left[\mathbf{K}(x-y,y) \circ \mathbf{B}(\mathbf{u}^t(y),y)\right] \mathbf{u}^t(y)\mathrm{d}y \tag{2.1}$$

where $\mathbf{u}^t(x)$ is the vector of population densities for each stage at location x and time t. $\mathbf{B}(\mathbf{u}^t(y),y)$ is the *population projection matrix*, and its (i,j)-th entry is the proportion of individuals in stage i transitioning to stage j. $\mathbf{K}(x-y,y)$ is the matrix of dispersal kernels $K_{i,j}(x-y,y)$, where the (i,j)-th entry is the dispersal kernel for individuals which have transitioned from demographic stage i to stage j in the preceding growth phase.

2.2.2 Sparse Periodic kernels and growth functions

Fragmented landscapes can be represented by one-dimensional landscapes in which the real line $\mathbb{R}$ is partitioned into periodically alternating patch types, *good patches* $\mathcal{G}_n = [nL - L_1/2, nL + L_1/2)$ of length L_1, and *bad patches* $\mathcal{B}_n = [nL + L_1/2, nL + L - L_1/2)$ of length $L - L_1$ (see Table 2.1 for a full table of parameters used in this chapter). Hence L is the period of the landscape. The dispersal kernel $\mathbf{K}(x-y,y)$ and the population projection matrix $\mathbf{B}(\mathbf{u}^t(y),y)$ depend on whether y is in a good or bad patch, and do not vary within patches.

We make two assumptions about the landscape scales, dispersal parameters and demographic rates. We assume (i) that the length L_1 of the good patches is much smaller than the scale of the dispersal distances from the good patches (see Condition IV in Subsection 2.2.3), and (ii) that all the demographic rates in the bad patches are

much lower than those in the good patches (see Condition V in Subsection 2.2.3).

Since the species has reduced fecundity in the bad patches (compared to the good patches), the population projection matrices in the good and bad patches are related by a small parameter $\epsilon \ll 1$, and are denoted respectively by $\mathbf{B}^{\mathcal{G}}(\mathbf{u}^t(y))$ and $\epsilon\mathbf{B}^{\mathcal{B}}(\mathbf{u}^t(y))$, where ϵ is chosen such that no element of the linearized population projection matrix $\mathbf{B}^{\mathcal{G}}(\mathbf{0})$ is larger than the corresponding element in $\mathbf{B}^{\mathcal{B}}(\mathbf{0})$. For brevity, the good and bad patch projection matrices are combined to form a spatially and density dependent population projection matrix,

$$\mathbf{B}(\mathbf{u}^t(y), y) = \begin{cases} \mathbf{B}^{\mathcal{G}}(\mathbf{u}^t(y)) & \text{for} \quad y \in \mathcal{G}_j \\ \\ \epsilon\mathbf{B}^{\mathcal{B}}(\mathbf{u}^t(y)) & \text{for} \quad y \in \mathcal{B}_j \end{cases} \qquad j \in \mathbb{Z} \ . \tag{2.2}$$

We also allow dispersal from y to depend on whether y is in $\mathcal{G}_j$ or $\mathcal{B}_j$, and let $\mathbf{K}^{\mathcal{G}}(x-y)$ and $\mathbf{K}^{\mathcal{B}}(x-y)$ be the matrices of dispersal kernels from the good and bad patches, with our spatially dependent matrix of dispersal kernels given by

$$\mathbf{K}(x-y, y) = \begin{cases} \mathbf{K}^{\mathcal{G}}(x-y) & \text{for} \quad y \in \mathcal{G}_j \\ \\ \mathbf{K}^{\mathcal{B}}(x-y) & \text{for} \quad y \in \mathcal{B}_j \end{cases} \qquad j \in \mathbb{Z} \ . \tag{2.3}$$

2.2.3 Conditions

We will explore solutions to (2.1) analytically by linearising the (2.1) about the constant zero population state, discretising the good habitat patches and finding travelling wave solutions to the discretised and linearised equations. Solutions to IDEs corresponding to real populations have initial conditions with compact support. For a solution's asymptotic wave-speed to be determined by its linearisation, we need the spatially dependent demographic matrix $\mathbf{B}(\mathbf{x}, y)$ and matrix of dispersal kernels $\mathbf{K}(x-y, y)$ to satisfy conditions which are typical for IDE wave-speed analysis (Neubert and Caswell, 2000) and are commonly satisfied for population matrix modelling

(Caswell, 2000):

I. The demographic matrix $\mathbf{B}(\mathbf{u}, y)$ is non-negative and irreducible for all $\mathbf{u}$ and y, i.e. the transition rate between every pair of stages is non-negative, and the presence of individuals in any demographic stage will affect the number of individuals in any other stage at some future time.

II. The intrinsic growth rate is greater than one (the zero population state is linearly unstable in the non-spatial model), and at every $y \in \mathbb{R}$ the non-linear population projection matrix $\mathbf{B}(\mathbf{u}, y)$ is bounded elementwise by its linearisation at zero, $\mathbf{A}(y) := \mathbf{B}(\mathbf{0}, y)$,

$$\mathbf{B}(\mathbf{u}, y)\mathbf{u} \leq \mathbf{A}(y)\mathbf{u} \quad \text{for all} \quad \mathbf{u} \geq \mathbf{0} \ .$$

This ensures *linearly determinacy* (Weinberger et al., 2002) (that the asymptotic wave-speed of solutions to a nonlinear IDE are the same as for the solutions of its linearisation). This is satisfied whenever higher populations cause reduced growth rates (through competition for resources, overcrowding, etc), which is true for most species.

III. Each element of the matrices of dispersal kernels from the good patches, $\mathbf{K}^{\mathcal{G}}(z)$ and bad patches, $\mathbf{K}^{\mathcal{B}}(z)$ have moment generating functions, i.e. the dispersal kernels are *exponentially bounded*. This ensures that solutions have a constant wave-speed and do not accelerate (Kot et al., 1996).

For our analysis of the heterogeneous landscape, we require two additional conditions,

IV. For the stage transitions where dispersal occurs, the scale of dispersal is much greater than the length L_1 of the good patches $\mathcal{G}_j$ (see Figure 2.1b). For this we require the $(i,j)^{\text{th}}$ element of the matrix of dispersal kernels from the good patch, $K^{\mathcal{G}}_{i,j}(z)$ to be either

(a) a Dirac delta function $\delta(z)$. No dispersal occurs for individuals transitioning from the i^{th} to the j^{th} demographic stage.

(b) approximately constant over other (neighbouring) good patches, i.e. for landscape period L and good patch length L_1,

$$\mathbf{K}^{\mathcal{G}}(nL+z) \approx \mathbf{K}^{\mathcal{G}}(nL) \quad \text{for} \quad z \in \left[-\frac{L_1}{2}, \frac{L_1}{2}\right] \quad \text{and} \quad n \in \mathbb{Z}\backslash\{0\} \ .$$

For dispersal within the same good patch ($n = 0$), we do not require the dispersal kernel to be approximately constant, and allow the kernel to vary more quickly. For most dispersal kernels, this condition can be expressed as

$$L_1 \ll \sigma$$

where σ is the scale of dispersal. This condition is satisfied by species in habitats where the scale of dispersal is greater than the sizes of the individual habitat patches.

V. The elements of the population projection matrix in the good patches $\mathbf{B}^{\mathcal{G}}(\mathbf{x})$ are much larger than the corresponding elements of the population projection matrix in the bad patches $\epsilon\mathbf{B}^{\mathcal{B}}(\mathbf{x})$, i.e.

$$\mathbf{B}^{\mathcal{G}}(\mathbf{x}) \gg \epsilon\mathbf{B}^{\mathcal{B}}(\mathbf{x})$$

where inequalities are calculated component-wise. Generally, and by definition, the demographic rates of species are much lower in the bad patches than in the good patches.

2.2.4 Method Outline

To find an analytical approximation c^{app} to the asymptotic wavespeed c^* of solutions to (2.1) where $\mathbf{B}$ and $\mathbf{K}$ are respectively the demographic matrix and kernel given by (2.2) and (2.3), and where the solution has compact initial conditions (the initial distribution $\mathbf{u}^0(x)$ has compact support), we first linearise around the zero-population state. Since the zero-steady state is unstable, the population projection matrix is bounded by its linearisation at zero (Condition II) and density dependence is local, the dynamics of the invasion are dominated by the wavefront (van den Bosch et al., 1990; Mollison, 1991). For the mathematical analysis, though not the later simulations, we will assume this *Linear Conjecture*, which has been proved rigorously for a narrower class of problem (Mollison, 1991). This allows us to explore solutions of a simpler, linear IDE, which has solutions with the same wave-speed as (2.1).

We then look for solutions to the linearised IDE which are the product of an L-periodic stage-structured (vector-valued) population distribution and an exponential travelling wave $\exp(s(c(s)t - x))$ (Weinberger, 2002) which propagates with speed $c(s)$, where s is the wave-number, and arbitrary *a priori*. This gives us an eigenvalue equation for $\rho_s := \exp(s\, c(s))$, with the principal eigenvalue corresponding to the physically meaningful solution of the linearised IDE (Neubert and Caswell, 2000).

Given the small demographic rates in the bad patches, we can write the operator in the eigenvalue equation as the sum of an O(1) operator, $F_{s,0}$, and an O(ϵ) operator, $\epsilon F_{s,1}$, i.e.

$$F_s = F_{s,0} + \epsilon F_{s,1} \ . \tag{2.4}$$

This allows us to solve the eigenvalue equation as a perturbation problem. We then approximate the $O(1)$ operator with a more tractable one, $F_{s,0}^{\text{app}}$, by approximating the dispersal from the good patches by dispersal from a point source (we justify this numerically in Subsection 2.3.1). This gives us the eigenvalue problem

$$F_s^{\text{app}}\left[\boldsymbol{\phi}_s^{\text{app}}\right](x) = \rho_s^{\text{app}}\boldsymbol{\phi}_s^{\text{app}}(x) \tag{2.5}$$

where ρ_s^{app} is the principal eigenvalue of the approximated operator F_s^{app}, with corresponding eigenvector $\boldsymbol{\phi}_s^{\text{app}}$. The approximation affects the $O(1)$ operator $F_{s,0}$ but does not affect the $O(\epsilon)$ component $F_{s,1}$, with F_s^{app} given by

$$F_s^{\text{app}} = F_{s,0}^{\text{app}} + \epsilon F_{s,1} \ . \tag{2.6}$$

Finally, we expand ρ_s^{app} and $\boldsymbol{\phi}_s^{\text{app}}(x)$ in terms of the small parameter ϵ and equate the coefficients of ϵ^n $(n = 0, 1, ...)$ in the expansion of (2.5). The expansion of ρ_s^{app} is given by

$$\rho_s^{\text{app}} = \rho_{s,0}^{\text{app}} + \epsilon\, \rho_{s,1}^{\text{app}} + \cdots \ .$$

Our approximation to the wave-speed c^{app} depends only on $\rho_{s,0}^{\text{app}}$ and (where non-zero higher order terms exist) the second non-zero term in the expansion of ρ_s^{app}. i.e.

$$c^{\text{app}} = \begin{cases} \min_{s>0}\left[\frac{1}{s}\log\left(\rho_{s,0}^{\text{app}}\right)\right] & \text{if } \rho_{s,j}^{\text{app}} = 0 \text{ for all } j \neq 0 \\ \min_{s>0}\left[\frac{1}{s}\log\left(\rho_{s,0}^{\text{app}} + \epsilon^n \rho_{s,n}^{\text{app}}\right)\right] & \text{where } n \text{ is the smallest integer s.t. } \rho_{s,n}^{\text{app}} \neq 0 \end{cases} . \tag{2.7}$$

So if $\rho_{s,1}^{\text{app}}$ is non-zero, then our approximation to the wave-speed is given by

$$c^{\text{app}} = \min_{s>0}\left[\frac{1}{s}\log\left(\rho_{s,0}^{\text{app}} + \epsilon\rho_{s,1}^{\text{app}}\right)\right] \ .$$

If the $\mathrm{O}(\epsilon)$ terms cancel to make $\rho_{s,1}^{\text{app}} = 0$, then we use the $\mathrm{O}(\epsilon^2)$ term and take

$$c^{\text{app}} = \min_{s>0}\left[\frac{1}{s}\log\left(\rho_{s,0}^{\text{app}} + \epsilon^2\rho_{s,2}^{\text{app}}\right)\right] \ .$$

If the $O(\epsilon^2)$ terms also cancel and $\rho_{s,2}^{\text{app}} = 0$, we go to even higher order terms, and if all higher order terms are trivial, we take $c^{\text{app}} = \min_{s>0}\left[\frac{1}{s}\log\left(\rho_{s,0}^{\text{app}}\right)\right]$.

2.2.5 Linear Conjecture

Following Neubert and Caswell (2000), we assume that Condition II (Subsection 2.2.3) is sufficient to guarantee that the wave-speeds of solutions to stage-structured IDEs propagating into an unstable zero population state are determined by their linearisation around the zero population state (the wave-speed is linearly determined), and that these conditions extend to periodic stage-structured IDEs.

Weinberger (2002) and Lui (1989) rigorously proved linear determinacy for non-stage-structured periodic IDEs and multi-species co-operative homogeneous IDEs (mathematically, this includes single-species stage-structured IDEs) under the conditions in Subsection 2.2.3, together with the condition that the IDE is order-preserving, which is guaranteed when the population projection matrix or growth function is order preserving, i.e. for stage-structured populations

$$\mathbf{u}(x) \geq \mathbf{v}(x) \implies \mathbf{B}(\mathbf{u}(x), x)\mathbf{u}(x) \geq \mathbf{B}(\mathbf{v}(x), x)\mathbf{v}(x)$$

where the inequalities are calculated component-wise.

No rigorous analytical result exists for stage-structured periodic IDEs and we assume that Condition II is sufficient to guarantee linear determinacy. The linearisation of (2.1) about $\mathbf{0}$ is

$$\mathbf{u}^{t+1}(x) = \int_{-\infty}^{\infty} \left[\mathbf{K}(x-y, y) \circ \mathbf{A}(y)\right] \mathbf{u}^t(y)\mathrm{d}y \tag{2.8}$$

where the L-periodic linearised population projection matrix $\mathbf{A}(y)$ is $\mathbf{B}(\mathbf{u}^t(y), y)$ evaluated at the zero population state. This has solutions of the form

$$\mathrm{e}^{s(c(s)t-x)}\boldsymbol{\phi}_s(x) \ , \tag{2.9}$$

where $\boldsymbol{\phi}_s(x)$ is L-periodic (Weinberger, 2002). Solutions to (2.8) with compact initial conditions are bounded above by a multiple of a solution of the form (2.9) for every $s > 0$. Furthermore, since the wavefronts of solutions to (2.1) decay exponentially as $t \to \infty$, the asymptotic invasion speed of solutions to (2.8) with compact initial conditions must attain one of the wavespeeds of these solutions. Therefore, this wavespeed is the minimum of the wavespeeds of the solutions of form (2.9), and we have

$$c^* = \min_{s>0} c(s) \ .$$

Substituting (2.9) into (2.8), we have that for $s > 0$,

$$\mathrm{e}^{s\,c(s)}\boldsymbol{\phi}_s(x) = \int_{-\infty}^{\infty} [\mathbf{K}(x-y,y) \circ \mathbf{A}(y)]\, \mathrm{e}^{s(x-y)}\boldsymbol{\phi}_s(y)\mathrm{d}y \tag{2.10}$$

for some L-periodic function $\boldsymbol{\phi}_s(y)$. For each s, this is an eigenvalue problem, with the principal eigenfunction $\boldsymbol{\phi}_s(x)$ and eigenvalue $\rho_s := \mathrm{e}^{s\,c(s)}$ corresponding to the physical solution (Neubert and Caswell, 2000).

Since $\boldsymbol{\phi}_s(y)$, $\mathbf{K}(z,y)$ and $\mathbf{A}(y)$ are L-periodic in y, we will write (2.10) as

$$\rho_s\boldsymbol{\phi}_s(x) = \sum_{n\in\mathbb{Z}} \int_0^L [\mathbf{K}(x-y-nL,y) \circ \mathbf{A}(y)]\, \mathrm{e}^{s(x-y-nL)}\boldsymbol{\phi}_s(y)\mathrm{d}y \ . \tag{2.11}$$

2.2.6 Asymptotic Expansion in ϵ

We now use Conditions IV and V to find an analytic expansion for ρ_s, by (i) formulating the integral operator in (2.11) as the sum of an $O(1)$ and $O(\epsilon)$ operator, (ii) approximating the unperturbed operator with an analytically tractable one, and (iii) finding asymptotic expansions for the eigenvalues and eigenvectors of the approximation to the operator.

In Subsection 2.2.2, we chose $\mathbf{B}$ such that its linearisation on $[-L_1/2, L - L_1/2)$ can be written as

$$\mathbf{A}(y) = \mathbf{A}^{\mathcal{G}}\mathcal{I}_{\left[\frac{-L_1}{2},\frac{L_1}{2}\right)}(y) + \epsilon\mathbf{A}^{\mathcal{B}}\mathcal{I}_{\left[\frac{L_1}{2},L-\frac{L_1}{2}\right)}(y)$$

where $\mathbf{A}^{\mathcal{G}} = \mathbf{B}^{\mathcal{G}}(\mathbf{0})$ and $\mathbf{A}^{\mathcal{B}} = \mathbf{B}^{\mathcal{B}}(\mathbf{0})$. This allows us to write (2.11) as

$$\begin{aligned}\rho_s\boldsymbol{\phi}_s(x) =& \sum_{n\in\mathbb{Z}}\left(\int_{\frac{-L_1}{2}}^{\frac{L_1}{2}}\left[\mathbf{K}^{\mathcal{G}}(x-y-nL)\circ\mathbf{A}^{\mathcal{G}}\right]\mathrm{e}^{s(x-y-nL)}\boldsymbol{\phi}_s(y)\mathrm{d}y\right.\\ &\left.+\epsilon\int_{\frac{L_1}{2}}^{L-\frac{L_1}{2}}\left[\mathbf{K}^{\mathcal{B}}(x-y-nL)\circ\mathbf{A}^{\mathcal{B}}\right]\mathrm{e}^{s(x-y-nL)}\boldsymbol{\phi}_s(y)\mathrm{d}y\right)\\ =&(F_{s,0}\,\boldsymbol{\phi}_s\,)(x)+\epsilon\,(F_{s,1}\,\boldsymbol{\phi}_s\,)(x)\ .\end{aligned}$$

To find the approximate value of ρ_s, we will use a more analytically tractable operator $F_{s,0}^{\text{app}}$ to approximate the operator $F_{s,0}$

$$(F_{s,0}\mathbf{u}\,)(x) = \sum_{n\in\mathbb{Z}}\int_{\frac{-L_1}{2}}^{\frac{L_1}{2}}\left[\mathbf{K}^{\mathcal{G}}(x-y-nL)\circ\mathbf{A}^{\mathcal{G}}\right]\mathrm{e}^{s(x-y-nL)}\mathbf{u}(y)\mathrm{d}y\ . \tag{2.12}$$

By Condition IV in Subsection 2.2.3 we have that the dispersal kernel $K_{i,j}^{\mathcal{G}}(x)$ for individuals transitioning from stage j to stage i is either (i) a Dirac delta function (individuals going from stage j to stage i do not disperse), or (ii) an exponentially bounded (Condition III) dispersal kernel, such that for $|x| > L_1/2$ and $y \in \left[\frac{-L_1}{2},\frac{L_1}{2}\right)$ we have that $K_{i,j}^{\mathcal{G}}(x-y) \approx K_{i,j}^{\mathcal{G}}(x)$. This means that the integrand of each integral in the sum corresponding to dispersal between a good patch and a bad patch or a different good patch ($n \neq 0$ or $|x| > L_1/2$) in (2.12) is approximately constant over $y \in \left[\frac{-L_1}{2},\frac{L_1}{2}\right]$. The terms corresponding to dispersal between a good patch and a bad patch or a different good patch ($n \neq 0$ or $n = 0$ but $|x| > L_1/2$), can therefore be approximated by taking the Taylor expansion of

$$\left[\mathbf{K}^{\mathcal{G}}(x-y-nL)\circ\mathbf{A}^{\mathcal{G}}\right]\mathrm{e}^{s(x-y-nL)}\mathbf{u}(y) \tag{2.13}$$

in y and taking the limit $L_1 \to 0$. For each of the terms in the summation in (2.12) where $n \neq 0$ or where $n = 0$ but $|x| > L_1/2$, we have

$$\begin{aligned}
&\lim_{L_1\to 0}\int_{-L_1/2}^{L_1/2}\left[\mathbf{K}^{\mathcal{G}}(x-y-nL)\circ\mathbf{A}^{\mathcal{G}}\right]\mathrm{e}^{s(x-y-nL)}\mathbf{u}(y)\mathrm{d}y\\
&\qquad=\lim_{L_1\to 0}\int_{-L_1/2}^{L_1/2}\left[\left(\mathbf{K}^{\mathcal{G}}(x-nL)+y\mathbf{J}(x,y)\right)\circ\mathbf{A}^{\mathcal{G}}\right]\left(\mathrm{e}^{s(x-nL)}+y\,f(x,y)\right)\left(\mathbf{u}(0)+y\mathbf{w}(y)\right)\mathrm{d}y\\
&\qquad=\lim_{L_1\to 0}\int_{-L_1/2}^{L_1/2}\left[\mathbf{K}^{\mathcal{G}}(x-nL)\circ\mathbf{A}^{\mathcal{G}}\right]\mathrm{e}^{s(x-nL)}\mathbf{u}(0)+y\mathbf{w}'(x,y)\mathrm{d}y\\
&\qquad=\lim_{L_1\to 0}\left\{\int_{-L_1/2}^{L_1/2}\left[\mathbf{K}^{\mathcal{G}}(x-nL)\circ\mathbf{A}^{\mathcal{G}}\right]\mathrm{e}^{s(x-nL)}\mathbf{u}(0)\mathrm{d}y+\mathrm{O}\left(L_1^2\right)\right\}\\
&\qquad=L_1\,\left[\mathbf{K}^{\mathcal{G}}(x-nL)\circ\mathbf{A}^{\mathcal{G}}\right]\mathrm{e}^{s(x-nL)}\mathbf{u}(0)\ .
\end{aligned}$$

Using the $L_1\to 0$ approximation, we have

$$\int_{\frac{-L_1}{2}}^{\frac{L_1}{2}}\left[\mathbf{K}^{\mathcal{G}}(x-y-nL)\circ\mathbf{A}^{\mathcal{G}}\right]\mathrm{e}^{s(x-y-nL)}\mathbf{u}(y)\mathrm{d}y\approx L_1\left[\mathbf{K}^{\mathcal{G}}(x-nL)\circ\mathbf{A}^{\mathcal{G}}\right]\mathrm{e}^{s(x-nL)}\mathbf{u}(0)\ ,$$

where higher order terms, of $\mathrm{O}(L_1^2)$ or higher, are ignored.

On the other hand, when $n=0$ and $|x|\le L_1/2$ (i.e. $|x|,|y|\le L_1/2$) we find that for the $n=0$ term, the integrand varies more quickly. To approximate this integral, we consider the volume of propagules remaining in their original good patch (having dispersed from some point y in the patch). This quantity shows little sensitivity to the location of x in the good patch (as L_1 is small compared to the scale of dispersal), and is equal to the integral of $K_{i,j}^{\mathcal{G}}(x-y)$ over $y\in\left[\frac{-L_1}{2},\frac{L_1}{2}\right]$. Due to this lack of sensitivity to x, we take the first term in the Taylor expansion of (2.13) in x around $x=0$ in the limit $L_1\to 0$,

$$\lim_{L_1\to 0}\int_{\frac{-L_1}{2}}^{\frac{L_1}{2}}\left[\mathbf{K}^{\mathcal{G}}(x-y)\circ\mathbf{A}^{\mathcal{G}}\right]\mathrm{e}^{s(x-y)}\mathbf{u}(y)\mathrm{d}y$$

$$= \lim_{L_1\to 0}\int_{\frac{-L_1}{2}}^{\frac{L_1}{2}}\left[\left(\mathbf{K}^{\mathcal{G}}(-y)+x\mathbf{J}(x,y)\right)\circ\mathbf{A}^{\mathcal{G}}\right]\left(\mathrm{e}^{-sy}+x\,f(x,y)\right)\,\mathbf{u}(y)\mathrm{d}y$$

$$= \lim_{L_1\to 0}\left\{\int_{\frac{-L_1}{2}}^{\frac{L_1}{2}}\left[\mathbf{K}^{\mathcal{G}}(y)\circ\mathbf{A}^{\mathcal{G}}\right]\mathrm{e}^{sy}\mathbf{u}(y)\mathrm{d}y + x\int_{\frac{-L_1}{2}}^{\frac{L_1}{2}}\mathbf{w}(x,y)\mathrm{d}y\right\}\ .$$

Given that $|x|, |y| \leq L_1/2$, the first and leading order term inside the limit is $\mathrm{O}(L_1)$, while the second term is $\mathrm{O}(L_1)$, and can be ignored,

$$\lim_{L_1\to 0}\int_{\frac{-L_1}{2}}^{\frac{L_1}{2}}\left[\mathbf{K}^{\mathcal{G}}(x-y)\circ\mathbf{A}^{\mathcal{G}}\right]\mathrm{e}^{s(x-y)}\mathbf{u}(y)\mathrm{d}y = \lim_{L_1\to 0}\int_{\frac{-L_1}{2}}^{\frac{L_1}{2}}\left[\mathbf{K}^{\mathcal{G}}(y)\circ\mathbf{A}^{\mathcal{G}}\right]\mathrm{e}^{sy}\mathbf{u}(y)\mathrm{d}y\ ,$$

with terms of $\mathrm{O}(L_1^2)$ and higher ignored. Additionally, we expect that for stable periodic travelling wave solutions to the IDE, the dispersal kernel $\mathbf{K}^{\mathcal{G}}(y)$ will vary more rapidly for $|y| < L_1/2$ than the population distribution $\mathbf{u}(y)$ or the exponential function e^{sy}. Thus, in the limit $L_1 \to 0$, we can approximate $\mathrm{e}^{sy}\,\mathbf{u}(y)$ by the constant function $\mathbf{u}(0)$,

$$\lim_{L_1\to 0}\int_{\frac{-L_1}{2}}^{\frac{L_1}{2}}\left[\mathbf{K}^{\mathcal{G}}(x-y)\circ\mathbf{A}^{\mathcal{G}}\right]\mathrm{e}^{s(x-y)}\mathbf{u}(y)\mathrm{d}y = \lim_{L_1\to 0}\int_{\frac{-L_1}{2}}^{\frac{L_1}{2}}\left[\mathbf{K}^{\mathcal{G}}(y)\circ\mathbf{A}^{\mathcal{G}}\right]\,\mathbf{u}(0)\mathrm{d}y\ .$$

Therefore, the discretised kernel, $\hat{K}^{\mathcal{G}}_{i,j}(nL)$ is either (i) the Kroenecker delta function (corresponding to the integrals of the Dirac delta functions), or (ii) an approximate integral of $K^{\mathcal{G}}_{i,j}(z)$ over the interval $\left[x-nL-\frac{L_1}{2}, x-nL+\frac{L_1}{2}\right]$,

$$\hat{K}^{\mathcal{G}}_{i,j}(x-nL) = \begin{cases} \int_{-L_1/2}^{L_1/2} K^{\mathcal{G}}_{i,j}(y)\mathrm{d}y & \text{for } n=x=0 \\ \\ L_1 K^{\mathcal{G}}_{i,j}(x-nL) & \text{otherwise} \end{cases}$$

and $F_{s,0}$ can be approximated by the operator $F_{s,0}^{\text{app}}$

$$F_{s,0}^{\text{app}}\mathbf{u}(x) = \sum_{n\in\mathbb{Z}} \left[\mathbf{K}_{\text{app}}^{\mathcal{G}}(x-nL) \circ \mathbf{A}^{\mathcal{G}}\right] \mathrm{e}^{s(x-nL)}\mathbf{u}(0) \ , \tag{2.14}$$

where $\mathbf{K}_{\text{app}}^{\mathcal{G}}(z) = \left(\hat{K}_{i,j}^{\mathcal{G}}(z)\right)_{i,j=1}^{N}$. This is the Point-Source approximation, which we justify numerically in Subsection 2.3.1. We expect the principal eigenvalue ρ_s^{app} to be a good approximation to ρ_s and that

$$\min_{s>0}\left[\frac{1}{s}\log\left(\rho_s^{\text{app}}\right)\right] \approx \min_{t>0}\left[\frac{1}{t}\log\left(\rho_t\right)\right] \ .$$

The problem now is to find the principal eigenvalue ρ_s^{app} of $F_s^{\text{app}} = F_{s,0}^{\text{app}} + \epsilon F_{s,1}$ for each $s > 0$. To do this, we expand the principal eigenvalue, ρ_s^{app}, and eigenfunction, $\boldsymbol{\phi}_s^{\text{app}}(x)$, of F_s^{app},

$$\begin{aligned}
\rho_s^{\text{app}} &= \rho_{s,0}^{\text{app}} + \epsilon\,\rho_{s,1}^{\text{app}} + \epsilon^2\,\rho_{s,2}^{\text{app}} + \cdots \\
\boldsymbol{\phi}_s^{\text{app}}(x) &= \boldsymbol{\phi}_{s,0}^{\text{app}}(x) + \epsilon\,\boldsymbol{\phi}_{s,1}^{\text{app}}(x) + \epsilon^2\,\boldsymbol{\phi}_{s,2}^{\text{app}}(x) + \cdots \ .
\end{aligned}$$

At O(1), we have that $\rho_{s,0}^{\text{app}}$ and $\boldsymbol{\phi}_{s,0}^{\text{app}}$ are the principal eigenvalue and eigenvector, respectively of the unperturbed problem

$$F_{s,0}^{\text{app}}\,\boldsymbol{\phi}_{s,0}^{\text{app}} = \rho_{s,0}^{\text{app}}\boldsymbol{\phi}_{s,0}^{\text{app}}$$

and at $\mathrm{O}(\epsilon^n)$ (for $n \geq 1$), we have

$$F_{s,0}^{\text{app}}\,\boldsymbol{\phi}_{s,n}^{\text{app}} + F_{s,1}\,\boldsymbol{\phi}_{s,n-1}^{\text{app}} - \sum_{j=0}^{n}\rho_{s,j}^{\text{app}}\boldsymbol{\phi}_{s,n-j}^{\text{app}} = 0 \ . \tag{2.15}$$

2.2.7 Properties of $F_{s,0}^{\text{app}}$

Evaluating $(F_{s,0}^{\text{app}}\boldsymbol{\phi}_{s,0}^{\text{app}})(x)$ at $x = 0$ we have that

$$(F_{s,0}^{\text{app}}\boldsymbol{\phi}_{s,0}^{\text{app}})(0) = \sum_{n\in\mathbb{Z}} \left[\mathbf{K}_{\text{app}}^{\mathcal{G}}(nL) \circ \mathbf{A}^{\mathcal{G}}\right] \mathrm{e}^{snL} \boldsymbol{\phi}_{s,0}^{\text{app}}(0)$$

and that the principal eigenvalue $\rho_{s,0}^{\text{app}}$ of $F_{s,0}^{\text{app}}$ is the principal eigenvalue of

$$\sum_{n\in\mathbb{Z}} \left[\mathbf{K}_{\text{app}}^{\mathcal{G}}(nL) \circ \mathbf{A}^{\mathcal{G}}\right] \mathrm{e}^{snL} \quad , \tag{2.16}$$

with the corresponding eigenfunction given by

$$\boldsymbol{\phi}_{s,0}^{\text{app}}(x) = \sum_{n\in\mathbb{Z}} \left[\mathbf{K}_{\text{app}}^{\mathcal{G}}(x - nL) \circ \mathbf{A}^{\mathcal{G}}\right] \mathrm{e}^{s(x-nL)} \boldsymbol{\psi} \tag{2.17}$$

where $\boldsymbol{\psi}$ is the principal eigenvector of (2.16). In order to find $\rho_{s,1}^{\text{app}}$ from (2.15), we will need to consider the adjoint operator $F_{s,0}^{\text{app}*}$ of $F_{s,0}^{\text{app}}$ in the inner product space $L^2\left(\left[\frac{-L_1}{2}, L - \frac{L_1}{2}\right)\right)$, where the inner product is given by

$$\langle \mathbf{u} | \mathbf{v} \rangle = \frac{1}{L} \int_{-L_1/2}^{L-L_1/2} \left[\mathbf{u}(x) \cdot \mathbf{v}(x)\right] \mathrm{d}x \quad .$$

To calculate the adjoint operator $F_{s,0}^{\text{app}*}$, we rearrange the expression for $F_{s,0}^{\text{app}}$ in (2.14) in terms of an integral in an additional variable y and the Dirac delta function $\delta(y)$,

$$\left(F_{s,0}^{\text{app}}\,\mathbf{u}\right)(x) = \sum_{n\in\mathbb{Z}} \left[\mathbf{K}_{\text{app}}^{\mathcal{G}}(x - nL) \circ \mathbf{A}^{\mathcal{G}}\right] \mathrm{e}^{s(x-nL)} \int_{-L_1/2}^{L-L_1/2} \delta(y)\, \mathbf{u}(y) \mathrm{d}y \quad ,$$

and take the inner product of $\left(F_{s,0}^{\text{app}}\,\mathbf{u}\right)(x)$ with an arbitrary member $\mathbf{v}(x)$ of the adjoint space,

$$
\begin{aligned}
&\left\langle \mathbf{v} | F_{s,0}^{\mathrm{app}}\, \mathbf{u} \right\rangle \\
&\quad = \frac{1}{L} \int_{-L_1/2}^{L-L_1/2} \mathbf{v}(x) \cdot \left(\sum_{n\in\mathbb{Z}} \left[\mathbf{K}_{\mathrm{app}}^{\mathcal{G}}(x-nL) \circ \mathbf{A}^{\mathcal{G}} \right] \mathrm{e}^{s(x-nL)} \int_{-L_1/2}^{L-L_1/2} \delta(y)\, \mathbf{u}(y) \mathrm{d}y \right) \mathrm{d}x \\
&\quad = \frac{1}{L} \int_{-L_1/2}^{L-L_1/2} \delta(y) \int_{-L_1/2}^{L-L_1/2} \left(\sum_{n\in\mathbb{Z}} \left[\mathbf{K}_{\mathrm{app}}^{\mathcal{G}}(x-nL) \circ \mathbf{A}^{\mathcal{G}} \right]^{\mathrm{T}} \mathrm{e}^{s(x-nL)} \right) \mathbf{v}(x) \mathrm{d}x \cdot \mathbf{u}(y) \mathrm{d}y \\
&\quad = \left\langle F_{s,0}^{\mathrm{app}*}\, \mathbf{v} | \mathbf{u} \right\rangle \ .
\end{aligned}
$$

Thus the adjoint operator $F_{s,0}^{\mathrm{app}*}$ of $F_{s,0}^{\mathrm{app}}$ is given by

$$
(F_{s,0}^{\mathrm{app}*}\mathbf{u})(x) = \delta(x) \sum_{n\in\mathbb{Z}} \int_{\frac{-L_1}{2}}^{L-\frac{L_1}{2}} \left[\mathbf{K}_{\mathrm{app}}^{\mathcal{G}}(y-nL) \circ \mathbf{A}^{\mathcal{G}} \right]^{\mathrm{T}} \mathrm{e}^{s(y-nL)} \mathbf{u}(y) \mathrm{d}y \ .
$$

Putting $\mathbf{u}(x) = \delta(x)\mathbf{v}(x)$, we find that

$$
(F_{s,0}^{\mathrm{app}*}\mathbf{u})(x) = \left(\sum_{n\in\mathbb{Z}} \left[\mathbf{K}_{\mathrm{app}}^{\mathcal{G}}(nL) \circ \mathbf{A}^{\mathcal{G}} \right]^{\mathrm{T}} \mathrm{e}^{snL} \right) \delta(x)\mathbf{v}(x)
$$

and that the principal eigenvalue of $F_{s,0}^{\mathrm{app}*}$ is the principal eigenvalue of the transpose of (2.16), which is ρ_s^{app}. The corresponding eigenfunction is

$$
\tilde{\boldsymbol{\phi}}_{s,0}^{\mathrm{app}}(x) = \delta(x)\tilde{\boldsymbol{\psi}} \tag{2.18}
$$

where $\tilde{\boldsymbol{\psi}}$ is the principal eigenvector of the transpose of (2.16). We can now reconsider (2.15)

$$
(F_{s,0}^{\mathrm{app}} - \rho_{s,0}^{\mathrm{app}})\, \boldsymbol{\phi}_{s,n}^{\mathrm{app}} + F_{s,1}\, \boldsymbol{\phi}_{s,n-1}^{\mathrm{app}} - \sum_{j=1}^{n} \rho_{s,j}^{\mathrm{app}} \boldsymbol{\phi}_{s,n-j}^{\mathrm{app}} = 0 \tag{2.19}
$$

which defines $\boldsymbol{\phi}_{s,n}^{\mathrm{app}}$ and $\rho_{s,n}^{\mathrm{app}}$ in terms of lower order terms. We find $\rho_{s,n}^{\mathrm{app}}$ by taking its inner product with $\tilde{\boldsymbol{\phi}}_{s,0}^{\mathrm{app}}$

$$\langle \tilde{\boldsymbol{\phi}}_{s,0}^{\text{app}} | (F_{s,0}^{\text{app}} - \rho_{s,0}^{\text{app}}) \boldsymbol{\phi}_{s,n}^{\text{app}} \rangle + \langle \tilde{\boldsymbol{\phi}}_{s,0}^{\text{app}} | F_{s,1} \boldsymbol{\phi}_{s,n-1}^{\text{app}} \rangle - \sum_{j=1}^{n} \rho_{s,j}^{\text{app}} \langle \tilde{\boldsymbol{\phi}}_{s,0}^{\text{app}} | \boldsymbol{\phi}_{s,n-j}^{\text{app}} \rangle = 0 \ . \quad (2.20)$$

By the properties of the inner product and the adjoint operator $F_{s,0}^{\text{app}*}$

$$\langle \tilde{\boldsymbol{\phi}}_{s,0}^{\text{app}} | (F_{s,0}^{\text{app}} - \rho_{s,0}^{\text{app}}) \boldsymbol{\phi}_{s,1}^{\text{app}} \rangle = \langle (F_{s,0}^{\text{app}*} - \rho_{s,0}^{\text{app}}) \tilde{\boldsymbol{\phi}}_{s,0}^{\text{app}} | \boldsymbol{\phi}_{s,1}^{\text{app}} \rangle = 0 \ .$$

Substituting this into (2.20) and rearranging, we have an expression for $\rho_{s,n}^{\text{app}}$ in terms of lower order terms in the asymptotic expansions of ρ_s^{app} and $\boldsymbol{\phi}_s^{\text{app}}$,

$$\begin{aligned} \rho_{s,1}^{\text{app}} &= \frac{\langle \tilde{\boldsymbol{\phi}}_{s,0}^{\text{app}} | F_{s,1} \boldsymbol{\phi}_{s,0}^{\text{app}} \rangle}{\langle \tilde{\boldsymbol{\phi}}_{s,0}^{\text{app}} | \boldsymbol{\phi}_{s,0}^{\text{app}} \rangle} \\ \rho_{s,n}^{\text{app}} &= \frac{\langle \tilde{\boldsymbol{\phi}}_{s,0}^{\text{app}} | F_{s,1} \boldsymbol{\phi}_{s,n-1}^{\text{app}} \rangle - \sum_{j=1}^{n-1} \rho_{s,j}^{\text{app}} \langle \tilde{\boldsymbol{\phi}}_{s,0}^{\text{app}} | \boldsymbol{\phi}_{s,n-j}^{\text{app}} \rangle}{\langle \tilde{\boldsymbol{\phi}}_{s,0}^{\text{app}} | \boldsymbol{\phi}_{s,0}^{\text{app}} \rangle} \qquad \text{for } n > 1 \ . \end{aligned} \quad (2.21)$$

For $\boldsymbol{\phi}_{s,n}^{\text{app}}$, we must solve (2.19). Since $F_{s,0}^{\text{app}} - \rho_{s,0}^{\text{app}}$ has a non-trivial null-space, we are free to choose $\boldsymbol{\phi}_{s,n}^{\text{app}}$ such that

$$\langle \tilde{\boldsymbol{\phi}}_{s,0}^{\text{app}} | \boldsymbol{\phi}_{s,n}^{\text{app}} \rangle = 0 \ .$$

Combining this projection constraint with (2.21), we have that

$$\rho_{s,n}^{\text{app}} = \frac{\langle \tilde{\boldsymbol{\phi}}_{s,0}^{\text{app}} | F_{s,1} \boldsymbol{\phi}_{s,n-1}^{\text{app}} \rangle}{\langle \tilde{\boldsymbol{\phi}}_{s,0}^{\text{app}} | \boldsymbol{\phi}_{s,0}^{\text{app}} \rangle} \qquad \text{for } n \geq 1 \ . \quad (2.22)$$

For $\rho_{s,1}^{\text{app}}$, we use the definitions of $\boldsymbol{\phi}_{s,0}^{\text{app}}$ and $\tilde{\boldsymbol{\phi}}_{s,0}^{\text{app}}$ from (2.17) and (2.18), to give us an expression for the numerator and denominator in (2.22) in terms of $\mathbf{K}$ and $\mathbf{B}$,

$$\langle \tilde{\boldsymbol{\phi}}_{s,0}^{\text{app}} | F_{s,1} \boldsymbol{\phi}_{s,0}^{\text{app}} \rangle = \tilde{\boldsymbol{\psi}} \cdot \left[\sum_{m,n \in \mathbb{Z}} \int_{\frac{L_1}{2}}^{L-\frac{L_1}{2}} \left(\mathbf{K}^{\mathcal{B}}(nL - y, y) \circ \mathbf{A}^{\mathcal{B}}(y) \right) \right.$$
$$\left. \cdot \left(\mathbf{K}_{\text{app}}^{\mathcal{G}}(mL + y) \circ \mathbf{A}^{\mathcal{G}} \right) \mathrm{e}^{s(n+m)L} \mathrm{d}y \right] \boldsymbol{\psi} \tag{2.23}$$

$$\langle \tilde{\boldsymbol{\phi}}_{s,0}^{\text{app}} | \boldsymbol{\phi}_{s,0}^{\text{app}} \rangle = \tilde{\boldsymbol{\psi}} \cdot \left[\sum_{n \in \mathbb{Z}} \left(\mathbf{K}_{\text{app}}^{\mathcal{G}}(nL) \circ \mathbf{A}^{\mathcal{G}} \right) \mathrm{e}^{snL} \right] \boldsymbol{\psi} \tag{2.24}$$
$$= \rho_{s,0}^{\text{app}} \tilde{\boldsymbol{\psi}} \cdot \boldsymbol{\psi} \ .$$

Substituting these into (2.22) gives us $\rho_{s,1}^{\text{app}}$.

2.2.8 The Approximation

We have found (Subsection 2.2.7) that the first term $\rho_{s,0}^{\text{app}}$ in the expansion of ρ_s^{app} is the principal eigenvalue of

$$\mathbf{M}_0(s) = \sum_{n \in \mathbb{Z}} \left[\mathbf{K}_{\text{app}}^{\mathcal{G}}(nL) \circ \mathbf{A}^{\mathcal{G}} \right] \mathrm{e}^{snL} \ , \tag{2.25}$$

where $\mathbf{K}_{\text{app}}^{\mathcal{G}}(nL)$ is a discretisation of the dispersal kernel of propagules from the good patches given by

$$\mathbf{K}_{\text{app}}^{\mathcal{G}}(x - nL) = \begin{cases} \int_{-L_1/2}^{L_1/2} \mathbf{K}_{\text{app}}^{\mathcal{G}}(y) \mathrm{d}y & \text{for } n = x = 0 \\ L_1 \mathbf{K}_{\text{app}}^{\mathcal{G}}(x - nL) & \text{otherwise} \end{cases} \tag{2.26}$$

and where $\mathbf{A}^{\mathcal{G}}$ is the linear population projection matrix in the good patches (i.e. $\mathbf{B}^{\mathcal{G}}(\mathbf{u}^t(x))$ at the zero-population state).

The second term $\rho_{s,1}^{\text{app}}$ in the expansion of ρ_s^{app} is given by substituting (2.23) and (2.24) into (2.22),

$$\rho_{s,1}^{\text{app}} = \frac{\tilde{\boldsymbol{\psi}} \cdot [\mathbf{M}_1(s) \boldsymbol{\psi}]}{\rho_{s,0}^{\text{app}} \tilde{\boldsymbol{\psi}} \cdot \boldsymbol{\psi}} \tag{2.27}$$

where $\boldsymbol{\psi}$ and $\tilde{\boldsymbol{\psi}}$ are the principal eigenvectors of (2.25) and its transpose, where $\mathbf{M}_1(s)$ is given by

$$\mathbf{M}_1(s) = \left[\sum_{m,n\in\mathbb{Z}} \int_{\frac{L_1}{2}}^{L-\frac{L_1}{2}} \left(\mathbf{K}^{\mathcal{B}}(nL-y) \circ \mathbf{A}^{\mathcal{B}}(y) \right) \left(\mathbf{K}^{\mathcal{G}}_{\text{app}}(mL+y) \circ \mathbf{A}^{\mathcal{G}} \right) \mathrm{e}^{s(n+m)L} \mathrm{d}y \right]$$

and where $\mathbf{A}^{\mathcal{B}}$ is the linear population projection matrix in the bad patches.

Therefore, using the definition of c^{app} in (2.7), the asymptotic wavespeed of the solution to (2.1) can be approximated by

$$c^{\text{app}} = \min_{s>0} \left[\frac{1}{s} \log \left(\rho^{\text{app}}_{s,0} + \epsilon \rho^{\text{app}}_{s,1} \right) \right] \quad . \tag{2.28}$$

This is the spatially heterogeneous equivalent to the expression for the asymptotic wave-speed of solutions to the spatially homogeneous IDE (1.15).

2.2.9 Inhospitable Bad Patches

If the bad patches are completely inhospitable, i.e. all elements of the demographic matrix in the bad patches are zero, i.e. $\mathbf{B}^{\mathcal{B}} \equiv \mathrm{O}$, then the higher order terms $\rho^{\text{app}}_{s,j}$ $(j > 0)$ in the expansion of ρ^{app}_{s} are equal to zero. So, by the definition of c^{app} in (2.7),

$$c^{\text{app}} = \min_{s>0} \left[\frac{1}{s} \log \left(\rho^{\text{app}}_{s,0} \right) \right]$$

where $\rho^{\text{app}}_{s,0}$ is the principal eigenvalue of $\mathbf{M}_0(s)$ in (2.25). The principal eigenvalue of this matrix is the ratio of the density distributions at $t+1$ and t, where the density distribution at t is an exponential wave with wave-number s.

2.2.10 Numerical Methods

In Section 2.3 (Examples), we compare our analytical results to simulations of the IDE. We now discuss some of the methods used.

Analytical Approximation

For exponentially bounded kernels, the terms in (2.25) and (2.27) corresponding to large n, m become exponentially small. We have found numerically that the relative errors from taking only the $|n| \leq 20$ terms in (2.25) and the $|n|, |m| \leq 20$ terms in (2.27) are less than 10^{-2} for both kernels studied (Gaussian and Laplace). Therefore, in calculating our approximations, we use only the terms where $|n|, |m| \leq 20$.

Simulations

We simulate the IDEs using MATLAB by restricting the domain to $[0, D]$ (where D is sufficiently large that ignoring behaviour outside $[0, D]$ does not affect the spreading speed of the travelling wave) and discretising the population density distribution for each stage and the dispersal kernels for individuals transitioning between each pair of stages into elements of non-dimensional length ≈ 0.0015. This allows us to treat the population densities for each stage and the dispersal kernel as vectors.

The approximation presented in Subsection 2.2.8 is valid for any initial conditions with compact support. We choose our initial conditions to be zero everywhere except for a small interval starting from zero in the spatial domain. Here the density of juveniles is small and constant and the densities of all other stages are zero. This allows the species to spread, and the wave to propagate outward from the origin and the initial population.

In the growth phase of the numerical model, at each spatial element of the domain, we form a diagonal matrix with the densities of the M demographic stages on the diagonal. This is multiplied by the density dependent population projection matrix for that element. This projection matrix is calculated for each element of the

discretised domain at each time-step (this changes as the population density in that element changes). The resulting matrices for each spatial element of the domain are incorporated into a three-dimensional array $\mathbf{Q}$ in which the (i, j, k)th element is the density of individuals from the ith spatial element transitioning between demographic stages j and k.

Since the kernel in the good patch $\mathbf{K}^{\mathcal{G}}(x-y)$ and the kernel in the bad patch $\mathbf{K}^{\mathcal{B}}(x-y)$ are dependent only on the dispersal distance $x-y$, the RHS of (2.1) can be written as the sum of two terms, with one referring to dispersal from the good patches, and the other to dispersal from the bad patches. Since the dispersal pattern from each type of patch does not vary within that patch type, the integrals are convolutions of the density of individuals transitioning between each demographic stage in that patch type and the dispersal kernel from that patch type for the relevant pair of demographic stages. Under the discretisation, the integral convolution of the population density functions and dispersal kernel between demographic stages m and n become a discrete convolution of the restriction of the vector $\mathbf{Q}(m, n, j)$ $(j = 1, 2, ...)$ to the relevant patch type and the corresponding dispersal kernel. We calculate this convolution using the Fourier convolution theorem and Fast Fourier Transform (FFT) (Andersen, 1991). To incorporate dispersal between all pairs of elements including those at either end of the domain, the kernels have $2n-1$ elements, where n is the number of elements in the domain. For each pair of demographic stages, convolution gives a vector of length $3n-2$, with the middle n elements corresponding to the domain $[0, D]$. We assume that anything outside the domain is totally inhospitable (and has no effect on the dynamics of the invasion), and take only the middle part of the vector as the population density at time $t+1$.

We observe that the solution settles into a travelling wave by $t \sim 50$ for the parameter values considered in this chapter (see Figure 2.2 for plots of the wave-front locations of solutions to IDEs with Laplace and Gaussian kernels), so we run the simulation for 100 time-steps and use the positions of the wave-front (the maximum of x such that the juvenile stage of the non-dimensional population density $u_1^t(x) > \mu$)

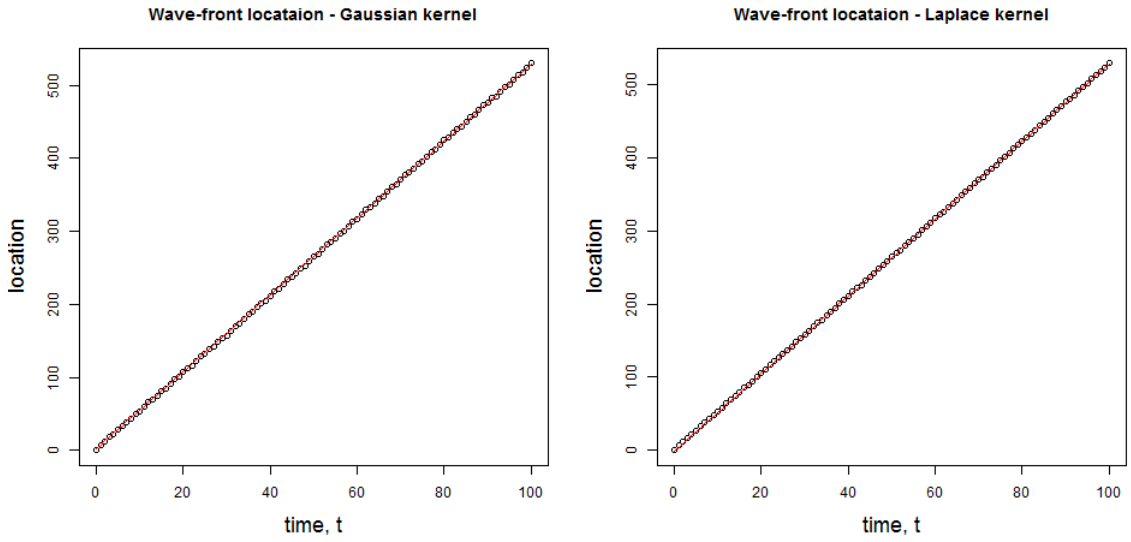

Figure 2.2: Location of the wave-front (black circles) of numerical solutions to (2.1), as measured by the largest x such that $u^t(x) > 0.0005$, for $t = 0, ..., 100$ for non-stage structured IDEs with $\alpha = 1$, $r = 10$, $\epsilon = 0$, $p = 1$ with (a) Gaussian dispersal and $L = 4$ and (b) Laplace dispersal and $L = 8$. All other parameters are given in Table 2.1. The red line is the line of best fit fitted to the wave-front locations for $t = 75, ..., 100$, and its slope is taken to be the wave-speed of the solution to the IDE. The red line is a good fit as the R^2 values are (a) 0.9994059 and (b) 0.9998585.

for $t = 75, ..., 100$ to find the asymptotic wave-speed by fitting a linear function to the data. Numerically, we find that (after an initial transient) the wave-front maintains the same exponential shape and shifts by a fixed distance. Therefore, the observed wave-speed is independent of the final time choice, and our choice of numerical threshold for invasion μ which we hereafter take as $\mu = 0.0005$.

2.3 Examples

2.3.1 Analytical Approximations

In this section, we first present approximations for the asymptotic wave speed of solutions to (2.1) where the demographic parameters vary between good and bad patches, but the choice of dispersal kernel (Gaussian or Laplace) and the dispersal parameters do not. We will find the first two non-zero terms in the expansion for ρ_s^{app} for non-stage-structured populations with Laplace and Gaussian dispersal ker-

nels and stage-structured populations with Laplace and Gaussian dispersal kernels. Additionally, we will justify the approximation of dispersal from a good patch with dispersal from a point source (the replacement of the integral operator $F_{s,0}$ by $F_{s,0}^{\text{app}}$) used in Subsection 2.2.6.

Throughout our non-stage-structured simulations we use the Beverton-Holt growth function for $\mathbf{B}$. This is widely used as a population growth function and has been used to model plant populations (Poulsen et al., 2007), with the population after the growth phase being given by the current population u multiplied by the growth rate

$$f(u) = \frac{rK}{K + (r-1)u} \ ,$$

where u is the scalar population before the growth phase, r is the zero-population growth rate ($f(0) = r$) and K is the carrying capacity of the environment (here, without loss of generality, we set $K = 1$). Since the approximation depends only on the zero-population growth rate, we could have used any growth function satisfying Condition II in Subsection 2.2.3 (Kot et al., 1996).

Example with Laplace Kernel

The non-stage-structured Laplace dispersal kernel (Dewhirst and Lutscher, 2009) is

$$k(x-y) = \frac{1}{2\alpha} \exp\left(-\frac{|x-y|}{\alpha}\right)$$

with mean dispersal distance given by α for dispersal from any point in the landscape. Since this is a non-stage-structured population, the linearised demographic matrices are the scalar growth rates r (in the good patches) and ϵr (in the bad patches). For the good patches, the discretised kernel, given by (2.26), is

$$\mathrm{K}_{\text{app}}^{G}(x - nL) = \begin{cases} 1 - \mathrm{e}^{\frac{-L_1}{2\alpha}} & \text{for } n = x = 0 \\ \\ \frac{L_1}{2\alpha}\mathrm{e}^{-\frac{|x-nL|}{\alpha}} & \text{otherwise} \end{cases} . \tag{2.29}$$

Using the result (2.25) from Subsection 2.2.8, we find an expression for $\rho_{s,0}^{\text{app}}$,

$$\begin{aligned}\rho_{s,0}^{\text{app}} &= r\left[\frac{L_1}{2\alpha}\sum_{n\neq 0}\mathrm{e}^{\frac{-L|n|}{\alpha}+sLn}+\left(1-\mathrm{e}^{\frac{L_1}{2\alpha}}\right)\right]\\ &= \frac{rL_1}{2\alpha}\left[\left(\mathrm{e}^{\frac{L}{\alpha}+sL}-1\right)^{-1}+\left(\mathrm{e}^{\frac{L}{\alpha}-sL}-1\right)^{-1}\right]+r\left(1-\mathrm{e}^{\frac{L_1}{2\alpha}}\right)\quad .\end{aligned}$$

Similarly, substituting (2.29) and the scalar growth rate into (2.27), we obtain an expression for $\rho_{s,1}^{\text{app}}$,

$$\begin{aligned}\rho_{s,1}^{\text{app}} &= \frac{1}{\rho_{s,0}}\frac{\epsilon r^2 L_1}{4\alpha^2}\sum_{n,m\in\mathbb{Z}}\mathrm{e}^{sL(n+m)}\int_{\frac{L_1}{2}}^{L-\frac{L_1}{2}}\mathrm{e}^{\frac{-1}{\alpha}(|Ln-y|+|Lm+y|)}\mathrm{d}y\\ &= \frac{1}{\rho_{s,0}}\frac{\epsilon r^2 L_1}{4\alpha^2}\sum_{n,m\in\mathbb{Z}}\mathrm{e}^{\frac{-L}{\alpha}sL(n+m)}A_{n,m}\end{aligned}$$

where

$$A_{n,m}=\begin{cases}\frac{1}{4\alpha^2}(L-L_1)\mathrm{e}^{\frac{-1}{\alpha}|(m+n)L|} & \text{where}\quad \operatorname{sign}\left(m+\frac{1}{2}\right)=\operatorname{sign}\left(n-\frac{1}{2}\right)\\ \frac{1}{4\alpha}\mathrm{e}^{\frac{-1}{\alpha}\operatorname{sign}\left(m+\frac{1}{2}\right)(m-n+1)L}\sinh\left(\frac{L-L_1}{\alpha}\right) & \text{where}\quad \operatorname{sign}\left(m+\frac{1}{2}\right)\neq\operatorname{sign}\left(n-\frac{1}{2}\right)\end{cases}.$$

We then substitute our expressions for $\rho_{s,0}^{\text{app}}$ and $\rho_{s,1}^{\text{app}}$ into (2.28) to get an analytical expression for the wave-speed which we will compare with numerical results in Subsection 2.3.2.

Example with Gaussian Kernel

The non-stage-structured Gaussian dispersal kernel (Dewhirst and Lutscher, 2009) is

$$k(x-y)=\frac{1}{\alpha\sqrt{2\pi}}\exp\left(\frac{-(x-y)^2}{2\alpha^2}\right)$$

with dispersal parameter α throughout the good and bad patches. The linear (zero-population) growth rates are r (in the good patches) and ϵr (in the bad patches). Given the smoothness of the Gaussian kernel around $x - y = 0$, we can take our discretised kernel

$$\mathrm{K}^G_{\mathrm{app}}(z) = L_1 k(z) \quad \text{for all } z \in \mathbb{R} \tag{2.30}$$

further simplifying the expression for $\mathrm{K}^G_{\mathrm{app}}$ in (2.26). By (2.25) we have that

$$\rho^{\mathrm{app}}_{s,0} = \frac{rL_1}{\alpha\sqrt{2\pi}} \sum_{n\in\mathbb{Z}} \mathrm{e}^{\frac{-n^2L^2}{2\alpha^2}+snL}$$

and where erf is the error function, we have by (2.27),

$$\begin{aligned}
\rho^{\mathrm{app}}_{s,1} &= \frac{1}{\rho^{\mathrm{app}}_{s,0}} \frac{r^2L_1}{2\pi\alpha^2} \sum_{m,n\in\mathbb{Z}} \mathrm{e}^{sL(n+m)} \int_{\frac{L_1}{2}}^{L-\frac{L_1}{2}} \mathrm{e}^{\frac{-(Ln-y)^2-(Lm+y)^2}{2\alpha^2}} \mathrm{d}y \\
&= \frac{r^2L_1}{4\sqrt{\pi}\alpha\rho^{\mathrm{app}}_{s,0}} \sum_{m,n\in\mathbb{Z}} \mathrm{e}^{\frac{-L^2(n+m)^2}{4\alpha^2}+sL(n+m)} \left[\mathrm{erf}\left(\frac{L(m-n+2)-L_1}{2\alpha}\right)\right. \\
&\left. -\mathrm{erf}\left(\frac{L(m-n)+L_1}{2\alpha}\right)\right] \quad .
\end{aligned}$$

We again substitute our expressions for $\rho^{\mathrm{app}}_{s,0}$ and $\rho^{\mathrm{app}}_{s,1}$ into (2.28) for an analytical expression for the wave-speed. The numerical evaluation of these expressions is straightforward, and as the terms in the infinite series become exponentially small as n or m tend to $\pm\infty$, they can be truncated to a finite number of terms (see Subsection 2.2.10).

Stage-Structured Example with Laplace and Gaussian Kernels

We now find the first two non-zero terms in the expansion of ρ^{app}_s for a stage-structured population with both Laplace and Gaussian kernels. The population has two stages (juveniles and adults), in which dispersal occurs only as juveniles are born. This is a modified version of the example in Neubert and Caswell (2000). The population

projection matrix in the good patches is

$$\mathbf{B}^{\mathcal{G}}(\mathbf{u}^t(x)) = \begin{bmatrix} \nu(1-\gamma) & \phi\exp(-u_1^t(x) - u_2^t(x)) \\ \nu\gamma & \theta \end{bmatrix},$$

where ν and θ respectively, are the juvenile and adult survival rates (the proportion of individuals surviving to the next time-step), with γ denoting the maturation rate (the proportion of juveniles advancing to adulthood) and $\phi\exp(-u_1^t(x) - u_2^t(x))$ is the density dependent birth rate (the number of births per adult). The population projection matrix in the bad patches is $\epsilon\mathbf{B}^{\mathcal{G}}(\mathbf{u}^t(x))$. Where new juveniles disperse with parameter α, the dispersal kernel is

$$\mathbf{K}(z) = \begin{bmatrix} \delta(z) & K(z) \\ \delta(z) & \delta(z) \end{bmatrix}$$

where

$$K(z) = \begin{cases} \frac{1}{2\alpha}\exp\left(\frac{-|z|}{\alpha}\right) & \text{for the Laplace kernel} \\ \frac{1}{\alpha\sqrt{2\pi}}\exp\left(\frac{-z^2}{2\alpha^2}\right) & \text{for the Gaussian kernel} \end{cases}. \tag{2.31}$$

We use (2.26) to define the discretised kernel

$$\mathbf{K}_{\text{app}}(z) = \begin{bmatrix} \delta(z) & K_{\text{app}}(z) \\ \delta(z) & \delta(z) \end{bmatrix}$$

where, for the Gaussian and Laplace kernels, K_{app} is defined as for the non-stage-structured Gaussian and Laplace examples in (2.29) and (2.30). Substituting $\mathbf{K}_{\text{app}}$ and the linearisation of $\mathbf{B}^{\mathcal{G}}$ into (2.25), we find that for the Laplace kernel, $\rho_{s,0}^{\text{app}}$ is the principal eigenvalue of

$$\left(\sum_{n\neq 0}\begin{bmatrix}\delta_{n,0} & \frac{L_1}{2\alpha}\exp\left(\frac{-|nL|}{\alpha}\right)\\ \delta_{n,0} & \delta_{n,0}\end{bmatrix}\mathrm{e}^{snL}+\begin{bmatrix}\delta_{n,0} & 1-\exp\left(\frac{-L_1}{2\alpha}\right)\\ \delta_{n,0} & \delta_{n,0}\end{bmatrix}\right)\circ\begin{bmatrix}\nu(1-\gamma) & \phi\\ \nu\gamma & \theta\end{bmatrix} \tag{2.32}$$

and for the Gaussian kernel, $\rho_{s,0}^{\text{app}}$ is the principal eigenvalue of

$$\sum_{n\in\mathbb{Z}}\begin{bmatrix}\delta_{n,0} & \frac{L_1}{\alpha\sqrt{2\pi}}\exp\left(\frac{-(nL)^2}{2\alpha^2}\right)\\ \delta_{n,0} & \delta_{n,0}\end{bmatrix}\circ\begin{bmatrix}\nu(1-\gamma) & \phi\\ \nu\gamma & \theta\end{bmatrix}\mathrm{e}^{snL}\ . \tag{2.33}$$

This means that

$$\rho_{s,0}^{\text{app}}=\frac{1}{2}\left(\nu(1-\gamma)+\theta+\sqrt{(\nu(1-\gamma)+\theta)^2-4\nu\gamma\phi B(s)}\right)$$

where

$$B(s)=\begin{cases}\frac{L_1}{2\alpha}\left[\left(\mathrm{e}^{\frac{L}{\alpha}+sL}+1\right)^{-1}+\left(\mathrm{e}^{\frac{L}{\alpha}-sL}+1\right)^{-1}\right]+\left(1-\mathrm{e}^{\frac{-L_1}{2\alpha}}\right) & \text{for the Laplace kernel}\\ \frac{L_1}{\alpha\sqrt{2\pi}}\sum_{n\in\mathbb{Z}}\mathrm{e}^{\frac{-(nL)^2+snL}{2\alpha^2}} & \text{for the Gaussian kernel}\ .\end{cases}$$

With $\tilde{\boldsymbol{\psi}}_s$ and $\boldsymbol{\psi}_s$, respectively, denoting the left and right eigenvectors of (2.32) for the Laplace kernel, or (2.33) for the Gaussian kernel, by (2.27), $\rho_{s,1}$ is given by

$$\rho_{s,1}^{\text{app}}=\frac{\tilde{\boldsymbol{\psi}}_s\mathbf{M}_1\boldsymbol{\psi}_s}{\rho_{s,0}\tilde{\boldsymbol{\psi}}_s\boldsymbol{\psi}_s}$$

where

$$\mathbf{M}_1 = \sum_{m,n\in\mathbb{Z}} \int_{\frac{L_1}{2}}^{L-\frac{L_1}{2}} \left(\begin{bmatrix} 0 & K_{\text{app}}(nL-y)\mathrm{e}^{snL} \\ 0 & 0 \end{bmatrix} \circ \begin{bmatrix} \nu(1-\gamma) & \phi \\ \nu\gamma & \theta \end{bmatrix} \right) \times \left(\begin{bmatrix} 0 & K_{\text{app}}(mL+y)\mathrm{e}^{smL} \\ 0 & 0 \end{bmatrix} \circ \begin{bmatrix} \nu(1-\gamma) & \phi \\ \nu\gamma & \theta \end{bmatrix} \right) \mathrm{d}y = \mathbf{O} \ .$$

So, for both kernels, we have that $\rho_{s,1}^{\text{app}} = 0$, and to find the second non-zero term in the expansions of ρ_s^{app}, we must investigate the third term $\rho_{s,2}^{\text{app}}$ in the expansion of ρ_s^{app}. To do this, we must find an expression for the second term $\boldsymbol{\phi}_{s,1}^{\text{app}}$ in the expansion of the eigenvector $\boldsymbol{\phi}_s^{\text{app}}$. Since $\rho_{s,1}^{\text{app}} = 0$, the coefficients of ϵ in the expansion of the eigenvalue problem (2.5) satisfy

$$(F_{s,0}^{\text{app}} - \rho_{s,0}^{\text{app}})\boldsymbol{\phi}_{s,1}^{\text{app}} + F_{s,1}\boldsymbol{\phi}_{s,0}^{\text{app}} = 0 \tag{2.34}$$

and by choice of $\boldsymbol{\phi}_{s,1}^{\text{app}}$

$$\langle \tilde{\boldsymbol{\phi}}_{s,0}^{\text{app}} | \boldsymbol{\phi}_{s,1}^{\text{app}} \rangle = 0 \ . \tag{2.35}$$

Both conditions (2.34) and (2.35) are satisfied by

$$\boldsymbol{\phi}_{s,1}^{\text{app}} = \frac{1}{\rho_{s,0}^{\text{app}}} \mathcal{I}_{\left[\frac{L_1}{2}, L-\frac{L_1}{2}\right)}(x) \sum_{m\in\mathbb{Z}} \begin{bmatrix} 0 & \nu(1-\gamma)\phi \\ 0 & \nu\gamma\phi \end{bmatrix} K(x-mL)\ \mathrm{e}^{s(x-mL)}\boldsymbol{\psi}_s$$

where $K(z)$ is the dispersal kernel of newborn juveniles defined in (2.31). Taking the coefficients of ϵ^2 in (2.5), we have

$$(F_{s,0}^{\text{app}} - \rho_{s,0}^{\text{app}})\boldsymbol{\phi}_{s,2}^{\text{app}} + (F_{s,1} - \rho_{s,1}^{\text{app}})\boldsymbol{\phi}_{s,1}^{\text{app}} = \rho_{s,2}^{\text{app}}\boldsymbol{\phi}_{s,0}^{\text{app}} \quad .$$

Taking the inner-product with $\tilde{\boldsymbol{\phi}}_{s,0}^{\text{app}}$, the first term on the left hand side becomes zero ($\tilde{\boldsymbol{\phi}}_{s,0}^{\text{app}}$ is the eigenvector of the adjoint operator of $F_{s,0}^{\text{app}}$ with eigenvalue $\rho_{s,0}^{\text{app}}$), and so

$$\begin{aligned}
\rho_{s,2}^{\text{app}} =& \frac{\langle \tilde{\boldsymbol{\phi}}_{s,0}^{\text{app}} | F_{s,1}\boldsymbol{\phi}_{s,1}^{\text{app}} \rangle}{\langle \tilde{\boldsymbol{\phi}}_{s,0}^{\text{app}} | \boldsymbol{\phi}_{s,0}^{\text{app}} \rangle} \\
=& \frac{L_1\phi^2\nu\gamma\tilde{\psi}_s^1\psi_s^2}{(\rho_{s,0}^{\text{app}})^2\tilde{\boldsymbol{\psi}}_s\boldsymbol{\psi}_s} \sum_{m,n\in\mathbb{Z}} \mathrm{e}^{sL(m+n)} \int_{\frac{L_1}{2}}^{L-\frac{L_1}{2}} K(nL-y)K(mL+y)\mathrm{d}y \\
=& \frac{L_1\phi^2\nu\gamma\tilde{\psi}_s^1\psi_s^2}{(\rho_{s,0}^{\text{app}})^2\tilde{\boldsymbol{\psi}}_s\boldsymbol{\psi}_s} \sum_{m,n\in\mathbb{Z}} \mathrm{e}^{sL(m+n)} A_{n,m}
\end{aligned}$$

where $\tilde{\psi}_s^1$ and ψ_s^2 are, respectively, the first and second elements of $\tilde{\boldsymbol{\psi}}_1$ and $\boldsymbol{\psi}_2$, and where for the Laplace kernel,

$$A_{n,m} = \begin{cases} \frac{1}{4\alpha^2}(L-L_1)\mathrm{e}^{\frac{-1}{\alpha}|(m+n)L|} & \text{where} \quad \text{sign}\left(m+\frac{1}{2}\right) = \text{sign}\left(n-\frac{1}{2}\right) \\ \frac{1}{4\alpha}\mathrm{e}^{\frac{-1}{\alpha}\text{sign}\left(m+\frac{1}{2}\right)(m-n+1)L}\sinh\left(\frac{L-L_1}{\alpha}\right) & \text{where} \quad \text{sign}\left(m+\frac{1}{2}\right) \neq \text{sign}\left(n-\frac{1}{2}\right) \end{cases}$$

and for the Gaussian kernel

$$A_{n,m} = \frac{1}{4\sqrt{\pi}\alpha}\mathrm{e}^{\frac{-L^2(n+m)^2}{4\alpha^2}}\left[\text{erf}\left(\frac{L(m-n+2)-L_1}{2\alpha}\right) - \text{erf}\left(\frac{L(m-n)+L_1}{2\alpha}\right)\right] \quad .$$

We now have expressions for $\rho_{s,0}^{\text{app}}$ and $\rho_{s,2}^{\text{app}}$ and have found that $\rho_{s,1}^{\text{app}} = 0$. The approximation to the asymptotic wave-speed is given by (2.7),

$$c^{\text{app}} = \min_{s>0}\left[\frac{1}{s}\log\left(\rho_{s,0}^{\text{app}} + \epsilon^2\rho_{s,2}^{\text{app}}\right)\right] \quad . \tag{2.36}$$

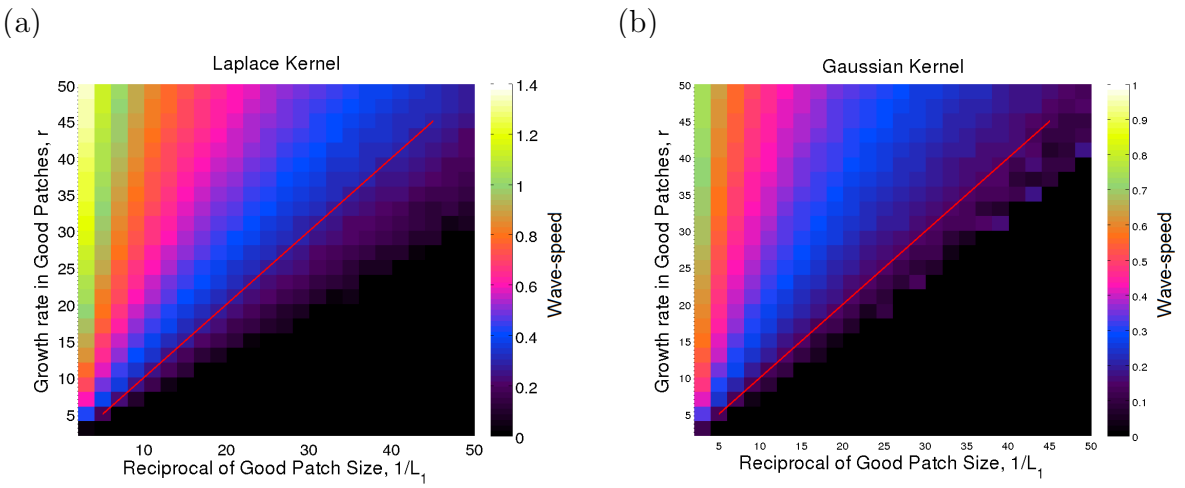

Figure 2.3: Wave-speeds of numerical solutions to IDEs of the form (2.1) for $2 \leq r \leq 50$ and $2 \leq 1/L_1 \leq 50$ for $r_2 = 0.1$, $L = 1$, $\alpha = 0.3$ for (a) a Laplace kernel and (b) a Gaussian kernel. The wave-speed is constant along the lines of the form $r = A/L_1$ (explicitly highlighted for $A = 1$). The approximations presented in Section 2.2.6 lead us to expect the wave-speed to be constant along these lines when L_1 is small (and when $1/L_1$ is large)

Justification of the Point Source Approximation

By approximating dispersal from each good patch with dispersal from a point source (approximating the integral operator $F_{s,0}$ with $F_{s,0}^{\text{app}}$) in Subsection 2.2.6, we assumed that the widths of the good patches are sufficiently small that neglecting the effect of spatial structure within each good patch, except when considering the quantity of dispersers remaining in the same patch, does not affect the asymptotic wave-speed of solutions to (2.1).

For small populations, the quantity of propagules leaving the good patch is proportional to the linearised scalar population growth rate multiplied by the width of the good patches, $r\,L_1$. For our approximation to hold, the asymptotic wave-speeds of solutions to (2.1) must be constant as $L_1 \to 0$ with constant $r\,L_1$.

We simulated solutions to the non-stage-structured IDE (2.1) for the Laplace and Gaussian dispersal kernels defined in Subsection 2.3.1 using the Beverton-Holt population growth function with different values of the good patch zero-population growth rate r and good patch width L_1 while keeping the dispersal parameters (which do not vary between the good and bad patches), landscape period L and bad patch

zero-population growth rate r_2 constant (see Figure 2.3). We found that the contour lines (lines of constant wave-speed) are given by

$$r\, L_1 = \text{Const} \ . \tag{2.37}$$

and that changing the landscape parameter's position on the line (2.37) does not affect the asymptotic wave-speed of solutions to (2.1). This justifies the use of a point source approximation in Subsection 2.2.6 and hence using $F_{s,0}^{\text{app}}$ as an approximation to $F_{s,0}$ to get the analytical results in Subsection 2.2.8.

2.3.2 Numerical Results

We simulate solutions to (2.1) for the population projection matrices $\mathbf{B}(\mathbf{u}^t(x), x)$ and dispersal kernels $\mathbf{K}(x-y)$ of each of the above examples (see Subsection 2.2.10 for numerical details). We simulate solutions for a range of values of the total proportion of good habitat $p = L_1/L$ and landscape period L (see Figure 2.4). Since the dispersal pattern of a given plant species is somewhat fixed, we fix the dispersal parameter $\alpha = 1$, and vary the total proportion of good habitat in the landscape p and the landscape period L.

Additionally, we choose the population growth rates in the good patches (i.e. the principal eigenvalue of the demographic matrix) to be higher than those used in applications of homogeneous IDEs (e.g. Bullock et al., 2008). For homogeneous IDEs, the most appropriate approach would be take a spatial average of demographic rates. In the heterogeneous model, we distinguish between the demographic rates in the good and bad patches, and would expect higher and lower demographic rates in good and bad habitat patches, respectively.

We investigate the effect of these parameters on the relative errors of the approximations from Subsection 2.3.1 compared to the simulated wave-speed, and investigate their effect on the simulated wave-speed in Subsection 2.3.2.

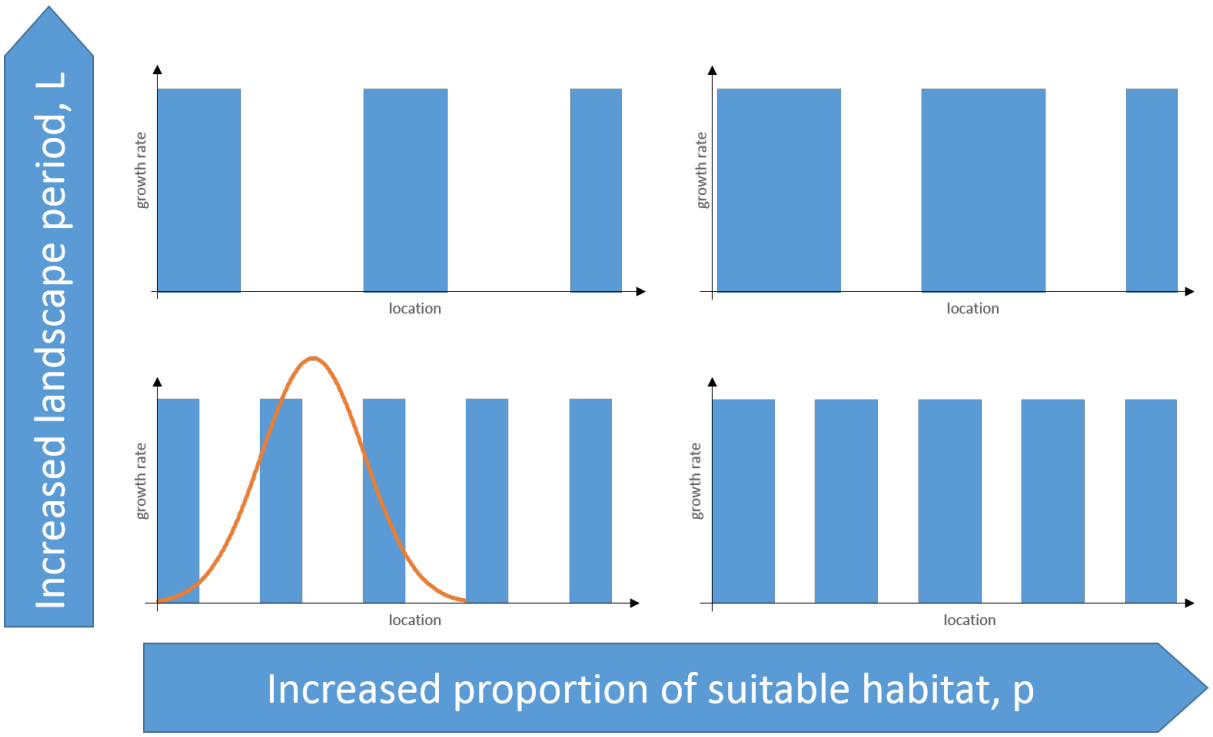

Figure 2.4: Schematic diagram showing the effects of varying the landscape period L and the proportion of suitable habitat p on the landscape structure.

Effect of the Bad patches on the wave-number

For both the Laplace and Gaussian kernels, the first-order approximation of the wave-speed is given by (2.28) in Subsection 2.2.8. In Figure 2.5, we plot the zeroth (considering only $\rho_{s,0}^{\text{app}}$) and first order approximations to the wave-speed $c(s)$ for a range of wave-numbers s for both non-stage-structured examples. The minima of the first order approximation give significantly better agreement with the simulated wave-speed than the minima of the zeroth order approximation. The first order approximations also have higher minimum wavespeeds than their respective zeroth order approximations, and these minima correspond to different wave-numbers (see Figure 2.5).

Relative Errors

For the examples in Subsection 2.3.1, we found that for the values of the total proportion of good habitat $p = L_1/L$ and landscape period L where the simulated wave-speed, $c^{\text{sim}} \neq 0$ (the relative error is not defined for $c^{\text{sim}} = 0$) the relative error

(a) (b)

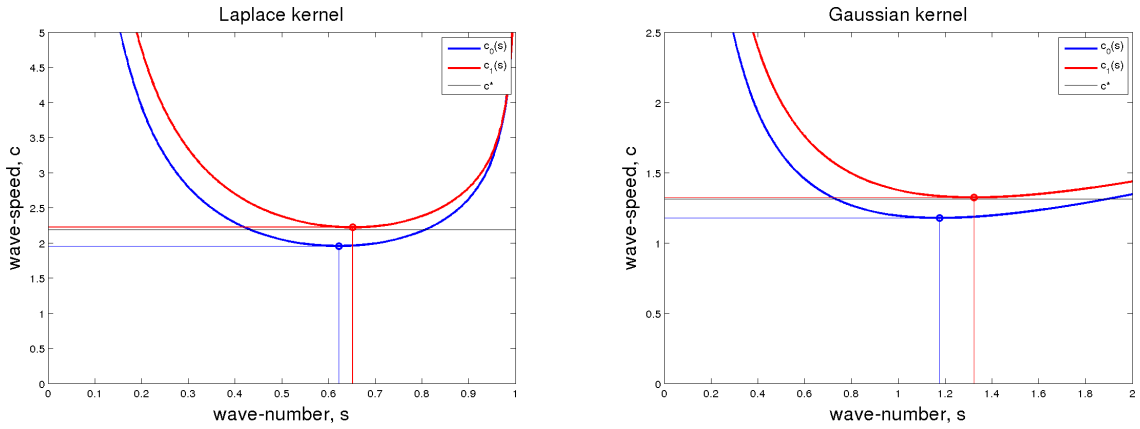

Figure 2.5: Zeroth order $c_0(s)$ (blue) and first order $c_1(s)$ (red) approximations to the wave-speed $c(s)$ of a travelling wave of the linearised IDE where $r = 10$, $L_1 = 0.2$, $L = 1$ and $\alpha = 1$ as a function of the wave-number s, for (a) a Laplace kernel and (b) a Gaussian kernel. The red and blue dots show the location of the minima of $c_1(s)$ and $c_0(s)$ respectively. The horizontal black line shows the asymptotic wave-speed c^* found through simulation.

$$E = \left| \frac{c^{\text{app}} - c^{\text{sim}}}{c^{\text{sim}}} \right|$$

is no more than 0.1, except for values of c^{sim} close to 0 (see Figures 2.6 and 2.7). The relative errors are small, and for parameter values that are not on the persistence/propagation thresholds, varying ϵ (when $\epsilon < 0.05$ in the non-stage-structured case, or $\epsilon < 0.25$ for the stage-structured case) does not significantly increase the size of the error. We have shown that the minima of the log of the first two non-zero terms of the expansion of ρ_s^{app} divided by the wave-number, s gives good agreement to the long-term wave-speed of simulated solutions to (2.1). Therefore the first two non-zero terms in the expansion of ρ_s^{app} correspond to an accurate approximation to the asymptotic wave-speed for the range of parameters studied for both (1) cases where the first two non-zero terms are $\rho_{s,0}^{\text{app}}$ and $\rho_{s,1}^{\text{app}}$ (see Figure 2.6), and for (2) cases where the first two non-zero terms are $\rho_{s,0}^{\text{app}}$ and $\rho_{s,2}^{\text{app}}$ (see Figure 2.7)

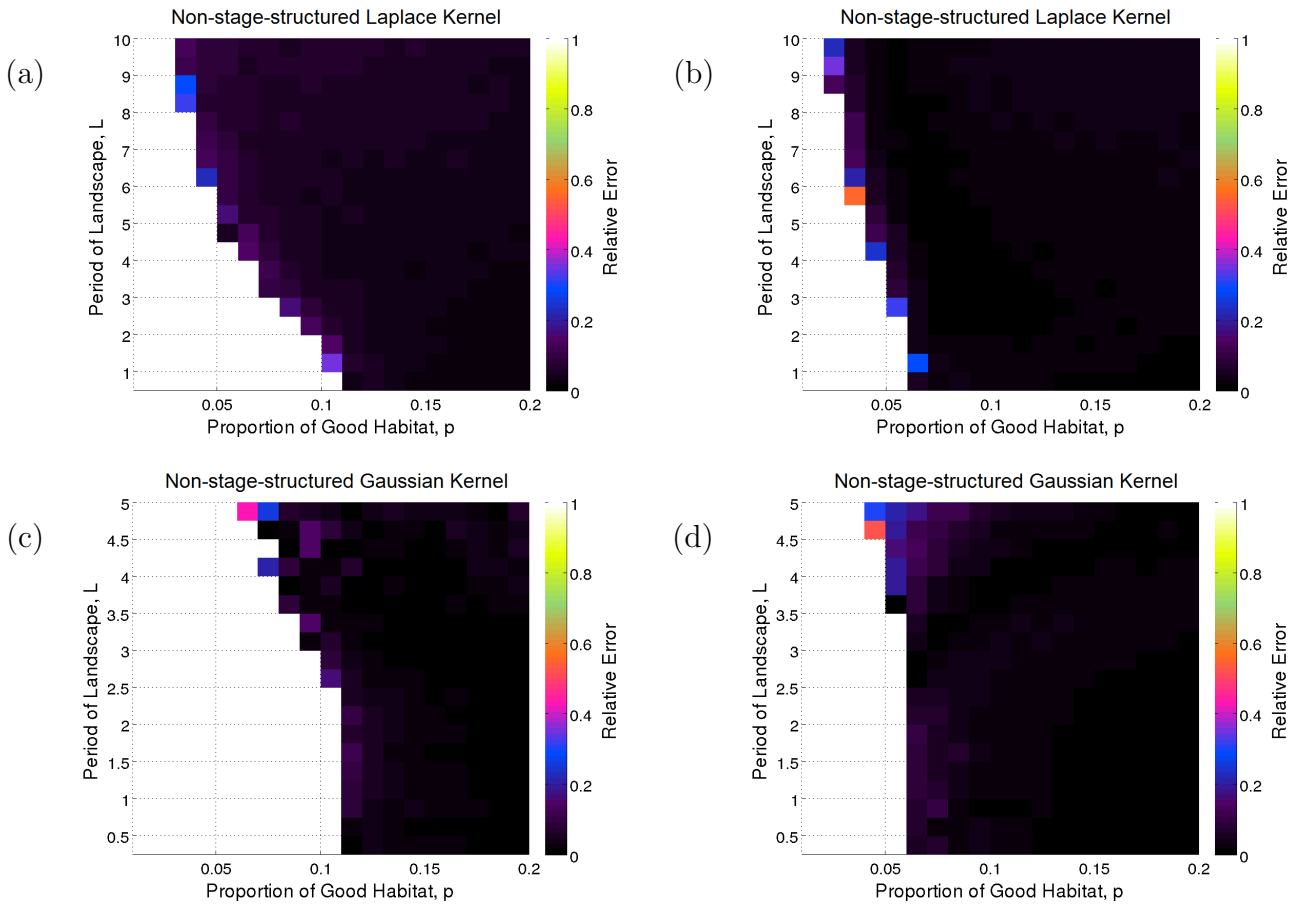

Figure 2.6: The relative errors of the first order analytic approximation (2.28) to the simulated wave-speeds of the non-stage-structured IDEs with $r = 10$ and (a)-(b) Laplace Kernel with $\alpha = 1$ and (a) $\epsilon = 0$, (b) $\epsilon = 0.05$. (c)-(d) Gaussian kernel with $\alpha = 1$ and (c) $\epsilon = 0$, (d) $\epsilon = 0.05$. The blank space at the left of each plot corresponds to values of L and p for which the wave cannot propagate, and the relative error is not defined. For both kernels, where the relative error is defined, it is less than 0.1 for a wide range of the parameters of interest. The parameters are given in Table 2.1.

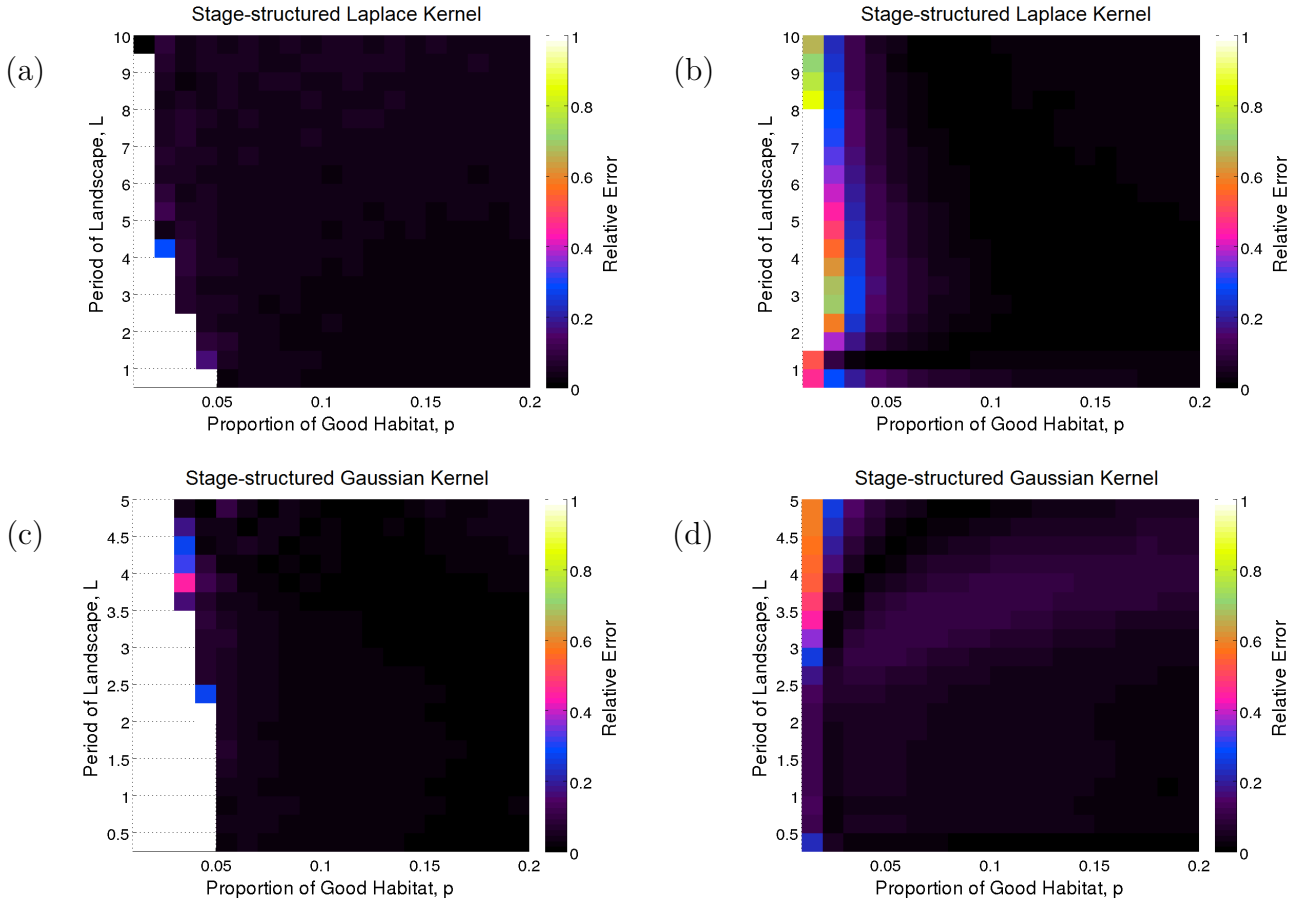

Figure 2.7: Relative errors of the second order analytic approximation (2.36) to the stage-structured IDE with $\nu = 0.8$, $\gamma = 0.625$, $\theta = 0.2$, $\phi = 30$ and $\alpha = 1$ and (a)-(b) Laplace kernel with $\alpha = 1$ and (a) $\epsilon = 0$, (b) $\epsilon = 0.25$. (c)-(d) Gaussian kernel with $\alpha = 1$ and (c) $\epsilon = 0$, (d) $\epsilon = 0.25$. The blank space at the left of each plot corresponds to values of L and p for which the wave cannot propagate, and the relative error is not defined. For both kernels, where the relative error is defined, it is less than 0.1 for a wide range of the parameters of interest. The parameters are given in Table 2.1.

Effects of Fragmentation

When studying the effect of fragmentation on landscape invasibility and invasion speed, we consider both the overall amount of habitat and the level of isolation of the patches. To explore the effect of habitat loss, we vary the total proportion of good habitat $p = L_1/L$, and to explore the effect of patch isolation, we vary the landscape period L (the scale of the landscape relative to the scale of dispersal). Figure 2.4 shows the effects of varying both parameters on landscape structure.

For all examples, increasing the total proportion of good habitat p increases the wave-speed (For each of the plots in Figures 2.8 and 2.9, increased p corresponds to higher wave-speeds). Similarly, increasing the ratio ϵ of the demographic rates in the bad patches relative to the rates in the good patches increases the wave-speed (the wave-speeds in Figure 2.8b,d and 2.9b,d are higher than for the corresponding values of L and p in Figure 2.8a,c and 2.9a,c).

For both the non-stage-structured and stage-structured examples, the relationship between the landscape period L and invasion speed differs between the two dispersal kernels. For the Gaussian kernel, and the values of p (the proportion of good habitat) for which an invasion occurs when the landscape period $L \sim 1$, the wave-speed decreases with increased L (except for a small region of parameter space in Figure 2.8d, where a minor increase occurs). For the Laplace kernel, increasing L increases the wave-speed.

For both non-stage-structured examples (Figure 2.8) and for both stage-structured examples with $\epsilon = 0$ (Figure 2.9a,c), we found that increasing the landscape period L decreases the total proportion of good habitat, p, needed for an invasion to occur. Our results do not show this for the stage-structured examples with $\epsilon = 0.25$ (Figure 2.9b,d) as all values of p and L correspond to an invasion.

To spread, a species with given dispersal and growth parameters requires a lower total proportion of good habitat when the landscape period is greater (the width of the black region corresponding to no spreading decreases as L increases in Figure 2.8

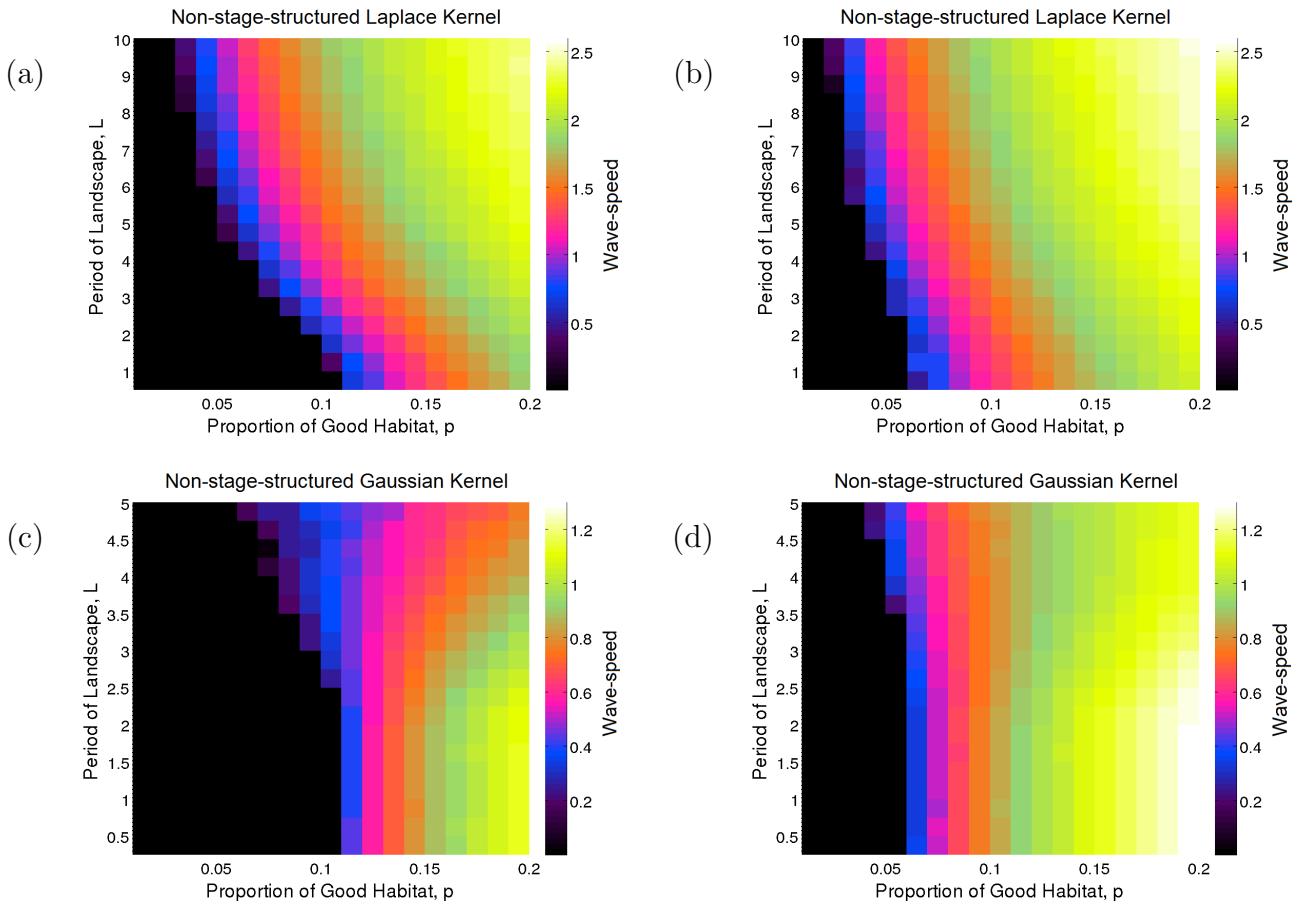

Figure 2.8: Simulated asymptotic wave-speeds of non-stage-structured IDEs with $r = 10$ for $0.01 \leq L_1/L \leq 0.2$ with (a)-(b) Laplace kernel with $\alpha = 1$ and (a) $\epsilon = 0$, (b) $\epsilon = 0.05$. (c)-(d) Gaussian kernel with $\alpha = 1$ and (c) $\epsilon = 0$, (d) $\epsilon = 0.05$.

and 2.9a,c).

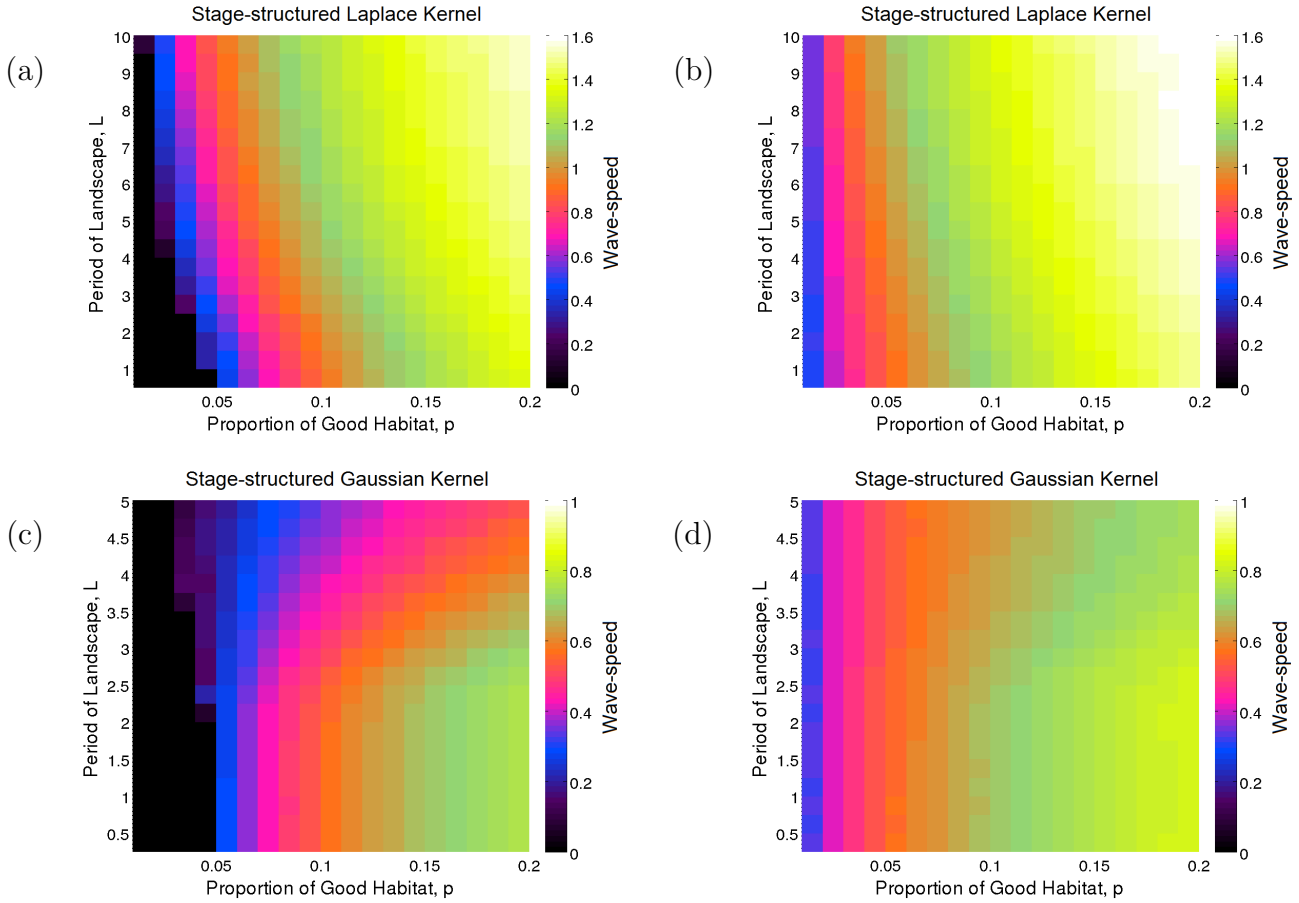

Figure 2.9: Simulated wave-speeds of the stage-structured IDE with $\nu = 0.8$, $\gamma = 0.625$, $\theta = 0.2$, $\phi = 30$ and $\alpha = 1$ and (a)-(b) Laplace kernel with (a) $\epsilon = 0$, (b) $\epsilon = 0.25$. (c)-(d) Gaussian kernel with (c) $\epsilon = 0$, (d) $\epsilon = 0.25$.

2.4 Discussion

In this chapter, we have derived an approximation for the asymptotic wave-speeds of solutions to stage-structured IDEs on periodic landscapes where the wave-speed is expressed as the minimum of the principal eigenvalues of approximations to the operators F_s. Approximating wave-speeds is useful because it yields analytically justified results and does not rely on numerical simulation, which is time-consuming, does not provide the same insight as an analytical approximation (e.g. sensitivity to certain parameters) and does not allow extensive parameter sweeps.

This is the first approximation to incorporate both stage-structure and landscape heterogeneity. The averaging approximation of Dewhirst and Lutscher (2009), which approximates the sum of the density of dispersal from each patch as a Riemann integral, is valid only for landscapes in which the landscape period L (and therefore the extent of the good/bad patches) is much less than the dispersal scale, $L \ll \sigma$, and breaks down when the landscape period is too large. Here, we have removed any condition on the landscape period, and replaced it with the less restrictive condition that the length scale of the good patch L_1 satisfies $L_1 \ll \sigma$ (Condition IV). This is sufficient to justify the approximation of the operator F_s in Subsection 2.2.6 with the discretised operator F_s^{app}. Additionally, we require the demographic rates in the bad patches to be related to the corresponding rates in the good patches by the small parameter $\epsilon \ll 1$ (Condition V). Taken together, these two assumptions allow us to express the principal eigenvalue ρ_s^{app} of F_s^{app} as an expansion in ϵ, with the terms in the expansion given as expressions of the demographic and dispersal parameters. Breaking the first of these assumptions (that $L_1 \ll \sigma$) makes our approximation of F_s by F_s^{app} unreasonable. Therefore, we do not expect this approximation to work when L_1 is of the same or a greater scale than the dispersal parameter. Increasing ϵ will increase the impact of higher order terms on the wave-speed, and when $\epsilon \sim 1$ we would no longer expect the first few terms in the expansion in ϵ to correspond to an approximation to the wave-speed.

We compared our approximation against numerical simulations for a range of parameters for Laplace and Gaussian dispersal kernels and for stage-structured and non-stage-structured populations. We found that the relative error of the approximation (compared to the simulations) is small (Figures 2.6 and 2.7), i.e. that the approximation of c^* given by c^{app} is accurate for the values of the parameters studied. The approximation is valid for any of the more complex exponentially bounded kernels which are often used in ecology (Clobert et al., 2012). For these kernels, terms in the expansion of the eigenvalue in ϵ may not have explicit analytical expressions and will need to be calculated numerically.

In this chapter, we showed that increasing the quality of the bad patches increases invasion speed. This is in agreement with previous studies showing the importance of the bad patches (habitat matrix) (Prugh et al., 2008; Franklin and Lindenmayer, 2009). For both kernels, increasing the landscape period L reduces the total proportion of good habitat required for an invasion to occur. This is in agreement with the theoretical findings of Shigesada et al. (1986) and Kinezaki et al. (2010), who found that larger fragmentation scales L reduced the total proportion of suitable habitat needed for an invasion to occur in partial differential equation (PDE) models of invasion. Furthermore, we found, with the exception of a small region of parameter space in Figure 2.8d, that for proportions of good habitat p corresponding to a successful invasion for low landscape periods L, increasing the landscape period increases the wave speed c^* for the Laplace kernel, and decreases the wave speed for the Gaussian kernel.

It is important and interesting that the choice of kernel affects the relationship between landscape structure and wave-speed, and further work is needed to explore this finding for a range of kernels. Given that increasing good patch size L_1 increases the wave-speed, and increasing the distance between good patches $L - L_1$ decreases the wave-speed, we hypothesise that the effect of increasing the landscape period (i.e. both patch-size and isolation simultaneously) will depend on the relative strengths of the two effects. For the Laplace kernel, the increase in wave-speed due to the

increased L_1 outweighs the decrease due to increased distance between good patches. For the Gaussian kernel, its thinner tail (compared to the Laplace kernel) strengthens the effect of increased distance between good patches, to the extent that the effect of increased distance outweighs the effect of increased patch-size. In general, therefore, it is important to have a detailed characterisation of the kernel, if we are to determine the effects of spatial heterogeneity on spread.

From a conservation perspective, the relationship between bad patch quality and spreading speed suggests that where spread is undesirable (i.e. invasive species), making the bad patches (habitat matrix) less hospitable may be an effective way to reduce the spreading speed. The implications for conservation efforts to reduce the spread of invasive species or promote the spread of populations tracking shifting habitat depend on the speed of spread and whether the system is close to the invasion threshold (at which the population neither spreads nor retreats). If the spreading population is close to this threshold, then the relationship between landscape scale L and the threshold of suitable habitat p required for an invasion suggests that where spread is desirable (e.g. spread to track shifting ranges), then fewer larger isolated patches will allow the population to keep up with its shifting habitat better than many smaller patches. Where spread is not desirable (e.g. invasive species), then a larger number of smaller but better connected patches may help to reduce spread. On the other hand, if the population is not close to the invasion threshold then the effects of landscape scale (and therefore the desired landscape configuration) depends on the population's dispersal kernel. Larger spatial scales increase spread for the Laplace kernel and reduce it for the Gaussian kernel, so the effect of patch size depends on the dispersal kernel. One situation where landscape managers can effectively change the landscape scale is in a hypothetical choice between developing habitat corridors and stepping stones or adding an equivalent area to existing habitat fragments. For populations far from the invasion threshold, habitat corridors and stepping stones would be desirable for reducing the spreading speed of an invasive organism with a Laplace dispersal kernel or for helping a species with Gaussian dispersal keep up with shifting habitat,

while they would be undesirable for invasive species with Gaussian dispersal or range shifting species with Laplace dispersal.

The dispersal kernel of a species may vary with habitat quality (Bullock et al., 2008). For example, plant height is affected by habitat quality (Soons and Heil, 2002), and mechanistic models (e.g. Katul et al., 2005) demonstrate that seed release height strongly affects the dispersal kernel. Here, we have presented a method for deriving the propagation speeds of populations in an IDE model where the kernel, the population projection matrix and their associated parameters take different values in the good and bad patches, but for simplicity, have looked only at examples where the dispersal kernel and parameters are constant throughout the landscape. Incorporating heterogeneous dispersal could help understand the way in which spatially heterogeneous dispersal affects populations' spreading speeds.

Here, we have required the ratio of all the demographic rates in the bad patches to the corresponding rates in the good patches to be $\mathrm{O}(\epsilon)$, and have found that the wave-speeds of stage-structured populations with two demographic stages differ from the $\epsilon = 0$ case by $\mathrm{O}(\epsilon^2)$. Ecologically, some species may only be affected by patch type at particular points in their life history, e.g. it may be much more difficult for a juvenile to become established outside the good habitat, but once established will exhibit similar demographic rates to established individuals in the good habitat (for example, see Bullock et al., 2008). This is not strictly in the range of validity of the method presented here, however, in some of these cases, it may still be possible for our model to work (by weakening Condition V). For example, our analysis would still be valid where the $\mathrm{O}(1)$ rates in the bad patches could be incorporated into the operator $F_{s,0}$ without affecting the value of the principal eigenvalue $\rho_{s,0}^{\mathrm{app}}$ (i.e. $F_{s,0}$ is determined only by behaviour in the good patches). Whether this is possible will depend on which demographic stages disperse and which stages are adversely affected by poor habitat. Weakening this condition would allow us to incorporate a wider range of behaviours in the bad patches.

We have considered single species invasions. A natural extension would be to

consider multi-species invasions, either where multiple co-operative species invade together, or where an invader out-competes an existing species. The possibility of extending this methodology to multi-species systems depends on whether solutions are propagating into unstable steady states, and on whether the wave-speeds of the solutions are determined by their linearisation around the unstable population state. Multi-species systems differ from single-species systems in that the linearisation $\mathbf{A}$ of the demographic matrix $\mathbf{B}$ is not generally irreducible. Weinberger et al. (2002) has shown analytically that systems with reducible matrices in which the population projection matrix is cooperative/order-preserving (i.e. $\mathbf{u}(x) \geq \mathbf{v}(x) \implies \mathbf{B}(\mathbf{u}(x), x)\mathbf{u}(x) \geq \mathbf{B}(\mathbf{v}(x), x)\mathbf{v}(x)$ element-wise) or can be transformed to one by a change of variables have linearly determined wave-speeds, but this is not applicable in general. Whether the cooperativity requirement can be relaxed to Condition II for reducible matrices requires further investigation.

In summary, we have provided analytical approximations to the wave-speeds of solutions to IDEs in periodic landscapes in which the landscape scale is not constrained by the dispersal scale. We have found them to be accurate, highlighting the sensitivity of the relationship between the landscape parameters and the spreading speed with respect to the choice of kernel.

Chapter 3

Landscapes with Low Environmental Variation

This chapter is based on the paper *Spreading Speeds for Plant Populations in Landscapes with Low Environmental Variation* by Gilbert, Gaffney, Bullock and White, which has been published in the Journal of Theoretical Biology (Gilbert et al., 2014a).

3.1 Introduction

Landscape structure is a decisive factor in determining whether a population spreads and its spreading speed (Bennie et al., 2013; King and With, 2002). While some modelling work has explicitly represented fragmented landscapes (Chapter 2; Lamoureaux et al., 2015), many researchers have used homogeneous landscapes in their models (see Table 1.2). One might expect that neglecting to incorporate the landscape structure explicitly would result in inaccurate predictions of spread. However, homogeneous approximations have been relatively successful when compared with real data (for example, Bullock et al., 2008; Caswell et al., 2003) and their use has been analytically justified in landscapes where the period of the landscape is much smaller than the scale of dispersal (Dewhirst and Lutscher, 2009). In this chapter, we will address the question of under what circumstances the details of landscape

structure can be ignored and a homogeneous IDE used, and when they must be taken into account if accurate predictions are to be made.

Specifically, we derive results for landscapes with low environmental variation, in which the environmentally driven variation ϵ in demographic parameters relative to the mean is small (i.e. $\epsilon \ll 1$). For example, fecundity may be slightly higher than the mean in some locations and slightly lower in others. Low environmental variation in population measures and environmental conditions is a feature of many different landscapes, including within forests (Hoshizaki et al., 2004) and grasslands (Jurena and Archer, 2003; Miller et al., 1995). For example, Janišová et al. (2012) measured the demographic matrices of the endangered flowering plant *Tephroseris longifolia* across five locations in a grassland/scrub landscape in the Czech Republic and Slovakia and found their principal eigenvalues to vary between 1.25 and 2.04 (a maximum relative variation of 0.31 from the mean). Generally, one might expect a population to encounter low environmental variation when spreading across a single continuous habitat, such as prairie, boreal forest, or regions converted to arable agriculture.

We show that when the environmental variation coefficient ϵ is small and the landscape is spatially periodic, the asymptotic wave-speeds $c^*(\epsilon)$ and $c^*(0)$ corresponding to the heterogeneous landscape and its homogenisation differ by an additive factor of size ϵ^2. This unexpected result provides a justification for homogenising a landscape with low environmental variation in modelling studies. Given that heterogeneous landscapes must in general be simulated, being able to use a homogeneous approximation avoids the computational costs of simulation and enables the application of analytical results that would otherwise not apply.

We will also derive a *second order* approximation for the wave-speed in these *weakly heterogeneous* landscapes which will act as a better approximation for larger ϵ. We will derive both results for non-stage-structured (scalar) populations with a conjecture that these results will also hold for stage-structured populations, providing a framework which can incorporate both the stage-structured and non-stage-structured cases. In most practical ecological scenarios, we would expect only a small number of

habitat types corresponding to different values of the spatially varying parameters. Using numerical simulation, we will show that in non-stage-structured populations, both the homogeneous and second order approximations are accurate for $\epsilon < 0.3$, with the second order approximation dramatically reducing the error. We will also explore the relationship between ϵ and the wave-speed in a non-periodic (stochastically generated) landscape, and will find a similar lack of sensitivity to ϵ for sufficiently small values of ϵ. For both periodic and stochastically generated landscapes, we find that environmental variation can both speed up and slow down invasions, with the specific effect having complex dependencies on the difference between landscape variation and dispersal scales, on the mean demographic/dispersal rates and on the dispersal kernel. This is in contrast to the effects of stochasticity caused by discrete individuals (intrinsic stochasticty) studied by Lewis (2000) which were found to slow down spread. How small ϵ needs to be in practice for the homogeneous approximation to work will depend on the average parameters of the organism and the landscape itself and will therefore be explored.

3.2 Method

This section considers the difference between (1) the asymptotic wave-speed of solutions to an IDE with spatially periodic heterogeneous parameters and compact initial conditions, and (2) the wave-speed of solutions to the homogeneous IDE with compact initial conditions, where the parameters are the spatial averages of the parameters of the heterogeneous IDE (the homogeneous approximation). In Subsections 3.2.1-3.2.2, this difference is found to be proportional to ϵ^2, with the homogeneous approximation found to be accurate for sufficiently small ϵ. A second order approximation is then derived in Subsection 3.2.3, which incorporates the second non-zero term in the eigenvalue of the dispersion relation. Finally, the extension of the periodic results to non-periodic landscapes is discussed in Subsection 3.2.4.

The spreading populations considered in this chapter are solutions to stage-structured

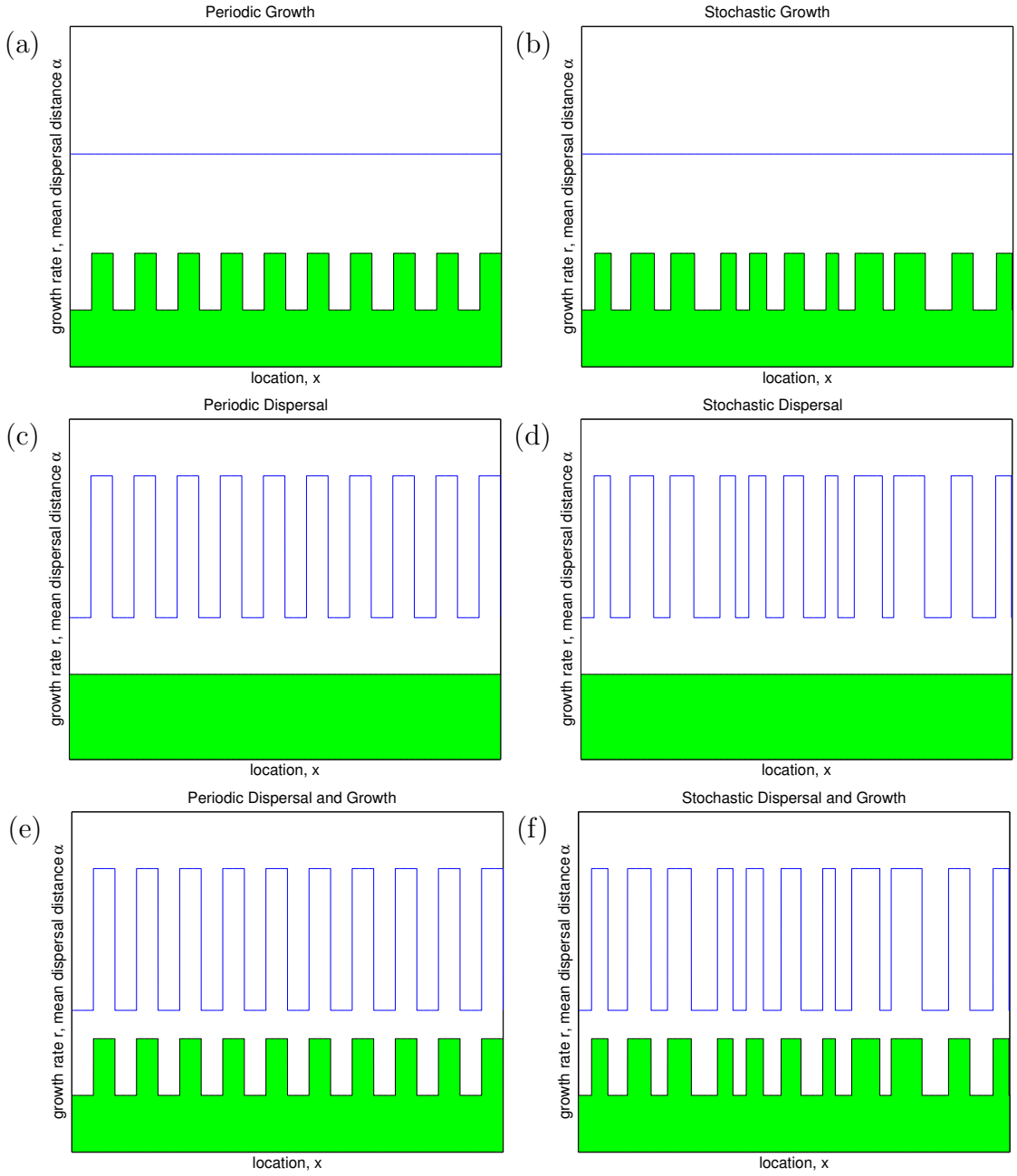

Figure 3.1: The intrinsic growth rate r (green solid area) and the mean dispersal distance α (blue solid line) for the three landscape scenarios considered for the non-stage-structured examples with periodic (a),(c),(e) and stochastic (b),(d),(f) landscapes. In (a),(b) only the intrinsic growth rate r depends on the region type. In (c),(d) only the mean dispersal distance α depends on region type. In (e),(f) both parameters depend on region type. The landscapes shown here have $\epsilon = 0.333$. When growth and dispersal are both varied, as in (e),(f), they need not be correlated but we consider the correlated case as an example.

IDEs of the form,

$$\mathbf{u}^{t+1}(x) = \int_{\Omega} \left[\mathbf{K}(x-y,y) \circ \mathbf{B}\left(\mathbf{u}^t(y),y\right)\right] \mathbf{u}^t(y)\mathrm{d}y \ , \tag{3.1}$$

or non-stage-structured IDEs,

$$u^{t+1}(x) = \int_{\Omega} k(x-y,y) r\left(u^t(y),y\right) u^t(y)\mathrm{d}y \ , \tag{3.2}$$

which have initial population distributions $\mathbf{u}^0(x)$ (or $u^0(x)$ for non-stage-structured IDEs) at $t = 0$ that are non-zero only on some closed interval $[x_{\min}, x_{\max}]$ such that $x_{\min}$ and $x_{\max}$ are finite. The landscape parameters in (3.1) are periodic and *weakly heterogeneous*, i.e. each dispersal and growth parameter exhibits only $\mathrm{O}(\epsilon)$ proportional variation from its spatial mean, where $0 < \epsilon \ll 1$.

If the spreading population is not stage-structured (it has only one demographic stage), then provided some conditions are satisfied, it can be shown analytically that the difference between the population's asymptotic spreading speed and the homogeneous approximation is $\mathrm{O}(\epsilon^2)$. It is conjectured that under these conditions, the results also hold for stage-structured populations. The following conditions guarantee the result for non-stage-structured populations (Weinberger et al., 2008).

I. The demographic matrix $\mathbf{B}(\mathbf{u}, x)$ is either positive, or non-negative and primitive for all values of the population density $\mathbf{u}$ and location x. If the model is not stage-structured (has only one demographic stage), then the scalar growth rate must be positive. Ecologically, this condition requires that the presence of individuals in any demographic stage will affect the number of individuals in any other stage at some future time.

II. The population projection matrix $\mathbf{B}(\mathbf{v}, y)$ is twice differentiable with respect to $\mathbf{v}$ at $\mathbf{v} = \mathbf{0}$, piecewise continuous in y, and population growth is highest when $\mathbf{v} = \mathbf{0}$, i.e.

$$\mathbf{B}(\mathbf{v}, x)\mathbf{v} \leq \mathbf{B}(\mathbf{0}, x)\mathbf{v} \quad \text{for all} \quad \mathbf{v} \geq \mathbf{0} \tag{3.3}$$

where inequalities are computed component-wise, and only a (locally) zero population before the growth phase can result in a zero population after the growth phase,

$$\mathbf{B}(\mathbf{v}, x)\mathbf{v} = \mathbf{0} \quad \text{if and only if} \quad \mathbf{v} = \mathbf{0} \ . \tag{3.4}$$

For non-stage-structured populations, the same conditions are required but with the population projection matrix replaced by the scalar growth rate $r(\mathbf{v}, y)$. Condition II is equivalent to requiring that larger populations have reduced demographic rates compared to small populations, that the demographic rates are non-zero and have a piecewise continuous relationship to the population density, which is reasonable for most species.

III. Each element of the matrix of dispersal kernels $\mathbf{K}(x-y, y)$ is (a) uniformly continuous in x and piecewise continuous in y, and (b) has a moment generating function in x, i.e. the dispersal kernel from each point y between each pair of demographic stages is *exponentially bounded* (i.e. that the dispersal kernel's tail be bounded by a positive exponential curve as $x \to -\infty$ and bounded by a negative exponential curve as $x \to \infty$). This condition ensures that solutions have a constant wave-speed and do not accelerate (Kot et al., 1996). Furthermore, at least one pair of stages has a kernel $K_{i,j}(x - y, y)$ which (for all $y \in \mathbb{R}$) is strictly non-zero for all x in an open interval of $\mathbb{R}$.

IV. The extinction (constant zero population) state is invadable (globally unstable), i.e. any initial arbitrarily small population, located anywhere, will invade and tend towards the non-zero equilibrium of the habitat as $t \to \infty$.

V. The dispersal kernel $\mathbf{K}(z, x)$ is determined by a finite number of spatially varying

parameters $\alpha^j(x)$ which determine the shape of the dispersal kernel at each x.

This condition allows the analysis to be related to experimental data, which due to the finite resolution of measurement, are represented as a finite number of measurements in ecological studies. The $\alpha^j(x)$ represent observable characteristics of the dispersion kernel, such as mean dispersal distance, variance and skewness etc. To put this in an explicit context, in the examples in Section 3.3, α is a scalar multiple of the mean dispersal distance.

VI. The population projection matrix and the parameters affecting the dispersal kernel are spatially L-periodic for some $L \in (0, \infty)$. This means that

$$\mathbf{B}(\mathbf{v}, x + L) = \mathbf{B}(\mathbf{v}, x) \quad \text{for all } \mathbf{v} \geq 0 \quad \text{and for all } x \in \mathbb{R} \tag{3.5}$$

$$\alpha^j(x + L) = \alpha^j(x) \quad \text{for all } x \in \mathbb{R} \quad \text{and for all } j = 1, \cdots \ . \tag{3.6}$$

Mathematically, this condition is sufficient to require that the operator on the RHS of Equation 3.1 is a periodic operator (Weinberger, 2002), i.e. it is invariant under translations of distance nL, where L is the period of the landscape and $n \in \mathbb{Z}$. This condition requires the landscape structure to be a regular pattern that repeats in space.

VII. The spatially varying (periodic) parameters $\alpha^j(x)$ and $A^{i,j}(x)$ exhibit only small levels of relative spatial variation and are small bounded perturbations from their spatial mean. In detail, let α_0^j and $A_0^{i,j}$ denote, respectively, the spatial means of $\alpha^j(x)$ and $A^{i,j}(x)$, i.e.

$$\alpha_0^j = \frac{1}{L}\int_0^L \alpha^j(x)\mathrm{d}x \quad \text{and} \quad A_0^{i,j} = \frac{1}{L}\int_0^L A^{i,j}(x)\mathrm{d}x \ ; \tag{3.7}$$

then for $\epsilon \ll 1$, we have that for all $x \in [0, L)$

$$\frac{\alpha^j(x) - \alpha_0^j}{\alpha_0^j} \sim \mathrm{O}(\epsilon) \quad \text{and} \quad \frac{A^{i,j}(x) - A_0^{i,j}}{A_0^{i,j}} \sim \mathrm{O}(\epsilon) \ . \tag{3.8}$$

Incorporating the size of the variation ϵ as a parameter in our model, the demographic and dispersal parameters can be written as the sum of their spatially constant mean α_0^j and $A_0^{i,j}$, and a small spatially varying component with zero spatial mean. As a result, the population projection matrix and dispersal kernel also have dependence on ϵ, i.e. $\mathbf{B}(\mathbf{u}, x, \epsilon)$ and $\mathbf{K}(x - y, y, \epsilon)$. When $\epsilon = 0$, there is no spatial variation in the demographic or dispersal parameters and the IDE is homogeneous, with the spatially constant parameters equal to the spatial means α_0^j and $A_0^{i,j}$ of the spatially varying parameters in the $\epsilon \neq 0$ case.

Condition I is a standard assumption for stage-structured models (Neubert and Caswell, 2000). For non-stage-structured populations, Conditions II - VI guarantee that conditions (i)-(vi) and (viii)-(ix) in Hypotheses 2.1 in Weinberger et al. (2008) are satisfied. These conditions are sufficient to prove that the asymptotic spreading speed of a non-stage-structured IDE on a periodic landscape is given by the minimum of the spreading speeds $c(\epsilon, s)$ of the periodic travelling wave solutions parameterised by s, and we hypothesise that this result also holds for stage-structured IDEs. The asymptotic spreading speed is given by

$$c^*(\epsilon) = \min_{s>0} \left[c(\epsilon, s)\right] \ . \tag{3.9}$$

The spreading speeds of the periodic travelling waves are given by

$$c(s, \epsilon) = \frac{1}{s} \log\left(\rho(s, \epsilon)\right) \ , \tag{3.10}$$

where ϵ is the size of the spatial variation and $\rho(s, \epsilon)$ is the principal eigenvalue of the stage-structured operator

$$F^{s,\epsilon}\left[\boldsymbol{\phi}\right](x) = \int_{-\infty}^{\infty} \left[\mathbf{K}(x - y, y, \epsilon) \circ \mathbf{A}\left(y, \epsilon\right)\right] \mathrm{e}^{s(x-y)} \boldsymbol{\phi}(y) \mathrm{d}y \ . \tag{3.11}$$

Condition VII enables us to use regular perturbation methods. We will assume Conditions I-VII for IDEs on periodic landscapes. However, when considering non-periodic landscapes in Section 3.2.4, we will assume Conditions I-V, together with a modified form of Condition VII (that the homogeneous parameters are the spatial averages of the parameters over the whole landscape). For non-periodic landscapes, the conditions in Weinberger et al. (2008) have not been shown analytically to guarantee results on spreading behaviour, so this will be justified numerically.

In Subsections 3.2.1 - 3.2.2, we consider the relationship betweeen the asymptotic spread rate $c^*(\epsilon)$ of a weakly heterogeneous IDE, and the spread rate $c^*(0)$ of the spatially homogeneous IDE with demographic and dispersal parameters given by the spatial means of the parameters in the heterogeneous IDE. We show that the speed of the weakly heterogeneous IDE differs from the speed of the homogeneous IDE by $\mathrm{O}(\epsilon^2)$. We demonstrate this by doing the following:

1. (Subsection 3.2.1) Find the first two terms ($\mathrm{O}(1)$ and $\mathrm{O}(\epsilon)$) in the expansion of the IDE in terms of ϵ. This defines the first two terms in the expansion of the operator $F^{s,\epsilon}$ in terms of ϵ around the spatially homogeneous landscape,

$$F^{s,\epsilon} = F^{s,0} + \epsilon F_1^s + \mathrm{O}(\epsilon^2) \quad \text{as} \quad \epsilon \to 0 \ . \tag{3.12}$$

2. (Subsection 3.2.2) Solve a regular perturbation problem to find the principal eigenvalue of $F^{s,\epsilon}$ as an expansion in ϵ,

$$\rho(s,\epsilon) = \rho_0(s) + \epsilon\rho_1(s) + \mathrm{O}(\epsilon^2) \quad \text{as} \quad \epsilon \to 0 \ , \tag{3.13}$$

and show that the $\mathrm{O}(1)$ term $\rho_0(s)$ is equal to the eigenvalue $\rho(s,0)$ of the spatially homogeneous operator $F^{s,0}$, which can be calculated using the formulae in Section 1.5.3, and that the coefficient $\rho_1(s)$ of ϵ is equal to zero, i.e.

$$\rho(s,\epsilon) = \rho(s,0) + \mathrm{O}(\epsilon^2) \quad \text{as} \quad \epsilon \to 0 \ , \tag{3.14}$$

and therefore that the spreading speed of the periodic travelling wave solution to the heterogeneous IDE with decay parameter s differs from the spreading speed of the travelling wave solution to the homogeneous IDE with decay parameter s, i.e.

$$c(s,\epsilon) = c(s,0) + \mathrm{O}(\epsilon^2) \quad \text{as} \quad \epsilon \to 0 \ . \tag{3.15}$$

3. Use this to show that the asymptotic spread rates $c^*(\epsilon)$ and $c^*(0)$ of initially compact solutions to the heterogeneous and homogeneous IDEs differ by only $\mathrm{O}(\epsilon^2)$, i.e.

$$c^*(\epsilon) = c^*(0) + \mathrm{O}(\epsilon^2) \quad \text{as} \quad \epsilon \to 0 \ . \tag{3.16}$$

In Subsection 3.2.3, we will build on this approximation by finding the $\mathrm{O}(\epsilon^2)$ term in the expansion for $\rho(s,\epsilon)$ and using the first two non-zero terms in its expansion to approximate it, and therefore to generate an improved approximation for the asymptotic wave-speed $c^*(\epsilon)$. In Subsection 3.2.4, we will discuss extending the results in Subsections 3.2.1 - 3.2.2 to non-periodic stochastically generated landscapes.

3.2.1 Expansion of the Integral Operator

To show that the asymptotic wave-speeds of IDEs on weakly heterogeneous and homogeneous landscapes differ by $\mathrm{O}(\epsilon^2)$, it is necessary to expand the IDE and integral operator $F^{s,\epsilon}$ in terms of ϵ. To do this, the linearised population projection matrix $\mathbf{A}(y)$ and the dispersal kernel $\mathbf{K}(x-y,y)$ are expanded in terms of ϵ. Since the terms in (3.8) are $\mathrm{O}(\epsilon)$, the difference in each parameter from its spatial mean can be characterised by

$$q_1^i(x) = \frac{\alpha^i(x) - \alpha_0^i}{\epsilon \alpha_0^i} \quad \text{and} \quad Q_1^{i,j}(x) = \frac{A^{i,j}(x) - A_0^{i,j}}{\epsilon A_0^{i,j}} \ , \tag{3.17}$$

where $q_1^i(x)$ and $Q_1^{i,j}(x)$ are O(1) for all x in $[0, L)$. Rearranging in terms of the dispersal and demographic parameters,

$$\alpha^i(x) = \alpha_0^i(1 + \epsilon q_1^i(x)) = \alpha_0^i q^i \text{ and } A^{j,k}(x) = A_0^{j,k}(1 + \epsilon Q_1^{j,k}(x)) \ . \tag{3.18}$$

This allows the linearised population projection matrix to be written as

$$\mathbf{A}(x) = \mathbf{A}_0 + \epsilon \mathbf{A}_0 \circ \mathbf{Q}_1(x) \ . \tag{3.19}$$

To write the dispersal kernel in terms of the homogeneous kernel and terms of size ϵ, the heterogeneous dispersal kernel is expanded in terms of ϵ. The form of the dispersal kernel $\mathbf{K}(x - y, y)$ of dispersers from point y is dependent on the value of each of the scalar parameters $\alpha^1(y), \cdots, \alpha^n(y)$. At each y, the kernel can be written as

$$\begin{aligned}
\mathbf{K}(z, y) &= \mathbf{K}(z, \alpha^1(y), \cdots, \alpha^n(y)) \\
&= \mathbf{K}(z, \alpha_0^1 q^1, \cdots, \alpha_0^n q^n) \\
&= \mathbf{K}(z, \alpha_0^1[1 + \epsilon q_1^1(y)], \cdots, \alpha_0^n[1 + \epsilon q_1^n(y)]) \ .
\end{aligned}$$

The kernel can be expanded in terms of its Taylor series in the variables $q^1, \cdots, q^n$,

$$\begin{aligned}
\mathbf{K}(z, y) = \mathbf{K}(z, \alpha_0^1, \cdots, \alpha_0^n) &+ \epsilon \sum_{j=1}^{n} q_1^j(y) \frac{\partial \mathbf{K}}{\partial q^j}(z, \alpha_0^1, \cdots, \alpha_0^n) \\
&+ \frac{1}{2}\epsilon^2 \sum_{i,j=1}^{n} q_1^i(y) q_1^j(y) \frac{\partial^2 \mathbf{K}}{\partial q^i \partial q^j}(z, \alpha_0^1, \cdots, \alpha_0^n) + \mathrm{O}(\epsilon^3) \\
= \mathbf{K}_0(z) &+ \epsilon \sum_{j=1}^{n} q_1^j(y) \mathbf{K}^j(z) + \frac{1}{2}\epsilon^2 \sum_{i,j=1}^{n} q_1^i(y) q_1^j(y) \mathbf{K}^{i,j}(z) + \mathrm{O}(\epsilon^3)
\end{aligned}$$

where $\mathbf{K}^j(z)$ is the parital derivative of $\mathbf{K}$ with respect to q^j and $\mathbf{K}^{i,j}(z)$ is the second partial derivative of $\mathbf{K}$ with respect to q^i and q^j. Defining the matrix coefficients of

ϵ and ϵ^2 as $\mathbf{K}_1(z,y)$ and $\mathbf{K}_2(z,y)$, the dispersal kernel can be written as

$$\mathbf{K}(z,y) = \mathbf{K}_0(z) + \epsilon\mathbf{K}_1(z,y) + \epsilon^2\mathbf{K}_2(z,y) + \mathrm{O}(\epsilon^3) \ . \tag{3.20}$$

Substituting the asymptotic expansions of the demographic dispersal matrix (3.19) and the dispersal kernel (3.20) into the expression for the operator $F^{s,\epsilon}$ (3.11), yields

$$\begin{aligned}
F^{s,\epsilon}\left[\boldsymbol{\phi}\right](x) =& \int_{-\infty}^{\infty} \left[\mathbf{K}(x-y,y) \circ \mathbf{A}\left(y\right)\right] \mathrm{e}^{s(x-y)}\boldsymbol{\phi}(y)\mathrm{d}y \\
=& \int_{-\infty}^{\infty} \left[(\mathbf{K}_0(x-y) + \epsilon\mathbf{K}_1(x-y,y)) \circ (\mathbf{A}_0 + \epsilon\mathbf{A}_0 \circ \mathbf{Q}_1(y))\right] \mathrm{e}^{s(x-y)}\boldsymbol{\phi}(y)\mathrm{d}y + \mathrm{O}(\epsilon^2) \\
=& \int_{-\infty}^{\infty} \left[\mathbf{K}_0(x-y) \circ \mathbf{A}_0\right] \mathrm{e}^{s(x-y)}\boldsymbol{\phi}(y)\mathrm{d}y \\
&+ \epsilon \int_{-\infty}^{\infty} \left[\mathbf{A}_0 \circ (\mathbf{K}_0(x-y) \circ \mathbf{Q}_1(y) + \mathbf{K}_1(x-y,y))\right] \mathrm{e}^{s(x-y)}\boldsymbol{\phi}(y)\,\mathrm{d}y + \mathrm{O}(\epsilon^2) \\
=& F^{s,0}\left[\boldsymbol{\phi}\right](x) + \epsilon F_1^s\left[\boldsymbol{\phi}\right](x) + \mathrm{O}(\epsilon^2) \ ,
\end{aligned} \tag{3.21}$$

giving the expansion of the operator $F^{s,\epsilon}$ in ϵ. In addition, by Conditions VI and VII, $q_1^i(x)$ and $Q_1^{i,j}(x)$ satisfy

$$\int_0^L q_1^i(x)\mathrm{d}x = 0 \quad \text{and} \quad \int_0^L Q_1^{j,k}(x)\mathrm{d}x = 0 \ . \tag{3.22}$$

Given that $\int_0^L q_1^j(y)\mathrm{d}y = 0$ (Condition VI), the spatial average of $\mathbf{K}_1(z,x)$ in x over $[0,L)$ is given by

$$\begin{aligned}
\int_0^L \mathbf{K}_1(z,y)\mathrm{d}y &= \sum_{j=1}^{n} \left(\int_0^L q_1^j(y)\mathrm{d}y\right) \mathbf{K}^j(z) \\
&= 0
\end{aligned}$$

for all $z \in \mathbb{R}$.

3.2.2 Expansion of the Principal Eigenvalue

The wave-speed in (3.9) depends on the principal eigenvalues $\rho(s,\epsilon)$ of the family of operators $F^{s,\epsilon}$. In the previous subsection, the operator $F^{s,\epsilon}$ was expanded in terms of ϵ, with expressions found explicitly for the first two terms, and the spatial means of $\mathbf{Q}(x)$ and $\mathbf{K}_1(z,x)$ in x over $[0,L)$ shown to be zero. This expansion of $F^{s,\epsilon}$ is now used to find an expansion for the principal eigenvalues of $F^{s,\epsilon}$, which satisfy the dispersion relation

$$\rho(s,\epsilon)\boldsymbol{\phi}_s(x) = F^{s,\epsilon}[\boldsymbol{\phi}_s](x) \ . \tag{3.23}$$

Substituting (3.21) into (3.23), the dispersion relation becomes

$$\rho(s,\epsilon)\boldsymbol{\phi}_s(x) = F^{s,0}\left[\boldsymbol{\phi}_s\right](x) + \epsilon F_1^s\left[\boldsymbol{\phi}_s\right](x) + \mathrm{O}(\epsilon^2) \ . \tag{3.24}$$

This is a regular perturbation problem, and can be solved by substituting asymptotic expansions of $\boldsymbol{\phi}_s(x)$ and $\rho(s,\epsilon)$ in ϵ,

$$\begin{aligned}\boldsymbol{\phi}_s(x) =& \boldsymbol{\phi}_{s,0}(x) + \epsilon\boldsymbol{\phi}_{s,1}(x) + \epsilon^2\boldsymbol{\phi}_{s,2}(x) + \cdots \\ \rho(s,\epsilon) =& \rho_0(s) + \epsilon\rho_1(s) + \epsilon^2\rho_2(s) + \cdots \ .\end{aligned}$$

Substituting these into (3.24), the O(1) terms satisfy

$$\rho_0(s)\boldsymbol{\phi}_{s,0}(x) = (F^0\boldsymbol{\phi}_{s,0})(x) \ , \tag{3.25}$$

i.e. $\rho_0(s)$ is the principal eigenvalue of the unperturbed homogeneous operator $F^{s,0}$,

$$\rho_0(s) = \rho(s,0) \tag{3.26}$$

and has the corresponding eigenvector $\boldsymbol{\phi}_{s,0}$. This eigenvector is a constant vector-

valued function and is equal to the principal eigenvector of the element-wise product of the moment-generating function $\mathbf{M}_0(s)$ of the O(1) component of the dispersal kernel $\mathbf{K}_0(z)$ and the demographic matrix $\mathbf{A}_0$. As $\mathbf{M}_0(s) \circ \mathbf{A}_0$ is either positive, or nonnegative and primitive (Condition I), by the Perron-Frobenius Theorem, every element of its principal eigenvector $\boldsymbol{\psi}_s$ (corresponding to the principal eigenvalue) is positive. Aside from multiples of this eigenvector, it has no other eigenvectors with non-negative elements. The spatially constant vector-valued function equal to $\boldsymbol{\psi}_s$ is an eigenvector of $F^{s,0}$ with eigenvalue λ,

$$\begin{aligned} F^{s,0}\boldsymbol{\psi}_s &= \int_{-\infty}^{\infty} \left[\mathbf{K}_0(x-y) \circ \mathbf{A}_0\right] \mathrm{e}^{s(x-y)} \boldsymbol{\psi}_s \mathrm{d}y \\ &= \left[\int_{-\infty}^{\infty} \mathbf{K}_0(z) \mathrm{e}^{sz} \mathrm{d}z \circ \mathbf{A}_0\right] \boldsymbol{\psi}_s \\ &= \left[\mathbf{M}_0 \circ \mathbf{A}_0\right] \boldsymbol{\psi}_s \\ &= \lambda \boldsymbol{\psi}_s \ . \end{aligned}$$

We now show that $\boldsymbol{\psi}_s$ is the principal eigenvector of $F^{s,0}$. As the principal eigenvalue is the largest eigenvalue, $\rho(s,0) \geq \lambda$. In addition, any eigenvector of $F^{s,0}$ is a bounded periodic function, so is bounded above by some multiple of any spatially constant positive vector-valued function. Thus the principal eigenvector $\mathbf{w}$ is bounded above by some multiple C of $\boldsymbol{\psi}_s$. Since $F^{s,0}$ is order-preserving for non-negative vector-valued functions,

$$\left(F^{s,0}\right)^N \mathbf{w} \leq C \left(F^{s,0}\right)^N \boldsymbol{\psi}_s \quad \text{for all } N > 0$$

and

$$\rho(s,0)^N \mathbf{w} \leq C\lambda^N \boldsymbol{\psi}_s \quad \text{for all } N > 0$$

so, $\rho(s,0) \geq \lambda$ and $\lambda = \rho(s,0)$. So $\boldsymbol{\psi}_s$ is the principal eigenvector of $F^{s,0}$.

In the inner product space $L^2([0,L))$, the adjoint operator $F^{s,0\,*}$ of $F^{s,0}$ is given by

$$(F^{s,0\,*}\mathbf{u})(x) = \int_{-\infty}^{\infty} \left[\mathbf{K}_0(x-y)\mathrm{e}^{s(x-y)} \circ \mathbf{A}_0\right]^T \mathbf{u}(y)\,\mathrm{d}y \ . \tag{3.27}$$

The principal eigenvector $\boldsymbol{\phi}^*_{s,0}$ of the adjoint operator corresponding to the principal eigenvalue $\rho(s,0)$ is equal to the spatially constant left eigenvector $\tilde{\boldsymbol{\psi}}_s$ of $\mathbf{M}_0(s) \circ \mathbf{A}_0$. The $\mathrm{O}(\epsilon)$ terms in the eigenvalue equation satisfy

$$(F^{s,0} - \rho(s,0))\boldsymbol{\phi}_{s,1} + (F^s_1 - \rho_1(s))\boldsymbol{\phi}_{s,0} = 0 \ . \tag{3.28}$$

Taking the inner product of the first term on the LHS with $\boldsymbol{\phi}^*_{s,0}$ yields

$$\langle \boldsymbol{\phi}^*_{s,0} | (F^{s,0} - \rho(s,0))\boldsymbol{\phi}_{s,1}\rangle = \langle (F^{s,0\,*} - \rho(s,0))\boldsymbol{\phi}^*_{s,0} | \boldsymbol{\phi}_{s,1}\rangle = 0 \tag{3.29}$$

so the inner product of the second term in (3.28) and $\boldsymbol{\phi}^*_{s,0}$ is equal to zero, i.e.

$$\langle \boldsymbol{\phi}^*_{s,0} | (F^s_1 - \rho_1(s))\boldsymbol{\phi}_{s,0}\rangle = 0 \ ; \tag{3.30}$$

rearranging, this gives an expression for $\rho_1(s)$,

$$\rho_1(s) = \frac{\langle \boldsymbol{\phi}^*_{s,0} | F^s_1 \boldsymbol{\phi}_{s,0}\rangle}{\langle \boldsymbol{\phi}^*_{s,0} | \boldsymbol{\phi}_{s,0}\rangle} \ . \tag{3.31}$$

We have found $\boldsymbol{\phi}^*_{s,0}$ and $\boldsymbol{\phi}_{s,0}$ to be constant and equal to $\tilde{\boldsymbol{\psi}}_s$ and $\boldsymbol{\psi}_s$, respectively. Without loss of generality, we choose $\langle \tilde{\boldsymbol{\psi}}_s | \boldsymbol{\psi}_s\rangle = 1$, so

$$\rho_1(s) = \frac{1}{L}\int_0^L \tilde{\boldsymbol{\psi}}_s \cdot (F^s_1 \boldsymbol{\psi}_s)(x)\mathrm{d}x \ . \tag{3.32}$$

Using the definition of F^s_1 in (3.21), (3.32) becomes

$$\rho_1(s) = \frac{1}{sL}\int_0^L \tilde{\boldsymbol{\psi}}_s \cdot \int_{-\infty}^{\infty} \left[\mathbf{A}_0 \circ (\mathbf{K}_0(x-y) \circ \mathbf{Q}_1(y) + \mathbf{K}_1(x-y,y))\right] \mathrm{e}^{s(x-y)}\, \boldsymbol{\psi}_s \mathrm{d}y\mathrm{d}x \ . \tag{3.33}$$

To evaluate this, the following change of variables is introduced

$$w = x - y \quad \text{and} \quad z = y \tag{3.34}$$

and (3.33) becomes

$$\begin{aligned}\rho_1(s) &= \frac{1}{sL}\tilde{\boldsymbol{\psi}}_s \cdot \left[\mathbf{A}_0 \circ \int_{-\infty}^{\infty}\int_{-w}^{L-w} (\mathbf{K}_0(w) \circ \mathbf{Q}_1(z) + \mathbf{K}_1(w,z))\, \mathrm{e}^{sw}\, \mathrm{d}z\mathrm{d}w\right] \boldsymbol{\psi}_s \\ &= \frac{1}{sL}\tilde{\boldsymbol{\psi}}_s \cdot \left[\mathbf{A}_0 \circ \left(\mathbf{M}_0(s) \circ \int_{-w}^{L-w} \mathbf{Q}_1(z)\mathrm{d}z + \int_{-\infty}^{\infty}\int_{-w}^{L-w} \mathbf{K}_1(w,z)\mathrm{d}z\, \mathrm{e}^{sw}\, \mathrm{d}w\right)\right] \boldsymbol{\psi}_s \ .\end{aligned} \tag{3.35}$$

Since $\mathbf{Q}_1(z)$ and $\mathbf{K}_1(w,z)$ are L-periodic in z and $\int_0^L \mathbf{Q}_1(x)\mathrm{d}x = \mathbf{O}$ and $\int_0^L \mathbf{K}_1(w,x)\mathrm{d}x = \mathbf{O}$ for all $w \in \mathbb{R}$,

$$\int_{-w}^{L-w} \mathbf{Q}_1(z)\mathrm{d}z = \mathbf{O} \quad \text{and} \quad \int_{-w}^{L-w} \mathbf{K}_1(w,z)\mathrm{d}z = \mathbf{O} \ , \tag{3.36}$$

and therefore

$$\rho_1(s) = 0 \ . \tag{3.37}$$

This means that

$$\rho(s,\epsilon) = \rho(s,0) + \mathrm{O}(\epsilon^2) \quad \text{as} \quad \epsilon \to 0 \tag{3.38}$$

and

$$c(s,\epsilon) = \frac{1}{s}\log(\rho(s,0) + \mathrm{O}(\epsilon^2)) \\ = c(s,0) + \mathrm{O}(\epsilon^2) \quad \text{as} \quad \epsilon \to 0 \ . \tag{3.39}$$

Specifically, for each value of s, the difference between the wave-speeds of the solutions to the heterogeneous and homogeneous IDEs are bounded by a multiple of ϵ^2,

$$|c(s,\epsilon) - c(s,0)| < R(s)\epsilon^2 \quad \text{as} \quad \epsilon \to 0 \ . \tag{3.40}$$

However the s-dependence (a lack of *uniform convergence*) means that, on its own, this is not enough to show that the asymptotic wave-speeds $c^*(\epsilon)$ and $c^*(0)$ (the minima of $c(s,\epsilon)$ and $c(s,0)$) differ by $\mathrm{O}(\epsilon^2)$ in the $\epsilon \to 0^+$ limit. To overcome this, we assume that

$$A(s,\epsilon) = \frac{c(s,\epsilon) - c(s,0)}{\epsilon^2} \tag{3.41}$$

is bounded and that for sufficiently small ϵ (i.e. $\epsilon \in [0,\epsilon^*]$, where $\epsilon^* > 0$),

$$|A(s,\epsilon)| < \tilde{A} \quad \text{for all} \ \ s > 0 \ , \tag{3.42}$$

otherwise the perturbation theory breaks down, with such terms dominating leading terms. However, we do not exclude the possibility that a solution lies beyond the scope of perturbation theory. This means that

$$|c(s,\epsilon) - c(s,0)| < \tilde{A}\epsilon^2 \quad \text{as} \quad \epsilon \to 0 \quad \text{for all} \ \ s > 0 \ . \tag{3.43}$$

This gives us the following inequalities for all $s > 0$ and $0 \leq \epsilon \leq \epsilon^*$

$$c(s,\epsilon) < c(s,0) + \tilde{A}\epsilon^2 \quad \text{and} \quad c(s,0) < c(s,\epsilon) + \tilde{A}\epsilon^2 \ . \tag{3.44}$$

This allows us to show that,

$$c^*(\epsilon) = \min_{s>0} c(s,\epsilon) \leq c(s,\epsilon) < c(s,0) + \tilde{A}\epsilon^2 \tag{3.45}$$

$$c^*(0) = \min_{s>0} c(s,0) \leq c(s,0) < c(s,\epsilon) + \tilde{A}\epsilon^2 \ . \tag{3.46}$$

Taking the minimum of the RHS in s in (3.45) and (3.46), we have that

$$c^*(\epsilon) < c^*(0) + \tilde{A}\epsilon^2 \quad \text{and} \quad c^*(0) < c^*(\epsilon) + \tilde{A}\epsilon^2 \ . \tag{3.47}$$

Rearranging, we have that for all $0 \leq \epsilon \leq \epsilon^*$,

$$|c^*(\epsilon) - c^*(0)| < \tilde{A}\epsilon^2 \ . \tag{3.48}$$

So the asymptotic wave-speeds $c^*(\epsilon)$ and $c^*(0)$ satisfy

$$c^*(\epsilon) = c^*(0) + \mathrm{O}(\epsilon^2) \ \text{ as } \ \epsilon \to 0^+ \ .$$

Thus the spreading speed of the weakly heterogeneous and homogeneous IDEs differ by a factor of ϵ^2, justifying the use of the homogeneous spreading speed as an approximation to the spreading speeds of IDEs on weakly heterogeneous landscapes. The homogeneous (zeroth order) appproximation is given by

$$c_0^*(\epsilon) = c^*(0) = \min_{s>0} \left\{ \frac{1}{s} \log \left(\tilde{\boldsymbol{\psi}}_s \cdot \mathbf{M}_0(s) \boldsymbol{\psi}_s \right) \right\} \ . \tag{3.49}$$

3.2.3 Derivation of the Wave-Speed Approximation

We have seen that the homogeneous approximation is better than expected (the error scales with the square of the environmental variation coefficient ϵ^2 rather than ϵ). However, as ϵ is increased, the homogeneous approximation becomes less accurate. When this occurs, or a more exact result is required, a second order approximation can be found. When Conditions I-VII are satisfied, this approach is justified for

non-stage-structured populations. The extension of these results to stage-structured populations implicitly requires the conjecture that the spreading speeds of populations satisfying Conditions I-VII are linearly determined, which has not been proven. To find the second order approximation, the asymptotic analysis developed in Section 3.2.2 is used to find the coefficient of the $\mathrm{O}(\epsilon^2)$ term in the expansion of the wave-speed $c^*(\epsilon)$. The $\mathrm{O}(\epsilon^2)$ approximation $c_2^*(\epsilon)$ is given by approximating the eigenvalue $\rho(s,\epsilon)$ by the first two non-zero terms in its expansion in ϵ. The $c_2^*(\epsilon)$ approximation to $c^*(\epsilon)$ is given by

$$c_2^*(\epsilon) = \min_{s>0}\left[\frac{1}{s}\log\left(\rho(s,0) + \epsilon^2\rho_2(s)\right)\right] \ , \tag{3.50}$$

where $\rho(s,0)$ is the eigenvalue of the element-wise product of the linearised homogeneous population projection matrix $\mathbf{A}_0$ and the moment generating function of the homogeneous matrix of dispersal kernels $\int_{-\infty}^{\infty} K_0(z)\mathrm{e}^{sz}\mathrm{d}z$. To express $\rho_2(s)$ in terms of known quantities, $F^{s,\epsilon}$ is expanded to second order, i.e.

$$\rho(s,\epsilon)\boldsymbol{\phi}_s(x) = \left(F^{s,0} + \epsilon F_1^s + \epsilon^2 F_2^s\right)\left[\boldsymbol{\phi}_s\right](x) + \mathrm{O}(\epsilon^3) \ , \tag{3.51}$$

where F_2^s is given by

$$F_2^s[\boldsymbol{\phi}](x) = \int_{-\infty}^{\infty}\left[\mathbf{A}_0 \circ (\mathbf{K}_1(x-y,y)\circ\mathbf{Q}_1(y) + \mathbf{K}_2(x-y,y))\right]\mathrm{e}^{s(x-y)}\boldsymbol{\phi}(y)\,\mathrm{d}y \ . \tag{3.52}$$

The $\mathrm{O}(\epsilon^2)$ terms in the eigenvalue equation (3.23) are

$$(F^{s,0} - \rho(s,0))\boldsymbol{\phi}_{s,2} + (F_1^s - \rho_1(s))\boldsymbol{\phi}_{s,1} + (F_2^s - \rho_2(s))\boldsymbol{\phi}_{s,0} = 0 \ . \tag{3.53}$$

Taking the inner product with $\boldsymbol{\phi}_{s,0}^*$, and using the properties of adjoint operators, we eliminate the $\boldsymbol{\phi}_{s,2}$ term,

$$\langle\boldsymbol{\phi}_{s,0}^*|(F^{s,0} - \rho(s,0))\boldsymbol{\phi}_{s,2}\rangle = \langle(F^{s,0*} - \rho(s,0))\boldsymbol{\phi}_{s,0}^*|\boldsymbol{\phi}_{s,2}\rangle = 0 \ , \tag{3.54}$$

and so, given that $\rho_1(s) = 0$, the inner product of $\boldsymbol{\phi}^*_{s,0}$ and the remaining terms in (3.53) is

$$\langle \boldsymbol{\phi}^*_{s,0} | F^s_1 \boldsymbol{\phi}_{s,1} \rangle + \langle \boldsymbol{\phi}^*_{s,0} | (F^s_2 - \rho_2(s)) \boldsymbol{\phi}_{s,0} \rangle = 0 \ . \tag{3.55}$$

Rearranging and using the definitions of the spatially constant eigenvectors in Section 3.2.2, $\boldsymbol{\phi}^*_{s,0} = \tilde{\boldsymbol{\psi}}_s$ and $\boldsymbol{\phi}_{s,0} = \boldsymbol{\psi}_s$ such that $\langle \tilde{\boldsymbol{\psi}}_s | \boldsymbol{\psi}_s \rangle = 1$, we have

$$\rho_2(s) = \frac{1}{L} \langle \boldsymbol{\phi}^*_{s,0} | F^s_1 \boldsymbol{\phi}_{s,1} + F^s_2 \boldsymbol{\phi}_{s,0} \rangle \tag{3.56}$$

$$\begin{aligned} = \frac{1}{L} \tilde{\boldsymbol{\psi}}_s \cdot \Bigg\{ & \int_0^L \int_{-\infty}^{\infty} \mathbf{A}_0 \circ \left[\sum_{j=1}^{n} q_1^j(y) \mathbf{K}^j(x-y) + \mathbf{K}_0(x-y) \circ \mathbf{Q}_1(y) \right] \\ & \mathrm{e}^{s(x-y)} \boldsymbol{\phi}_{s,1}(y) \mathrm{d}y \mathrm{d}x + \int_0^L \int_{-\infty}^{\infty} \mathbf{A}_0 \circ \Bigg[\frac{1}{2} \sum_{i,j=1}^{n} q_1^i(y) q_1^j(y) \mathbf{K}^{i,j}(x-y) \\ & + \sum_{j=1}^{n} q_1^j(y) \mathbf{K}^j(x-y) \circ \mathbf{Q}_1(y) \Bigg] \mathrm{e}^{s(x-y)} \mathrm{d}y \mathrm{d}x \, \boldsymbol{\psi}_s \Bigg\} \ . \end{aligned} \tag{3.57}$$

To evaluate this, we need an expression for $\boldsymbol{\phi}_{s,1}$. To do this, we again consider the $\mathrm{O}(\epsilon)$ terms in (3.23) which, given that $\rho_1(s) = 0$, is

$$(F^{s,0} - \rho(s,0)) \boldsymbol{\phi}_{s,1} + F^s_1 \boldsymbol{\phi}_{s,0} = 0 \tag{3.58}$$

where $\boldsymbol{\phi}_{s,1}$ is L-periodic. This becomes

$$\begin{aligned} & \int_{-\infty}^{\infty} \left[\mathbf{A}_0 \circ \mathbf{K}_0(x-y) \mathrm{e}^{s(x-y)} \right] \boldsymbol{\phi}_{s,1}(y) \mathrm{d}y - \rho(s,0) \boldsymbol{\phi}_{s,1}(x) \\ & + \int_{-\infty}^{\infty} \left[\sum_{j=1}^{n} q_1^j(y) \mathbf{K}^j(x-y) \circ \mathbf{A}_0 + \mathbf{K}_0(x-y) \circ \mathbf{A}_0 \circ \mathbf{Q}_1(y) \right] \mathrm{e}^{s(x-y)} \boldsymbol{\psi}_s \mathrm{d}y = 0 \ , \end{aligned} \tag{3.59}$$

with boundary conditions $\boldsymbol{\phi}_{s,1}(0) = \boldsymbol{\phi}_{s,1}(L)$. To find $\boldsymbol{\phi}_{s,1}(x)$, we take the Fourier

transform of (3.59). This gives us the following expression for $\boldsymbol{\phi}_{s,1}(x)$,

$$\begin{aligned}\hat{\boldsymbol{\phi}}_{s,1}(\eta) =& \left[\rho(s,0)\mathbf{I} - \mathbf{A}_0 \circ \mathbf{M}_0(s-2\pi i\eta)\right]^{-1} \mathbf{A}_0 \\ & \circ \left[\mathbf{M}_0(s-2\pi i\eta) \circ \hat{\mathbf{Q}}_1(\eta) + \sum_{j=1}^{n} \hat{q}_1^j(\eta)\mathbf{M}^j(s-2\pi i\eta)\right] \boldsymbol{\psi}_s \ .\end{aligned}$$

where $\hat{}$ denotes the Fourier transform.

The expression for $\rho_2(s)$ is then given by

$$\begin{aligned}\rho_2(s) =& \frac{1}{L}\int_0^L \tilde{\boldsymbol{\psi}}_s \int_{-\infty}^{\infty}\int_{-\infty}^{\infty} \Big[\mathbf{A}_0 \circ \Big(\mathbf{M}_0(s-2\pi i\xi) \circ \hat{\mathbf{Q}}_1(\xi-\eta) \\ & + \sum_{j=1}^{n} \hat{q}_1^j(\xi-\eta)\mathbf{M}^j(s-2\pi i\xi)\Big)\Big] \left[\rho(s,0)\mathbf{I} - \mathbf{A}_0 \circ \mathbf{M}_0(s-2\pi i\eta)\right]^{-1} \\ & \cdot \left[\mathbf{A}_0 \circ \left(\mathbf{M}_0(s-2\pi i\eta) \circ \hat{\mathbf{Q}}_1(\eta) + \sum_{j=1}^{n} \hat{q}_1^j(\eta)\mathbf{M}^j(s-2\pi i\eta)\right)\right] \\ & + \left[\mathbf{A}_0 \left(\sum_{j=1}^{n} \hat{q}_1^j(\xi-\eta)\mathbf{M}^j(s-2\pi i\xi) \circ \hat{\mathbf{Q}}_1(\eta)\right.\right. \\ & \left.\left. + \frac{1}{2}\sum_{i,j=1}^{n} \hat{q}_1^i(\xi-\eta)\hat{q}_1^j(\eta)\mathbf{M}^{i,j}(s-2\pi i\xi)\right)\right] \mathrm{d}\eta\boldsymbol{\psi}_s \mathrm{e}^{2\pi i\xi x}\mathrm{d}\xi\mathrm{d}x \ . \end{aligned} \tag{3.60}$$

Since $\mathbf{Q}_1(x)$ and $q_1^j(x)$ are L-periodic and have spatial average $\mathbf{O}_N$ (the $N \times N$ matrix of zeros) and 0, we can write them as Fourier series with the constant terms $\mathbf{C}_0$ and γ_0^j equal to zero,

$$\mathbf{Q}_1(x) = \sum_{n\neq 0} \mathbf{C}_n \exp\left(\frac{2\pi inx}{L}\right) \quad \text{and} \quad q_1^j(x) = \sum_{n\neq 0} \gamma_n^j \exp\left(\frac{2\pi inx}{L}\right) \tag{3.61}$$

where $\mathbf{C}_{-n} = \bar{\mathbf{C}}_n$ and $\gamma_{-n} = \bar{\gamma}_n$ for all j and all $n \in \mathbb{N}$. The Fourier transforms of $\mathbf{Q}_1(x)$ and q_1^j are

$$\hat{\mathbf{Q}}_1(\xi) = \sum_{n\neq 0} \mathbf{C}_n \delta\left(\xi - \frac{n}{L}\right) \quad \text{and} \quad \hat{q}_1^j(\xi) = \sum_{n\neq 0} \gamma_n^j \delta\left(\xi - \frac{n}{L}\right) \ . \tag{3.62}$$

Substituting these into (3.60), we get

$$\begin{aligned}\rho_2(s) = \tilde{\boldsymbol{\psi}}_s \Bigg(& \sum_{n\neq 0} \left[\mathbf{A}_0 \circ \left(\mathbf{M}_0(s) \circ \mathbf{C}_{-n} + \sum_{j=1}^{n} \gamma_{-n}^{j} \mathbf{M}^{j}(s) \right) \right] \\ & \cdot \left[\rho(s,0)\mathbf{I} - \mathbf{A}_0 \circ \mathbf{M}_0 \left(s - \frac{2\pi i n}{L} \right) \right]^{-1} \\ & \cdot \left[\mathbf{A}_0 \circ \left(\mathbf{M}_0 \left(s - \frac{2\pi i n}{L} \right) \circ \mathbf{C}_n + \sum_{j=1}^{n} \gamma_n^j \mathbf{M}^j \left(s - \frac{2\pi i n}{L} \right) \right) \right] \\ & + \left[\mathbf{A}_0 \circ \left(\sum_{j=1}^{n} \gamma_{-n}^{j} \mathbf{M}^{j}(s) \circ \mathbf{C}_n + \frac{1}{2} \sum_{i,j=1}^{n} \gamma_{-n}^{i} \gamma_n^j \mathbf{M}^{i,j}(s) \right) \right] \Bigg) \boldsymbol{\psi}_s \ . \end{aligned} \tag{3.63}$$

In (3.50), we defined the second order approximation for the asymptotic wave-speed of solutions to the models with initial compact support in terms of $\rho(s,0)$ and $\rho_2(s)$. Substituting (3.63) into (3.50), we obtain the expressions for c_2^*,

$$c_2^*(\epsilon) = \min_{s>0} \left\{ \frac{1}{s} \log \left(\tilde{\boldsymbol{\psi}}_s \cdot \left[\mathbf{M}_0(s) \circ \mathbf{A}_0 + \epsilon^2 \mathbf{H}_2(s) \right] \boldsymbol{\psi}_s \right) \right\} \tag{3.64}$$

where $\mathbf{M}_0(s)$ is the moment generating function of the homogeneous kernel matrix $\mathbf{K}_0(z)$ and $\mathbf{A}_0$ is the homogeneous intrinsic population projection matrix. $\tilde{\boldsymbol{\psi}}_s$ and $\boldsymbol{\psi}_s$ are respectively, left and right eigenvectors of $\mathbf{M}_0(s) \circ \mathbf{A}_0$ chosen such that $\langle \tilde{\boldsymbol{\psi}}_s | \boldsymbol{\psi}_s \rangle = 1$, ϵ is the parameter determining the relative scale of the heterogeneity and $\mathbf{H}_2(s)$ is

$$\begin{aligned}\mathbf{H}_2(s) = \sum_{n\neq 0} \Bigg(& \left[\mathbf{A}_0 \circ \left(\mathbf{M}_0(s) \circ \mathbf{C}_{-n} + \sum_{j=1}^{n} \gamma_{-n}^{j} \mathbf{M}^{j}(s) \right) \right] \\ & \cdot \left[\left(\tilde{\boldsymbol{\psi}}_s \cdot \left[\mathbf{A}_0 \circ \mathbf{M}_0(s) \right] \boldsymbol{\psi}_s \right) \mathbf{I} - \mathbf{A}_0 \circ \mathbf{M}_0 \left(s - \frac{2\pi i n}{L} \right) \right]^{-1} \\ & \cdot \left[\mathbf{A}_0 \circ \left(\mathbf{M}_0 \left(s - \frac{2\pi i n}{L} \right) \circ \mathbf{C}_n + \sum_{j=1}^{n} \gamma_n^j \mathbf{M}^j \left(s - \frac{2\pi i n}{L} \right) \right) \right] \\ & + \left[\mathbf{A}_0 \circ \left(\sum_{j=1}^{n} \gamma_{-n}^{j} \mathbf{M}^{j}(s) \circ \mathbf{C}_n + \frac{1}{2} \sum_{i,j=1}^{n} \gamma_{-n}^{i} \gamma_n^j \mathbf{M}^{i,j}(s) \right) \right] \Bigg) \ . \end{aligned} \tag{3.65}$$

$\mathbf{M}^j(s)$ is the moment generating function of the first derivative of the kernel $\mathbf{K}$ with respect to q^j, $\mathbf{M}^{i,j}(s)$ is the moment generating function of the second derivative of

$\mathbf{K}$ with respect to q^i and q^j, and $\mathbf{C}_n$ and γ_n^j are the coefficients in the Fourier series of $\mathbf{Q}_1(x)$ and $q_1^j(x)$, i.e.

$$\mathbf{Q}_1(x) = \sum_{n\neq 0} \mathbf{C}_n \exp\left(\frac{2\pi i n x}{L}\right) \quad \text{and} \quad q_1^j(x) = \sum_{n\neq 0} \gamma_n^j \exp\left(\frac{2\pi i n x}{L}\right) \ . \tag{3.66}$$

For non-stage-structured populations, the expression for $c_2^*(\epsilon)$ is more concise. The $\mathrm{O}(\epsilon^2)$ approximation $c_2^*(\epsilon)$ to the asymptotic wave-speed is given by

$$c_2^*(\epsilon) = \min_{s>0}\left\{\frac{1}{s}\log\left(r_0 M_0(s) + \epsilon^2 H_2(s)\right)\right\} \ , \tag{3.67}$$

where r_0 is the intrinsic population growth rate, $M_0(s)$ is the moment generating function of the homogeneous kernel $K_0(z)$ and $H_2(s)$ is given by

$$\begin{aligned} H_2(s) =& r_0 \sum_{n\neq 0}\left[\left(M_0(s) - M_0\left(s - \frac{2\pi i n}{L}\right)\right)^{-1}\left(C_{-n}M_0(s) + \sum_{j=1}^{n}\gamma_{-n}^j M^j(s)\right)\right. \\ &\cdot\left(C_n M_0\left(s - \frac{2\pi i n}{L}\right) + \sum_{j=1}^{n}\gamma_n^j M^j\left(s - \frac{2\pi i n}{L}\right)\right) \\ &\left. + \sum_{j=1}^{n}\gamma_{-n}^j M^j(s) C_n + \frac{1}{2}\sum_{i,j=1}^{n}\gamma_{-n}^i\gamma_n^j M^{i,j}(s)\right] \ , \end{aligned} \tag{3.68}$$

where $M^j(s)$ is the moment generating function of the first derivative of the kernel K with respect to q^j, $M^{i,j}(s)$ is the moment generating function of the second derivative of K with respect to q^i and q^j, and where the C_n and γ_n^j are the coefficients in the Fourier series of $Q_1(x)$ and $q_1^j(x)$, i.e.

$$Q_1(x) = \sum_{n\neq 0} C_n \exp\left(\frac{2\pi i n x}{L}\right) \quad \text{and} \quad q_1^j(x) = \sum_{n\neq 0} \gamma_n^j \exp\left(\frac{2\pi i n x}{L}\right) \ . \tag{3.69}$$

3.2.4 Extension to Non-Periodic Landscapes

In the previous subsections, we showed analytically that the homogeneous approximation is better than expected for periodic landscapes with small ϵ and derived a second order approximation to the wave-speed for periodic landscapes. To do this, we have required the landscape to be periodic. We now discuss the possibility of extending these results to non-periodic landscapes.

For periodic landscapes, we can assume that solutions to the linearised IDE are periodic travelling waves. This allows us to formulate a dispersion relation (the eigenvalue problem) for the wave-speed $c(s)$ of the solution to the linearised IDE for each value of the decay rate s. We can then take the minimum of $c(s)$ as the asymptotic wave-speed for solutions with initial conditions with compact support.

If the landscape is non-periodic (e.g. stochastically generated or quasi-periodic), then these methods cannot be applied. However, while it is not clear whether the approximation presented in Subsection 3.2.3 can be generalised to non-periodic landscapes, through the numerical simulations presented in Subsection 3.3.2 we see that the wave-speeds of solutions to IDEs on weakly heterogeneous stochastically-generated landscapes differ from their spatial homogenisations by $\mathrm{o}(\epsilon)$ (i.e. as ϵ is made arbitrarily small, the difference becomes smaller than any factor of ϵ). In Subsection 3.3.2 we will consider IDEs on landscapes satisfying Conditions I-V and an additional condition:

VII.b. The dispersal kernel $\mathbf{K}(z,x)$ is determined by a number of spatially varying parameters $\alpha^j(x)$. These parameters, together with the elements $A^{i,j}(x)$ of the intrinsic population projection matrix $\mathbf{A}(x) = \mathbf{B}(\mathbf{0},x)$, are small bounded perturbations from their spatial mean. In detail, let α_0^j and $A_0^{i,j}$ denote the spatial means of $\alpha^j(x)$ and $A^{i,j}(x)$, i.e.

$$\alpha_0^j = \lim_{P\to\infty} \frac{1}{2P}\int_{-P}^{P} \alpha^j(x)\mathrm{d}x \quad \text{and} \quad A_0^{i,j} = \lim_{L\to\infty} \frac{1}{2P}\int_{-P}^{P} A^{i,j}(x)\mathrm{d}x \ ; \qquad (3.70)$$

then, for $\epsilon \ll 1$, we have that for all $x \in \mathbb{R}$

$$\left|\frac{\alpha^j(x) - \alpha_0^j}{\alpha_0^j}\right| \sim \mathrm{O}(\epsilon) \quad \text{and} \quad \left|\frac{A^{i,j}(x) - A_0^{i,j}}{A_0^{i,j}}\right| \sim \mathrm{O}(\epsilon) \ . \tag{3.71}$$

This condition ensures that while the spatial average of any parameter over a given interval is stochastically generated, the spatial average of a given parameter tends to a fixed value as $P \to \infty$.

As in the periodic case, this enables us to write $\alpha^j(x)$ and $A^{i,j}(x)$ as

$$\alpha^i(x) = \alpha_0^i(1 + \epsilon q_1^i(x)) \ \text{ and } \ A^{j,k}(x) = A_0^{j,k}(1 + \epsilon Q_1^{j,k}(x)) \tag{3.72}$$

where the environmental variation coefficient $\epsilon \ll 1$ and the relative perturbations $q_1^j(x), Q_1^{i,j}(x)$ are O(1) and satisfy

$$\int_{-\infty}^{\infty} q_1^i(x)\mathrm{d}x = 0 \ , \qquad \int_{-\infty}^{\infty} Q_1^{j,k}(x)\mathrm{d}x = 0 \ . \tag{3.73}$$

3.2.5 Numerical Methods

In Section 3.3 (Examples), we compare our analytical results to simulations of the IDE. We now discuss the numerical methods used in carrying out the simulations.

We simulate the IDEs by discretising the population density function and dispersal kernels into domains of non-dimensional length ≈ 0.0015. A total of $2^{14} - 1 = 16383$ grid points are used in the simulations. In Section 3.3, we consider only IDEs where the landscape is composed of two types of alternating regions, where demographic and dispersal parameters are constant within each region. The regions with the higher demographic rates are denoted as good, and the ones with the lower demographic rates as bad. Since the kernels in each type of region (good) are dependent only on the dispersal distance $x - y$, the RHS of (1.10) can be written as the sum of two terms, with one referring to dispersal from one region type, and the other to dispersal from the other type. Since the dispersal pattern from each type of region does not

vary within that region type, the integrals are convolutions of the population density function in that region type and the dispersal kernel from that region type. Under the discretisation, the integral convolution of the population density function and dispersal kernel becomes a discrete convolution which we calculate using the Fourier convolution theorem and Fast Fourier Transform (FFT) (Andersen, 1991). We assume (and observe numerically) that the solution will have settled into a travelling wave by the time the wave-front (the locations such that the population density $u^t(x) > \mu$) has reached $x = 100$. We run the simulations until $x = 200$ and use the position of the wave-front at each time-step between these two events to find the asymptotic wave-speed by fitting a linear function to the data. Numerically, we find that (after an initial transient) the wave-front maintains the same exponential shape and shifts by a fixed distance. Therefore, the observed wave-speed is independent of the final time choice, and our choice of numerical threshold for invasion μ which we thereafter take as $\mu = 0.0005$.

3.3 Examples

In this section, we explore the homogeneous and second order approximations discussed in Section 3.2 for two types of landscape with a range of parameters. Although we have derived the approximations for general (stage-structured) populations, in the interests of brevity we detail only non-stage-structured examples, and consider two examples. In the first example (Subsection 3.3.1), the simulated wave-speeds of solutions to IDEs on periodic landscapes are compared with the homogeneous (zeroth order) and the second order approximation introduced in Subsection 3.2.3. The dispersal kernel, growth function and landscape all satisfy Conditions I-VI at the beginning of Section 3.2. Both approximations are shown to be accurate for a range of ϵ, with the second order approximation being more accurate, and appropriate for larger values of ϵ. In the second example (Subsection 3.3.2), we consider solutions of IDEs on stochastically generated (non-periodic) landscapes which satisfy Conditions I-V at

the start of Section 3.2 and Condition VI.b in Subsection 3.2.4. The wave-speeds of IDEs on these non-periodic landscapes are found to exhibit $o(\epsilon)$ dependence on the environmental variation coefficient ϵ and therefore that the homogeneous approximation is appropriate for at least some stochastically generated landscapes with very low environmental variation.

For the periodic example, we find the second order approximation presented in Subsection 3.2.3 for populations with Gaussian and Laplace kernels on an infinite landscape with two types of alternating regions of equal size, in which the growth/dispersal parameters take different sets of values (see Figure 3.1a,c,e). We compare this with the asymptotic wave-speeds of simulated solutions to (1.10), showing that this approximation is accurate. For the non-periodic example, numerical simulation is used to find the asymptotic wave-speeds of (1.10) for landscapes of two types of alternating region in which the size of each individual region is randomly generated from the Uniform distribution (see Figure 3.1b,d,f), to show that the asymptotic wave-speeds of IDEs on non-periodic landscapes exhibit $o(\epsilon)$ sensitivity to the environmental variation coefficient ϵ.

For both the periodic and stochastically generated landscapes, the Beverton-Holt growth function is used for the growth rate (scalar population projection matrix), $\mathbf{B}(\mathbf{u}^t(x), x)$. This has been widely used in population modelling (e.g. for plants, see Poulsen et al., 2007), with the population after the growth phase being given by the current population u multiplied by the growth rate

$$f(u) = \frac{r}{1+u} \ . \tag{3.74}$$

where u is the scalar population before the growth phase and r is the zero-population growth rate ($f(0) = r$). Since the approximation depends only on the zero-population growth rate, any growth function satisfying Condition II in Section 3.2 (Kot et al., 1996) could also have been used. For both the periodic and non-periodic examples, we consider the same three landscape scenarios:

1. Only growth is varied and $(m_r, m_\alpha) = (1, 0)$ (Figure 3.1 a,b)

2. Only dispersal is varied and $(m_r, m_\alpha) = (0, 1)$ (Figure 3.1 c,d)

3. Growth and dispersal are varied and correlated and $(m_r, m_\alpha) = (1, 1)$ (Figure 3.1 e,f)

where m_r and m_α are indicators of the relative strength of the heterogeneity in the growth and dispersal parameters respectively.

3.3.1 Periodic Landscapes

A non-stage-structured population on a landscape of two alternating habitat types of equal size is considered. For each landscape scenario, dispersal is given by either the Gaussian or Laplace kernel. The growth and dispersal parameters at location $x \in \mathbb{R}$ depend only on which type of region x is in.

Derivation of the Analytical Approximation

We calculate the analytical approximation (2.7) for a landscape of two types of alternating region with either a Gaussian or Laplace dispersal kernel. The non-structured growth rate $r(x)$ is given by

$$r(x) = \begin{cases} r_0(1 + \epsilon m_r) & \text{for } x \in \left[nL, nL + \frac{L}{2}\right) \\ r_0(1 - \epsilon m_r) & \text{for } x \in \left[nL + \frac{L}{2}, (n+1)L\right) \end{cases}, \tag{3.75}$$

where r_0 is the spatial mean of the growth rate, L is the landscape period and the value of m_r depends on the landscape scenario under investigation. The dispersal parameter $\alpha(x)$ (which is equal to the mean dispersal distance for the Laplace kernel, and is equal to the mean dispersal distance multiplied by $\sqrt{\pi/2}$ for the Gaussian kernel) is given by

$$\alpha(x) = \begin{cases} \alpha_0(1+\epsilon m_\alpha) & \text{for } x \in \left[nL, nL+\frac{L}{2}\right) \\ \\ \alpha_0(1-\epsilon m_\alpha) & \text{for } x \in \left[nL+\frac{L}{2}, (n+1)L\right) \end{cases}, \tag{3.76}$$

where α_0 is the spatial mean of $\alpha(x)$ and where m_r and m_α are the strengths of the growth and dispersal heterogeneity. Therefore, using the definitions for the non-stage-structured approximation in Subsection 3.2.3, $Q_1(x)$ and $q_1(x)$ are given by

$$Q_1(x) = \begin{cases} m_r & \text{for } x \in \left[nL, nL+\frac{L}{2}\right) \\ \\ -m_r & \text{for } x \in \left[nL+\frac{L}{2}, (n+1)L\right) \end{cases}, \tag{3.77}$$

and

$$q_1(x) = \begin{cases} m_\alpha & \text{for } x \in \left[nL, nL+\frac{L}{2}\right) \\ \\ -m_\alpha & \text{for } x \in \left[nL+\frac{L}{2}, (n+1)L\right) \end{cases}. \tag{3.78}$$

Expressing $Q_1(x)$ and $q_1(x)$ as Fourier series,

$$Q_1(x) = \sum_{n \in \text{Odd}} \frac{2m_r}{\pi i n} \exp\left(\frac{2\pi i n x}{L}\right) \quad \text{and} \quad q_1(x) = \sum_{n \in \text{Odd}} \frac{2m_\alpha}{\pi i n} \exp\left(\frac{2\pi i n x}{L}\right) \tag{3.79}$$

so

$$C_n = \begin{cases} \frac{2m_r}{n\pi i} & \text{if } n \text{ is odd} \\ \\ 0 & \text{if } n \text{ is even} \end{cases} \quad \text{and} \quad \gamma_n = \begin{cases} \frac{2m_\alpha}{n\pi i} & \text{if } n \text{ is odd} \\ \\ 0 & \text{if } n \text{ is even} \end{cases}. \tag{3.80}$$

Substituting these values of C_n and γ_n into the expression for $H_2(s)$ (3.65),

$$H_2(s) = r_0 \sum_{n\in\text{Odd}} \frac{4}{\pi^2 n^2} \left(\left[m_r M_0(s) + m_\alpha M^1(s) \right] \left[M_0(s) - M_0\left(s - \frac{2\pi i n}{L} \right) \right]^{-1} \cdot \left[m_r M_0\left(s - \frac{2\pi i n}{L} \right) + m_\alpha M^1\left(s - \frac{2\pi i n}{L} \right) \right] + m_r m_\alpha M^1(s) + \frac{m_\alpha^2}{2} M^{1,1}(s) \right) . \tag{3.81}$$

To compare this result with numerical simulations, we evaluate this for some specific kernels. We choose the widely used Gaussian and Laplace kernels due to their analytical tractability. The Gaussian dispersal kernel is given in terms of the distance $z = x - y$ and the dispersal heterogeneity function $q(x) := 1 + q_1(x)$,

$$K(z, q) = \frac{1}{\alpha_0 q \sqrt{2\pi}} \exp\left(\frac{-z^2}{2(\alpha_0 q)^2} \right) \tag{3.82}$$

with the first $K^1(z, 1)$ and second $K^{1,1}(z, 1)$ derivatives of the Gaussian kernel $K(z, q)$ with respect to q evaluated at $q = 1$

$$K^1(z, 1) = \frac{1}{\alpha_0 \sqrt{2\pi}} \left(\frac{z^2}{\alpha_0^2} - 1 \right) \exp\left(\frac{-z^2}{2\alpha_0^2} \right) \tag{3.83}$$

$$K^{1,1}(z, 1) = \frac{1}{\alpha_0 \sqrt{2\pi}} \left(\frac{z^4}{\alpha_0^4} - 5\frac{z^2}{\alpha_0^2} + 2 \right) \exp\left(\frac{-z^2}{2\alpha_0^2} \right) . \tag{3.84}$$

The Moment Generating Functions $M_0(s)$, $M^1(s)$ and $M^{1,1}(s)$ of $K_0(z) = K(z, 1)$, $K^1(z)$ and $K^{1,1}(z)$ are

$$M_0(s) = \exp\left(\frac{\alpha_0^2 s^2}{2} \right) \quad M^1(s) = \alpha_0^2 s^2 \exp\left(\frac{\alpha_0^2 s^2}{2} \right) \tag{3.85}$$

$$M^{1,1}(s) = \left(\alpha_0^2 s^2 + \alpha_0^4 s^4 \right) \exp\left(\frac{\alpha_0^2 s^2}{2} \right) \tag{3.86}$$

and $H_2(s)$ is given by

$$H_2(s) = r_0 \sum_{n \in \text{Odd}} \frac{4}{\pi^2 n^2} \left(\left[m_r + m_\alpha \alpha_0^2 s^2 \right] \left[\exp\left(\frac{2\pi i n \alpha_0^2 s}{L} + \frac{2\pi^2 n^2 \alpha_0^2}{L^2} \right) - 1 \right]^{-1} \right.$$
$$\left. \cdot \left[m_r + m_\alpha \alpha_0^2 \left(s - \frac{2\pi i n}{L} \right)^2 \right] + m_r m_\alpha \alpha_0^2 s^2 + \frac{m_\alpha^2}{2} \left(\alpha_0^2 s^2 + \alpha_0^4 s^4 \right) \right) \exp\left(\frac{\alpha_0^2 s^2}{2} \right) \quad . \tag{3.87}$$

The second kernel we consider is the Laplace dispersal kernel, which is given by

$$K(z, q) = \frac{1}{2\alpha_0 q} \exp\left(\frac{-|z|}{\alpha_0 q} \right) \tag{3.88}$$

with the first $K^1(z, 1)$ and second $K^{1,1}(z, 1)$ derivatives of the Laplace kernel $K(z, q)$ with respect to q evaluated at $q = 1$

$$K^1(z, 1) = \frac{1}{2\alpha_0} \left(\frac{|z|}{\alpha_0} - 1 \right) \exp\left(\frac{-|z|}{\alpha_0} \right) \tag{3.89}$$

$$K^{1,1}(z, 1) = \frac{1}{2\alpha_0} \left(\frac{|z|^2}{\alpha_0^2} - \frac{4|z|}{\alpha_0} + 2 \right) \exp\left(\frac{-|z|}{\alpha_0} \right) \quad . \tag{3.90}$$

The Moment Generating Functions $M_0(s)$, $M^1(s)$ and $M^{1,1}(s)$ of $K_0(z) = K(z, 1)$, $K^1(z)$ and $K^{1,1}(z)$ are

$$M_0(s) = \frac{1}{1 - s^2 \alpha_0^2} \quad M^1(s) = \frac{2 s^2 \alpha_0^2}{(1 - s^2 \alpha_0^2)^2} \tag{3.91}$$

$$M^{1,1}(s) = \frac{2 s^2 \alpha_0^2}{(1 - s^2 \alpha_0^2)^2} + \frac{8 s^4 \alpha_0^4}{(1 - s^2 \alpha_0^2)^3} \tag{3.92}$$

and $H_2(s)$ is given by

$$H_2(s) = r_0 \sum_{n\in \text{Odd}} \frac{4}{\pi^2 n^2} \left(\frac{L^2}{4\pi\alpha_0^2 n\left(\pi n + iLs\right)} \left[m_r + \frac{2m_\alpha s^2\alpha_0^2}{(1-s^2\alpha_0^2)} \right] \right.$$
$$\left. \cdot \left[m_r + \frac{2m_\alpha \left(s - \frac{2\pi i n}{L}\right)\alpha_0^2}{(1-\left(s-\frac{2\pi i n}{L}\right)^2\alpha_0^2)^2} \right] + \frac{m_\alpha s^2\alpha_0^2}{(1-s^2\alpha_0^2)^2} \left[2m_r + m_\alpha \left(1 + \frac{4s^2\alpha_0^2}{1-s^2\alpha_0^2} \right) \right] \right) \quad . \tag{3.93}$$

Numerical accuracy of analytical approximations

We simulate solutions to (1.10) for non-stage-structured populations with Gaussian and Laplace dispersal kernels and Beverton-Holt growth function on an alternating landscape with two types of region of equal size (see Section 3.2.5 for numerical details) for a range of values of the environmental variation coefficient ϵ and landscape period L (with fixed values for the mean growth rate and dispersal parameter). We then calculate the relative error of the simulated wave-speed when compared to both the homogeneous approximation c_0^*, and the second order analytical approximation $c_2^*(\epsilon)$ presented in (3.67). The relative error E_j of the j-th order approximation (for $j = 0, 2$) is given in terms of the approximation c_j^* and the simulated wave-speed c^{sim} by

$$E_j = \frac{c_j^* - c^{\text{sim}}}{c^{\text{sim}}} \quad . \tag{3.94}$$

E_j is a measure of the accuracy of the approximation, and is positive when the approximation is an over-estimate of the numerical wave-speed, and negative when it is an under-estimate. When E_j is close to zero, c_j^* is a good approximation to the simulated wave-speed c^{sim} and hence to the asymptotic wave-speed of solutions to (1.10).

In Figures 3.2 and 3.3, we present the relative error of the homogeneous (zeroth order) and second order approximations to the wave-speed for a range of values of landscape period L and environmental variation coefficient ϵ. For both Gaussian and

Laplace dispersal kernels, we consider the cases where spatial heterogeneity affects only growth, only dispersal, and both growth and dispersal together. We find that the simulated wave-speeds have a monotone dependence on ϵ, although in the interests of brevity we do not present the simulated wave-speeds.

In Figure 3.2, we see that, for all scenarios, the relative error $E_0 \sim \mathrm{o}(\epsilon)$ as $\epsilon \to 0$ (the difference can be made arbitrarily smaller than ϵ for sufficiently small ϵ), and that for relatively large ϵ, the relative error remains small. The relationship between ϵ and the relative error is monotone (except for a small region of parameter space in the top right of Figure 3.2e). However, the precise effect of increased ϵ on E_0 (i.e. whether the homogeneous approximation over- or underestimates the simulated wave-speed) depends on the value of the landscape period L. When heterogeneity only affects growth (Figures 3.2a,b), E_0 is positive for large L. On the other hand, when heterogeneity only affects dispersal (Figures 3.2c,d), E_0 is positive for small L. When L is large, E_0 is close to zero (Laplace kernel, Figure 3.2d) or negative (Gaussian kernel, Figure 3.2c). When both growth and dispersal vary together (Figures 3.2e,f) and dispersal is given by the Laplace kernel (Figure 3.2f), E_0 is positive for all values of L. When dispersal is given by the Gaussian kernel, E_0 is positive for small L and negative for large L.

The relative error E_2 of the second order approximation $c_2^*(\epsilon)$ is presented in Figure 3.3. When heterogeneity affects only the growth rate (Figures 3.3a,b) or only the dispersal parameter (Figure 3.3c,d), the relative error of this approximation is small for all values of ϵ and L and both dispersal kernels. In these cases, the second order approximation is much more accurate than the homogeneous approximation for large values of ϵ and generally slightly over-estimates the simulated wave-speed. When heterogeneity affects both growth and dispersal together (Figure 3.3e,f), E_2 is close to zero for moderately large ϵ and small L. However, when ϵ and L are both larger, E_2 becomes large and negative (it underestimates the simulated wave-speed). This is due to the growth of higher order terms in the asymptotic expansion of the eigenvalue $\rho(s) = \mathrm{e}^{sc(s)}$ of the dispersion relation with respect to ϵ. In general, the

second order approximation is more accurate than the homogeneous approximation, particularly when ϵ is too large for the homogeneous approximation to be reliable.

3.3.2 Stochastically Generated Landscapes

We now consider the relationship between the environmental variation coefficient ϵ and the spread rate in stochastically generated landscapes by numerically simulating solutions to IDEs on stochastic analogues of the periodic landscapes considered in Subsection 3.3.1 (where the landscapes consisted of two alternating types of region of equal size $L/2$). In the stochastically generated landscapes, the size of region (regardless of its type) is an independent random variable with mean $L/2$. The landscape parameter L is the expected length of two neighbouring patches of different types, so is analogous to the landscape period L used in the periodic example. We fix the distribution of the random variables as the uniform distribution on $[L/4, 3L/4]$. An advantage of the uniform distribution is that the lengths of the patches are bounded above by $3L/4$. This prevents populations becoming arbitrarily small in a region with low growth rate and the resulting difficulties in simulation. We take the representative value $r_0 = 1.5$ for the mean growth rate. More formally, the lengths of the regions L_j (irrespective of region type) are independent and identically distributed (i.i.d.) with distribution

$$L_j \sim \mathcal{U}\left(\frac{L}{4}, \frac{3L}{4}\right) \quad . \tag{3.95}$$

To explore the relationship between the environmental variation coefficient ϵ and the asymptotic wave-speed, we generated landscapes with independently uniformly distributed region sizes for each combination of dispersal kernel, landscape scenario (spatially varying growth, spatially varying dispersal and both spatially varying growth and dispersal) and representative landscape parameters $L = 2$ and $L = 4$. We found that generating 50 landscapes for each scenario was sufficient in this case, as further runs did not change our conclusions. For each combination of kernel, landscape sce-

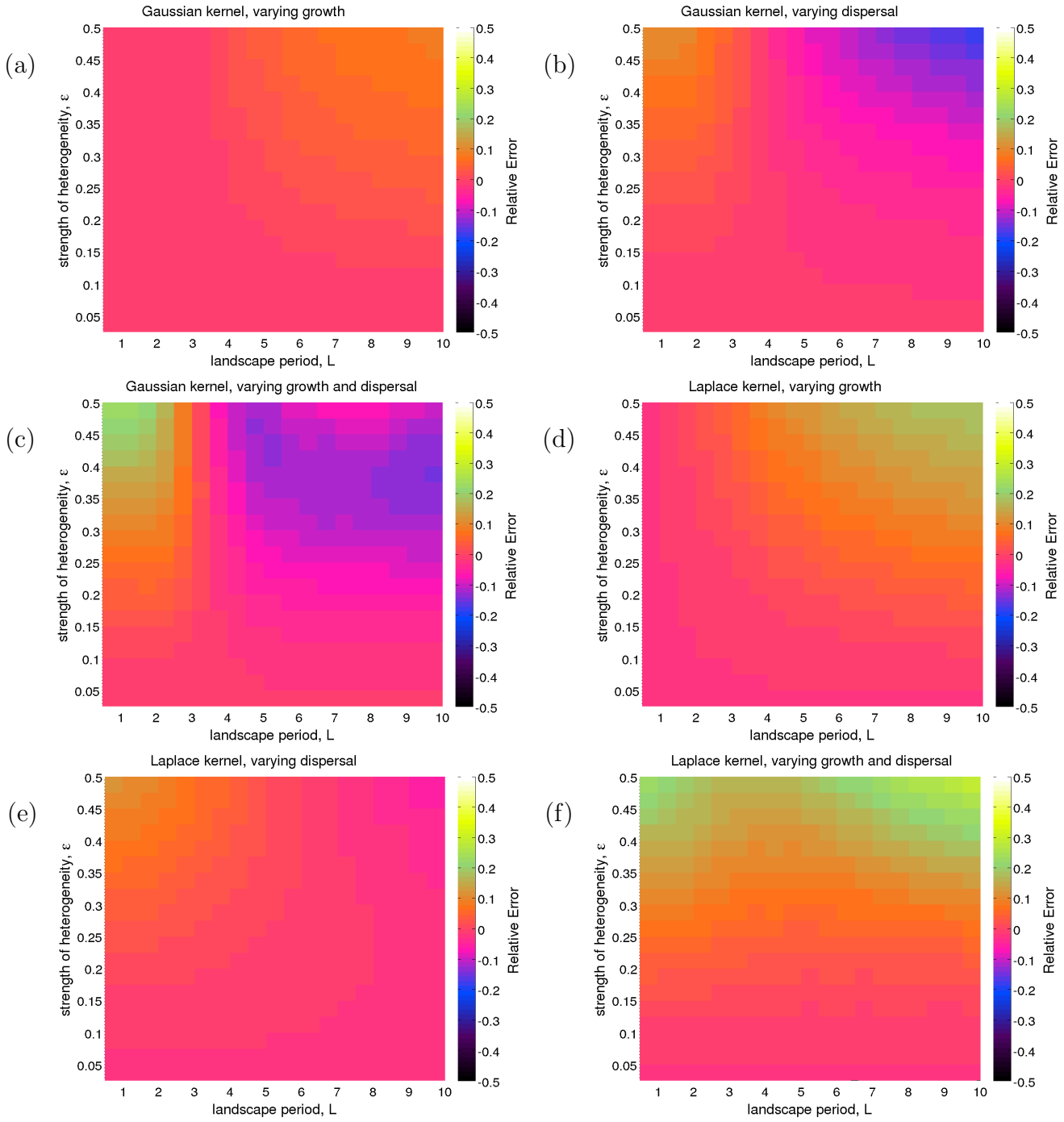

Figure 3.2: Relative Error of the homogeneous (zeroth order) approximation (3.49) for Gaussian (a),(c),(e) and Laplace (b),(d),(f) kernels for a range of heterogeneity strength ϵ and landscape period L, where spatial heterogeneity is present in the growth rate (a),(b), the mean dispersal distance (c),(d) and both the growth rate and mean dispersal distance (e)-(f). The spatially averaged growth rate and the spatial average of the mean dispersal distances are $r_0 = 1.2$ and $\alpha_0 = 1$.

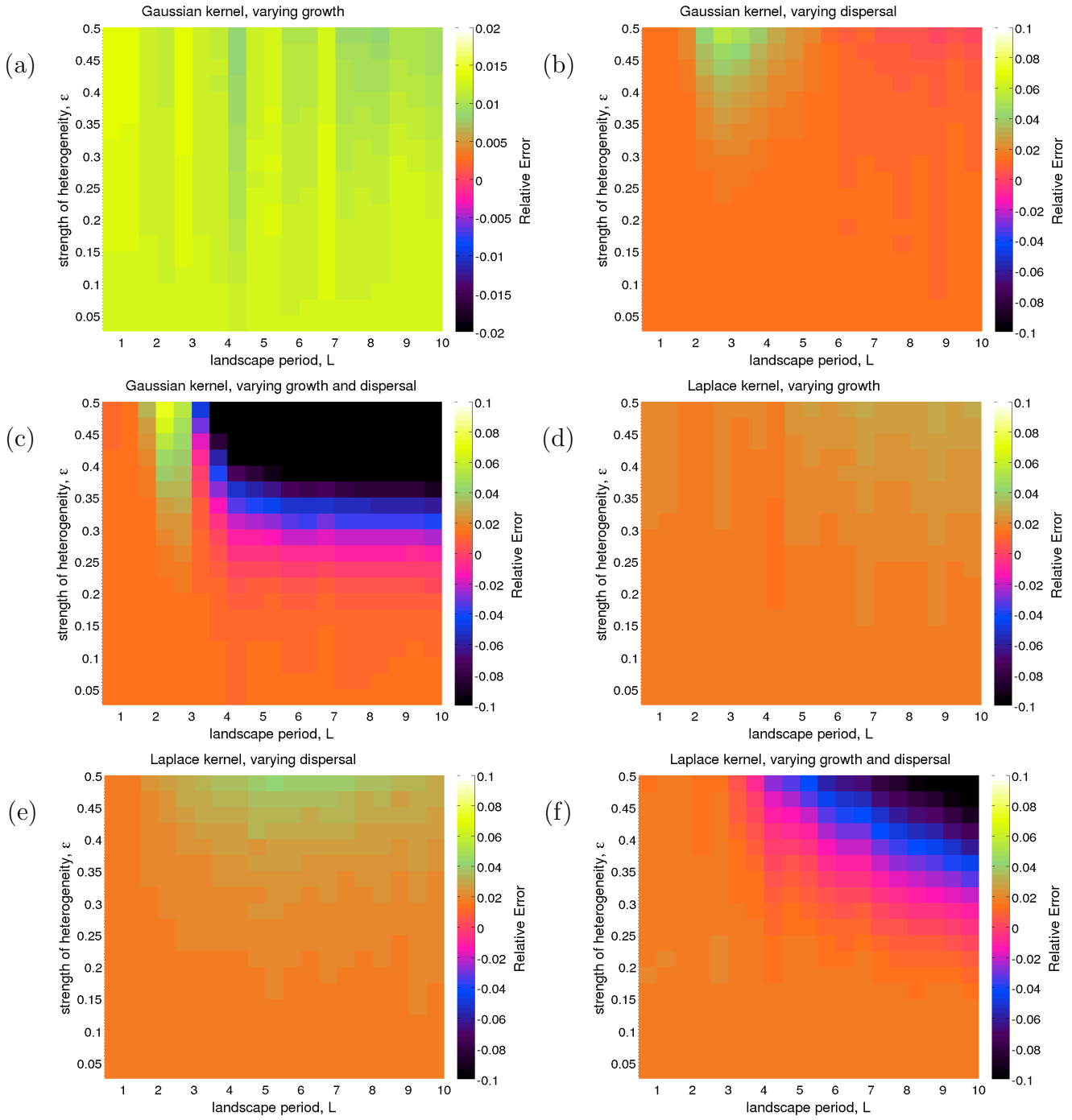

Figure 3.3: Relative Errors ($\min\{0.1, \max\{-0.1, E\}\}$) of the second order wave-speed approximation (3.67) for Gaussian (a),(c),(e) and Laplace (b),(d),(f) kernels for a range of heterogeneity strength ϵ and landscape period L, where spatial heterogeneity is present in the growth rate (a),(b), the mean dispersal distance (c),(d) and both the growth rate and mean dispersal distance (e)-(f). The spatially averaged growth rate and the spatial average of the mean dispersal distances are $r_0 = 1.2$ and $\alpha_0 = 1$.

nario and landscape parameter L and each value of ϵ, we take the average wave-speed for the different landscapes.

We present these results in Figure 3.4 and find that for each kernel, heterogeneity scenario and landscape parameter, the change in mean wave-speed for values of ϵ close to zero is very small. For the parameters considered here, the relationship between ϵ and the simulated wave-speed c is found to be monotone increasing or decreasing and smooth. We observe that the relationship between ϵ and the mean wave-speed is either convex with a minimum at $\epsilon = 0$ or concave with a maximum at $\epsilon = 0$. This shows that wave-speed sensitivity reduces massively for small ϵ, demonstrating a dependence of the form $o(\epsilon)$ and thus a lack of sensitivity to sufficiently small perturbations of the landscape.

3.3.3 Comparison of Periodic and Stochastically Generated Landscapes

We now present the relative change in wave-speed between the homogeneous landscape ($\epsilon = 0$) and the heterogeneous one ($\epsilon = 0.3$) for both the periodic landscapes and the stochastically generated landscapes introduced in Subsection 3.3.2. We compare the homogeneous and heterogeneous wave-speeds for the three landscape scenarios presented in Figure 3.1 and for a range of values of mean growth rate and landscape period (for the periodic landscapes) or landscape parameter (for the stochastically generated landscapes). We present only the results for the Gaussian dispersal kernel (Figure 3.5), but find a similar relationship between the periodic and stochastically generated plots for the Laplace kernel.

When comparing the plots for periodic landscapes (Figures 3.5 a,c,e) and the corresponding plots for the stochastically generated landscapes (Figures 3.5 b,d,f), the qualitative relationships between r, L and the relative change in wave-speed are the same, but are quantitatively different. This suggests that the wave-speeds on stochastically generated landscapes have similar behaviour to wave-speeds on peri-

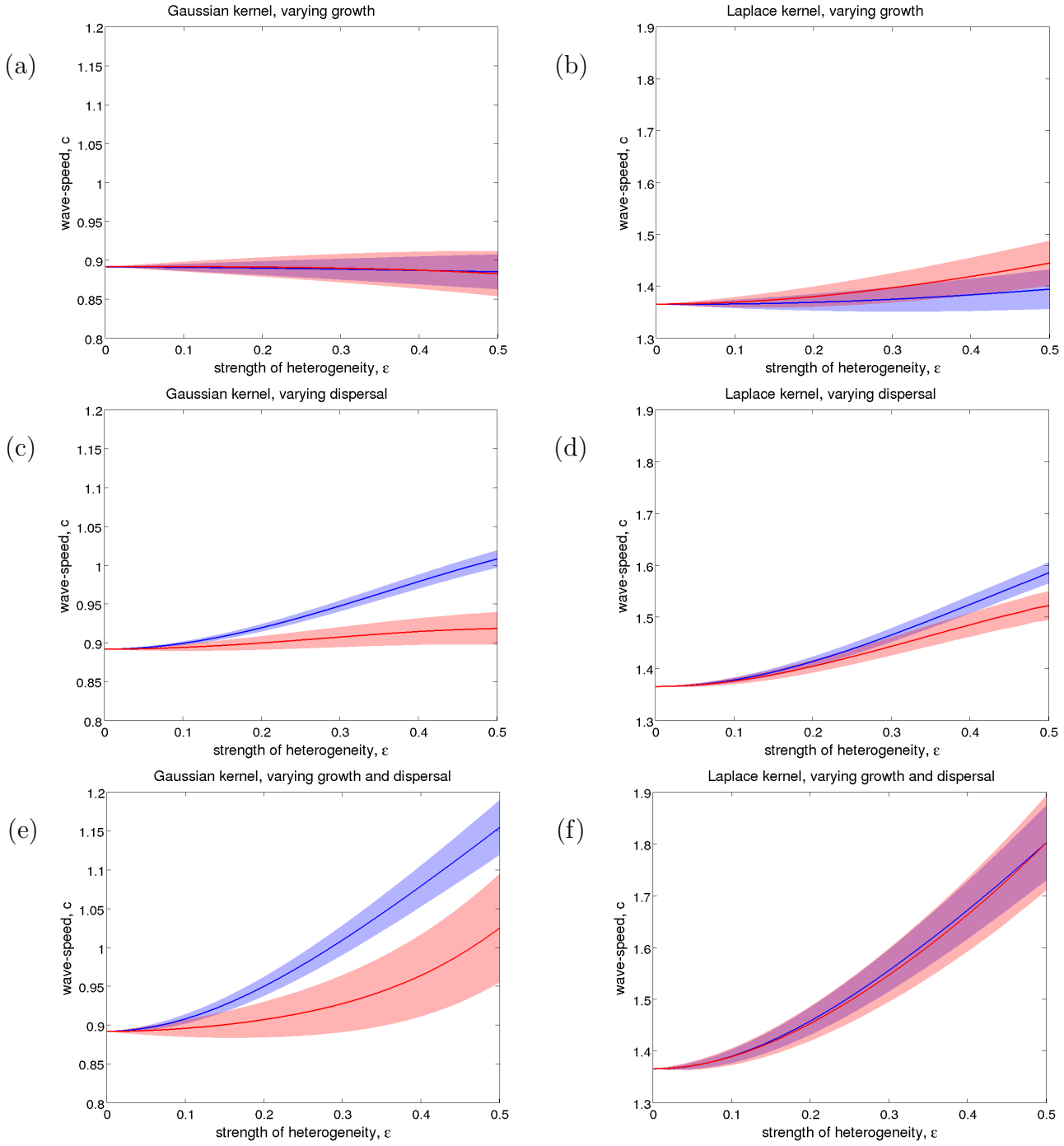

Figure 3.4: Mean (solid lines) simulated wave-speeds, with standard deviations (transparent) of IDEs for Gaussian (a),(c),(e) and Laplace (b),(d),(f) kernels with the spatial average of the mean dispersal distance $\alpha_0 = 1$ for landscape period $L = 2$ (blue) and $L = 4$ (red) on stochastically generated landscapes, where spatial heterogeneity is present in the growth rate (a),(b), the mean dispersal distance (c),(d) and both the growth rate and mean dispersal distance (e)-(f).

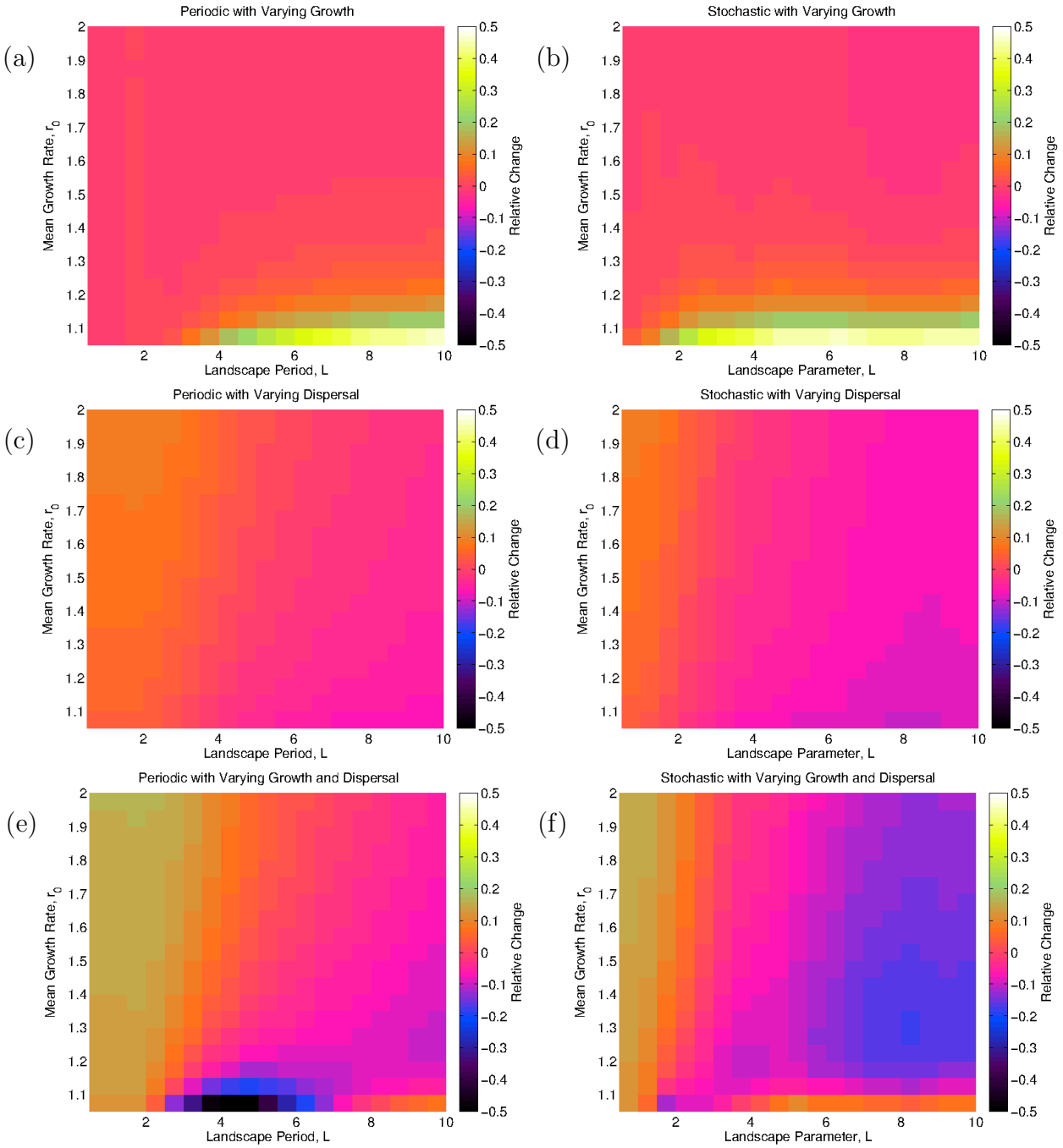

Figure 3.5: Relative change in the wave-speed of numerical solutions to IDEs (3.2) with $\epsilon = 0.3$ compared to the wave-speed of the corresponding homogeneous IDE (i.e. the same IDE with $\epsilon = 0$). The wave-speeds are for periodic (a),(c),(e) and the mean wave-speed of fifty stochastically generated (b),(d),(f) landscapes with Gaussian dispersal, where heterogeneity is present only in the growth (a),(b), where heterogeneity is present only in the dispersal (c),(d) and where heterogeneity is present both in the growth and dispersal (e),(f).

odic landscapes, giving us greater confidence in extending our main result (that the difference between heterogeneous and homogeneous landscapes is $o(\epsilon)$) to non-periodic landscapes.

Since we have found the relationship between the heterogeneity parameter ϵ and the wave-speed to be monotone for periodic (Subsection 3.3.1) and stochastically generated landscapes (Subsection 3.3.2), we expect the relative change in wave-speed between heterogeneous landscapes with a given value of ϵ and the homogeneous case to be representative of the general change in wave-speed as ϵ increases from zero. Where heterogeneity only affects growth (Figures 3.5 a,b), the change in wave-speed is only significant where r is small (the persistence/invasion threshold for homogeneous landscapes) and L is large. Where heterogeneity only affects dispersal (Figures 3.5 c,d), the change is quite small for all parameter values, with smaller values of L corresponding to increases in wave-speed. Hence, where heterogeneity only affects either growth or dispersal, the homogeneous approximation is still close to the simulated results for moderately large ϵ. On the other hand, when heterogeneity affects both growth and dispersal together (Figures 3.5 e,f), the relative change has complex dependencies on r and L (i.e. heterogeneity increases the wave-speed if L is small, or if L is large and r is small, but decreases wave-speed if L is large, or for some values of L when r is small), and is much larger. This means that when both growth and dispersal are heterogeneous, the homogeneous approximation may not be reliable for all parameter values as ϵ increases.

3.4 Discussion

In this chapter, we have shown analytically that the wave-speeds of solutions to periodic IDEs with low environmental variation differ from the wave-speeds of solutions to their homogenisations by a factor proportional to ϵ^2, where ϵ is the environmental variation coefficient, and have shown numerically that a similar result (that the wave-speeds differ by $o(\epsilon)$) extends to the non-periodic landscapes considered. Through

numerical simulations, we have found that for the Laplace and Gaussian dispersal kernels, with fixed mean growth rate r_0 and mean dispersal parameter α_0 and a range of values of the environmental variation coefficient ϵ and landscape period L, the magnitude of the relative error of the homogeneous approximation is small. Additionally, for the Gaussian kernel with fixed α_0 and ϵ, all three heterogeneity scenarios and a range of values of r_0 and L, the relative change in wave-speed between the homogenised and the heterogeneous IDE is small unless r_0 is very close to the persistence threshold. This means that the wave-speed of the invasion in homogeneous landscapes is often a very good approximation to the wave-speed even when ϵ is only moderately small. Additionally, our finding that the error was very small for $\epsilon \sim 0$ is in agreement with the analytical result.

This means that for small values of ϵ, the homogeneous approximation is better than might initially be expected. Therefore, for any landscape with low environmental variation, with dispersal given by any exponentially bounded kernel, homogenising and using the comparatively simple formula for the asymptotic wave-speed in homogeneous landscapes may be a sensible approach to approximating the wave-speed c^*. This is useful for ecologists studying real landscapes, as small variations can be averaged out, making the analytical calculations of the wave-speed much simpler. The straightforward homogeneous IDE can be implemented, as in previous ecological studies (e.g. Bullock et al., 2012; Lewis, 2000; Neubert and Caswell, 2000), by taking these average values to parametrise the IDE. How small the level of variation should be if the homogeneous approximation is to be used will vary with the desired level of accuracy. The results in this chapter suggest that if a 10% error in the spreading speed is acceptable, then a homogeneous approximation is appropriate for $\epsilon < 0.25$.

For more complex landscapes with large variation on small spatial scales but with less variation over large scales, it may be possible to combine the methods presented in this chapter with the methods presented by Dewhirst and Lutscher (2009) to justify the use of the homogeneous approximation. Dewhirst and Lutscher used Riemann sums to show that rapidly varying landscapes could be approximated by

their homogenisation, but it seems reasonable that this could be extended to justify the removal of the rapidly oscillating frequencies from the Fourier decomposition of the landscape even in the presence of frequencies with larger periods. Assuming that the resulting smoothed landscape has low environmental variation, the analysis presented in this chapter could be used to justify the homogeneous approximation and thus enable the comparatively simple expressions for the wave-speed derived by Kot (1992) for non-stage-structured IDEs and by Neubert and Caswell (2000) for stage-structured IDEs to be used to approximate the speeds of real spreading populations on complex heterogeneous landscapes.

For IDEs on periodic landscapes where more analytical accuracy is required, or the specific effects of the heterogeneity on the wave-speed are being studied, we have derived a second order approximation $c_2^*(\epsilon)$ which incorporates the $\mathrm{O}(\epsilon^2)$ term in the asymptotic expansion of $\rho(s) = \mathrm{e}^{sc(s)}$. We have found $c_2^*(\epsilon)$ by linearising the IDE, considering periodic travelling wave solutions and using regular perturbation theory. Unlike the homogeneous approximation, the second order approximation has an ϵ dependence, so takes into account the details of the heterogeneity, but is much more complex than the homogeneous approximation. Numerically, for the landscape scenarios, dispersal kernels and parameters studied, and for moderately small ϵ, the relative error was very small, thus demonstrating a greater degree of accuracy.

While intrinsic stochasticity and variation have been found to reduce populations' spreading speeds (Lewis, 2000; Snyder, 2003; Metz et al., 1999), we have found that the effects of extrinsic/landscape variation to be more complex. Although the relationship between the heterogeneity coefficient ϵ and the wave-speed is typically monotone, the precise effect that increasing environmental variation has on the wave-speed has a complex dependence on the dispersal kernel and mean dispersal parameter α_0, the mean growth rate r_0 and the landscape period/parameter L. It is likely that this is due to a complex interplay between increasing isolation of suitable habitat as ϵ increases (which we would expect to reduce the spreading speed) and the clustering of good habitat (which we would expect to increase the spreading speed). Which

of these effects is stronger depends on the values of r_0 and L (Skelsey et al., 2013). Therefore, to characterise the precise effects of increased ϵ on the spread rate accurately, it is of utmost importance to accurately characterise the precise shape of the dispersal kernel and the structure of the landscape (i.e. the degree and type of environmental variation).

For both dispersal kernels in the periodic example, we have found that for fixed mean growth rate r_0, the effect of increased heterogeneity (increased ϵ) on the accuracy of the homogeneous approximation depends on the landscape period L, the choice of dispersal kernel and the heterogeneity scenario (whether heterogeneity is present only in the growth rate, the dispersal parameters, or in both simultaneously). Additionally, we have found that for the Gaussian kernel and both periodic and stochastically generated landscapes, when ϵ is fixed and r_0 and L vary, the relative change in wave-speed is qualitatively similar for the periodic and non-periodic cases.

In this chapter, we have shown the $\mathrm{O}(\epsilon^2)$ dependence of the wave-speed on the environmental variation coefficient for general stage-structured IDEs, but in the interests of brevity, have only considered non-stage-structured examples. We anticipate that the approximation would show similar effectiveness on stage-structured examples. Conversely, we have been able to show a lack of sensitivity in the wave-speed in non-periodic landscapes to ϵ numerically, but have not been able to do so analytically. In Section 3.3, due to their wide use and analytical tractability, we have used the Laplace and Gaussian kernels. However, all the results presented here are valid for any of the more complex exponentially bounded kernels which are often used in ecology (Clobert et al., 2012).

In summary, we have shown for periodic and non-periodic landscapes that the asymptotic wave-speed of the model shows a lack of sensitivity to the environmental variation coefficient ϵ and therefore that the simpler homogeneous approximation to the wave-speed is valid for landscapes with low environmental variation. For situations where more accuracy is required, we have derived a second order approximation to the wave-speed in terms of ϵ for periodic landscapes, and have shown it to be

accurate for low environmental variation through numerical simulation.

Chapter 4

Speeding up Simulaltion

This chapter is based on the paper *Speeding Up The Simulation of Population Spread Models* by Gilbert, White, Bullock and Gaffney, which has been accepted for publication in Methods in Ecology and Evolution.

A paper which uses the algorithm presented in this chapter, *Emerging opportunities for landscape ecological modelling* by Synes, Brown, Watt, White, Gilbert and Travis, has been published in Current Landscape Ecology Reports. The paper reviews different modelling approaches used in landscape ecology and uses the simulation algorithm to simulate the spread of spruce (Picea) trees at Glacier Bay, Alaska.

4.1 Introduction

Spatial variation in abiotic and biotic factors is a feature of all landscapes, and therefore affects the habitats of all biological organisms. When modelling its effects on population spread, some spatial variation can be ignored by approximating the heterogeneous landscape with a homogeneous one, in which the demographic and dispersal parameters are spatially constant. IDE models on these landscapes have the benefit of simple analytical expressions for spreading speeds and sensitivity to life-history and dispersal parameters (see Sections 1.5.2-3 and Kot et al., 1996; Neubert and

Caswell, 2000; Shigesada et al., 1986). Approximation by a homogeneous landscape is justified for landscapes where spatial variation is highly localised (Dewhirst and Lutscher, 2009) or very slight (see Chapter 3 and Gilbert et al., 2014a). Other types of variation that cannot be homogenised may be spatially periodic, with landscape features repeating after a particular distance. Such landscapes also have analytical approximations for spread rates (Chapters 2-3 and Gilbert et al., 2014b,a) which can be calculated without extensive computational resources.

Other landscapes are more complex and exhibit strong variation across large spatial scales, rendering homogeneous and periodic approximations inaccurate (see Figure 4.1; Svenning et al., 2014; Miller and Tenhumberg, 2010). Instead, to make predictions on complex landscapes, numerical simulations of the models are required. Accurate predictions require accurate simulations, which in turn require a large number of calculations (Scheffer et al., 1995). This means that intense computational power is needed to simulate spread in large two-dimensional landscapes. This is a particular problem for IBMs, such as RangeShifter (Bocedi et al., 2014a), where a large number of individual mechanisms can be modelled, but where each organism must be explicitly represented in the numerical framework.

Since predictions of species spread rely on computationally expensive simulations, the ability to predict spread is often limited by the model's scale and the available computational resources. This limitation inhibits the types of scientific questions and problems that can be investigated. For example, fitting spread models to data requires numerous model runs, so if each model run is computationally intensive, then the time to fit the model to data will be prohibitively long.

To be simulated numerically, most mechanistic population models must first be discretised, with space and time represented as a mesh of points. In general, the simulation's accuracy depends on the number of points, with the accuracy increasing with the number of points (Bocedi et al., 2012). Simulating spatially explicit models involves a large number of calculations at each time-step. The computational complexity and computational resources (RAM, CPU-time etc) required to compute these

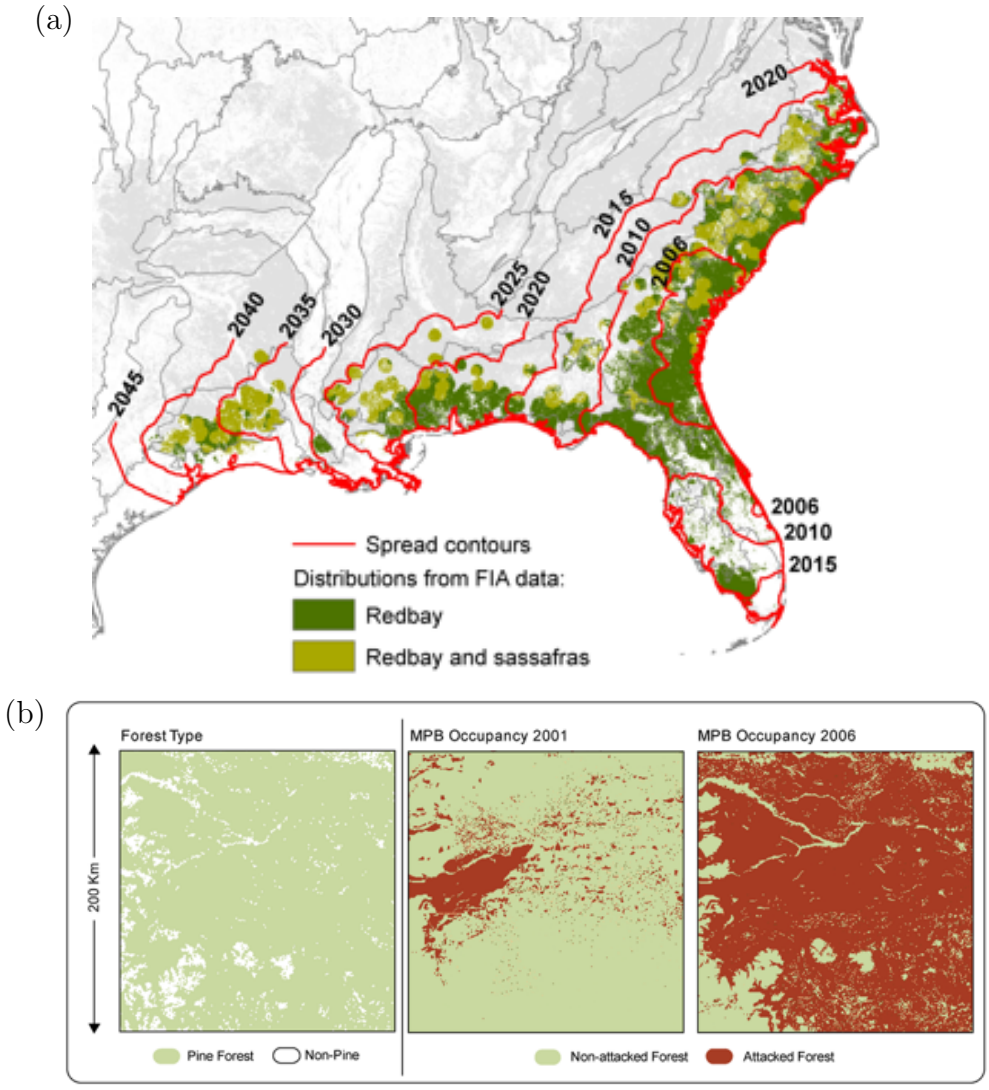

Figure 4.1: Maps of the spaptial spread of species in heterogeneous landscapes: (a) Redbay (*Xyleborus glabratus*) in the South-Eastern United States and (b) Mountain pine beetle (*Dendroctonus ponderosae*) in British Columbia, Canada. Reproduced (a) from Conkling (2011) with permission, (b) from Bone et al. (2013) under the Creative Commons Attribution license.

calculations increases linearly or faster with the total number of points or individuals (Solodovnikov, 1985; Cooley and Tukey, 1965). If simulations over large landscapes are to be accurate, they need a high density of points and a very large total number of points. Additionally, most models will require numerous iterations if the model is simulated over a long time, making simulations extremely computationally expensive. Large numbers of runs are also often required for parameter estimation and sensitivity studies, thus further motivating the need for efficient solvers (Csilléry et al., 2010). One way to improve efficiency has been developed for PDEs, using *adaptive mesh refinement* to allow the density of points (the resolution) to change in time and space (e.g. Berger and Oliger, 1984; Davis and Flaherty, 1982). The density of points is usually highest where the most accuracy is required (e.g. where the relative population change is greatest, such as in the wave-front). With only small reductions in accuracy (i.e. the accuracy of the simulations compared to the mathematical model), this approach allows limited computational resources to be focused on the spatial locations which have the greatest effect on the distribution as it changes. Adaptive mesh refinement has so far been restricted to PDEs. However, in cases where long distance dispersal or annual cycles play an important role in the model, IDEs may be a more appropriate choice of modelling framework than PDEs, as they can incorporate these processes (Kot et al., 1996) and are relatively easy to parameterise, e.g. by using data from the COMPADRE database (Salguero-Gómez et al., 2015) or population spread data (e.g. Gilbert et al., 2005), and thus, IDEs are extensively used in species modelling (Bullock et al., 2008; Le Corff and Horvitz, 2005; Neubert and Parker, 2004; Bullock et al., 2012; Miller and Tenhumberg, 2010; Zhou and Kot, 2011).

In this chapter we provide a solution to large-scale spread problems by developing an adaptive-mesh refinement algorithm to simulate IDEs. At each iteration, the algorithm divides the landscape up into square *regions* of equal area, that are either *high resolution* (containing a large number of mesh-points) or *low resolution* (containing only one mesh-point). We present the algorithm for stage-structured

populations with homogeneous dispersal and heterogeneous demography in Section 4.2. In Section 4.3, we demonstrate that the algorithm is both highly accurate and uses fewer computational resources (RAM, CPU-time) than non-adaptive algorithms for a given problem, as well as enabling us to tackle problems that were previously impossible due to insufficient computational resources. Finally, we discuss extending the algorithm to landscapes with heterogeneous dispersal in the Discussion (Section 4.4). We provide an executable application and source code with a worked example via GitHub (Gilbert et al., 2016) so that others may use this algorithm to simulate the spread of species under a variety of scenarios.

4.2 Method

In this section, we introduce the adaptive algorithm, outline its structure and features. We restrict our attention to single-species stage-structured IDEs with constant/homogeneous dispersal on two-dimensional landscapes. These have the general form

$$\mathbf{u}^{t+1}(\mathbf{x}) = \int_{\Omega} \left[\mathbf{K}(\mathbf{x}-\mathbf{y}) \circ \mathbf{B}\left(\mathbf{u}^{t}(\mathbf{y}), \mathbf{y}\right)\right] \mathbf{u}^{t}(\mathbf{y})\, \mathrm{d}\mathbf{y}\,, \tag{4.1}$$

where Ω is a bounded subset of $\mathbb{R}^2$. Locations outside of Ω are non-habitat, so the boundary conditions are absorbing. The dispersal is homogeneous in that it depends only on the displacement $\mathbf{x}-\mathbf{y}$ between the initial location of the disperser $\mathbf{y}$ and its destination $\mathbf{x}$ (as in Figure 4.6d). In Section 4.4, we will discuss prospects for incorporating dispersal that depends on the initial location (see Figure 4.6e). The method can also be easily restricted to one spatial dimension ($\Omega \subseteq \mathbb{R}$).

With the exception of homogeneous landscapes with no variation in demography or dispersal (see Section 1.5.2) or where an approximate spread rate is sufficient (e.g. Chapters 2,3), quantifying spread requires numerical simulation, with the landscape typically discretised into a mesh (Powell et al., 1998). If dispersal is homogeneous,

such as in (4.1), then the integral can be computed efficiently using fast-Fourier transforms (FFTs) (Andersen, 1991). If dispersal varies spatially, then the discretised spatial distributions at t and $t+1$ are related by a matrix multiplication. Considering either case, the computational resources required increase linearly or faster with the number of mesh-points, leading to very large computational costs for simulating the model accurately over large and complex landscapes (see Section 1.5.5). To reduce these computational requirements, we propose a simulation algorithm with adaptive mesh refinement.

In spreading populations, there is usually little change in the population density in the *wave-back* (or within range), where the population has reached carrying capacity, or in the *far-field*, where the population is very small (see Figure 4.2). Behaviour in these regions has only a small effect on the wave-front's behaviour, so computational resources can be focused on the wave-front (or leading edge) with a loss of resolution in the wave-back and far-field. For our novel algorithm, we subdivide the landscape into non-overlapping square *regions* of equal width Dx, which are further divided into an equal number M of *cells*. Cells are the smallest unit of discretisation for the simulation, are all square and of equal size with width dx. To ensure that the regions can be of equal size, the total width and length of the domain (in cells) is divisible by the square-root of the number of cells in each region. Regions can be either *High Resolution* (HR) or *Low Resolution* (LR). In high resolution regions, each cell has a stage-structured population density, while in low resolution regions, the region has a single stage-structured population density. To achieve reductions in CPU-time and RAM-usage, we (1) reduce some of the resolution in the tail of the dispersal kernel and (2) reduce the resolution in regions which are not in the wave-front.

The algorithm requires several maps and parameters as inputs. There are two types of maps which must both be provided as raster, i.e. gridded, data at the desired resolution. These are (1) the initial population distribution for each demographic stage, and (2) the value of each parameter that affects the population projection matrix (growth function) and the (spatially homogeneous) dispersal kernel. Threshold

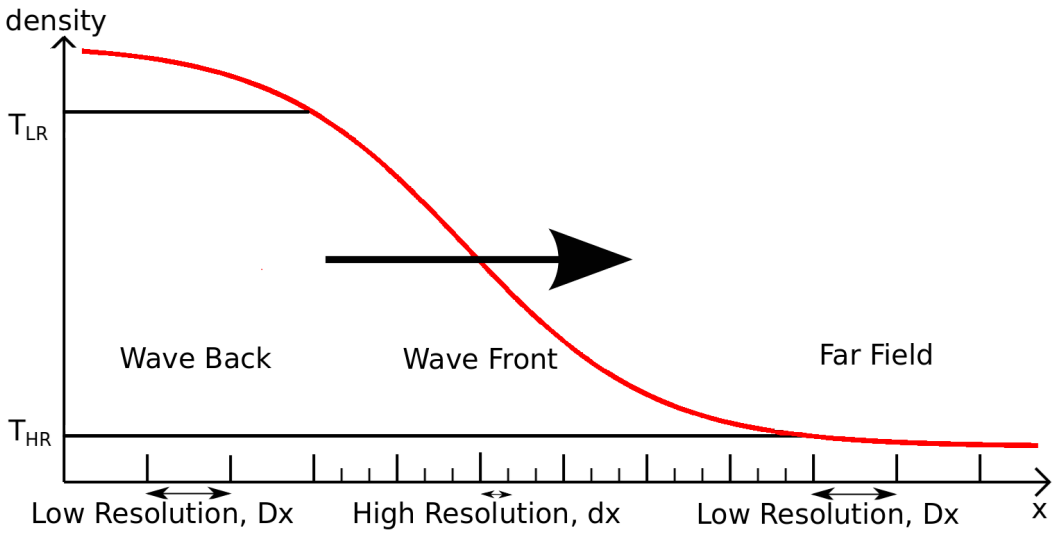

Figure 4.2: Schematic diagram of a travelling wave showing the algorithm parameters: the upper threshold T_{LR} where the population returns to low-resolution LR, the lower threshold T_{HR} where the population becomes HR, the distances between each cell dx and between each region Dx in relation to the spreading population (red online).

values for transitions between low and high resolution and the sizes of the domain, the cells and the regions are required, as are the structure of the population projection matrix and dispersal kernels.

The IDE model can have any number, N, of demographic stages. The first of which is referred to as the *juvenile* stage. In an IDE with a single demographic stage (a non-stage-structured IDE), this instead refers to the whole (non-stage-structured) population. Initially, any region in which any mesh-point is in the *wave-front* is high-resolution (see Figure 4.2). The wave-front is any location where the juvenile (or lowest) demographic stage, $u_1^t(\mathbf{x})$ has population density between the thresholds T_{LR} and T_{HR} and has changed more than $T_{LR,2}$ since the previous time-step (this ensures that locations where the population never grows past T_{HR} are not always counted as part of the wave-back). The upper threshold T_{LR} is taken as a proportion of the carrying capacity and T_{HR} and $T_{LR,2}$ are set as small as required to allow small populations to be resolved (for example, $T_{HR} = 10^{-13}$ and $T_{LR,2} = 10^{-10}$ in the examples in Sections 2-3), with suitable values provided for these parameters in the worked example.

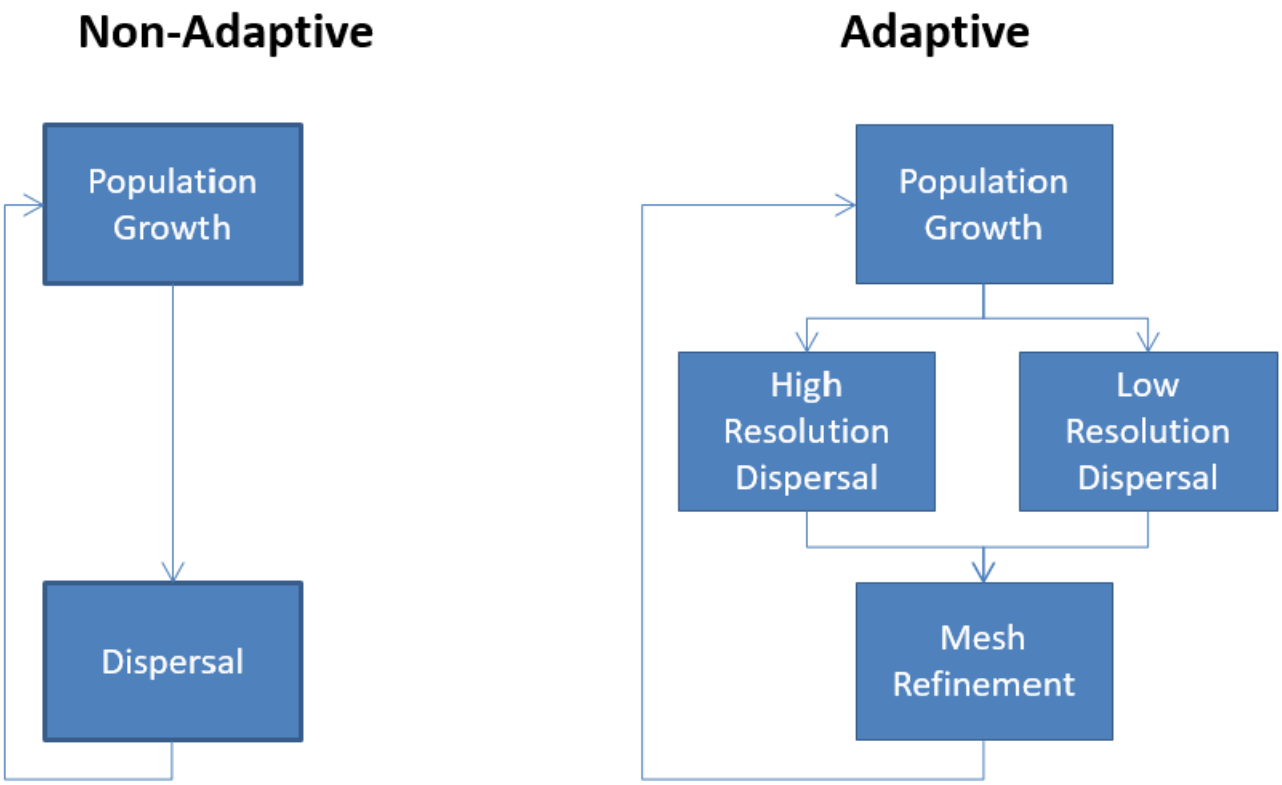

Figure 4.3: Flow diagrams detailing the non-adaptive and adaptive algorithms for simulating IDEs.

In standard simulations of IDEs there are two sequential processes during each generation: population growth and dispersal. However, the adaptive algorithm also incorporates the additional process of mesh-refinement (see Figure 4.3).

4.2.1 Population Growth

The population growth function at each cell depends on the cell's intrinsic demographic rates and carrying capacity, which define the population projection matrix and are supplied by the user. At the start of each time-step, prior to the population growth phase, individuals' behaviour is determined purely by their current demographic stage. However in order to facilitate different dispersal patterns between different pairs of demographic stages, individuals' behaviour after the growth phase depends on both the demographic stages occupied before and after the growth phases.

For high resolution regions, population growth is calculated by applying each cell's

population projection matrix $\mathbf{B}(\cdot, \mathbf{y})$ to its stage-structured population density $\mathbf{u}^t(\mathbf{y})$. For low resolution regions, each demographic stage's population density is represented by a single scalar, so the growth phase for the whole region is calculated using the mean of the population projection matrix over the region.

In high-resolution regions, the population density $u^{\tilde{t}}_{\beta,j,s_1,s_2}$ after the growth phase at time $\tilde{t}$ for cell j of region β transitioning from stage s_1 to s_2 is related to the population density u^t_{β,j,s_1} of individuals at stage s_1 in cell j of region β and the density dependent population projection matrix $\mathbf{B}_{\beta,j}(\cdot) = (B_{\beta,j,s_1,s_2}(\cdot))^N_{s_1,s_2=1}$ in cell j of region β by

$$u^{\tilde{t}}_{\beta,j,s_1,s_2} = B_{\beta,j,s_1,s_2}(\mathbf{u}^t_{\beta,j})\, u^t_{\beta,j,s_1} \ , \tag{4.2}$$

where $\mathbf{u}^t_{\beta,j} = \left(u^t_{\beta,j,s_1}\right)^N_{s_1=1}$. In low-resolution regions, we simulate the region's population by a single scalar U^t_{β,s_1} for each stage (before the growth phase) or by a single scalar U^t_{β,s_1,s_2} for each pair of stages (after the growth phase). With $\bar{B}_{\beta,s_1,s_2}(\mathbf{U}^t_\beta)$ denoting the (s_1, s_2) element of the mean population projection matrix in region β at density $\mathbf{U}^t_\beta = \left(U^t_{\beta,s_1}\right)^N_{s_1=1}$, as given by

$$\bar{B}_{\beta,s_1,s_2}(\mathbf{U}^t_\beta) = \frac{1}{M} \sum_j B_{\beta,j,s_1,s_2}(\mathbf{U}^t_\beta) \ , \tag{4.3}$$

where M is the number of cells in the region. The region's population density at $\tilde{t}$ is then given by

$$U^{\tilde{t}}_{\beta,s_1,s_2} = \bar{B}_{\beta,s_1,s_2}\left(\mathbf{U}^t_\beta\right)\, U^t_{\beta,s_1} \ . \tag{4.4}$$

4.2.2 Dispersal

The assumption of homogeneous dispersal reduces the integral for each pair of demographic stages in (4.1) to a convolution and allows dispersal within a regular square mesh to be calculated using FFTs (Andersen, 1991). Since dispersal is the transfer of

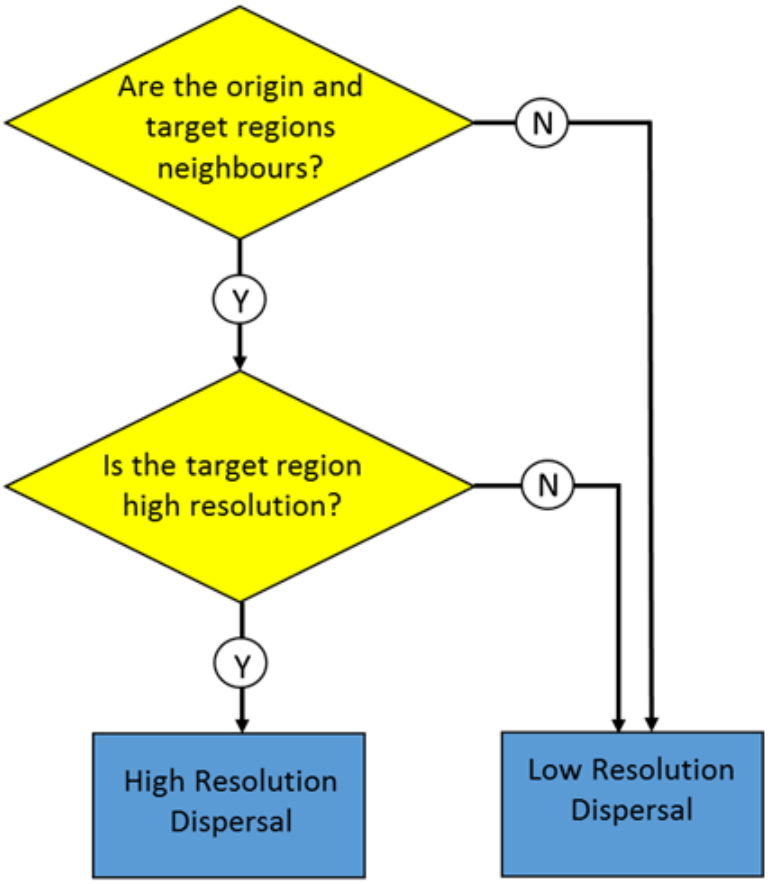

Figure 4.4: Flow diagram detailing the conditions for dispersal between an origin and target to be high resolution and low resolution.

density between cells and regions, we refer to dispersal being between an *origin* cell (or region) and a *target* cell (or region).

The key idea with our method is to divide dispersal into two categories of *dispersal resolution*: *high-resolution dispersal* and *low-resolution dispersal*. Which category the dispersal between a particular origin and target belongs to depends on (1) whether the origin and target are in neighbouring regions and (2) whether the target is in the wave-front. If the origin and target are in adjacent or diagonally neighbouring regions then the dispersal is classed as *local* and if they are not neighbouring it is classed as long-distance or *global dispersal*. Global dispersal is always low-resolution, whereas local dispersal is high-resolution if the target region is high-resolution and low-resolution otherwise (see Figure 4.4).

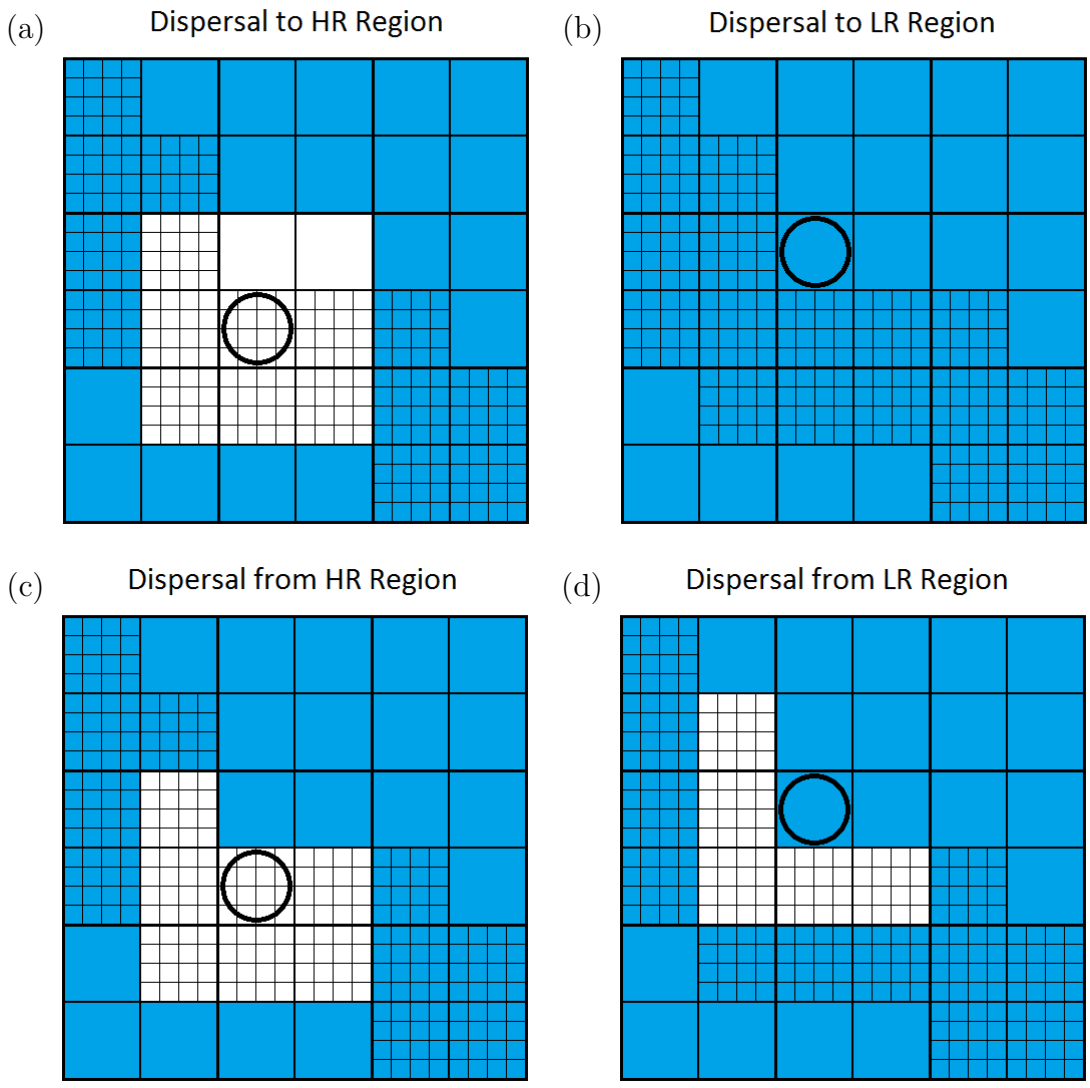

Figure 4.5: Schematic diagrams of the types of dispersal between different regions. (a)-(b) show regions where the resolution of dispersal destined for the circled region is low (blue) and high (white). (c)-(d) show regions where the resolution of dispersal originating from the circled region is low (blue) and high (white).

High-resolution dispersal

High resolution dispersal is used to denote the dispersal processes which require more computational resources for simulations to be accurate. High-resolution is required for dispersal that (i) is relatively short distance and (ii) has its destination in the wave-front (see Figures 4.4 and 4.5). In practice, this is dispersal to a high-resolution region (a region in the wave-front) from any neighbouring region (short-distance). For a region containing high-resolution information, we take the pre-dispersal population density of each cell in the region and its neighbours (for low resolution neighbouring regions, all cells are assumed to have population density equal to the region's population density) and take the discrete convolution of this distribution with the *HR dispersal kernel* (a high resolution discretisation of the dispersal kernel) to get the post-dispersal population density distribution.

High resolution dispersal is characterised by a stage-structured $N \times N$ matrix of discretised dispersal kernels, where N is the number of stages; these are all represented as matrices. These are the *HR dispersal kernels* and there is one matrix for each pair of demographic stages. Each matrix defines local dispersal to regions with high resolution information and consists of the dispersal densities between the centres of all pairs of cells in neighbouring regions. If one of the neighbouring regions is low-resolution, then we assume all the cells in that region have the same population densities for each pair of demographic stages (i.e. we think of the densities as being on a high resolution grid but with equality between cells in the same region if a region is low resolution). For each pair of stages, we take the convolution of the high-resolution array with the corresponding HR dispersal kernel. The HR dispersal kernel $\tilde{k}_{s_1,s_2}$ for dispersal for individuals going from stage s_1 to s_2 and dispersing between two cells with displacement $\mathbf{i} = (i_1, i_2)$ in the array is given by the spatially homogeneous dispersal kernel evaluated at the mid-points of the two cells,

$$\tilde{k}_{s_1,s_2,\mathbf{i}} = k_{s_1,s_2}(\mathrm{d}x\,\mathbf{i}) \tag{4.5}$$

where $k_{s_1,s_2}(\mathbf{z})$ is the dispersal kernel for stages (s_1, s_2) with spatially constant dispersal. The section of the resulting array corresponding to region β gives us the local contribution to the new population density distribution in β.

Low-resolution dispersal

Low-resolution dispersal denotes the dispersal processes which can be simulated with fewer computational resources without significantly affecting the simulation's accuracy. This is dispersal between regions which are either not neighbours or not in the wave-front (Figure 4.4). This is justified by the observation that all realistic dispersal kernels eventually decay after sufficient distance from the origin. The low-resolution dispersal can be thought of as having two components: (1) global dispersal between non-neighbouring regions, and (2) local dispersal to low-resolution regions.

Dispersal between non-neighbouring regions (global dispersal) is always low-resolution. In particular, if two cells are in the same region, then the contributions to them from global dispersal will be the same. For each pair of demographic stages, global dispersal is simulated by taking the array of the means of the regions after the growth stage (each region is represented by a single element in this array) and taking its convolution with the *long-distance LR dispersal kernel* for that pair of stages. These kernels are low-resolution discretisations of the dispersal kernel restricted to dispersal between non-neighbouring regions. This means that they are zero for regions that are adjacent or diagonal neighbours, and that for all other pairs of regions, they are given by the elements of the dispersal kernel in (4.1) evaluated between the centres of the two regions. The result of the convolutions are arrays where each element corresponds to a region. If a region is low-resolution, then for each pair of demographic stages, the corresponding element of the array is simply added to its population density, and if it is high-resolution, the corresponding element is added to the population density of each cell in the region.

Low-resolution local dispersal occurs when the target cell is in a low-resolution region and the origin and target cells are in neighbouring regions. To calculate the

dispersal to a low-resolution target region from all its neighbours, we take the mean pre-dispersal stage-structured population densities for the region and its neighbours and for each pair of stages, take the discrete convolution of this distribution with the *local LR dispersal kernel*, a low-resolution discretisation of the dispersal kernel restricted to dispersal between neighbouring regions. This is composed of the dispersal densities between the centres of a region and itself and its adjacent and diagonal neighbours, i.e. the dispersal kernel in (4.1) evaluated at the distances between the mid-points of regions, i.e. the dispersal between neighbouring regions with difference $\mathbf{i}$ between their indices is given by

$$K_{s_1,s_2\mathbf{i}} = k_{s_1,s_2}(\mathrm{D}x\,\mathbf{i}) \ . \tag{4.6}$$

The middle entry of the resulting array gives us the local contribution to the new population density in the region.

After both the high and low resolution components have been calculated, they are added together. In low-resolution regions, this involves the addition of two scalars (for each pair of demographic stages). For high-resolution regions, the contribution of long-distance dispersal to a region is approximated as equal for all cells, so the region's global-dispersal density is added to each cell's population density.

In summary, picking and choosing which level of dispersal resolution to use, based on the change in population and distance between locations, allows gains in efficiency with little reduction in accuracy.

4.2.3 Mesh Refinement

Mesh refinement is where the resolution of each region is changed to ensure that while the population distribution and the wave-front (the area with population density between the lower T_{HR} and upper T_{LR} thresholds) change, the mesh always has high resolution where needed. Individuals in the far field may drive population expansion (Lewis, 2016), so the choice of T_{HR} will depend on the IDE model being studied

and is in general set as low as required to ensure no significant change in model prediction. The mesh-refinement phase enables regions which enter the wave-front to become high-resolution, and regions which leave to return to low-resolution. Regions in the far-field of the wave-front where the juvenile stage's minimum population density has crossed the T_{HR} threshold become high-resolution. Regions in the wave-back which have either a juvenile population that has crossed the T_{LR} threshold, or densities which have changed less than a further parameter $T_{LR,2}$, become low-resolution. Since regions with only zero intrinsic population growth rates will always have zero population, they will always remain low-resolution (making the algorithm very efficient for sparse landscapes). Defining the wave-front via the juvenile stage is reasonable for populations where the juvenile stage is the first demographic stage to arrive at a new location, but if this is not the case then the algorithm can be altered.

4.2.4 Implementation

The algorithm was implemented in C++. We used C++ because it offers improvements in speed on higher level languages such as MATLAB and R. An executable which runs on Windows operating systems together with the source code is downloadable from GitHub (Gilbert et al., 2016).

We measured the algorithm's accuracy in simulating a non-stage-structured spreading population compared to a non-adaptive simulation algorithm (Section 4.3.1), its efficiency in CPU-time and RAM-usage (Section 4.3.2) and tested it by simulating hypothetical biological invasions into coniferous woodland with (1) a single demographic stage across Great Britain, and (2) two demographic stages into the New Forest (Hampshire, UK). In both cases, we used fine-scale mapping data from the CEH Land Cover Map 2007 (LCM2007) in Section 4.3.3.

Throughout the following section, we simulate IDEs of the form (4.1) with a single demographic stage and the commonly-used 2D Laplace (exponential) dispersal kernel (Carrasco et al., 2010) with spatially constant dispersal parameter α, given by

$$\mathbf{K}(\mathbf{x}-\mathbf{y},\mathbf{y}) = \frac{1}{2\pi\alpha^2}\exp\left(\frac{-\|\mathbf{x}-\mathbf{y}\|}{\alpha}\right), \tag{4.7}$$

where $\|\mathbf{x}-\mathbf{y}\|$ is the distance between $\mathbf{y}$ and $\mathbf{x}$. We choose a piecewise-linear scalar population growth function due to its simplicity and its ease in coding. Other stage-structured population projection matrices and single stage growth rates, including those with Allee effects, can also be used. We have tested the algorithm for a growth function with an Allee effect and found that the simulations were accurate for selected examples. For the piecewise-linear growth function, the population growth rate is constant below the carrying capacity C, with the population after the growth phase at $\mathbf{x}$ given by

$$r\left(\mathbf{u}^t(\mathbf{x}),\mathbf{x}\right)\mathbf{u}^t(\mathbf{x}) = \min\left(r_0(\mathbf{x})\mathbf{u}^t(\mathbf{x}), C\right), \tag{4.8}$$

where $r_0(\mathbf{x})$ is the intrinsic population growth rate at $\mathbf{x}$. Without loss of generality, we take the carrying capacity $C = 1$ throughout the following section. In Subsections 4.3.1-2 we take $\alpha = 1$ in non-dimensionalised units, but in Subsection 4.3.3 we simulate over a large real landscape, and take $\alpha = 50\,\mathrm{m}$ to allow wider dispersal.

When measuring the algorithm's accuracy (§4.3.1) and efficiency (§4.3.2), we take the initial distribution to be along one side of the square domain. For the example of spread of a specialist into a fragmented coniferous habitat in the UK as given by the LCM 2007 (§4.3.3), we took the initial distribution to be localised at a single cell.

4.3 Results

4.3.1 Accuracy

We tested the accuracy of the adaptive algorithm presented in Section 4.2 by comparing its output with a high-resolution non-adaptive algorithm across a range of parameters and landscape types for non-stage-structured IDEs. We varied four user-defined

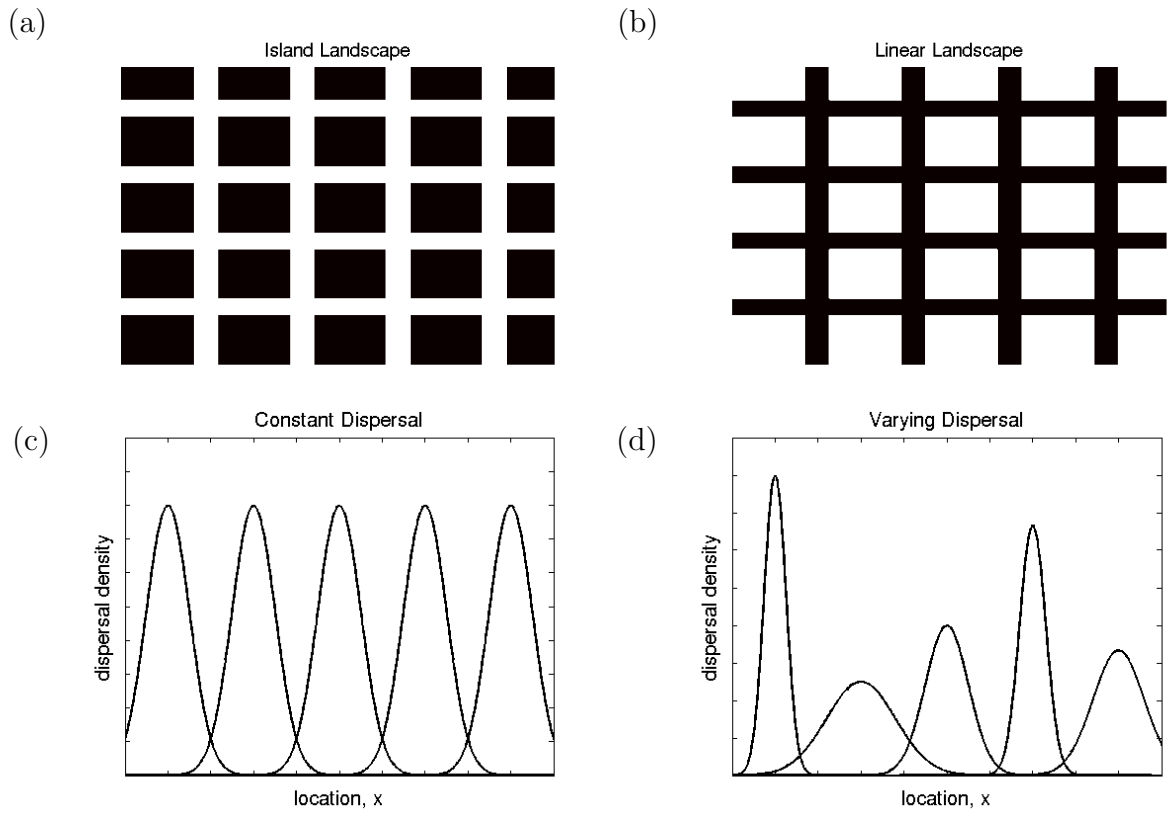

Figure 4.6: (a),(b) Heterogeneous Landscape Scenarios used to test the accuracy and efficiency of the adaptive simulation of IDEs of the form (4.1), with suitable habitat shown in black and unsuitable habitat in white. The suitable habitat in (a) is a regular grid of unconnected square islands separated by unsuitable habitat. The suitable habitat in (b) is a connected linear habitat with islands of unsuitable habitat. (c),(d) One-dimensional dispersal kernels at select points with (c) constant dispersal parameters, and (d) varying dispersal parameters (for comparison).

tolerance parameters to investigate the trade-off between accuracy and speed, as well as two model parameters to determine how the demography and landscape pattern affect the algorithm's accuracy. For a spatially homogeneous landscape and the spatially periodic linear and island landscapes presented in Figure 4.6a,b, we simulated both algorithms while varying six different parameters to explore the relationship between the parameter value, the landscape type and the algorithm's accuracy. To show that our algorithm gives accurate results for stage-structured populations, we demonstrated its accuracy against a stage-structured example.

For the non-stage-structured IDEs, we measured the accuracy using the relative error in (1) the area occupied by the population (where the population density exceeds

the threshold $\mu = 10^{-5}$) after 40 time-steps (at $t = 40$), and in (2) the furthest distance from the initial distribution that is occupied by the population at $t = 40$.

When considering the area-occupied, the relative error is given by

$$E_A = \frac{|A_a - A_n|}{A_n}, \tag{4.9}$$

where A_a and A_n are, respectively, predictions by the adaptive and non-adaptive algorithms for the area where the population density exceeds the threshold $\mu = 10^{-5}$ (area occupied) after 40 time-steps. Similarly, the relative error calculated using the furthest distances is given by

$$E_D = \frac{|D_a - D_n|}{D_n}, \tag{4.10}$$

where D_a and D_n are, respectively, predictions by the adaptive and non-adaptive algorithms for the maximum distance from the initial population of locations where the population density exceeds the threshold $\mu = 10^{-5}$ after 40 time-steps.

To systematically test the algorithm across a spectrum of variable landscape types and parameters, we varied: the density threshold at which a region returns to low-resolution once it is in the wave-back T_{LR}, the density threshold at which a region becomes high-resolution (from being in the far-field) T_{HR}, the size of each cell dx, the size of each region Dx, the growth rate in suitable habitat r and the period of the landscape, that is, the spatial distance taken for landscape features to repeat, p. Fifty values of each parameter were investigated under three landscape scenarios: one homogeneous scenario with the proportion of suitable habitat $d = 1$ and two periodic heterogeneous scenarios with $d = 0.5$. In the homogeneous landscape every location was suitable habitat ($d = 1$) and the landscape had the same growth rate everywhere, i.e. $r_0(\mathbf{x}) = r$ for all $\mathbf{x}$. We considered two heterogeneous landscape types, with differing levels of habitat connectivity, to test the effectiveness of the algorithm on a wide range of landscapes. In both heterogeneous landscapes, 50% of the landscape was suitable habitat ($d = 0.5$). In the *islands* scenario, each area

Parameter	**Description**	**Default Value (Accuracy)**	**Default Value (Efficiency)**
T_{LR}	HR to LR density threshold	0.5	0.5
$T_{LR,2}$	HR to LR density change threshold	10^{-10}	10^{-10}
T_{HR}	LR to HR density threshold	10^{-13}	10^{-13}
dx	cell size	0.1	0.4
Dx	region size	10	40
r	growth rate (suitable habitat)	3	3
p	landscape period	3	3
L_1	habitat length	160	800
L_2	habitat width	80	400
α	dispersal parameter	1	2
T	number of generations	40	40

Table 4.1: Table of default parameter values (used when the parameter is not being varied).

of suitable habitat was separated from other suitable habitat by unsuitable habitat (see Figure 4.6a) whereas in the *linear* scenario, all areas of suitable habitat were connected to all other areas of suitable habitat (see Figure 4.6b). Apart from the parameter being varied, all other parameters are fixed at their default values (see Table 4.1).

The effects of varying the different parameters on the two measures of error were fairly similar. When measuring the error using the area occupied, increasing the density threshold for regions to return to low resolution, T_{LR} increases the accuracy for all three landscape scenarios (Figure 4.7a). However, the effects of increasing T_{LR} above 10^{-3} are minimal. As the threshold where regions become high-resolution T_{HR} increases (Figure 4.7b), the accuracy decreases. For the homogeneous case, the simulation is highly accurate ($E_A < 0.05$) when $T_{HR} < 10^{-12}$ and the high-resolution region extends far out into the wave-front, but accuracy is lost for higher values of T_{HR}, i.e. $E = 0.35$ for all values of $T_{HR} > 10^{-11}$ investigated. For the two heterogeneous

cases, a similar pattern is observed but with the simulations remaining accurate for larger values of T_{HR} ($E < 0.05$ for all $T_{HR} < 10^{-9}$).

The size of each cell dx is positively correlated with the relative error E_A for all three scenarios, with a higher resolution mesh giving more accurate results (see Figure 4.7c). The effect of varying the region size Dx on the accuracy is more complicated. E_A is small for both small and large values of Dx and has a peak for intermediate values (see Figure 4.7d). This is because as the region width Dx becomes very small, the algorithm tends to the non-adaptive case. Similarly, when the region width Dx becomes very large, the requirement that regions containing any population with density between T_{HR} and T_{LR} that is changing faster than $T_{LR,2}$ be high-resolution means that most of the landscape is modelled as high-resolution, and that given the regions' size, most dispersal is modelled as high-resolution, bringing the algorithm close to the non-adaptive case.

Increasing the growth rate r does not much affect the accuracy for the two heterogeneous scenarios. However, for the homogeneous case, the accuracy is reduced for larger values of r considered, though the error remains below 2% (Figure 4.7e). Varying the landscape period does not have a straightforward effect on the accuracy, but for all values of p simulated, E_A was less than 0.5% (Figure 4.7f).

Qualitatively, the effects of varying the different parameters in the different scenarios on the relative error E_D of the furthest distance travelled are very similar to the effects on the relative error E_A of the area occupied. However, the values of the relative error E_D calculated using the furthest distances are often much larger than the E_A values, particularly for the two heterogeneous scenarios. This is likely to be due to the high degree of sensitivity of the furthest distance to small changes in dynamics in heterogeneous landscapes (if even a very small part of an additional island is colonised, the distance jumps to the island's location, while the area occupied grows only incrementally). This means that distance is often a misleading metric to use, but is included here in the interests of showing the robustness of our qualitative results. For all three scenarios, increasing T_{LR} decreases E_D (Fig 4.8a). As T_{HR} increases

beyond a threshold value ($\sim 10^{-12}$ for the homogeneous scenario and 10^{-9} for the heterogeneous cases), E_D begins to grow (Figure 4.8b). As dx is increased (and the resolution of each cell becomes coarser), E_D increases (Figure 4.8c), and decreases as r decreases (Figure 4.8e). For both the size of the regions Dx and the period of the heterogeneous landscapes, there is no clear relationship between the parameter and E_D (Figure 4.8d,f).

In summary, the algorithm gives accurate results for the scenarios considered when using both the area occupied and the maximum distance to measure the error. The high levels of accuracy attained using both measures demonstrate that our results are robust.

Analytically Tractable Example

In order to further study the adaptive algorithm and the behaviour of the errors it introduces, we compared the results of simulation with analytical results for an analytically tractable example. In our example, the landscape is homogeneous, the initial population distribution a small population concentrated at a single point source (Dirac delta function), dispersal is given by the Gaussian kernel with dispersal parameter $\sigma = 5$, the population growth function given by a linear population growth rate $r = 2.5$, with no non-linearities. The IDE is given by

$$\mathbf{u}^{t+1}(\mathbf{x}) = \int_{\mathbb{R}^2} \frac{r}{2\pi\sigma^2} \exp\left(\frac{-\|\mathbf{x}-\mathbf{y}\|^2}{2\sigma^2}\right) \mathbf{u}^t(\mathbf{y}) \mathrm{d}\mathbf{y} \ , \tag{4.11}$$

with the initial population distribution $\mathbf{u}^0(\mathbf{x})$ given by the Dirac delta function, $\mathbf{u}^0(\mathbf{x}) = \delta(\mathbf{x})$. Given that the convolution of (i) a Gaussian distribution and a delta function and of (ii) two Gaussian distributions are both Gaussian distributions, the analytical solution to the IDE is given by

$$\mathbf{u}^t(\mathbf{x}) = \frac{r^{\,t}}{2\pi\, t\, \sigma^2} \exp\left(\frac{-\|\mathbf{x}\|^2}{2\, t\, \sigma^2}\right) \ , \tag{4.12}$$

for $t > 0$. We compare this analytical expression for the solution of the linear IDE

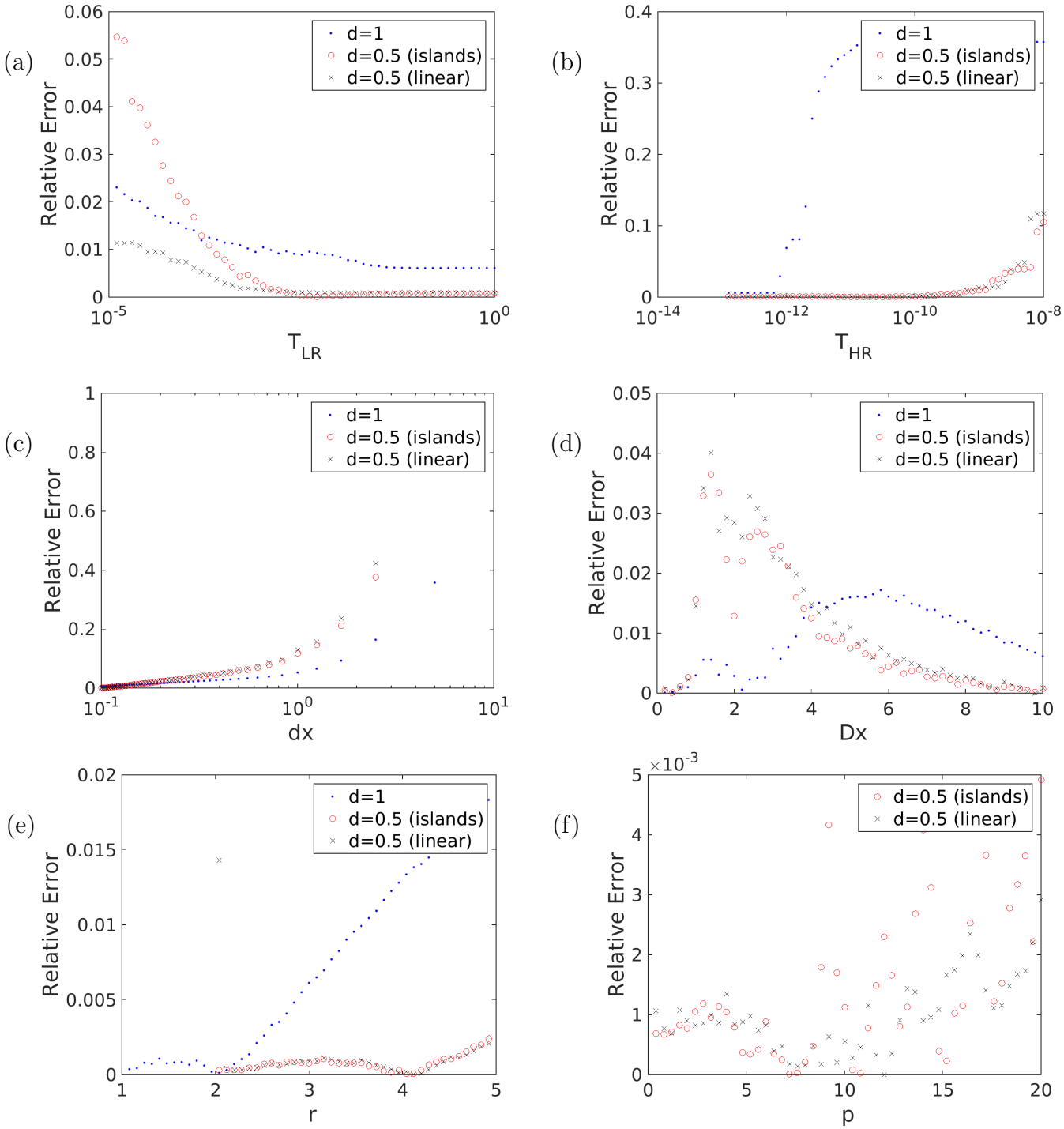

Figure 4.7: Effect of varying parameters on the Relative Error of the simulation as measured by the area occupied (4.9), i.e. $u > 10^{-5}$, by the invasion at $t = 40$ for three different landscape scenarios (i) homogeneous, with habitat density $d = 1$ (spots, blue online), (ii) islands, with $d = 0.5$ (circles, red online) and (iii) linear, with $d = 0.5$ (crosses, black online). We vary the density thresholds (a) T_{LR}, at which a region returns to low-resolution in the wave-back, (b) T_{HR}, at which a region becomes high-resolution in the wave-front. We vary the spatial extent (c) dx, of the individual cells and (d) Dx, of the regions. We vary (e) the growth rate, r and (f) the landscape period, p. For each parameter, we show all three landscape scenarios except for p, where varying the period has no effect on the homogeneous landscape.

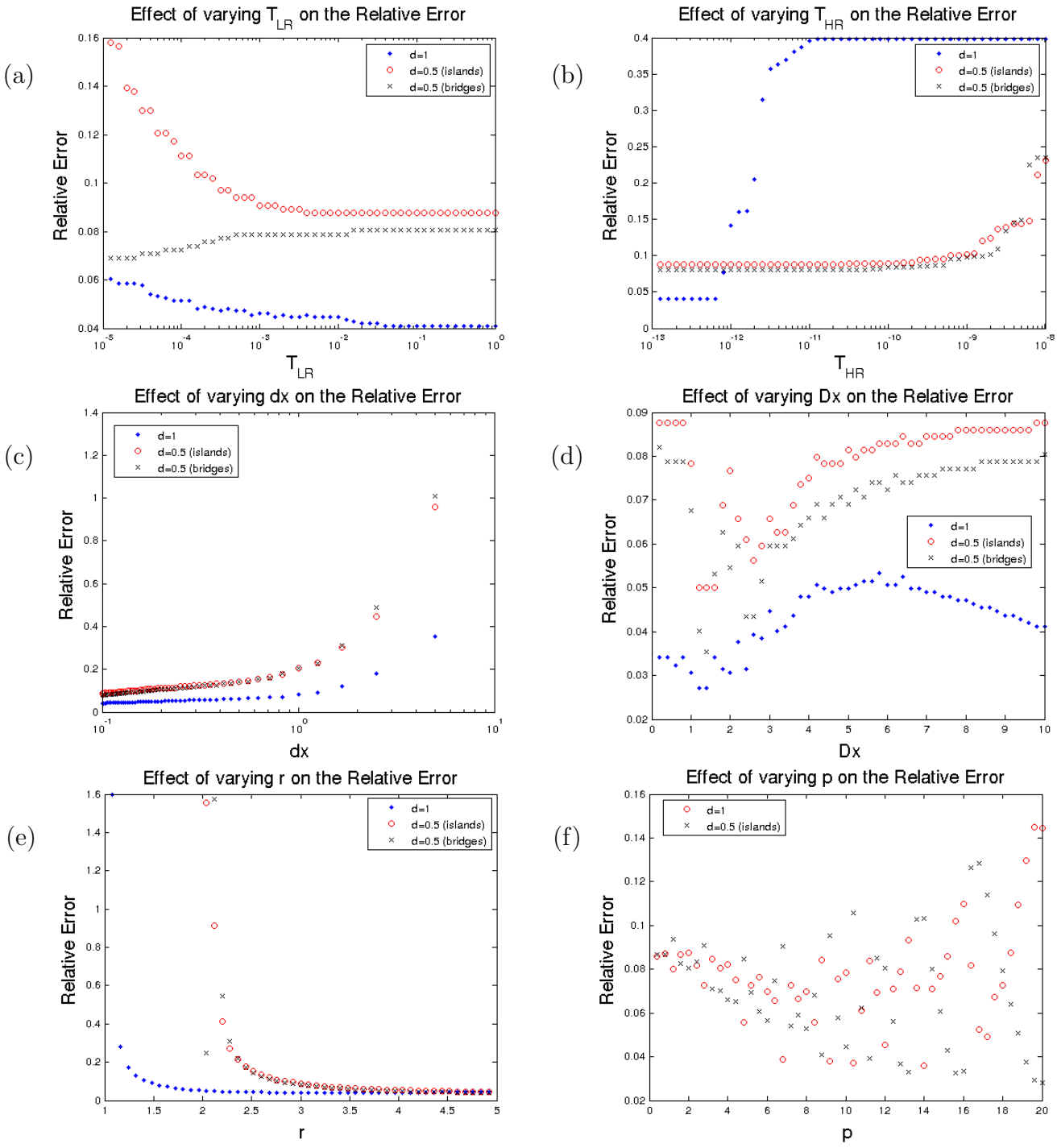

Figure 4.8: Effect of varying parameters on the Relative Error of the simulation as measured by the furthest point (from the original population) occupied (4.10), i.e. $u >$ 1e-5, by the invasion at $t = 40$. We vary the density thresholds (a) T_{LR}, at which a region returns to low-resolution in the wave-back, (b) T_{HR}, at which a region becomes high-resolution in the wave-front. We vary the spatial extent (c) dx, of the individual cells and (d) Dx, of the regions. We vary (e) the growth rate, r and (f) the landscape period, p. For each parameter, we show all three landscape scenarios except for p, where varying the period has no effect on the homogeneous landscape.

with the results of the adaptive algorithm for cell size dx = 0.1, region size Dx = 10, landscape length and width $L_1 = L_2 = 90$ and the values of T_{LR}, $T_{LR,2}$ and T_{HR} presented in Table 4.1. We plot the simulated population distribution and the absolute values of the error (the difference between the analytical and simulated results at each spatial location) in Figure 4.9.

We find that even for the relatively large ratio between the dispersal parameter σ and the region-size Dx, the errors remained small, with the maximum size of the error less than 4% the maximum size of the population. Figures 4.9(b),(d),(f) show that the main source of error is from the low-resolution dispersal, with the largest errors occurring when the low-resolution dispersal density is at its greatest, next to the boundaries between regions (see Figure 4.9(b)). These errors propagate to generate the patterns in Figures 4.9(d),(f).

Stage-Structured Example

While we have developed an algorithm that uses adaptive mesh refinement to simulate stage-structured IDEs with no restriction on the number of demographic stages, in the interests of brevity, we restricted the demonstration of accuracy to IDEs with a single demographic. To demonstrate that the algorithm could simulate populations with multiple demographic stages accurately, we simulated an IDE with two demographic stages (juvenile and adult) and spatially homogeneous demography and dispersal and compared the numerically simulated spreading speed with the analytical spreading speed.

In our example, population growth below a threshold at time t is given by a linear matrix $\mathbf{A}$

$$\mathbf{B}(\mathbf{u}^t(\mathbf{x})) = \begin{cases} \mathbf{A}\mathbf{u}^t(\mathbf{x}) & \text{if } \mathbf{c}\cdot\mathbf{u}^t(\mathbf{x}) \leq 1 \\ \\ \mathbf{u}^t(\mathbf{x}) & \text{if } \mathbf{c}\cdot\mathbf{u}^t(\mathbf{x}) > 1 \end{cases}, \tag{4.13}$$

where

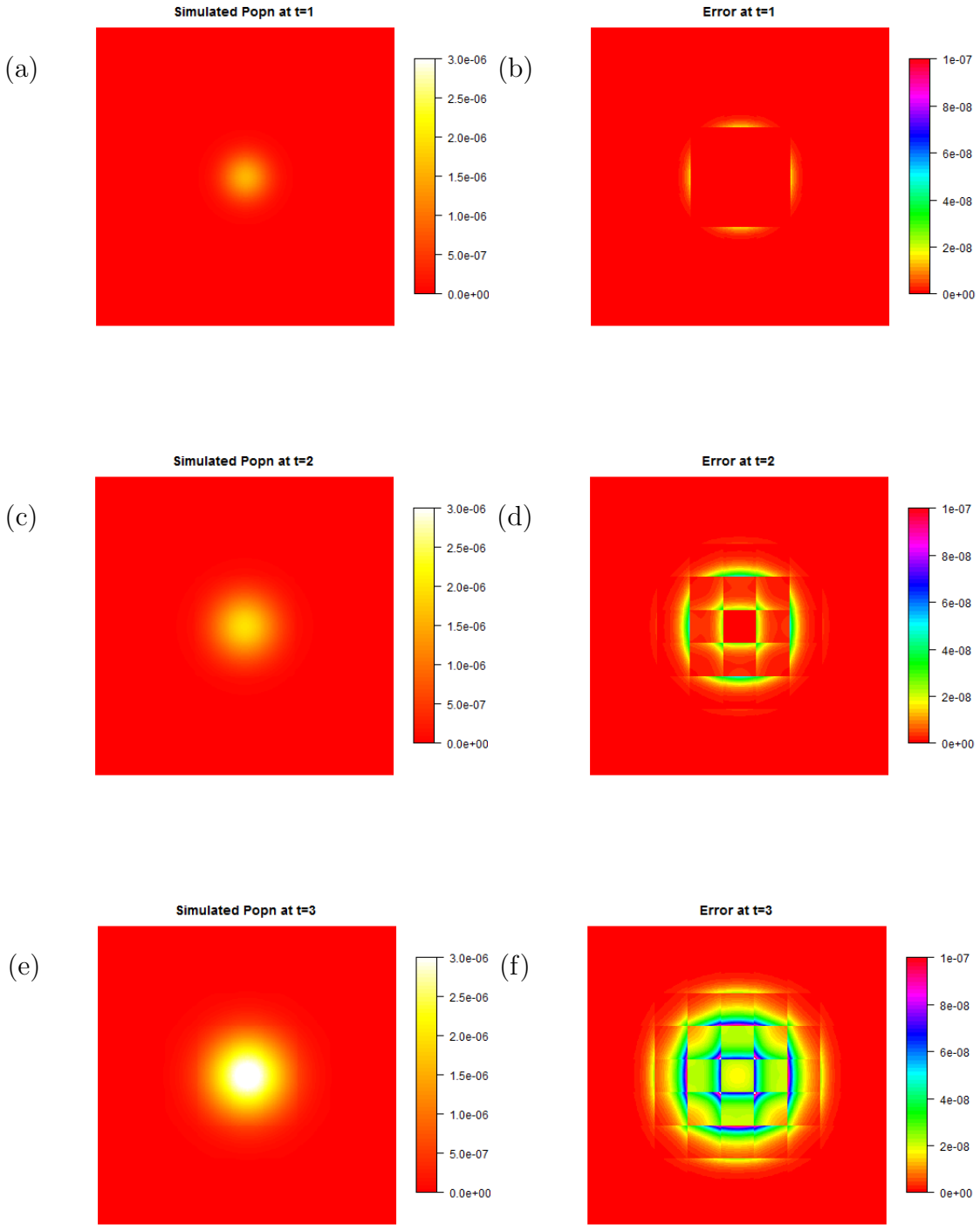

Figure 4.9: (a),(c),(e) Adaptive simulation of (4.11) at (a) $t = 1$, (c) $t = 2$, (e) $t = 3$ and error of the simulation compared to the exact analytical solution at (b) $t = 1$, (d) $t = 2$, (f) $t = 3$.

$$\mathbf{A} = \begin{bmatrix} 0.2 & 3 \\ 0.7 & 0.5 \end{bmatrix} \quad \text{and} \quad \mathbf{c} = \begin{bmatrix} 1 \\ 1 \end{bmatrix} \quad , \tag{4.14}$$

for all locations in the landscape. Dispersal occurs only between the adult and juvenile stage (for offspring generated at time t) and is given by the Gaussian dispersal kernel with $\sigma = 1$. All other pairs of stages do not disperse and their dispersal is represented by the Dirac delta function,

$$\mathbf{K}(\mathbf{z}) = \begin{bmatrix} \delta(\mathbf{z}) & \frac{1}{\sigma\sqrt{2\pi}} \exp\left(\frac{-\|\mathbf{z}\|^2}{2\sigma^2}\right) \\ \delta(\mathbf{z}) & \delta(\mathbf{z}) \end{bmatrix} \quad . \tag{4.15}$$

We used the analytical spreading speed given by equation (1.15) and Neubert and Caswell (2000) to calculate the asymptotic spreading speed from the population projection matrix and the matrix of dispersal kernels. Equation (1.17) generalises to

$$\int_{\mathbb{R}^2} \mathbf{K}(\mathbf{z}) \circ \mathbf{A} \mathrm{e}^{s\mathbf{j}\cdot\mathbf{z}} \mathrm{d}\mathbf{z} = \begin{bmatrix} 0.2 & 3\exp\left(\frac{1}{2}\sigma^2 s^2\right) \\ 0.7 & 0.5 \end{bmatrix} \quad , \tag{4.16}$$

and following the results of Neubert and Caswell (2000) and Equation (1.15), c^* is given by

$$c^* = \min_{s>0} \left[\frac{1}{s} \log\left(\rho(s)\right)\right], \tag{4.17}$$

where $\rho(s)$ is the principal eigenvalue of (4.16). The value of c^* and the analytical spreading speed of a two-dimensional travelling wave (where the wave-front is a straight line) is 0.7076. Simulating the IDE on a rectangular domain with constant non-zero initial conditions only in the cells closest to one of the vertices, we took $\mathrm{d}x = 0.1$, $\mathrm{D}x = 5$ and used the default values of T_{LR}, $T_{LR,2}$ and T_{HR} presented in

Table 4.1. To determine the wave-speed, we calculated the area occupied by a population density greater than 10^{-5} for $50 < t \leq 100$ and divided this by the width of the domain to get the average distance travelled by the population at each time step. We fitted a straight line to these distances, and found the spreading speed (the gradient) to be 0.693. This gave a relative error of around 2% when compared to the analytical result.

4.3.2 Efficiency

The adaptive algorithm was tested for efficiency against a non-adaptive algorithm. We varied the parameters that have the greatest effect on the algorithm's computational complexity as these demonstrated the differences in performance between the adaptive and non-adaptive algorithms. Different values to the ones used to test the accuracy were used as performance gains are only possible for larger simulations (see Table 4.1). We varied the landscape/domain length, L, the number of generations, T, and the ratio M of the region width $\mathrm{D}x$ to the cell width $\mathrm{d}x$, $M = \mathrm{D}x/\mathrm{d}x$ (Figure 4.10).

For each of the three parameters varied, 24 values were investigated under the three landscape scenarios introduced in Subsection 4.3.1. For each parameter value and landscape scenario, the average of 10 runs was taken. The following performance measures were used:

- **CPU time.** The total time used by the processor (AMD FX(tm)-4100 Quad-Core Processor) on the simulation. This ignores any interruptions from other tasks, so is generally less than the actual time taken for the simulation, and was measured via the UNIX command `time()`.

- **Maximum RAM** is measured by the maximum *resident set size* over the programme's run, that is the amount of main memory (RAM) occupied by the process.

In Figure 4.10, we plot the adaptive algorithm's performance against the performance of the non-adaptive algorithm for the three different landscape scenarios and

for the three different parameters. In all cases, the adaptive algorithm was generally faster than the non-adaptive algorithm, particularly as the domain length L, total number of generations, T and the width in cells of each region M increased, with the adaptive algorithm using up to ten times fewer resources than the non-adaptive algorithm (Figure 4.10a,c,e). The adaptive algorithm also achieved a lower maximum RAM usage than the non-adaptive algorithm, especially as the domain length L and the ratio of region width to cell width $M = \mathrm{D}x/\mathrm{d}x$ increased.

4.3.3 Examples

To run the algorithm, the landscape map must be saved in the same directory as the executable, and the model and algorithm parameters (which determine the speed and accuracy of the algorithm) must be set in the parameter text file. The parameter file includes the option of specifying the location of a point release for the spreading population, or of defining an initial population through another map file. The executable and source code are available from GitHub (Gilbert et al., 2016), with the User Guide presented in Appendix A.

UK Land Cover Map

To assess our algorithm's performance on high-resolution maps of large landscapes, we simulated an invasion of a hypothetical specialist non-stage-structured species that can only inhabit coniferous woodland habitat using data from the 25m resolution CEH Land Cover Map, LCM2007, covering the whole of Britain (Morton et al., 2011). LCM2007 has 1.456×10^9 individual cells and our ability to simulate the model over this scale demonstrates the usefulness of the algorithm (the maximum RAM used by the adaptive algorithm is seven times less than the non-adaptive).

We present the results of this simulation in Figure 4.11, with the parameter values: growth rate $r^* = 200$ in coniferous habitat and zero elsewhere (non-coniferous terrain and sea/ocean), dispersal parameter $\alpha = 50$m, region size $\mathrm{D}x = 2.5$km, landscape

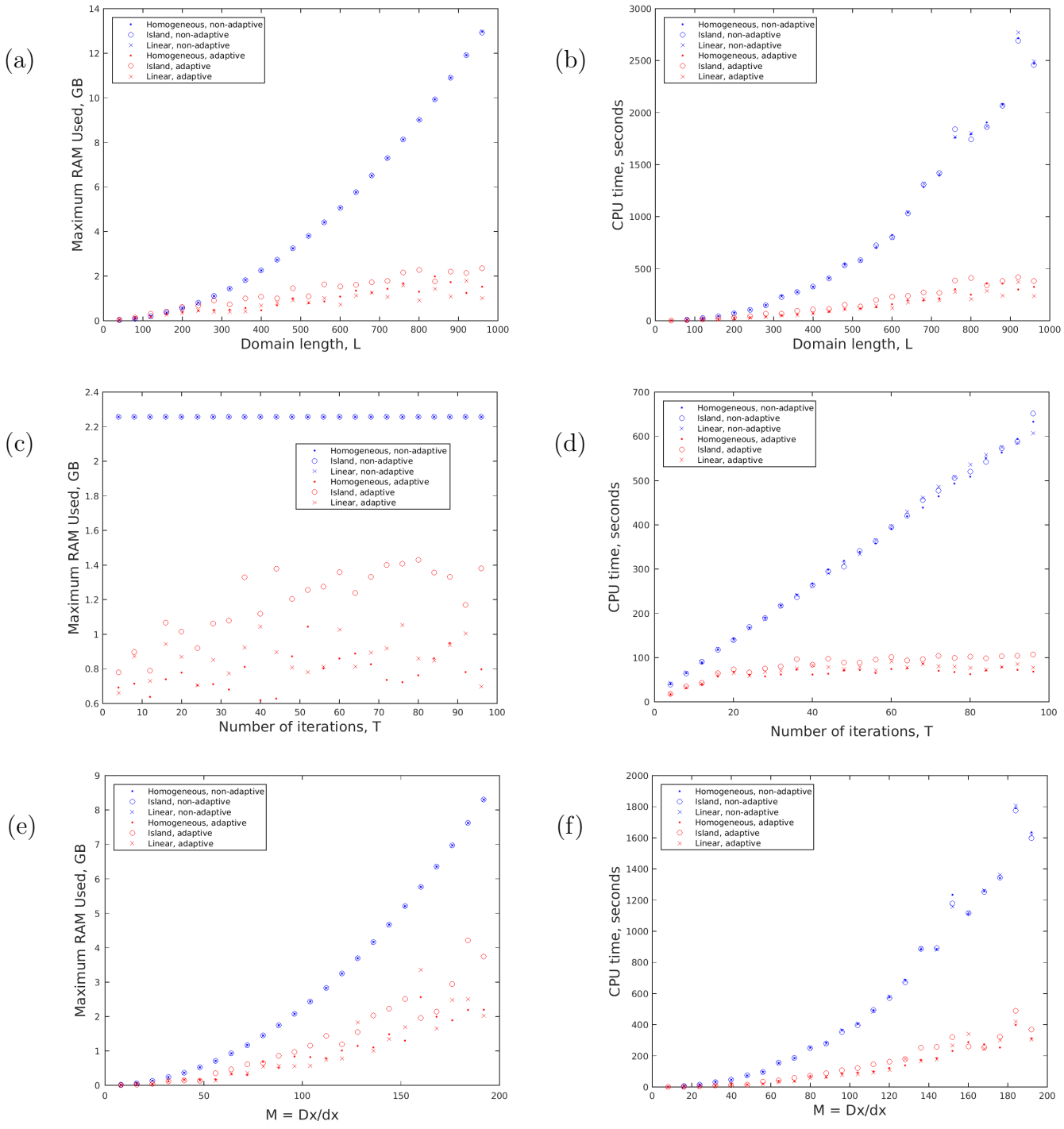

Figure 4.10: Effect of varying parameters on the average CPU time (a),(c),(e) and the maximum RAM (b),(d),(f) used by ten adaptive and non-adaptive simulations of (4.1) on an AMD FX(tm)-4100 Quad-Core Processor. We vary (a),(b) the domain length L, (c),(d) the number of generations T and (e),(f) the width of each region in cells $M = \mathrm{D}x/\mathrm{d}x$. For each parameter varied, we show the results for all three landscape scenarios for both the adaptive and non-adaptive algorithms.

length $L_1 = 1300$km and landscape width $L_2 = 700$km. All other model parameters took the values tabulated under default accuracy values in Table 4.1.

Stage-Structured Example

To demonstrate the opportunities our algorithm offers for modelling stage-structured spread, we simulated the spread of a population with two demographic stages (juvenile and adult) across part of the New Forest (Hampshire, UK). The hypothetical species has the same demographic and dispersal parameters as the stage-structured example in Section 4.3.1, except its population projection matrix is given by

$$\mathbf{A} = \begin{bmatrix} 0.2 & 30 \\ 0.7 & 0.5 \end{bmatrix} \tag{4.18}$$

in coniferous habitat, and zero elsewhere. The other (algorithm) parameters are given by the default values in Table 4.1. We present the results of this simulation in Figure 4.12, which show the areas occupied by juveniles (Figure 4.12a) and adults (Figure 4.12b) at each time-step.

4.4 Discussion

Spatially explicit, mechanistic population models facilitate a quantitative understanding of changing population distributions that incorporate dispersal and demographic behaviour. These models enable predictions of population spread for any species and landscape fitting the assumptions of the model. Under a limiting set of assumptions, spread rates of spatial models can be calculated analytically (Kot et al., 1996; Neubert and Caswell, 2000; Shigesada et al., 1986), but in general, numerical simulation must be used to predict the dynamics of changing population distributions in realistic scenarios, particularly when landscapes are either inhomogeneous or aperiodic. For all spatially explicit models, the accuracy of results obtained through simulation de-

(a) (b) (c)

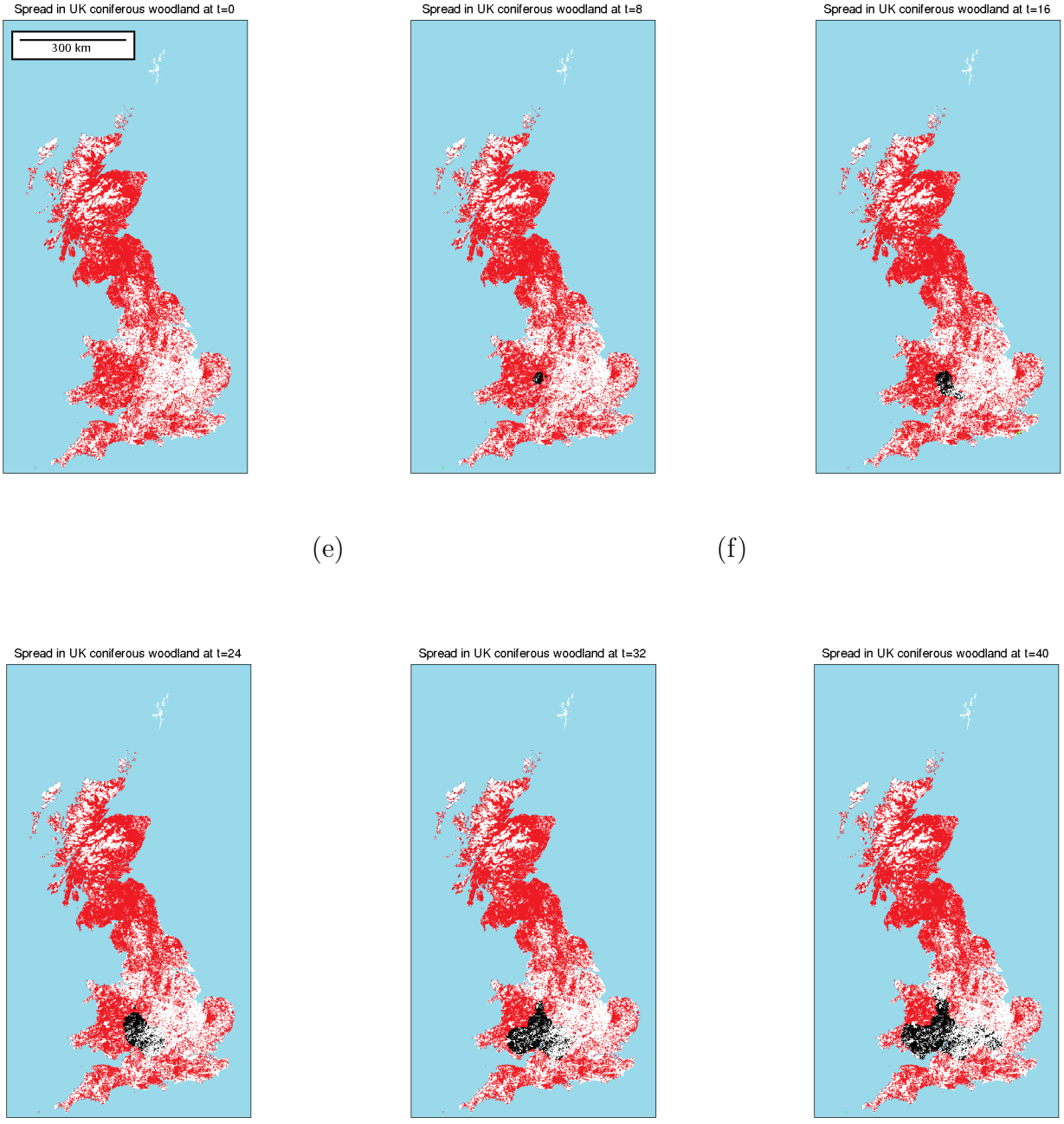

(d) (e) (f)

Figure 4.11: Spread of a hypothetical invasive species (black online) into UK coniferous woodland (red online) shown at 8-year intervals. The spread is given by an adaptive simulation of (4.1) using the CEH Land Cover Map, LCM 2007. The population growth rate in the coniferous habitat is $r = 200$ and the dispersal parameter $\alpha = 50$m. The blue region represents salt-water (oceans and seas) which together with terrestrial non-habitat has a zero population growth rate.

(a)

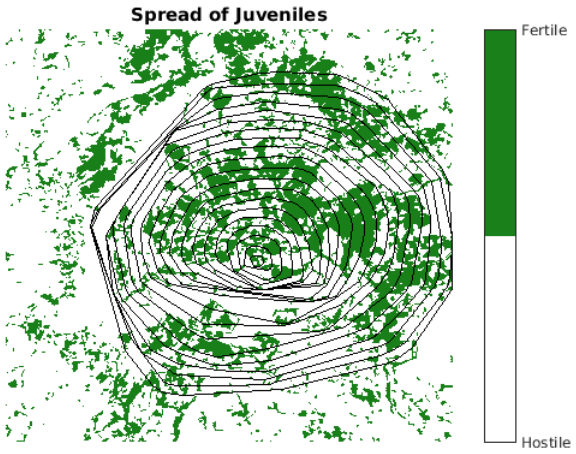

(b)

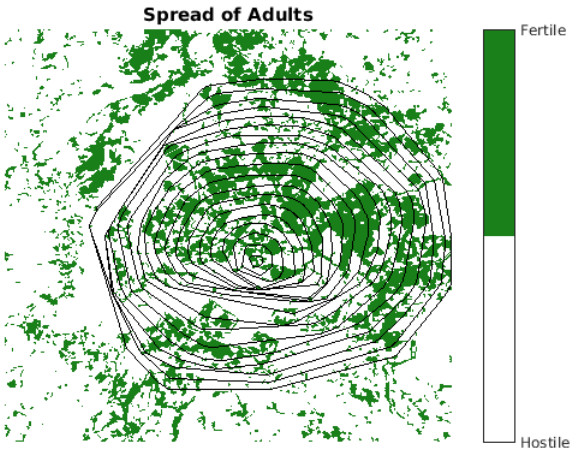

Figure 4.12: Spread of a hypothetical stage-structured invasive species modelled by (4.1) into an area of the New Forest (green online) with the areas occupied by (a) the juvenile and (b) the adult stage shown at one year intervals (black boundary).

pends on the quality of the data used as input to the model and on the resolution of the discretisation of the landscape, with more grid points providing greater accuracy, but requiring more computational resources.

In this chapter we have developed an adaptive mesh method that facilitates the simulation of IDE models of spatial spread efficiently and without significant losses in accuracy. This method allows ecologists to simulate spatial dynamics for cases that have previously been too computationally demanding even on computer clusters, and thus permits previously unachievable research questions to be addressed, and allows researchers to get more out of limited computational resources. In particular, we show that it is possible to simulate spread straightforwardly over very large areas with appropriate resolution. This adaptive algorithm has the additional cost of a mesh-refinement phase, but this is significantly smaller than the savings in computational resources in the growth and dispersal phases. We implemented this algorithm in C++ and have made an executable and source code available on GitHub (Gilbert et al., 2016).

For a range of parameter values and landscape types, we found that the adaptive algorithm was accurate and that for IDEs on large and/or high-resolution domains, in the tests (Sections 4.2-4.3), the adaptive algorithm used up to ten times less CPU-time

and maximum RAM than the non-adaptive algorithm. The algorithm was also applied to stage-structured IDE, and was found to be highly accurate in a homogeneous landscape, and has been used by Synes et al. (2016) to model the spread of spruce (Picea) trees at Glacier Bay, Alaska (see Figure 4.13).

The loss of resolution in the far-field and wave-back of the invading population introduces some error. In particular, if T_{LR} is too low, the errors in the wave-back may affect the spreading behaviour and if T_{HR} is too high, large errors will appear in the wave-front that may significantly affect spread. These effects are further exacerbated by landscape heterogeneity, which affects the spreading population. As with most numerical solvers (Berger and Oliger, 1984), there is a trade-off between model accuracy and efficiency, and the simulation parameters must be chosen to reduce both computational resources and the errors added by the numerical scheme. The acceptable level of error will depend on the application, but when calculating wave-speeds an error of a few percent will usually be acceptable. We suggest that users use the parameter values used in our examples (Table 4.1), and then lower the error tolerance and see if the solution significantly changes. If a significant change occurs, then a lower error tolerance is probably required.

To further demonstrate the algorithm's efficiency, we simulated a hypothetical invasive species' spread across coniferous woodland in Great Britain using the CEH LCM2007 habitat map of the UK. Using a non-adaptive algorithm to simulate over the whole of Great Britain at a resolution of 25m by 25m would require around 300 GB of RAM, which is not presently possible on a regular desktop computer. For the same problem, the adaptive algorithm used a maximum of 40 GB RAM and therefore enables the running of simulations that would have been impossible with non-adaptive algorithms.

In particular, the adaptive algorithm enables the simulation for the spread of species over large landscapes with variation in demographic parameters or complex fragmentation patterns. Spatial variation in demography is commonly observed (Oostermeijer et al., 1996), with environmental variation having a strong relationship

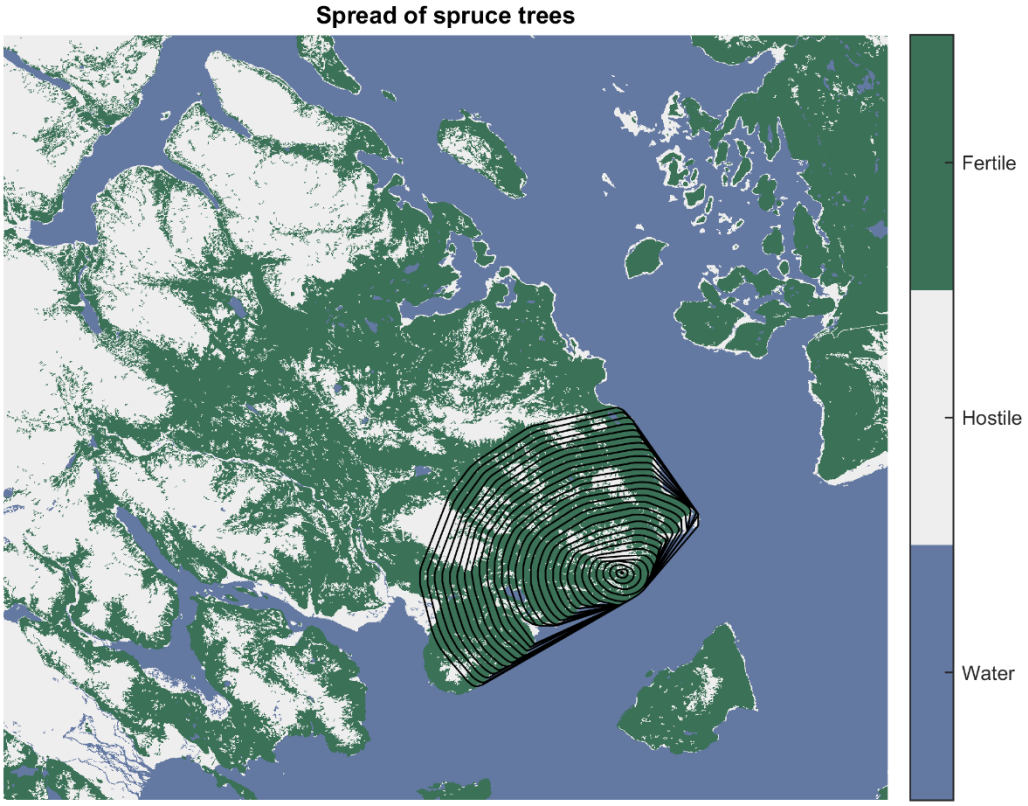

Figure 4.13: Simulated spread of spruce (Picea) trees at Glacier Bay, Alaska from Synes et al. (2016). The spread was simulated using the adaptive algorithm presented here with $r = 15\text{yr}^{-1}$ on fertile land and zero elsewhere. A 2D exponential dispersal kernel was assumed with a mean dispersal distance of 85m. The landscape suitability map was calculated from the National Land Cover Database 2011 (Homer et al., 2015). The figure shows areas of water, hostile and fertile land. The contours depict predicted annual maximal spread of the spruce trees from the initial location. For the given parameters, the IDE gives a spread rate of $367\text{m}\,\text{yr}^{-1}$, which closely matches empirical estimates (Fastie, 1995).

to parameter variation (Bullock et al., 1996). Fine-scale variation has been identified as a strong determinant of spread and persistence (Bennie et al., 2013; Carrasco et al., 2010). Therefore, incorporating high-resolution spatial variation into large scale models will enable more accurate predictions as well as greater insight into the effectiveness of fine scale ecological interventions such as landscape buffers and wildlife corridors in preventing and facilitating spread. Indeed, models of spread along corridors, stepping stones, etc in realistic landscapes have, to date, been limited with simplifying assumptions about spatial extent, structure and dynamics (Moilanen, 2011; Hodgson et al., 2012; Fennell et al., 2012). Our method will facilitate more complex modelling over scales and resolutions appropriate for conservation policy and planning.

A natural extension to the method presented in this paper is the inclusion of dispersal heterogeneity (Figure 4.6d) and density dependent dispersal, which is required to simulate organisms which settle based on habitat quality or population density as well as distance (e.g. Bonte et al., 2012). This is more computationally intensive to simulate, and simulating these IDEs adaptively would provide even greater relative improvements in speed and efficiency than for homogeneous IDEs. Without dispersal homogeneity, the integral in (4.1) cannot be calculated using FFTs. Instead dispersal is normally computed by multiplying the vector of discretised population densities by an $N \times N$ matrix, where N is the number of points in the discretisation, requiring $\mathrm{O}(N^2)$ floating point operations. An adaptive algorithm for simulating IDEs with heterogeneous dispersal would reduce the size of the matrix to $\hat{N}^2$, where $\hat{N}$ is the number of cells in regions with high-resolution information added to the number of regions with low-resolution information, leading to even larger reductions in computational resources than for the homogeneous cases presented in this paper. Extending the algorithm to heterogeneous and density dependent dispersal would vastly extend the types of models that could be simulated, and is for future development.

Chapter 5

Discussion

5.1 Summary

In this thesis, we have explored the problem of predicting the spread rate of species invasions in heterogeneous landscapes. Predicting spread is of great importance given the environmental and economic impacts of invasive species (Murray et al., 2014; Pimentel, 2011) and the necessity that populations keep pace with shifting habitats caused by climate change (Virkkala and Lehikoinen, 2014, Section 1.1). In particular, the distribution of suitable habitat and the spatial structure of the landscape are key in determining whether, and how, a population spreads (Section 1.2). Some spatial arrangements of habitat promote species invasions (Doherty et al., 2015), while others slow or prevent their spread (Hodgson et al., 2012). This may be due to the overall pattern of habitat: the size, shape and number of habitat patches (Bocedi et al., 2014b), connectivity (Vos et al., 2008) etc, or due to landscape barriers such as rivers, mountains and roads which may prevent spread in a particular direction (Marsh et al., 2005). Landscape barriers may be a particular problem for species affected by climate change (Meier et al., 2012). As temperatures increase, suitable ranges shift further north or to higher elevations. If barriers perpendicular to this direction prevent populations and communities from shifting (McInerny et al., 2007) then there is an increased risk of extinctions and reductions in biodiversity.

We reviewed a range of mathematical models for spreading populations (Section 1.4) including PDEs, SDMs, Metapopulation models, Integrodifferential Equationsa and IBMs. While the choice of model depends on the species and scenario being studied and the scientific question under consideration, IDEs have several benefits over other modelling approaches. In particular, they reflect the seasonal behaviour of many species by treating time as a discrete quantity (Wright and Hastings, 2007), can incorporate a wide variety of dispersal patterns (Kot et al., 1996), have a relatively small number of free parameters and are amenable to both simulation (Andersen, 1991) and analytical (Neubert and Caswell, 2000) methods. We gave an overview of the IDE literature and existing analytical and numerical techniques used to study them in Section 1.5.

To improve the applicability of IDEs and widen the range of mathematical techniques that can be used to investigate the behaviour of spreading populations, we developed novel analytical approximations to the wave-speeds of IDEs under two specific scenarios (Chapters 2 and 3) and developed an efficient simulation algorithm (Chapter 4). In Chapters 2 and 3, we used the fact that the wave-speed of an IDE on a periodic landscape with an exponentially bounded dispersal kernel and no Allee effect can be formulated as the minimum of a function of the principal eigenvalues of a family of operators (Weinberger et al., 2008), and used perturbation theory to find an asymptotic expansion for the eigenvalue in terms of a small parameter ϵ. In Chapter 4, we propose a novel algorithm to speed up the simulation of IDEs that have no exact or approximate analytical solution.

5.1.1 Sparse Fragmented Landscapes

In Chapter 2, we considered landscapes where suitable habitat is restricted to small isolated patches surrounded by a matrix of less suitable habitat or non-habitat. This is particularly relevant for predicting the spread of populations whose habitat patches are small and isolated, either due to geological processes (e.g. calcareous grassland,

see Hooftman and Bullock, 2012) or to habitat loss and fragmentation (e.g. forest habitat, see Figure 1.3 and Curtis, 1956).

We represented these sparse landscapes in one spatial dimension by periodic landscapes of alternating good and bad patches, where the dispersal scale is greater than the extent of each good patch and where the ratio of the demographic rates in the good and bad patches is given by a small parameter, denoted ϵ.

We derived an approximation to the asymptotic ($t \to \infty$) wave-speed of spreading populations in the sparse periodic landscape. This was based on the results for the asymptotic spreading speeds of spreading solutions to IDEs with spatially periodic variation in the demographic and dispersal parameters (Section 1.5.4 and Weinberger et al., 2008). Both the results of Section 1.5.4 and our approximation are justified for single species stage-structured populations where the dispersal kernel is exponentially bounded (or equivalently has moments of all orders) and the growth function has no Allee effect (the zero population steady state is locally unstable in the good patches).

In deriving our approximation to the wave-speed, we used two properties of the landscape. First, the much larger demographic rates in the good patches allowed us to formulate an asymptotic expansion in the parameter ϵ, with the leading order term depending only on the population dynamics between the good patches. Second, the much smaller spatial extent of the good patches compared to the scale of dispersal meant that dispersal from the good patches, and therefore the leading order term in the asymptotic expansion, could be modelled as dispersal from a *point source*. We derived the first two non-zero terms of the expansion for stage-structured single-species IDEs with exponentially bounded dispersal kernels and no Allee effect.

We applied this approximation for IDEs with Gaussian and Laplace dispersal kernels and with stage-structured and non-stage-structured populations, and compared the approximate spread rates against the results of numerical simulations. We found the analytical approximations to have low relative error and to be highly accurate across a range of parameters for the landscapes considered. Weaknesses of this approximation include its validity only for periodic landscapes and for growth functions

without Allee effects and exponentially bounded kernels, and the fact that it is unclear a-priori how small ϵ and L_1 need to be to obtain a given level of accuracy.

We also found that the choice of dispersal kernel affects the relationship between the spatial scales of variation and extent of the good patches and the spreading speed. In particular, for proportions of good habitat p corresponding to a successful invasion for low landscape periods L, increasing the landscape period increases the wave speed c^* for the Laplace kernel, and decreases the wave speed for the Gaussian kernel. The approximations developed in this chapter were published in the Journal of Theoretical Biology (Gilbert et al., 2014b).

5.1.2 Landscapes with Low Variation

In Chapter 3, we derived an approximation to the spreading speeds of IDEs over landscapes where the spatial variation in demographic and dispersal parameters occurs over arbitrarily large spatial scales, but where the amount of variation from the mean is small, with the maximum change in environmental parameters being $\mathrm{O}(\epsilon)$, where $\epsilon \ll 1$. Variation of this form has been documented by several authors (Jurena and Archer, 2003; Miller et al., 1995; Janisova et al., 2012), and is associated with spread across a single continuous habitat, such as prairie, boreal forest, or regions converted to arable agriculture.

We considered two classes of landscape with low environmental variation, landscapes with periodic spatial variation and those that were stochastically generated. For the spatially periodic landscapes, we used the methods in Section 1.5.4 to formulate the asymptotic spreading speed in terms of the minimum of a function of the principal eigenvalues of a family of periodic operators. We showed that each of these periodic operators could be formulated as the sum of a spatially homogeneous operator plus a small heterogeneous component. This enabled us to use perturbation methods and to formulate an asymptotic expansion for the eigenvalue in terms of the parameter ϵ, which governs the degree of environmental variation. For the

non-periodic, stochastically generated landscapes, we used numerical simulation to explore the impact of changing the value of ϵ on the simulated wave-speed.

For the periodic landscapes, we found that the $O(\epsilon)$ term in the expansions of both the principal eigenvalue, and of the asymptotic spreading speed were zero. This means that the difference between the wave-speeds of populations spreading in a spatially periodic landscape and its homogenisation is, in general, proportional to ϵ^2. For stochastically generated landscapes we numerically demonstrate that the error decays faster than $O(\epsilon)$. In both periodic and stochastic cases, this means that for sufficiently small ϵ, the homogeneous spreading speed is a suitable approximation for the spreading speed in the heterogeneous model. To provide a more accurate approximation for larger values of ϵ, we calculated the $O(\epsilon^2)$ term of the expansion of the wave-speed for periodic landscapes, which gave a higher order approximation. better but less analytically tractable approximation. This approximation provided more accuracy, but was less analytically tractable (had many more terms and involved infinite series) than the homogeneous approximations. Both the homogeneous and second order approximations shared some of the weaknesses of the sparse fragmented approximation (Chapter 2), namely being valid only for growth functions without Allee effects and exponentially bounded kernels, and having no a-priori estimate of the values of ϵ that satisfied given error tolerances. In addition, the second order approximation is valid only for periodic landscapes. However, the homogeneous approximation does not share this limitation and has been shown to have $o(\epsilon)$ error on periodic and stochastically generated landscapes.

We calculated both approximations for the spreading speed of IDEs on periodic landscapes of two alternating patches with Gaussian and Laplace dispersal kernels. We compared these results against numerical simulations of IDEs and found that the error of both approximations was very small sufficiently close to $\epsilon = 0$ and that the second order approximation had relative error less than 0.03 for $\epsilon < 0.3$. Finally, we compared the relationship between the mean growth rate, the scale of spatial variation and the spreading speed between the periodic and stochastically generated

landscapes, and found them to be qualitatively similar. This suggests that the insights gained for IDEs on periodic landscapes can be applied to a wider class of landscapes.

5.1.3 Speeding up Simulation

In Chapter 4, we addressed the problem of predicting spread for landscapes with no exact or approximate analytical expression for the spread rate. In these cases it is necessary to use numerical simulation by discretising the model and running it on a computer. Conventional approaches to simulating IDE models involve discretising the landscape into a regular mesh of cells of equal size and shape (Andersen, 1991; Legaspi Jr et al., 1998) and formulating the model as either a discrete convolution (for IDEs with homogeneous dispersal) or to a matrix multiplication (for heterogeneous dispersal), see Section 1.5.5. However, accurate simulations over large landscapes require a very large number of mesh points which use large amounts of computational resources.

To overcome this problem, we have developed a novel algorithm to simulate IDEs using *adaptive mesh refinement* techniques that have previously been applied to PDEs. Adaptive mesh refinement focuses computational resources on the parts of the landscape that have the greatest effect on the dynamics of the model's solution. The locations with the greatest impact on the model's dynamics change every time-step, so the algorithm updates the mesh every time-step so that it remains focused on the most relevant locations.

We implemented the algorithm in C++ for stage-structured single species IDEs, and have made our implementation available from GitHub (Gilbert et al., 2016). We analysed the accuracy of the algorithm and its efficiency compared to conventional methods. We found that when compared to a standard non-adaptive algorithm, the relative error of the population's spatial extent was low (< 0.05) for a range of parameter values. The adaptive algorithm was also extremely efficient and used up to ten times less CPU-time and RAM than the non-adaptive algorithm.

When running the adaptive algorithm, the numerical thresholds and region sizes must be pre-determined by the user (akin to error tolerance controls in ODE and PDE solvers). Setting the thresholds too low or high, or making the regions too small is likely to result in large numerical errors. However when these values are set correctly, its ability to provide improvements in efficiency without significant losses in accuracy enable the simulation of IDEs at scales, resolutions and speeds that were not previously feasible. We demonstrated these possibilities by simulating the spread of a hypothetical species over the UK at a resolution of 25m. A paper outlining the algorithm has been accepted for publication in Methods in Ecology and Evolution.

5.2 Future Work

The work presented in Chapters 2-4 motivates a range of ideas for future work. This includes extending the analytical and simulation methods to different ecological modelling frameworks, incorporating the adaptive algorithm presented in Chapter 4 into Bayesian inference methods that can infer ecological parameters from spread data, extending the adaptive algorithm to incorporate heterogeneous dispersal and answering scientific questions that can now be considered given the potential for simulating IDEs over larger landscapes given by the adaptive algorithm. In this section we sketch a brief outline of each of these ideas of further work.

5.2.1 Analytical Approximations of Spread for Other Models

The analytical approximations presented in Chapters 2 and 3 can be applied more generally and extended to other deterministic spatially explicit mathematical spread models. This allows the calculation of approximate spreading speeds in these models and may help to show that results are independent of the choice of modelling framework.

In particular, for PDEs with low periodic variation, it is possible to formulate approximations to the spreading speed of the same form as in Chapter 3 to show

that the degree of spatial variation ϵ has only an $O(\epsilon^2)$ effect on the asymptotic spreading speed c^*. This demonstrates that the results in Chapter 3 apply more widely to include populations where PDE models are more relevant and that for species spreading in landscapes with low environmental variation, the choice of deterministic model does not affect the reasonableness of the homogeneous approximation.

Periodic Travelling Waves in PDEs

Shigesada and Kawasaki (1997) showed that reaction-diffusion type PDEs with spatially periodic dispersal and growth have the same spread rates as their linearisation around the zero population steady state. In one spatial dimension, the linearised PDEs have the general form

$$\frac{\partial u}{\partial t}(t,x) = D(x)\,\frac{\partial^2 u}{\partial x^2}(t,x) + r(x)\,u(t,x) \tag{5.1}$$

where $D(x)$ and $r(x)$ are periodic with period L. The solutions to (5.1) are periodic travelling waves of the form

$$u(t,x) = \exp\left(s(c(s)t - x)\right)\phi(x,s) \tag{5.2}$$

where $c(s)$ is the wave-speed, s is the wave-number and ϕ is an L-periodic function in x. Substituting (5.2) into (5.1) gives us an expression for the wave-speed $c(s)$ of each travelling wave as the principal eigenvalue of a periodic operator F^s,

$$F^s\left[\phi(x,s)\right] = D(x)\left[s\,\phi(x,s) - 2\frac{\partial \phi}{\partial x}(x,s) + \frac{1}{s}\frac{\partial^2 \phi}{\partial x^2}(x,s)\right] + \frac{r(x)}{s}\phi(x,s)\ . \tag{5.3}$$

The asymptotic spreading speed of an initially bounded solution to (5.1) and therefore to a PDE with linearisation of the form (5.3) is given by the minimum of the periodic travelling wave-speeds, i.e.

$$c^* = \min_{s>0} c(s) \tag{5.4}$$

where $c(s)$ is the principal eigenvalue of (5.3).

Perturbation of the Operator

That the asymptotic spreading speed of a PDE with periodic dispersal and growth rates is the minimum of a family of principal eigenvalues of periodic operators allows us to use the same methods as in Chapter 4 to determine the spreading rate of periodic PDEs with low environmental variation. For these cases, the growth and dispersal functions have a periodic dependence on space and a dependence on the heterogeneity coefficient ϵ. This means that the PDE becomes

$$\frac{\partial u}{\partial t}(t,x,\epsilon) = D(x,\epsilon)\,\frac{\partial^2 u}{\partial x^2}(t,x,\epsilon) + r(x,\epsilon)\,u(t,x,\epsilon) \tag{5.5}$$

and that the periodic operator in (5.3) has ϵ dependence and is written as $F^{s,\epsilon}$. Similarly, the wave-speed $c(s)$ and periodic function $\phi(x,s)$ also have ϵ dependence and are now written as $c(s,\epsilon)$ and $\phi(x,s,\epsilon)$.

To find an asymptotic expression of the spreading speed $c(s,\epsilon)$, we start by expanding $c(s,\epsilon)$, $\phi(x,s,\epsilon)$, $D(x,\epsilon)$ and $r(x,\epsilon)$ in terms of ϵ. Since the growth rate and dispersal coefficient have weak variation, their O(1) terms are spatially constant. Similarly, we expect $\phi(x,s,\epsilon)$ to have a spatially constant O(1) term. The expansions are

$$D(x,\epsilon) = D_0 + \epsilon D_1(x) + \cdots \tag{5.6}$$

$$r(x,\epsilon) = r_0 + \epsilon r_1(x) + \cdots \tag{5.7}$$

$$\phi(x,s,\epsilon) = \phi_0(s) + \epsilon\phi_1(x,s) + \cdots \tag{5.8}$$

$$c(s,\epsilon) = c_0(s) + \epsilon c_1(s) + \cdots \ , \tag{5.9}$$

where

$$\int_0^L D_1(x)\mathrm{d}x = 0 \quad \text{and} \quad \int_0^L r_1(x)\mathrm{d}x = 0 \ . \tag{5.10}$$

In particular, substituting the expansions into (5.3) allows us to write the operator $F^{s,\epsilon}$ as the sum of a homogeneous operator and a small heterogeneous component, $F^{s,\epsilon} = F^{s,0} + \epsilon\, F^{s,1}$. Using the same algebraic manipulations as in Section 3.2.2, we find that $c_0(s)$ is the spreading speed of a spatially homogeneous PDE and is given by

$$c_0(s) = c(s,0) = sD(x) + \frac{r(x)}{s} \tag{5.11}$$

and $c_1(s)$ is given by

$$c_1(s) = \frac{1}{L}\int_0^L s\, D_1(x) + \frac{r_1(x)}{s}\mathrm{d}x = 0 \ . \tag{5.12}$$

This means that

$$c(s,\epsilon) = c(s,0) + \mathrm{O}(\epsilon^2) \ . \tag{5.13}$$

and by the same argument as in Section 3.2.3, the asymptotic wave-speed of the weakly varying PDE $c^*(\epsilon)$ differs from the spatially homogeneous PDE by $\mathrm{O}(\epsilon^2)$, i.e.

$$c^*(\epsilon) = c^*(0) + \mathrm{O}(\epsilon^2) \ . \tag{5.14}$$

5.2.2 Hybrid IDE/IBM models

The approach used in Chapter 4 of focusing resolution on the parts of the spatial domain that have the greatest effect on the system's future dynamics allows far more efficient simulation of PDEs and IDEs without significant losses of accuracy. The same approach could also be applied to other ecological models. This would widen the tool-kit of mathematical methods available to ecologists and would enable the

efficient simulation of species and scenarios where IDEs and PDEs are not realistic or useful modelling frameworks.

IDEs and PDEs are continuum models, so break down when individual behaviour has a significant effect on the dynamics. This can occur when populations are made up only of small numbers of individuals, or where there are a large number of individuals but where groups of individuals move as a single unit and it is desirable to model groups rather than individuals. Additionally, it is unknown how the small numbers of individuals in the wave-front of spreading populations affects spread. In these cases, models which incorporate intrinsic (population) stochasticity such as IBMs may be more realistic.

IBMs represent each individual explicitly and can incorporate a wide range of biological processes so can model the noisiness of small populations. However, modelling larger populations may become computationally expensive or even impossible. This would be a particular problem for modelling spreading populations where intrinsic noise plays a role in the spread dynamics, as the explicit modelling of each individual is necessary only in the wave-front and both unnecessary and extremely computationally expensive in the wave-back where populations are large.

One solution to this problem is to use different mathematical models in different spatial regions. For example, in the wave-front, where individual based stochasticity affects the population dynamics, the population could be represented by an IBM, while in the wave-back the population could be represented by a coarser IBM with the agents/individuals in the model representing communities or groups of organisms rather than single organisms. The hybrid model also incorporates rules for the movement of population across the interface between the two regimes and for the movement of the interface itself.

These methods have been used to model the dynamics of chemical reactions propagating through space. For example, Robinson et al. (2014) used an IBM model in the wave-front and a PDE model in the wave-back to model the spread of a travelling wave. Using a PDE model throughout the domain instead of the IBM significantly

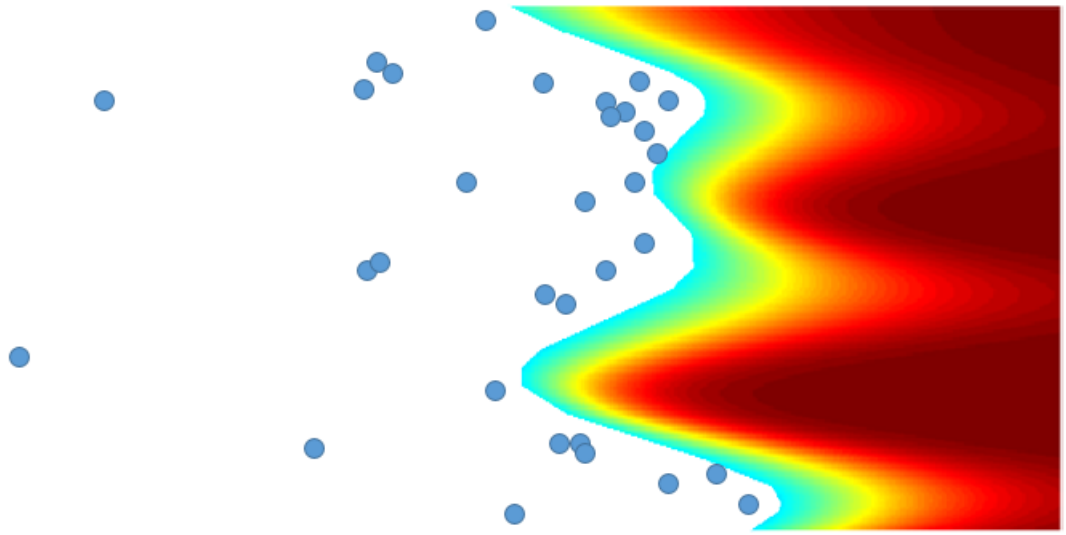

Figure 5.1: Sketch of a hybrid IDE/IBM simulation model. In the wave-back (right), an IDE is used, which is coupled to an IBM in the wave-front (left). The blue dots denote agents in the IBM.

over-estimated the spread rate as it ignored the important role of stochasticity in the wave-front. However, the *two-regime* model gave good agreement with the wave-speed of the IBM model solution. This means that computationally expensive IBMs need only be simulated in specific regions of space (the wave-front) and can be substituted with a deterministic PDE model which is less computationally expensive.

Extending these methods to problems in ecology would be relatively straightforward. For continuous time IBMs where organisms/propagules move by diffusion (dispersal is Gaussian), the methods of Robinson et al. (2014) could be used without modification. For IBMs which are discrete time or have a more complex dispersal process, then the wave-back continuum model would need to incorporate these aspects of the wave-front IBM. For many IBMs, an IDE in the wave-back would be the most obvious choice (see Figure 5.1).

For example, using a discrete time IBM and an IDE to model the spread of an invasive shrub, Travis et al. (2011) found that the spreading speed of the IBM model was slower than that of an IDE. In the IBM model, each individual's age was incremented by one each year. Then each of the reproductively mature plants

produced n seeds, each of which had dispersed to a location with displacement $\mathbf{x}_i$ from the parent. The number of offspring n of each plant were random variables, and the displacements were independently drawn from a distribution. This model could be coupled with a stage-structured IDE where the dispersal kernel for new individuals is given by the distribution of displacements in the IBM.

Using a hybrid IDE/IBM would provide very large benefits in efficiency over an IBM, especially given that most individuals are likely to be in the wave-back and therefore not modelled explicitly in the hybrid model. It would enable a model with the same behaviour as a full IBM to be simulated at scales that would otherwise be impossible.

5.2.3 Bayesian Inference and Data

Throughout this thesis, we have developed and presented methods to use IDE models to predict the future spreading behaviour of species invasions. In particular, we have derived analytical expressions for spreading speeds on particular landscape types (Chapters 2 and 3) and algorithms to simulate spread across a wider range of landscapes (Chapter 4). In all cases, we have assumed that the demographic and dispersal parameters and the forms of the life-cycle and dispersal kernel have been determined experimentally (Fujiwara et al., 2006, e.g.) or by observation in the field.

On the other hand, there may be species and scenarios for which experimental demographic or dispersal data are lacking, but where spatial data about population spread (e.g. presence-absence mapping data, mark-recapture data, counts at specific locations) are available. In these cases, it may be possible to solve the *inverse problem* of calculating the parameters from the data (Bellman et al., 1966) and to use the spatial population data to infer unknown demographic and dispersal parameters using either Bayesian (Wikle, 2002) or maximum likelihood approaches (Heavilin and Powell, 2008). This approach is not without its obstacles; insufficient or unreliable data and convergence issues (Huelsenbeck et al., 2002) may prevent accurate infer-

ence, and the form of the model (e.g. the type of dispersal kernel) must often be assumed *a priori*. On the other hand, if this approach is possible, then determining parameters using historical data improves understanding of the species' behaviour and allows the model to be run with the inferred parameters to make predictions of future spread, which can in turn be used to inform management strategies and risk assessment.

Bayesian Inference for IDEs

Work has been carried out on using Bayesian inference to determine the parameters of IDEs applied to meteorological systems (Wikle, 2002; Dewar et al., 2009; Scerri et al., 2009; Wikle and Hooten, 2010). However, these IDEs are exclusively linear, and are of limited applicability to ecological models. In ecology, Bayesian inference has been used to parameterise a Fisher-KPP PDE spread model (Habbal et al., 2014), process-based (hybrid SDM) models (Pagel and Schurr, 2012) and integral projection models (Merow et al., 2014).

In general, the ecological spatial data available to parameterise spread models fall into two categories: complete spatial maps obtained from field mapping or aerial photography over several years, or point data obtained through records at specific locations (Hastings et al., 2005). In the latter case, interpolation techniques can be used to generate complete maps. In the former case, the spatially continuous data are of the form $v^t(\mathbf{x})$ where $\mathbf{x} \in \Omega$, $t \in 1, ..., T$ where Ω is the spatial domain and T is the number of time-steps (e.g. years, days) for which data are available. If the data only refers to specific locations, then it will be of the form v_i^t such that $i \in 1, ..., K$ where K is the number of spatial locations.

In the Bayesian approach, the spread data v^t (denoted by the event $\mathbf{X}$) are used to calculate the *posterior* probability distribution $p(\boldsymbol{\theta}|\mathbf{X})$ of each of the possible sets of parameter values $\boldsymbol{\theta}$ given the spread data $\mathbf{X}$. Using Bayes' Theorem, the posterior probability can be expressed in terms of the *likelihood* function $p(\mathbf{X}|\boldsymbol{\theta})$ of the data, the *prior* probability distribution $p(\boldsymbol{\theta})$ and the probability of each set of parameters

in the absence of experimental data,

$$p(\boldsymbol{\theta}|\mathbf{X}) \propto p(\mathbf{X}|\boldsymbol{\theta})\, p(\boldsymbol{\theta}) \ . \tag{5.15}$$

If the desired output is a specific set of parameter values $\boldsymbol{\theta}$, then the parameter values corresponding to the maximum value of the posterior distribution can be inferred as the model parameters, which can then be used for running the model to make predictions. Depending on the shape of the likelihood function, the posterior distribution will show different levels of sensitivity to the prior distribution, which must be given as an input.

To fit an IDE to spatial spread data, two parts of the model (the process model and the observation model) must be assumed in order to calculate the likelihood function (Habbal et al., 2014), with the prior distribution also supplied in order to determine the posterior. Thus, to calculate the posterior distribution using the Bayesian approach, three inputs are required:

- **The process model** - The Bayesian approach can infer the likelihoods and probabilities of different parameter values, but it cannot in general determine the overall structure of the model (e.g. the growth function, the distribution of good and bad habitat, the dispersal kernel and the initial conditions). These must be assumed as an input. For example, a non-stage-structured IDE model with homogeneous dispersal may be assumed,

$$u^{t+1}(\mathbf{x}) = \int_{\Omega} k(\mathbf{x}-\mathbf{y}, \alpha)\, f(u^t(\mathbf{y}), \mathbf{y}, r)\, \mathrm{d}\mathbf{y} \ , \tag{5.16}$$

  where k is a specific dispersal kernel (e.g. Laplace), α is a dispersal parameter that controls the shape of k, f is a specific growth function (e.g. Ricker) which has growth rate r in good habitat and 0 elsewhere. Then $\boldsymbol{\theta}$ is given by $\boldsymbol{\theta} = \{\alpha, r\}$. The initial distribution $u^0(\mathbf{x})$ is also assumed.

- **The observation model** determines the probabilities of observing different

spread data v^t given a specific population distribution $u^t(\mathbf{x})$ (which is an output of the process/IDE model). This is not necessarily straightforward as the population distributions produced by the IDE are continuous valued and deterministic, while the data are likely to be noisy and may be discrete valued. To formulate an observation model, we can think of the observations as being random variables V^t that depend on the population distribution $u^t(\mathbf{x})$. The probability of observing the data $p(V^t = v^t)$, can be determined from the (joint) distributions of the random variables.

There may be several choices for the observation model. As an example, suppose that data are available only at specific points and continuous valued, with observations at each point independently exponentially distributed with mean equal to the population distribution at that point $u^t(\mathbf{x}_i)$, i.e.

$$V_i^t \sim \text{Exp}\left(\frac{1}{u^t(\mathbf{x}_i)}\right) \quad . \tag{5.17}$$

The likelihood function is then given in terms of the spread data v_k^t and the population model generated by the IDE with parameters $\boldsymbol{\theta}$ by

$$\begin{aligned} p(\mathbf{X}|\boldsymbol{\theta}) &= p(V_k^t = v_k^t, t \in \{1, ..., t\}, k \in \{1, ..., K\}|\boldsymbol{\theta}) && (5.18)\\ &= \prod_{t=1}^{T}\prod_{k=1}^{K} p(V_k^t = v_k^t|\boldsymbol{\theta}) && (5.19)\\ &= \prod_{t=1}^{T}\prod_{k=1}^{K} \frac{1}{u^t(\mathbf{x}_k)} \exp\left(\frac{v_k^t}{u^t(\mathbf{x}_k)}\right) && (5.20)\\ &= \exp\left(\sum_{t=1}^{T}\sum_{k=1}^{K} \frac{v_k^t}{u^t(\mathbf{x}_k)} - \log\left(u^t(\mathbf{x}_k)\right)\right) \quad . && (5.21) \end{aligned}$$

- **The prior distribution** expresses the probability of particular parameter values in the absence of the data. The choice of a prior distribution is likely to be subjective, however "with well-identied parameters and large sample sizes, reasonable choices of prior distributions will have minor effects on posterior

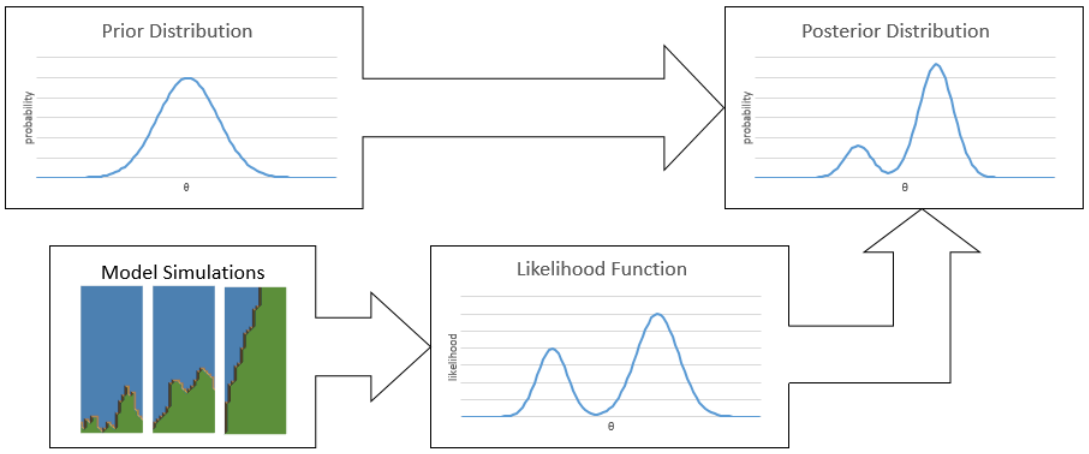

Figure 5.2: Flow diagram illustrating the role of model simulation, the likelihood function and the prior and posterior distributions in Bayesian inference

inferences" (Gelman, 2002).

In general, for some choices of process model, data model and prior distribution, it may be possible to derive analytical expressions for the likelihood and posterior distribution functions in terms of the data. However, this will not be possible for IDEs with nonlinear growth terms over heterogeneous landscapes. Instead, the posterior distribution must be sampled by simulating the IDE and data models for specific values. To determine the posterior distribution at a set of points $\boldsymbol{\theta} \in \Theta$, we must carry out the following steps (see Figure 5.2):

1. Simulate the IDE model for each value of $\boldsymbol{\theta}$.

2. Use this to calculate the likelihood function $p(\mathbf{X}|\theta)$.

3. Multiply the likelihood function $p(\mathbf{X}|\theta)$ by the prior distribution $p(\boldsymbol{\theta})$ to determine the posterior distribution $p(\boldsymbol{\theta}|\mathbf{X})$

These three steps can be used to determine the parameter values of IDEs and thus provide ecological insight and make future predictions about the spread of species where only spread data are available. For IDEs this can be extremely computationally costly, especially if (1) the parameter space Θ is very large, or (2) high-resolution

simulation over a large spatial domain is required to calculate the model population distributions $u^t(\mathbf{x})$. However, efficient simulation algorithms such as the adaptive algorithm presented in Chapter 4 would be able to achieve reductions in the computational cost of the high-resolution simulation required by Bayesian inference in these cases.

Adaptive Simulation and Approximate Bayesian Computation

The high computational cost of Bayesian inference on IDEs has two primary sources: (1) the cost of running simulations for each parameter value and (2) the cost of calculating the likelihood function from the model output. We propose that this computational cost can be reduced by using the adaptive simulation algorithm (Chapter 4) to reduce the cost of simulating IDEs and by using Approximate Bayesian Computation (ABC) to allow the calculation of the likelihood function to be parallelised, and to enable the use of clusters.

Approximate Bayesian Computation (Beaumont et al., 2002) involves running a number of model simulations in parallel, which are either accepted (and incorporated into the likelihood function) or discarded based on the size of the difference between the observations and the data. This difference is calculated using summary statistics for the data and distribution (Csilléry et al., 2010, 2012). For example, for discrete valued data over the complete map, one choice of summary statistic is the area occupied by the species. Combining this approach with the adaptive algorithm would allow much more efficient fitting of parameters to IDEs.

5.2.4 Incorporation of dispersal heterogeneity into simulation

In Chapter 4, we proposed and implemented a novel algorithm for simulating IDEs using adaptive mesh refinement. In the interests of brevity, we considered only cases where dispersal is homogeneous, i.e. where the form of the dispersal kernel does

not depend on the starting location of the dispersing individual or propagule. This assumption of homogeneity allowed the dispersal phase of the IDE to be formulated as a convolution and enabled the use of FFTs in their simulation. As a result, the adaptive algorithm developed for homogeneous landscapes simulates dispersal using FFTs for the low and high-resolution simulation of dispersal.

IDEs with heterogeneous dispersal cannot be simulated using FFTs. However, the adaptive mesh refinement approach can be extended to the heterogeneous dispersal case. Conventionally, an IDE with heterogeneous dispersal is simulated using standard quadrature. In the most simple case, the dispersal phase of a non-stage-structured IDE,

$$u^{t+1}(\mathbf{x}) = \int_{\Omega} k(\mathbf{x}-\mathbf{y},\mathbf{y})\, v^t(\mathbf{y})\, \mathrm{d}\mathbf{y} \tag{5.22}$$

where $v^t(\mathbf{y})$ is the population distribution after the growth phase ($v^t(\mathbf{y}) = r(u^t(\mathbf{y}),\mathbf{y})\, u^t(\mathbf{y})$) is represented by dividing the domain Ω into square compartments of equal width h, with mid-points $\{\mathbf{x}_j\}_{j=1}^{J}$. The IDE (5.22) can then be discretised, with the dispersal between compartments i and j given by the dispersal density between the mid-points multiplied by the area of the target compartment. The discretised form of the dispersal phase is then given by

$$u_i^{t+1} = h^2 \sum_{j=1}^{J} k(\mathbf{x}_i - \mathbf{x}_j, \mathbf{x}_j)\, v_j^t \tag{5.23}$$

$$= h^2 \sum_{j=1}^{J} K_{i,j} v_j^t \ , \tag{5.24}$$

which can be written as the matrix equation

$$\mathbf{u}^{t+1} = h^2 \mathbf{K} \mathbf{v}^t \ . \tag{5.25}$$

To incorporate adaptive mesh refinement, we allow the compartments used to

discretise (5.22) to be different sizes. This results in a matrix equation with the same form as (5.25) but with fewer elements for a given level of maximum resolution. The population growth and mesh refinement phases can then be simulated in precisely the same way as for the adaptive algorithm with homogeneous dispersal presented in Chapter 4.

5.2.5 Ecological Questions

The methods for quantifying spread presented in this thesis enable us to answer a range of ecological and scientific questions in ways that would previously have been impossible.

Chapters 2-4 present methods that facilitate the investigation of relationships between landscape variation, ecological parameters and spread. For example, it would be possible to explore how the variation in spatially varying factors such as soil chemistry/pH, temperature and drainage affect population spread, or how spread is affected ecological parameters specific to the spreading species, e.g. maturation rates, fecundity, dispersal behaviour. In particular, the analytical expressions for spread in periodic landscapes (Chapters 2-3) and the adaptive simulation algorithm (Chapter 4) allow faster parameter sweeps to determine these relationships. Additionally, in Chapter 3, we showed that landscape heterogeneity could be ignored in quantifying spread if the spatial variation were sufficiently weak. This justifies the use of existing analytical techniques that have been developed for homogeneous landscapes (e.g. Neubert and Caswell, 2000) on some heterogeneous landscapes.

The adaptive simulation algorithm presented in Chapter 4 allows predictions of spread at larger scales and higher resolutions than previously possible. This facilitates more accurate predictions over larger landscapes and time-scales, allowing better risk assessment and better informed management decisions. Previously, predictions of spread using IDEs have focused on calculating a specific scalar spreading speed (Buckley et al., 2005; Bullock et al., 2008) to quantify the threat of an invasive or the

ability of a range-shifting species to keep pace with its habitat. The advantages of this approach include the analytical tractability of expressions for spreading speeds and their sensitivity and elasticity to ecological parameters. However this approach cannot incorporate the complexities of spread over real heterogeneous landscapes. Using an efficient simulation algorithm allows future population distributions to be calculated more easily, and enables better informed and targeted conservation decision making.

Optimal control theory uses mathematical techniques to find the optimum management strategy in situations where a particular outcome (e.g. eradication of a pest, large harvest etc) is desired. Several authors have used optimal control for IDEs with the aims of maximising an objective functional such as profit from crop species (Joshi et al., 2006, 2007), finding the most effective way to release sterile insects (Gordillo, 2014) and to control pests (Martinez et al., 2015). These methods could easily be applied to species invasions with the aim of preventing or slowing the spread of an invasive species or encouraging the spread of range-shifting populations. In general, finding the optimal management strategy involves using an iterative algorithm such as the Forward-Backward sweep method (Martinez et al., 2015), which requires the IDE to be simulated a number of times, with the accuracy of the optimal control method determined by the resolution of the IDE. Incorporating the adaptive algorithm into these methods would allow more accurate and efficient calculation of optimal control methods, leading to more effective management decisions.

5.3 Conclusion

In this thesis, we have explored the relationship between landscape heterogeneity and the spread of species invasions (invasive species, range expansion). To do this we have modelled species invasions the IDE framework introduced to ecology by (Kot and Schaffer, 1986). Applying analytical and simulation techniques to IDEs have enabled us to develop the understanding of IDEs as mathematical systems and to draw wider conclusions about the ecological processes being modelled.

In particular, in Chapters 2 and 3 we derived analytical approximations to the spreading speeds of invasive species in specific landscape types. With the exception of landscapes with only low levels of environmental variation (Chapter 3), we found that the spread was highly sensitive to the spatial configuration of habitat as determined by parameters such as the landscape period and the proportion of good habitat. We also found that spread through heterogeneous landscapes was highly sensitive to the form of the dispersal kernel, with IDEs with Gaussian kernels having very different relationships between landscape period and spread rate than IDEs with Laplace kernels.

In summary, we have developed the understanding of both the relationship between landscape heterogeneity and population spread and the behaviour of IDE models, and have used mathematics to develop new methodology to enable ecological modellers to investigate spread more effectively. Specifically, we have justified the application of existing homogeneous approximations to IDEs with low environmental variation, have developed analytical approximations for spreading speeds in periodic landscapes which are either fragmented or have low variation (but where a greater degree of accuracy is required than given by the homogeneous approximation). Finally, we have developed a novel algorithm for the simulation of IDEs which provides large improvements in efficiency and accuracy on existing approaches.

Appendices

Appendix A

User Guide for the Adaptive Algorithm

AdaptiveIDE User Guide

AdaptiveIDE was written in C++, compiled using Visual Studio 2010 and has been tested on a Windows 7 PC. The steps below outline how to run the code.

Getting Started

To use AdaptiveIDE on Windows, simply download the zipped folder *AdaptiveIDE* from the GitHub repository (Gilbert et al., 2016). The folder (see Figure A.1) contains four files that are necessary for the simulation (we can ignore all others for now):

- **AdaptiveIDE.exe** - The compiled programme
- **libfftw3-3.dll** - The Dynamic Link Library (dll) file for the Fastest Fourier Transform in the West (FFTW) library. This precompiled dll file was downloaded from the fftw website, http://www.fftw.org/install/windows.html . Without this file, AdaptiveIDE.exe will not be able to run.

- **map.bin** - a binary file containing a map of the landscape as boolean variables. 1s denote suitable habitat and 0s denote unsuitable habitat.

- **Parameters.txt** - a text file containing all the (changeable) parameters used in the model and in the simulation algorithm.

In this user guide, we will briefly describe what type of integrodifference equation AdpativeIDE solves in **What AdpativeIDE Does**, list the **Inputs**, explain **How to Run a Simple Example**, and finally explain **How to Run Your Own Examples**.

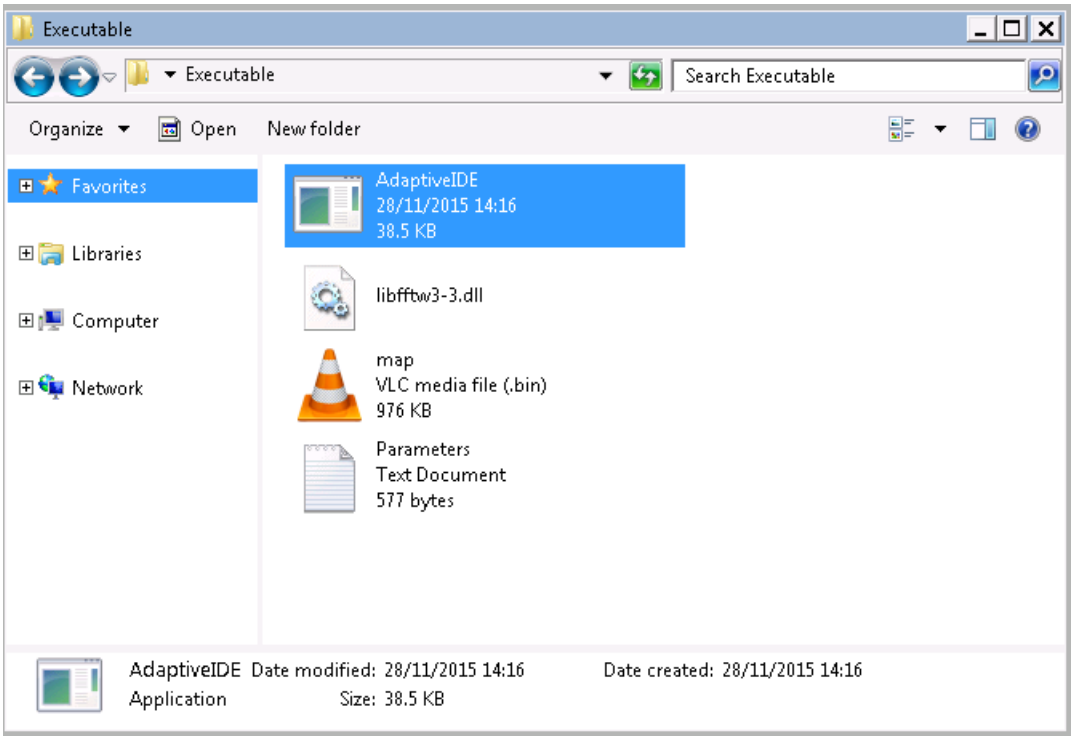

Figure A.1: The zipped folder *AdaptiveIDE*, available from the GitHub repository (Gilbert et al., 2016), contains four files.

What AdaptiveIDE Does

AdaptiveIDE simulates integrodifference equations using adaptive mesh refinement. It simulates integrodifference equations of the form

$$\mathbf{u}^{t+1}(\mathbf{x}) = \int_{\Omega} \left[\mathbf{K}(\mathbf{x}-\mathbf{y}) \circ \mathbf{B}(\mathbf{u}^{t}(\mathbf{x}))\right] \mathbf{u}^{t}(\mathbf{x}) \mathrm{d}\mathbf{y} \tag{A.1}$$

where $\mathbf{u}^t(\mathbf{x})$ is the population distribution, $\mathbf{K}(\mathbf{x}-\mathbf{y})$ is the spatially homogeneous dispersal kernel, Ω is the simulation domain and $\mathbf{B}(\mathbf{u}^t(\mathbf{x}))$ is the density and location dependent growth function. In AdaptiveIDE, the choices of dispersal kernel are restricted to Tophat, Cone, Hemisphere, Gaussian and Laplace and population growth below a threshold at time t is given by location dependent linear matrix $\mathbf{A}(\mathbf{x})$

$$\mathbf{B}(\mathbf{u}^t(\mathbf{x}),\mathbf{x}) = \begin{cases} \mathbf{A}(\mathbf{x}) & \text{if } \mathbf{q}\cdot\mathbf{u}^t(\mathbf{x}) \leq 1 \\ \\ \mathbf{I} & \text{if } \mathbf{q}\cdot\mathbf{u}^t(\mathbf{x}) > 1 \ , \end{cases} \tag{A.2}$$

where $\mathbf{q}$ determines the population carrying capacity (with each individual weighted by demographic stage), and $\mathbf{A}$ is the location dependent population projection matrix linearised around the zero population state. This is equal to the intrinsic population projection matrix in suitable habitat and zero in unsuitable habitat. The suitable and unsuitable habitat are defined by the binary file map.bin.

The initial population $\mathbf{u}^0(\mathbf{x})$ is constant and equal to 0.1 over a single region (the lower-resolution cells into which the landscape is partitioned) for its juvenile stage, all other locations and the initial populations of all other demographic stages are equal to zero.

A.1 Inputs

The zipped folder *AdaptiveIDE* contains four files. All the user-definable parameters are stored in Parameters.txt and a map of the landscape is stored in map.bin.

The map file is by default the random map shown in Figure A.2. This cannot be read directly into MATLAB using load but requires the fread and fwrite commands (see the How to Run Your Own Examples section).

Parameter	Description
initial_popn_loc_x	The x co-ordinate of the region containing the initial population
initial_popn_loc_y	The y co-ordinate of the region containing the initial population
initial_popn_density	Initial population density
kernel_no	Dispersal kernel (1 Tophat, 2 Cone, 3 Hemisphere, 4 Gaussian, 5 Laplace)
length	Landscape length
print	Print to file? (yes 1, no 0)
intrinsic_growth_rate	Population projection matrix in suitable habitat
output_resolution	Resolution of output map
T	Number of time-steps
landscape_width	Width of map in pixels
landscape_length	Length of map in pixels
region_width	Width of each region (in pixels)
threshcoarse	Population density threshold at which mesh returns to low-resolution
threshcoarse2	Population density change threshold at which mesh returns to low-resolution (if density threshold threshcoarse has not been reached)
threshcoarse3	Minimum population density that must be attained for mesh to return to low-resolution
threshfine	Population density threshold at which mesh becomes high-resolution

Table A.1: Table of parameters needed in the Parameters.txt file.

A.2 How to Run a Simple Example

To run AdaptiveIDE using the inputs in Parameters.txt and using the map in map.bin, just click on AdaptiveIDE.exe. If we assume that print = 1 in Parameters.txt, then this will result in the generation of an output file output.bin, which contains maps of the population distribution at each time-step which are concatenated together

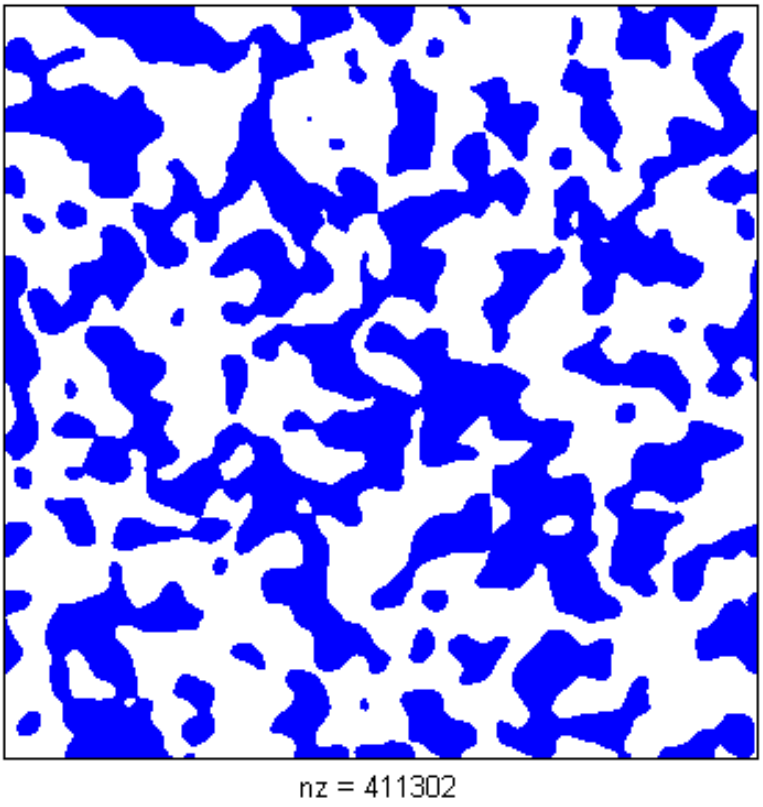

Figure A.2: The map provided in the zipped folder *AdaptiveIDE* is randomly generated.

(stacked on top of each other). To read them into MATLAB, use

```
>> load(PATH\output.bin);
>> for t = 0:(T-1)
       mesh(output((N*t+1):N*(t+1), : ));
       pause(.5);
   end
```

where N is the height of the map in pixels and T is the number of time-steps.

A.3 How to Run Your Own Examples

To run your own example with a different map, e.g. the 2000 x 2000 concentric circle jpeg figure included with the code (Figure A.3) using a Gaussian dispersal kernel,

with intrinsic growth rate equal to 20 and regions of size 200 x 200. We'll take the map to be of an area of 200km x 200km and the dispersal parameter to be 2 km.

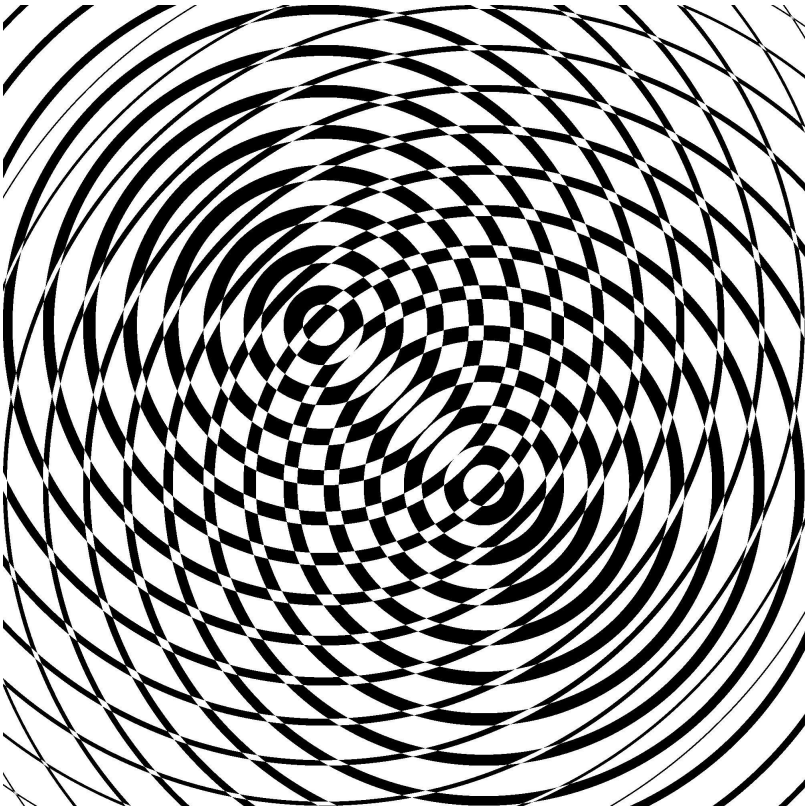

Figure A.3: The concentric circle jpeg figure included with the code can be used as a map of population growth rates.

Open the map image (e.g. jpeg) in MATLAB:

```
>> Z = imread(PATH\concentrics.jpeg');
>> Z = Z>100;
>> fileID = fopen('PATH\concentrics.bin','w');
>> fwrite(fileID,Z,'bool');
```

This turns a black and white map into a Boolean binary file. This should output concentrics.bin into the folder containing the AdaptiveIDE code. To run a simulation using this map, well need to rename concentrics.bin as map.bin. However to avoid losing the existing map, we should rename it as something else, e.g. random_map.bin, and then rename concentric.bin as map.bin (Figure A.4).

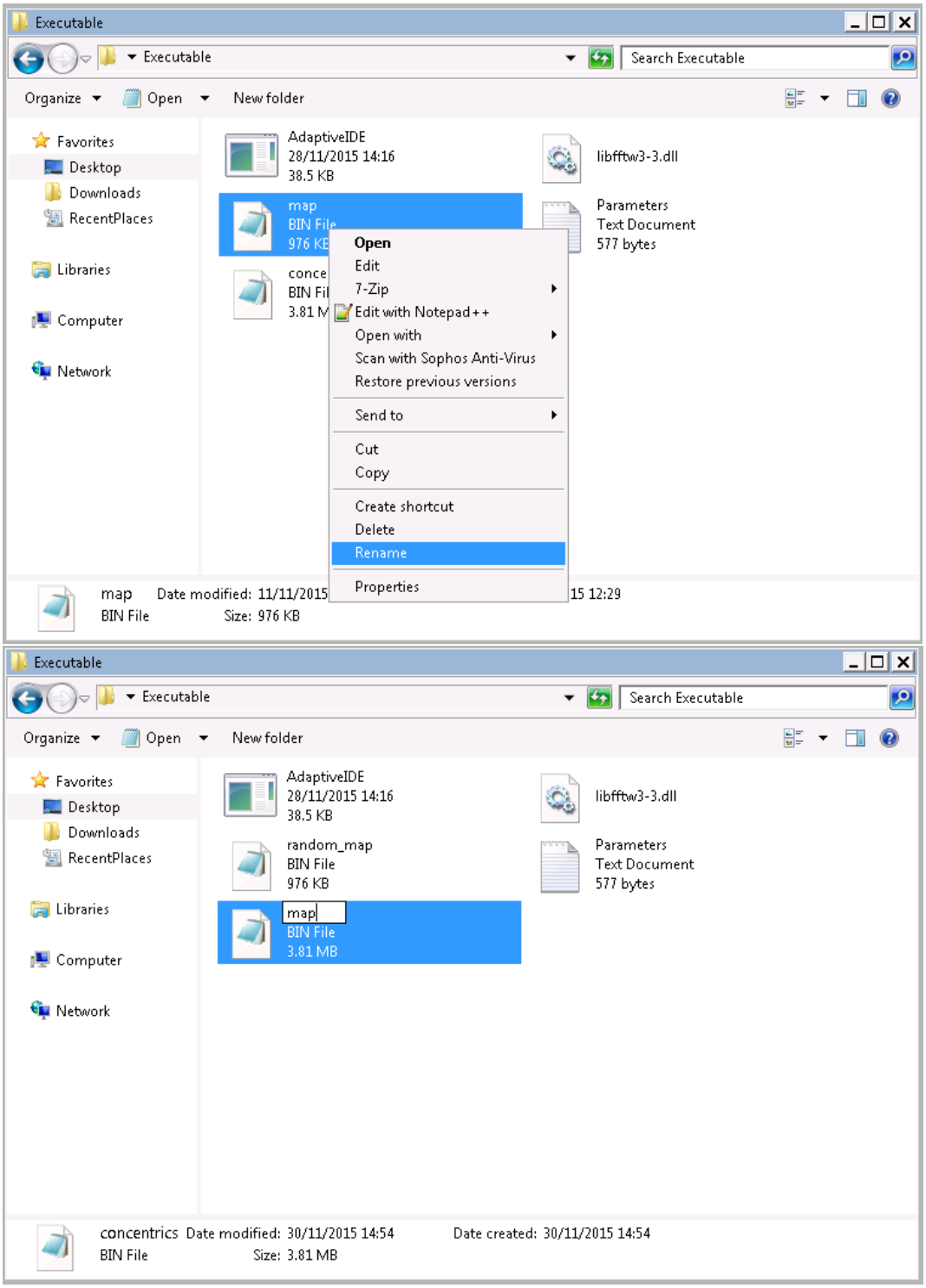

Figure A.4: To use the concentric circles image (Figure A.3), its name must be changed to map.bin, and the original map.bin given a different name.

This changes the map. We now need to change the Parameters file. Simply open the Parameters.txt file in a text editor (e.g. notepad). When initially opened, the text file should look like Figure A.5.

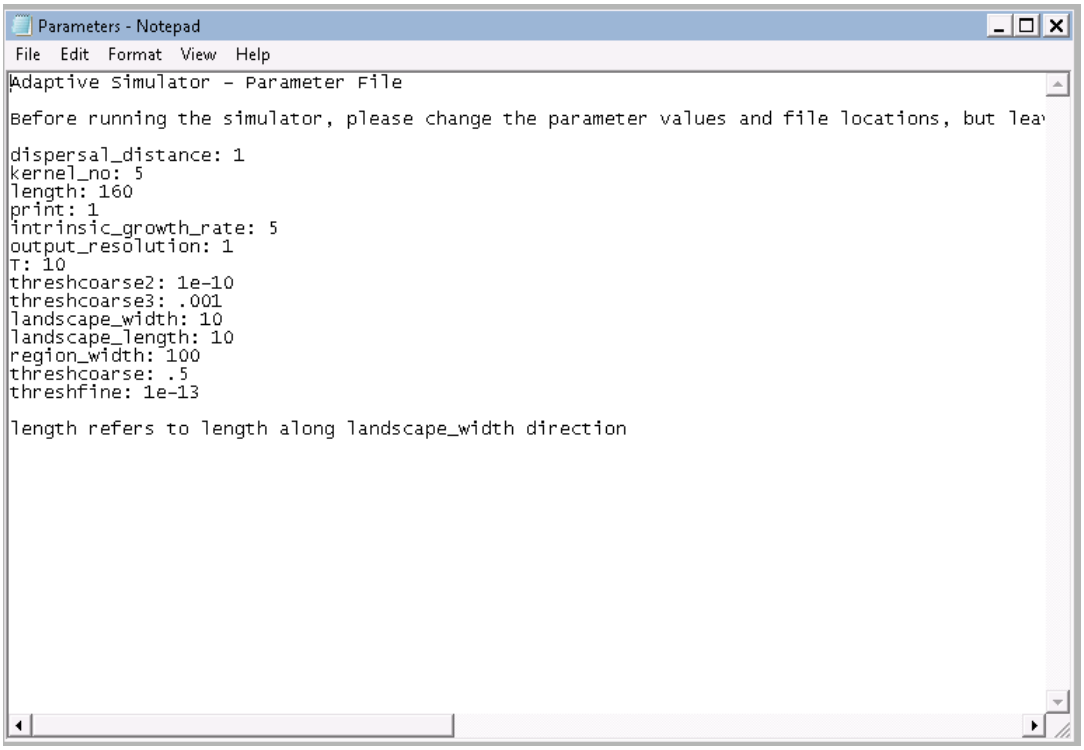

Figure A.5: The unedited Parameters.txt file downloaded from GitHub.

- Since the dispersal distance is 2km and the length of the landscape is 200km, we change the dispersal_distance to 2 and length to 200.
- The dispersal kernel is now Gaussian (kernel_no = 4), so we change the number after kernel_no to 4.
- The intrinsic growth rate is now 20, so we change this.
- The width of each region in cells is now 200, so we change region_width
- This means that the landscape is a 10 x 10 array of regions, so landscape_width and landscape_length stay as 10.

Changing these values (and saving the file) leaves us with a text file of the form shown in Figure A.6.

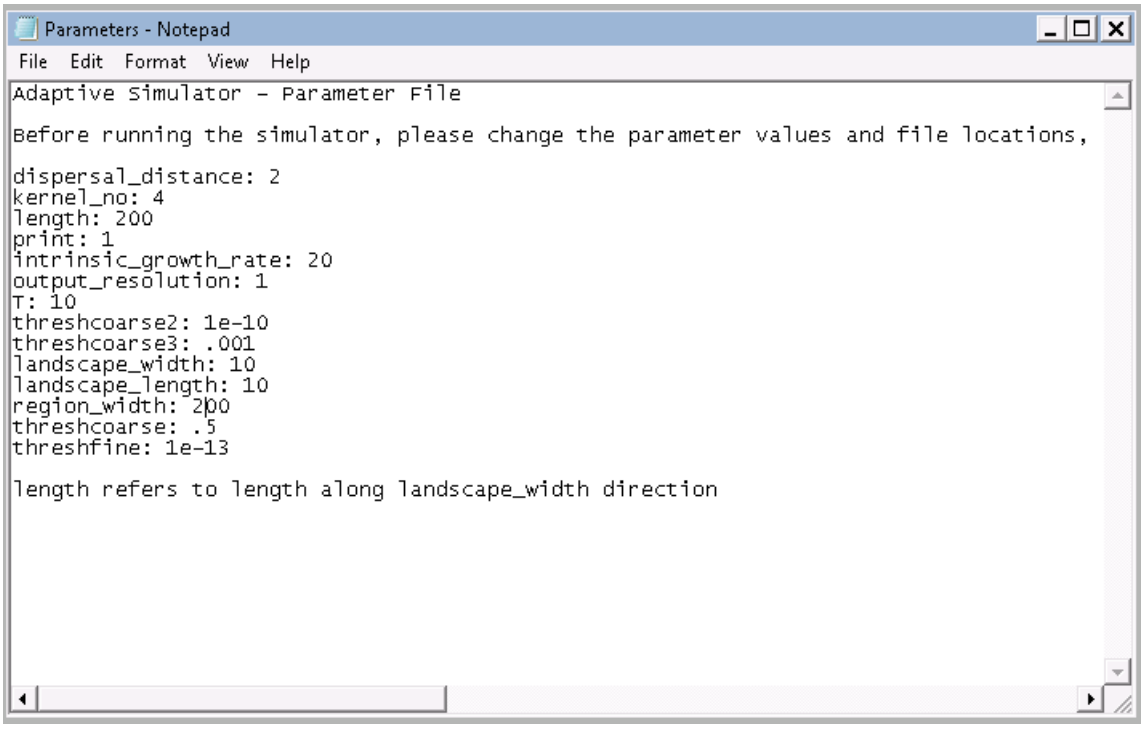

Figure A.6: The Parameters.txt file with changed parameter values.

Before running the programme with the new parameters and map, make sure you save previous outputs as anything called output.bin in the file will be over-written. Once youve done this , you can run the programme with the new map and parameters by clicking on the executable. This should generate output.bin, which you can read into MATLAB (for details, see How to Run a Simple Example). The map at the final time-step should look similar to Figurue A.7.

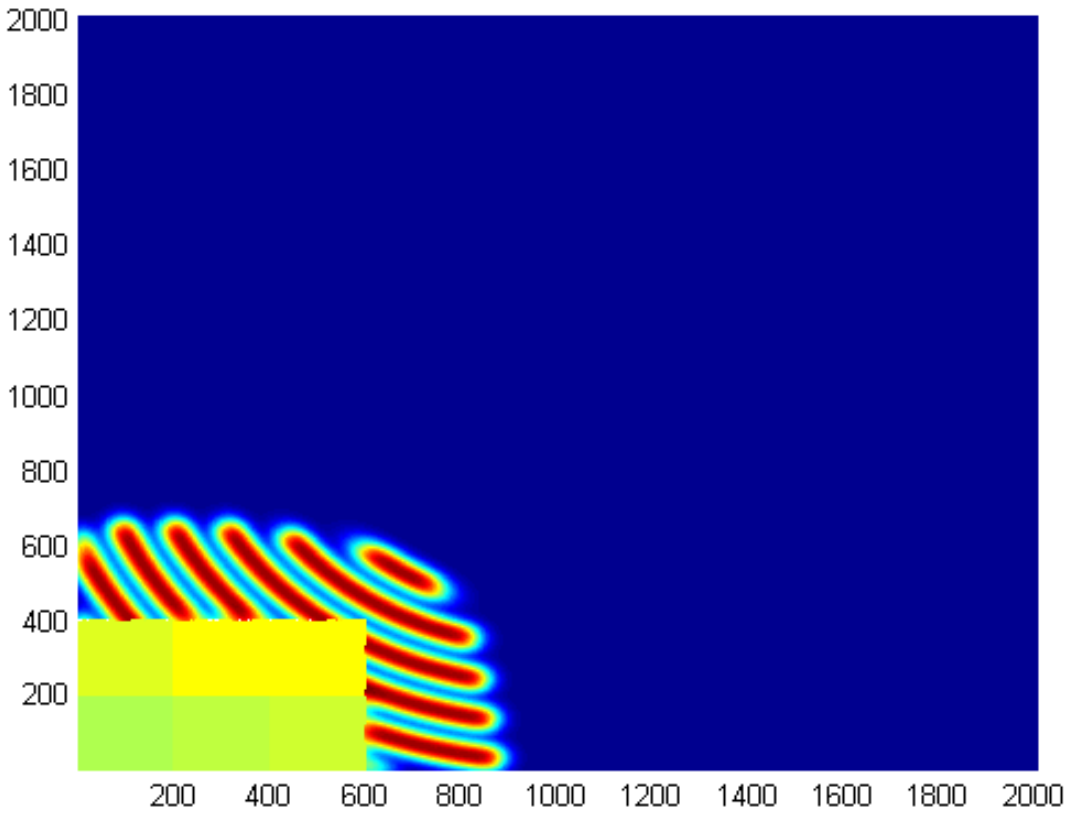

Figure A.7: Map of the population distribution at the final time-step output by the adaptive algorithm. The yellow/green blocks in the bottom left-hand corner correspond to regions with low spatial resolution.

References

R. Aguilar, M. Quesada, L. Ashworth, Y. Herrerias-Diego, and J. Lobo. Genetic consequences of habitat fragmentation in plant populations: susceptible signals in plant traits and methodological approaches. *Mol. Ecol.*, 17(24):5177–5188, 2008.

E. J. Allen, L. J. S. Allen, and X. Gilliam. Dispersal and competition models for plants. *J. Math. Biol.*, 34(4):455–481, 1996.

A. H. Altieri, B. K. van Wesenbeeck, M. D. Bertness, and B. R. Silliman. Facilitation cascade drives positive relationship between native biodiversity and invasion success. *Ecology*, 91(5):1269–1275, 2010.

M. Andersen. Properties of some density-dependent integrodifference equation population models. *Math. Biosci.*, 104(1):135–157, 1991.

P. Aram and D. R. Freestone. Estimation of the mixing kernel and the disturbance covariance in ide-based spatiotemporal systems. *Signal Process.*, 121:46–53, 2016.

M. Baguette, S. Blanchet, D. Legrand, V. M. Stevens, and C. Turlure. Individual dispersal, landscape connectivity and ecological networks. *Biol. Rev.*, 88(2):310–326, 2013.

J. K. Balch, B. A. Bradley, C. M. D'Antonio, and J. Gómez-Dans. Introduced annual grass increases regional fire activity across the arid western USA (1980–2009). *Glob. Chang. Biol.*, 19(1):173–183, 2013.

A. W. Bateman, M. G. Neubert, M. Krkošek, and M. A. Lewis. Generational spreading speed and the dynamics of population range expansion. *Am. Nat.*, 186(3): 362–375, 2015.

L. J. Beaumont, R. V. Gallagher, W. Thuiller, P. O. Downey, M. R. Leishman, and L. Hughes. Different climatic envelopes among invasive populations may lead to

underestimations of current and future biological invasions. *Divers. Distrib.*, 15(3): 409–420, 2009.

M. A. Beaumont, W. Zhang, and D. J. Balding. Approximate bayesian computation in population genetics. *Genetics*, 162(4):2025–2035, 2002.

R. Bellman, H. Kagiwada, and R. Kalaba. Inverse problems in ecology. *J. Theor. Biol.*, 11(1):164–167, 1966.

J. Belmonte-Beitia, T. Woolley, J. Scott, P. Maini, and E. Gaffney. Modelling biological invasions: individual to population scales at interfaces. *J. Theor. Biol.*, 334: 1–12, 2013.

J. Bennie, J. A. Hodgson, C. R. Lawson, C. T. R. Holloway, D. B. Roy, T. Brereton, C. D. Thomas, and R. J. Wilson. Range expansion through fragmented landscapes under a variable climate. *Ecol. Lett.*, 16(7):921–929, 2013.

M. J. Berger and J. Oliger. Adaptive mesh refinement for hyperbolic partial differential equations. *J. Comput. Phys.*, 53(3):484–512, 1984.

R. Binimelis, W. Born, I. Monterroso, and B. Rodríguez-Labajos. Socio-economic impact and assessment of biological invasions. In M. M. Caldwell, G. Heldmaier, R. B. Jackson, O. L. Lange, H. Mooney, E. D. Schulze, and U. Sommer, editors, *Biological Invasions*, pages 331–347. Springer, 2008.

G. Bocedi, G. Peer, R. K. Heikkinen, Y. Matsinos, and J. M. J. Travis. Projecting species range expansion dynamics: sources of systematic biases when scaling up patterns and processes. *Methods Ecol. Evol.*, 3(6):1008–1018, 2012.

G. Bocedi, S. C. F. Palmer, G. Pe'er, R. K. Heikkinen, Y. G. Matsinos, K. Watts, and J. M. J. Travis. Rangeshifter: a platform for modelling spatial eco-evolutionary dynamics and species' responses to environmental changes. *Methods Ecol. Evol.*, 5 (4):388–396, 2014a.

G. Bocedi, D. Zurell, B. Reineking, and J. M. Travis. Mechanistic modelling of animal dispersal offers new insights into range expansion dynamics across fragmented landscapes. *Ecography*, 37(12):1240–1253, 2014b.

C. Bone, J. C. White, M. A. Wulder, C. Robertson, and T. A. Nelson. Impact of forest fragmentation on patterns of mountain pine beetle-caused tree mortality. *Forests*, 4(2):279–295, 2013.

D. Bonte, H. Van Dyck, J. M. Bullock, A. Coulon, M. Delgado, M. Gibbs, V. Lehouck, E. Matthysen, K. Mustin, M. Saastamoinen, et al. Costs of dispersal. *Biol. Rev.*, 87(2):290–312, 2012.

D. B. Botkin, J. F. Janak, and J. R. Wallis. Some ecological consequences of a computer model of forest growth. *J. Ecol.*, 6(3):849–872, 1972.

M. S. Boyce, J. S. Mao, E. H. Merrill, D. Fortin, M. G. Turner, J. Fryxell, and P. Turchin. Scale and heterogeneity in habitat selection by elk in yellowstone national park. *Ecoscience*, 10(4):421–431, 2003.

S. C. Brenner and L. R. Scott. *The Mathematical Theory of Finite Element Methods*, volume 15. Springer, 2008.

K. H. Britton-Simmons and K. C. Abbott. Short-and long-term effects of disturbance and propagule pressure on a biological invasion. *J. Ecol.*, 96(1):68–77, 2008.

M. Buckland-Nicks, A. Heim, and J. Lundholm. Spatial environmental heterogeneity affects plant growth and thermal performance on a green roof. *Sci. Total Environ.*, 553:20–31, 2016.

Y. M. Buckley, D. T. Briese, and M. Rees. Demography and management of the invasive plant species *Hypericum perforatum.* ii. construction and use of an individual-based model to predict population dynamics and the effects of management strategies. *J. Appl. Ecol.*, 40(3):494–507, 2003.

Y. M. Buckley, E. Brockerhoff, L. Langer, N. Ledgard, H. North, and M. Rees. Slowing down a pine invasion despite uncertainty in demography and dispersal. *J. Appl. Ecol.*, 42(6):1020–1030, 2005.

J. M. Bullock, J. Silvertown, and B. C. Hill. Plant demographic responses to environmental variation: distinguishing between effects on age structure and effects on age-specific vital rates. *J. Ecol.*, 84(5):733–743, 1996.

J. M. Bullock, R. F. Pywell, and S. J. Coulson-Phillips. Managing plant population spread: prediction and analysis using a simple model. *Ecol. Appl.*, 18(4):945–953, 2008.

J. M. Bullock, S. M. White, C. Prudhomme, C. Tansey, R. Perea, and D. A. P. Hooftman. Modelling spread of British wind-dispersed plants under future wind speeds in a changing climate. *J. Ecol.*, 100(1):104–115, 2012.

M. T. Burrows, D. S. Schoeman, L. B. Buckley, P. Moore, E. S. Poloczanska, K. M. Brander, C. Brown, J. F. Bruno, C. M. Duarte, B. S. Halpern, et al. The pace of shifting climate in marine and terrestrial ecosystems. *Science*, 334(6056):652–655, 2011.

R. Bustamante, I. Serey, and S. Pickett. Forest fragmentation, plant regeneration and invasion processes across edges in central Chile. In G. A. Bradshaw and P. A. Marquet, editors, *How Landscapes Change*, pages 145–160. Springer, 2003.

R. S. Cantrell and C. Cosner. *Spatial Ecology via Reaction-Diffusion Equations*. John Wiley & Sons, 2004.

P. Caplat, R. Nathan, and Y. M. Buckley. Seed terminal velocity, wind turbulence, and demography drive the spread of an invasive tree in an analytical model. *Ecology*, 93(2):368–377, 2012.

N. O. Carlsson, O. Sarnelle, and D. L. Strayer. Native predators and exotic prey-an acquired taste? *Front. Ecol. Environ.*, 7(10):525–532, 2009.

N. O. L. Carlsson, C. Brönmark, and L. A. Hansson. Invading herbivory: the golden apple snail alters ecosystem functioning in asian wetlands. *Ecology*, 85(6):1575–1580, 2004.

L. Carrasco, T. Harwood, S. Toepfer, A. MacLeod, N. Levay, J. Kiss, R. Baker, J. Mumford, and J. Knight. Dispersal kernels of the invasive alien western corn rootworm and the effectiveness of buffer zones in eradication programmes in Europe. *Ann. Appl. Biol.*, 156(1):63–77, 2010.

C. Carrillo, K. Cherednichenko, N. Britton, and M. Mogie. Dynamic coexistence of sexual and asexual invasion fronts in a system of integro-difference equations. *Bull. Math. Biol.*, 71(7):1612–1625, 2009.

H. Caswell. *Matrix population models: construction, analysis and interpretation.* Sinauer, Sunderland, Massachusetts, USA, 2nd edition, 2000.

H. Caswell, R. Lensink, and M. G. Neubert. Demography and dispersal: life table response experiments for invasion speed. *Ecology*, 84(8):1968–1978, 2003.

H. Caswell, M. G. Neubert, and C. M. Hunter. Demography and dispersal: invasion speeds and sensitivity analysis in periodic and stochastic environments. *Theor. Ecol.*, 4(4):407–421, 2011.

D. S. Chapman, T. Haynes, S. Beal, F. Essl, and J. M. Bullock. Phenology predicts the native and invasive range limits of common ragweed. *Glob. Chang. Biol.*, 20 (1):192–202, 2014.

I. C. Chen, J. K. Hill, R. Ohlemüller, D. B. Roy, and C. D. Thomas. Rapid range shifts of species associated with high levels of climate warming. *Science*, 333(6045): 1024–1026, 2011.

W.-C. Chou, W.-T. Lin, and C.-Y. Lin. Vegetation recovery patterns assessment at landslides caused by catastrophic earthquake: A case study in central Taiwan. *Environ. Monit. Assess.*, 152(1-4):245–257, 2009.

J. S. Clark. Why trees migrate so fast: confronting theory with dispersal biology and the paleorecord. *Am. Nat.*, 152(2):204–224, 1998.

K. L. Clark, N. Skowronski, and J. Hom. Invasive insects impact forest carbon dynamics. *Glob. Chang. Biol.*, 16(1):88–101, 2010.

J. Clobert, M. Baguette, T. G. Benton, and J. M. Bullock. *Dispersal Ecology and Evolution*. Oxford University Press, 1st edition, 2012.

C. A. Cobbold, M. A. Lewis, F. Lutscher, and J. Roland. How parasitism affects critical patch-size in a host–parasitoid model: application to the forest tent caterpillar. *Theor. Popul. Biol.*, 67(2):109–125, 2005.

R. I. Colautti and H. J. MacIsaac. A neutral terminology to define invasive species. *Divers. Distrib.*, 10(2):135–141, 2004.

S. Condé, L. Jones-Walters, A. Torre-Marin, C. Romao, et al. EU 2010 biodiversity baseline. *Copenhagen: EEA Technical report*, (12), 2010.

B. L. Conkling. Forest health monitoring: 2007 national technical report. Technical report, United States Department of Agriculture, Forest Service, 2011.

D. B. Conn. Aquatic invasive species and emerging infectious disease threats: A one health perspective. *Aquat. Invasions*, 9(3):383–390, 2014.

J. W. Cooley and J. W. Tukey. An algorithm for the machine calculation of complex fourier series. *Math. Comput.*, 19(90):297–301, 1965.

J. K. Cooper, J. Li, and D. J. Montagnes. Intermediate fragmentation per se provides stable predator-prey metapopulation dynamics. *Ecol. Lett.*, 15(8):856–863, 2012.

R. M. Coutinho, W. A. C. Godoy, and R. A. Kraenkel. Integrodifference model for blowfly invasion. *Theor. Ecol.*, 5(3):363–371, 2012.

K. Csilléry, M. G. Blum, O. E. Gaggiotti, and O. François. Approximate bayesian computation (ABC) in practice. *Trends Ecol. Evol.*, 25(7):410–418, 2010.

K. Csilléry, O. François, and M. G. Blum. ABC: an R package for approximate bayesian computation (ABC). *Methods Ecol. Evol.*, 3(3):475–479, 2012.

K. Cuddington and A. Hastings. Invasive engineers. *Ecol. Model.*, 178(3):335–347, 2004.

J. T. Curtis. The modification of mid-latitude grasslands and forests by man. In W. L. Thomas, editor, *Man's Role in Changing the Face of the Earth*. University of Chicago Press Chicago, IL, 1956.

S. F. Davis and J. E. Flaherty. An adaptive finite element method for initial-boundary value problems for partial differential equations. *SIAM J. Sci. Stat. Comp.*, 3(1): 6–27, 1982.

D. DeAngelis, D. Cox, and C. Coutant. Cannibalism and size dispersal in young-of-the-year largemouth bass: experiment and model. *Ecol. Model.*, 8:133–148, 1980.

M. Dewar, K. Scerri, and V. Kadirkamanathan. Data-driven spatio-temporal modeling using the integro-difference equation. *IEEE T. Signal Proces.*, 57(1):83–91, 2009.

S. Dewhirst and F. Lutscher. Dispersal in heterogeneous habitats: thresholds, spatial scales, and approximate rates of spread. *Ecology*, 90(5):1338–1345, 2009.

W. Ding, X. Liang, and B. Xu. Spreading speeds of n-season spatially periodic integro-difference models. *Discrete Contin. Dyn. Syst*, 33:3443–3472, 2013.

T. S. Doherty, C. R. Dickman, D. G. Nimmo, and E. G. Ritchie. Multiple threats, or multiplying the threats? interactions between invasive predators and other ecological disturbances. *Biol. Conserv.*, 190:60–68, 2015.

C. F. Dormann. Promising the future? global change projections of species distributions. *Basic Appl. Ecol.*, 8(5):387–397, 2007.

C. F. Dormann, S. J. Schymanski, J. Cabral, I. Chuine, C. Graham, F. Hartig, M. Kearney, X. Morin, C. Römermann, B. Schröder, et al. Correlation and process in species distribution models: bridging a dichotomy. *J. Biogeogr.*, 39(12):2119–2131, 2012.

D. A. Driscoll, S. C. Banks, P. S. Barton, D. B. Lindenmayer, and A. L. Smith. Conceptual domain of the matrix in fragmented landscapes. *Trends Ecol. Evol.*, 28 (10):605–613, 2013.

J. Elith and J. Leathwick. The contribution of species distribution modelling to conservation prioritization. In A. Moilanen, K. A. Wilson, and H. Possingham, editors, *Spatial Conservation Prioritisation: Quantitative Methods and Computational Tools.* Oxford University Press, 2009a.

J. Elith and J. R. Leathwick. Species distribution models: ecological explanation and prediction across space and time. *Annu. Rev. Ecol. Evol. Syst.*, 40(1):677, 2009b.

J. A. Estes, J. Terborgh, J. S. Brashares, M. E. Power, J. Berger, W. J. Bond, S. R. Carpenter, T. E. Essington, R. D. Holt, J. B. Jackson, et al. Trophic downgrading of planet earth. *Science*, 333(6040):301–306, 2011.

R. Etienne, B. Wertheim, L. Hemerik, P. Schneider, and J. Powell. The interaction between dispersal, the allee effect and scramble competition affects population dynamics. *Ecol. Model.*, 148(2):153–168, 2002.

M. R. Evans, V. Grimm, K. Johst, T. Knuuttila, R. De Langhe, C. M. Lessells, M. Merz, M. A. OMalley, S. H. Orzack, M. Weisberg, et al. Do simple models lead to generality in ecology? *Trends Ecol. Evol.*, 28(10):578–583, 2013.

W. F. Fagan, M. Lewis, M. G. Neubert, C. Aumann, J. L. Apple, and J. G. Bishop. When can herbivores slow or reverse the spread of an invading plant? a test case from Mount St. Helens. *Am. Nat.*, 166(6):669–685, 2005.

W. F. Fagan, F. Lutscher, and K. Schneider. Population and community consequences of spatial subsidies derived from central-place foraging. *Am. Nat.*, 170(6):902–915, 2007.

L. Fahrig. How much habitat is enough? *Biol. Conserv.*, 100(1):65–74, 2001.

L. Fahrig. Effect of habitat fragmentation on the extinction threshold: A synthesis. *Ecol. Appl.*, 12(2):346–353, 2002.

L. Fahrig. Effects of habitat fragmentation on biodiversity. *Annu. Rev. Ecol. Evol. Syst.*, 34:487–515, 2003.

L. Fang, P. K. Wong, L. I. Lin, C. Lan, and J. W. Qiu. Impact of invasive apple snails in hong kong on wetland macrophytes, nutrients, phytoplankton and filamentous algae. *Freshwater Biol.*, 55(6):1191–1204, 2010.

C. L. Fastie. Causes and ecosystem consequences of multiple pathways of primary succession at Glacier Bay, Alaska. *Ecology*, 76(6):1899–1916, 1995.

M. Fennell, J. E. Murphy, C. Armstrong, T. Gallagher, and B. Osborne. Plant spread simulator: a model for simulating large-scale directed dispersal processes across heterogeneous environments. *Ecol. Model.*, 230:1–10, 2012.

J. Fischer and D. B. Lindenmayer. Landscape modification and habitat fragmentation: a synthesis. *Glob. Ecol. Biogeogr.*, 16(3):265–280, 2007.

R. A. Fisher. The wave of advance of advantageous genes. *Ann. Hum. Genet.*, 7(4): 355–369, 1937.

A. E. Fleming-Davies, V. Dukic, V. Andreasen, and G. Dwyer. Effects of host heterogeneity on pathogen diversity and evolution. *Ecol. Lett.*, 18(11):1252–1261, 2015.

C. E. Flower, K. S. Knight, and M. A. Gonzalez-Meler. Impacts of the emerald ash borer (*Agrilus planipennis Fairmaire*) induced ash (*Fraxinus spp.*) mortality on

forest carbon cycling and successional dynamics in the eastern United States. *Biol. Invasions*, 15(4):931–944, 2013.

J. Fort, J. Pérez-Losada, and N. Isern. Fronts from integrodifference equations and persistence effects on the neolithic transition. *Phys. Rev. E*, 76(3):031913, 2007.

J. Fort, J. Pérez-Losada, J. Suñol, L. Escoda, and J. Massaneda. Integro-difference equations for interacting species and the neolithic transition. *New J. Phys.*, 10(4): 043045, 2008.

J. F. Franklin and D. B. Lindenmayer. Importance of matrix habitats in maintaining biological diversity. *Proc. Natl. Acad. Sci. U.S.A.*, 106(2):349–350, 2009.

S. D. Fuhlendorf, D. M. Engle, J. Kerby, and R. Hamilton. Pyric herbivory: rewilding landscapes through the recoupling of fire and grazing. *Conserv. Biol.*, 23(3):588–598, 2009.

M. Fujiwara, K. E. Anderson, M. G. Neubert, and H. Caswell. On the estimation of dispersal kernels from individual mark-recapture data. *Environ. Ecol. Stat.*, 13(2): 183–197, 2006.

E. Fuller, E. Brush, and M. L. Pinsky. The persistence of populations facing climate shifts and harvest. *Ecosphere*, 6(9):1–16, 2015.

M. Gaertner, A. Den Breeyen, C. Hui, and D. M. Richardson. Impacts of alien plant invasions on species richness in mediterranean-type ecosystems: a meta-analysis. *Prog. Phys. Geogr.*, 33(3):319–338, 2009.

H. Gaff, H. R. Joshi, and S. Lenhart. Optimal harvesting during an invasion of a sublethal plant pathogen. *Environ. Dev. Econ.*, 12(05):673–686, 2007.

L. Gallien, R. Douzet, S. Pratte, N. E. Zimmermann, and W. Thuiller. Invasive species distribution models–how violating the equilibrium assumption can create new insights. *Glob. Ecol. Biogeogr.*, 21(11):1126–1136, 2012.

A. García-Romero, R. M. Alanís-anaya, and J. Muñoz-Jiménez. Environmental factors that affect primary plant succession trajectories on lahars (Popocatépetl volcano, Mexico). *J. Mt. Sci.*, 12(5):1254–1266, 2015.

A. Garnier and J. Lecomte. Using a spatial and stage-structured invasion model to assess the spread of feral populations of transgenic oilseed rape. *Ecol. Model.*, 194 (1):141–149, 2006.

A. Gelman. Prior distribution. In *Encyclopedia of Environmetrics, Volume 3*, pages 1634–1637. John Wiley & Sons, 2002.

M. Gilbert, S. Guichard, J. Freise, J.-C. Grégoire, W. Heitland, N. Straw, C. Tilbury, and S. Augustin. Forecasting *Cameraria ohridella* invasion dynamics in recently invaded countries: from validation to prediction. *J. Appl. Ecol.*, 42(5):805–813, 2005.

M. A. Gilbert, E. A. Gaffney, J. M. Bullock, and S. M. White. Spreading speeds for plant populations in landscapes with low environmental variation. *J. Theor. Biol.*, 363:436–451, 2014a.

M. A. Gilbert, S. M. White, J. M. Bullock, and E. A. Gaffney. Spreading speeds for stage structured plant populations in fragmented landscapes. *J. Theor. Biol.*, 349: 135–149, 2014b.

M. A. Gilbert, S. M. White, J. M. Bullock, and E. A. Gaffney. Adaptiveide: Adaptiveide version 1, doi: 10.5281/zenodo.45509, Feb. 2016. URL `http://dx.doi.org/10.5281/zenodo.45509`.

L. Gordillo. Optimal sterile insect release for area-wide integrated pest management in a density regulated pest population. *Math. Biosci. Eng.*, 11(3):511–521, 2014.

S. Gous, P. Raal, and M. S. Watt. Aerial spot treatment using an oil carrier to apply ester based herbicides for control of *Pinus contorta* and *P. nigra* in New Zealand. *New. Zeal. J. For. Sci.*, 44(1):23, 2014.

E. A. Graham, P. W. Rundel, W. Kaiser, Y. Lam, M. Stealey, and E. M. Yuen. Fine-scale patterns of soil and plant surface temperatures in an alpine fellfield habitat, White Mountains, California. *Arct. Antarct. Alp. Res.*, 44(3):288–295, 2012.

V. Grimm and S. F. Railsback. *Individual-Based Modeling and Ecology*. Princeton university press, 2013.

A. Guisan and W. Thuiller. Predicting species distribution: offering more than simple habitat models. *Ecol. Lett.*, 8(9):993–1009, 2005.

A. Guisan, R. Tingley, J. B. Baumgartner, I. Naujokaitis-Lewis, P. R. Sutcliffe, A. I. T. Tulloch, T. J. Regan, L. Brotons, E. McDonald-Madden, C. Mantyka-Pringle, et al. Predicting species distributions for conservation decisions. *Ecol. Lett.*, 16(12):1424–1435, 2013.

A. Habbal, H. Barelli, and G. Malandain. Assessing the ability of the 2D fisher–KPP equation to model cell-sheet wound closure. *Math. Biosci.*, 252:45–59, 2014.

M. Halwart. The golden apple snail *Pomacea canaliculata* in asian rice farming systems: present impact and future threat. *Int. J. Pest Manage.*, 40(2):199–206, 1994.

M. Hanewinkel, D. A. Cullmann, M.-J. Schelhaas, G.-J. Nabuurs, and N. E. Zimmermann. Climate change may cause severe loss in the economic value of European forest land. *Nat. Clim. Chang.*, 3(3):203–207, 2013.

I. Hanski and C. D. Thomas. Metapopulation dynamics and conservation: a spatially explicit model applied to butterflies. *Biol. Conserv.*, 68(2):167–180, 1994.

L. Hansson, L. Fahrig, and G. Merriam. *Mosaic Landscapes and Ecological Processes*. Springer Science & Business Media, 2012.

M. A. Harsch, Y. Zhou, J. HilleRisLambers, and M. Kot. Keeping pace with climate change: Stage-structured moving-habitat models. *Am. Nat.*, 184(1):25–37, 2014.

D. R. Hart and R. H. Gardner. A spatial model for the spread of invading organisms subject to competition. *J. Math. Biol.*, 35(8):935–948, 1997.

G. S. Hartshorn. A matrix model of tree population dynamics. In F. B. Golley and E. Medina, editors, *Tropical ecological systems*, pages 41–51. Springer, 1975.

A. Hastings. Persistence and management of spatially distributed populations. *Popul. Ecol.*, 56(1):21–26, 2014.

A. Hastings, K. Cuddington, K. F. Davies, C. J. Dugaw, S. Elmendorf, A. Freestone, S. Harrison, M. Holland, J. Lambrinos, U. Malvadkar, et al. The spatial spread of invasions: new developments in theory and evidence. *Ecol. Lett.*, 8(1):91–101, 2005.

K. A. Hayes, R. C. Joshi, S. C. Thiengo, and R. H. Cowie. Out of South America: multiple origins of non-native apple snails in Asia. *Divers. Distrib.*, 14(4):701–712, 2008.

J. Heavilin and J. Powell. A novel method of fitting spatio-temporal models to data, with applications to the dynamics of mountain pine beetles. *Nat. Resour. Model.*, 21(4):489–524, 2008.

S. I. Higgins, J. S. Clark, R. Nathan, T. Hovestadt, F. Schurr, J. M. V. Fragoso, M. R. Aguiar, E. Ribbens, and S. Lavorel. Forecasting plant migration rates: managing uncertainty for risk assessment. *J. Ecol.*, 91(3):341–347, 2003.

R. J. Hobbs. Synergisms among habitat fragmentation, livestock grazing, and biotic invasions in southwestern Australia. *Conserv. Biol.*, 15(6):1522–1528, 2001.

G. Hoch and C. Körner. Global patterns of mobile carbon stores in trees at the high-elevation tree line. *Global Ecol. Biogeogr.*, 21(8):861–871, 2012.

J. A. Hodgson, C. D. Thomas, C. Dytham, J. M. J. Travis, and S. J. Cornell. The speed of range shifts in fragmented landscapes. *PLoS One*, 7(10):e47141, 2012.

C. G. Homer, J. A. Dewitz, L. Yang, S. Jin, P. Danielson, G. Xian, J. Coulston, N. D. Herold, J. Wickham, and K. Megown. Completion of the 2011 National Land Cover Database for the conterminous United States-representing a decade of land cover change information. *Photogramm. Eng. Remote Sens*, 81(5):345–354, 2015.

D. A. Hooftman, B. Edwards, and J. M. Bullock. Reductions in connectivity and habitat quality drive local extinctions in a plant diversity hotspot. *Ecography*, 39 (6):583–592, 2015.

D. A. P. Hooftman and J. M. Bullock. Mapping to inform conservation: a case study of changes in semi-natural habitats and their connectivity over 70 years. *Biol. Conserv.*, 145(1):30–38, 2012.

F. G. Horgan, A. M. Stuart, and E. P. Kudavidanage. Impact of invasive apple snails on the functioning and services of natural and managed wetlands. *Acta Oecol.*, 54: 90–100, 2014.

C. C. Horvitz, A. L. Koop, and K. D. Erickson. Time-invariant and stochastic disperser-structured matrix models: Invasion rates of fleshy-fruited exotic shrubs. *Discrete Cont. Dyn. B*, 20(6), 2015.

K. Hoshizaki, K. Niiyama, K. Kimura, T. Yamashita, Y. Bekku, T. Okuda, E. S. Quah, and N. S. M. Noor. Temporal and spatial variation of forest biomass in relation to stand dynamics in a mature, lowland tropical rainforest, Malaysia. *Ecol. Res.*, 19(3):357–363, 2004.

J. P. Huelsenbeck, B. Larget, R. E. Miller, and F. Ronquist. Potential applications and pitfalls of bayesian inference of phylogeny. *Systematic biology*, 51(5):673–688, 2002.

P. E. Hulme, S. Bacher, M. Kenis, S. Klotz, I. Kühn, D. Minchin, W. Nentwig, S. Olenin, V. Panov, J. Pergl, et al. Grasping at the routes of biological invasions:

a framework for integrating pathways into policy. *J. Appl. Ecol.*, 45(2):403–414, 2008.

P. E. Hulme, A. Pauchard, P. Pyšek, M. Vilà, C. Alba, T. M. Blackburn, J. M. Bullock, M. Chytrỳ, W. Dawson, A. M. Dunn, et al. Challenging the view that invasive non-native plants are not a significant threat to the floristic diversity of Great Britain. *Proc. Natl. Acad. Sci. USA*, 112(23):E2988–E2989, 2015.

A. Hurford, M. Hebblewhite, and M. A. Lewis. A spatially explicit model for an allee effect: why wolves recolonize so slowly in greater Yellowstone. *Theor. Popul. Biol.*, 70(3):244–254, 2006.

V. Hutson, S. Martinez, K. Mischaikow, and G. Vickers. The evolution of dispersal. *J. Math. Biol.*, 47(6):483–517, 2003.

J. Jacobsen, Y. Jin, and M. A. Lewis. Integrodifference models for persistence in temporally varying river environments. *J. Math. Biol.*, 70(3):549–590, 2015.

H. Jacquemyn, R. Brys, and M. G. Neubert. Fire increases invasive spread of *Molinia caerulea* mainly through changes in demographic parameters. *Ecol. Appl.*, 15(6): 2097–2108, 2005.

M. Janišová, K. Hegedüšová, P. Král', and I. Škodová. Ecology and distribution of *tephroseris longifolia* subsp.*moravica* in relation to environmental variation at a micro-scale. *Biologia (Bratisl.)*, 67(1):97–109, 2012.

C. L. Jerde, C. J. Bampfylde, and M. A. Lewis. Chance establishment for sexual, semelparous species: overcoming the allee effect. *Am. Nat.*, 173(6):734–746, 2009.

E. Jongejans, K. Shea, O. Skarpaas, D. Kelly, A. W. Sheppard, and T. L. Woodburn. Dispersal and demography contributions to population spread of *Carduus nutans* in its native and invaded ranges. *J. Ecol.*, 96(4):687–697, 2008.

H. R. Joshi, S. Lenhart, and H. Gaff. Optimal harvesting in an integrodifference population model. *Optim. Contr. Appl. Met.*, 27(2):61–75, 2006.

H. R. Joshi, S. Lenhart, H. Lou, and H. Gaff. Harvesting control in an integrodifference population model with concave growth term. *Nonlinear Anal. Hybri.*, 1(3): 417–429, 2007.

P. Jurena and S. Archer. Woody plant establishment and spatial heterogeneity in grasslands. *Ecology*, 84(4):907–919, 2003.

R. Kachurivs kyi. Periodic solutions of systems of integrodifference equations. *Nonlinear Oscil.*, 13(2):172–177, 2010.

T. Kadoya and I. Washitani. Use of multiple habitat types with asymmetric dispersal affects patch occupancy of the damselfly *Indolestes peregrinus* in a fragmented landscape. *Basic Appl. Ecol.*, 13(2):178–187, 2012.

L. Kanary, J. Musgrave, R. C. Tyson, A. Locke, and F. Lutscher. Modelling the dynamics of invasion and control of competing green crab genotypes. *Theor. Ecol.*, 7(4):391–406, 2014.

S. Katsanevakis, I. Wallentinus, A. Zenetos, E. Leppäkoski, M. E. Çinar, B. Oztürk, M. Grabowski, D. Golani, A. C. Cardoso, et al. Impacts of invasive alien marine species on ecosystem services and biodiversity: a pan-European review. *Aquat. Invasions*, 9(4):391–423, 2014.

G. G. Katul, A. Porporato, R. Nathan, M. Siqueira, M. B. Soons, D. Poggi, H. S. Horn, and S. A. Levin. Mechanistic analytical models for long-distance seed dispersal by wind. *Am. Nat.*, 166(3):368–381, 2005.

K. Kawasaki and N. Shigesada. An integrodifference model for biological invasions in a periodically fragmented environment. *Jpn. J. Ind. Appl. Math.*, 24(1):3–15, 2007.

L. J. Kayes and D. B. Tinker. Forest structure and regeneration following a mountain pine beetle epidemic in southeastern Wyoming. *Forest Ecol. Manag.*, 263:57–66, 2012.

M. Kettunen, P. Genovesi, S. Gollasch, S. Pagad, U. Starfinger, P. ten Brink, and C. Shine. Technical support to EU strategy on invasive alien species (ias). *Institut for European Environnemental Policy (IEEP)*, 2009.

N. Kinezaki, K. Kawasaki, and N. Shigesada. The effect of the spatial configuration of habitat fragmentation on invasive spread. *Theor. Popul. Biol.*, 78(4):298–308, 2010.

A. W. King and K. A. With. Dispersal success on spatially structured landscapes: when do spatial pattern and dispersal behavior really matter? *Ecol. Model.*, 147 (1):23–39, 2002.

J. M. H. Knops, J. R. Griffin, and A. C. Royalty. Introduced and native plants of the Hastings Reservation, central coastal California: a comparison. *Biol. Conserv.*, 71 (2):115–123, 1995.

M. Kot. Discrete-time travelling waves: ecological examples. *J. Math. Biol.*, 30(4): 413–436, 1992.

M. Kot and M. G. Neubert. Saddle-point approximations, integrodifference equations, and invasions. *Bull. Math. Biol.*, 70(6):1790–1826, 2008.

M. Kot and A. Phillips. Bounds for the critical speed of climate-driven moving-habitat models. *Math. Biosci.*, 262:65–72, 2015.

M. Kot and W. M. Schaffer. Discrete-time growth-dispersal models. *Math. Biosci.*, 80(1):109–136, 1986.

M. Kot, M. A. Lewis, and P. van den Driessche. Dispersal data and the spread of invading organisms. *Ecology*, 77(7):2027–2042, 1996.

M. Kot, J. Medlock, T. Reluga, and D. Brian Walton. Stochasticity, invasions, and branching random walks. *Theor. Popul. Biol.*, 66(3):175–184, 2004.

J. Krauss, R. Bommarco, M. Guardiola, R. K. Heikkinen, A. Helm, M. Kuussaari, R. Lindborg, E. Öckinger, M. Pärtel, J. Pino, et al. Habitat fragmentation causes immediate and time-delayed biodiversity loss at different trophic levels. *Ecol. Lett.*, 13(5):597–605, 2010.

M. Krkošek, J. S. Lauzon-Guay, and M. A. Lewis. Relating dispersal and range expansion of California sea otters. *Theor. Popul. Biol.*, 71(4):401–407, 2007.

S. Lamoureaux, B. Basse, G. Bourdôt, and D. Saville. Comparison of management strategies for controlling *Nassella trichotoma* in modified tussock grasslands in New Zealand: a spatial and economic analysis. *Weed Res.*, 55(5):449–460, 2015.

J. Latore, P. Gould, and A. M. Mortimer. Spatial dynamics and critical patch size of annual plant populations. *J. Theor. Biol.*, 190(3):277–285, 1998.

J. Latore, P. Gould, and A. M. Mortimer. Effects of habitat heterogeneity and dispersal strategies on population persistence in annual plants. *Ecol. Model.*, 123(2): 127–139, 1999.

C. R. Lawson, J. J. Bennie, C. D. Thomas, J. A. Hodgson, and R. J. Wilson. Local and landscape management of an expanding range margin under climate change. *J. Appl. Ecol.*, 49(3):552–561, 2012.

J. Le Corff and C. C. Horvitz. Population growth versus population spread of an ant-dispersed neotropical herb with a mixed reproductive strategy. *Ecol. Model.*, 188(1):41–51, 2005.

S. S. Lee, R. Baker, E. Gaffney, and S. White. Modelling *Aedes aegypti* mosquito control via transgenic and sterile insect techniques: Endemics and emerging outbreaks. *J. Theor. Biol.*, 331:78–90, 2013.

L. P. Lefkovitch. The study of population growth in organisms grouped by stages. *Biometrics*, 21(1):1–18, 1965.

B. Legaspi Jr, J. Allen, C. Brewster, J. Morales-Ramos, and E. King. Areawide management of the cotton boll weevil: use of a spatio–temporal model in augmentative biological control. *Ecol. Model.*, 110(2):151–164, 1998.

M. Leps, J. D. Tonkin, V. Dahm, P. Haase, and A. Sundermann. Disentangling environmental drivers of benthic invertebrate assemblages: The role of spatial scale and riverscape heterogeneity in a multiple stressor environment. *Sci. Total Environ.*, 536:546–556, 2015.

P. H. Leslie. On the use of matrices in certain population mathematics. *Biometrika*, 33(3):183–212, 1945.

M.-R. Leung and M. Kot. Models for the spread of white pine blister rust. *J. Theor. Biol.*, 382:328–336, 2015.

R. Levins. Some demographic and genetic consequences of environmental heterogeneity for biological control. *Bull. Entomol. Soc. Am.*, 15(3):237–240, 1969.

E. G. Lewis. On the generation and growth of a population. *Sankhya*, 6:93–96, 1942.

M. A. Lewis. Spread rate for a nonlinear stochastic invasion. *J. Math. Biol.*, 41(5): 430–454, 2000.

M. A. Lewis. Finding the sweet spot for invasion theory. *Proc. Natl. Acad. Sci. U.S.A.*, 113(25):68196820, 2016.

B. Li. Traveling wave solutions in a plant population model with a seed bank. *J. Math. Biol.*, 65(5):855–873, 2012.

B. Li, W. F. Fagan, and K. I. Meyer. Success, failure, and spreading speeds for invasions on spatial gradients. *J. Math. Biol.*, 70(1-2):265–287, 2015.

G. Lin and W.-T. Li. Spreading speeds and traveling wavefronts for second order integrodifference equations. *J. Math. Anal. Appl.*, 361(2):520–532, 2010.

H.-T. Lin. On a system of integrodifference equations modelling the propagation of genes. *SIAM J. Math. Anal.*, 26(1):35–76, 1995.

D. B. Lindenmayer and J. Fischer. *Habitat Fragmentation and Landscape Change: an Ecological and Conservation Synthesis*. Island Press, 2013.

S. R. Loarie, P. B. Duffy, H. Hamilton, G. P. Asner, C. B. Field, and D. D. Ackerly. The velocity of climate change. *Nature*, 462(7276):1052–1055, 2009.

R. Lui. Biological growth and spread modeled by systems of recursions. i. mathematical theory. *Math. Biosci.*, 93(2):269–295, 1989.

F. Lutscher. A short note on short dispersal events. *Bull. Math. Biol.*, 69(5):1615–1630, 2007.

F. Lutscher and M. A. Lewis. Spatially-explicit matrix models. *J. Math. Biol.*, 48 (3):293–324, 2004.

F. Lutscher and N. Van Minh. Traveling waves in discrete models of biological populations with sessile stages. *Nonlinear Anal. Real World Appl.*, 14(1):495–506, 2013.

F. Lutscher, E. Pachepsky, and M. A. Lewis. The effect of dispersal patterns on stream populations. *SIAM Review*, 47(4):749–772, 2005.

F. Lutscher, R. M. Nisbet, and E. Pachepsky. Population persistence in the face of advection. *Theor. Ecol.*, 3(4):271–284, 2010.

S. Lv, Y. Zhang, P. Steinmann, G.-J. Yang, K. Yang, X.-N. Zhuo, and J. Utzinger. The emergence of angiostrongyliasis in the Peoples Republic of China: the interplay between invasive snails, climate change and transmission dynamics. *Freshwater Biol.*, 56(4):717–734, 2011.

R. N. Mack, D. Simberloff, W. Mark Lonsdale, H. Evans, M. Clout, and F. A. Bazzaz. Biotic invasions: causes, epidemiology, global consequences, and control. *Ecol. Appl.*, 10(3):689–710, 2000.

S. J. Manchester and J. M. Bullock. The impacts of non-native species on UK biodiversity and the effectiveness of control. *J. Appl. Ecol.*, 37(5):845–864, 2000.

K. M. Marchetto, E. Jongejans, K. Shea, and S. A. Isard. Plant spatial arrangement affects projected invasion speeds of two invasive thistles. *Oikos*, 119(9):1462–1468, 2010.

N. G. Marculis and R. Lui. Modelling the biological invasion of *Carcinus maenas* (the European green crab). *J. Biol. Dyn.*, 10(1):140–163, 2016.

D. M. Marsh, G. S. Milam, N. P. Gorham, and N. G. Beckman. Forest roads as partial barriers to terrestrial salamander movement. *Conserv. Biol.*, 19(6):2004–2008, 2005.

M. V. Martinez, S. Lenhart, and K. J. White. Optimal control of integrodifference equations in a pest-pathogen system. *Discrete Cont. Dyn. B*, 20(6):1759–1783, 2015.

M. Marvier, P. Kareiva, and M. G. Neubert. Habitat destruction, fragmentation, and disturbance promote invasion by habitat generalists in a multispecies metapopulation. *Risk. Anal.*, 24(4):869–878, 2004.

D. P. Matlaga and A. S. Davis. Minimizing invasive potential of *Miscanthus* × *giganteus* grown for bioenergy: identifying demographic thresholds for population growth and spread. *J. Appl. Ecol.*, 50(2):479–487, 2013.

R. A. McCleery, A. Sovie, R. N. Reed, M. W. Cunningham, M. E. Hunter, and K. M. Hart. Marsh rabbit mortalities tie pythons to the precipitous decline of mammals in the Everglades. *P. Roy. Soc. Lond. B Bio.*, 282(1805):20150120, 2015.

G. McInerny, J. Travis, and C. Dytham. Range shifting on a fragmented landscape. *Ecol. Inform.*, 2(1):1–8, 2007.

J. Medlock and M. Kot. Spreading disease: integro-differential equations old and new. *Math. Biosci.*, 184(2):201–222, 2003.

E. S. Meier, H. Lischke, D. R. Schmatz, and N. E. Zimmermann. Climate, competition and connectivity affect future migration and ranges of European trees. *Global Ecol. Biogeogr.*, 21(2):164–178, 2012.

C. Merow, A. M. Latimer, A. M. Wilson, S. M. McMahon, A. G. Rebelo, and J. A. Silander. On using integral projection models to generate demographically driven predictions of species' distributions: development and validation using sparse data. *Ecography*, 37(12):1167–1183, 2014.

J. Metz and M. Gyllenberg. How should we define fitness in structured metapopulation models? including an application to the calculation of evolutionarily stable dispersal strategies. *P. Roy. Soc. Lond. B Bio.*, 268(1466):499–508, 2001.

J. A. Metz, D. Mollison, and F. Van Den Bosch. The dynamics of invasion waves, 1999.

J. R. Miller and H. Zeng. Multidimensional stability of planar traveling waves for an integrodifference model. *Discrete Cont. Dyn. B*, 18(3):741–751, 2013.

R. Miller, J. Ver Hoef, and N. Fowler. Spatial heterogeneity in eight central Texas grasslands. *J. Ecol.*, 83(6):919–928, 1995.

T. E. Miller and B. Tenhumberg. Contributions of demography and dispersal parameters to the spatial spread of a stage-structured insect invasion. *Ecol. Appl.*, 20(3): 620–633, 2010.

T. E. Miller, A. K. Shaw, B. D. Inouye, and M. G. Neubert. Sex-biased dispersal and the speed of two-sex invasions. *Am. Nat.*, 177(5):549–561, 2011.

D. C. Mistro, L. A. D. Rodrigues, and W. C. Ferreira Jr. The africanized honey bee dispersal: a mathematical zoom. *Bull. Math. Biol.*, 67(2):281–312, 2005.

A. Moilanen. On the limitations of graph-theoretic connectivity in spatial ecology and conservation. *J. Appl. Ecol.*, 48(6):1543–1547, 2011.

D. Mollison. Dependence of epidemic and population velocities on basic parameters. *Math. Biosci.*, 107(2):255–287, 1991.

W. F. Morris, W. G. Wilson, J. L. Bronstein, and J. H. Ness. Environmental forcing and the competitive dynamics of a guild of cactus-tending ant mutualists. *Ecology*, 86(12):3190–3199, 2005.

A. Mortelliti, G. Amori, D. Capizzi, C. Cervone, S. Fagiani, B. Pollini, and L. Boitani. Independent effects of habitat loss, habitat fragmentation and structural connectivity on the distribution of two arboreal rodents. *J. Appl. Ecol.*, 48(1):153–162, 2011.

D. Morton, C. Rowland, C. Wood, L. Meek, C. Marston, G. Smith, R. Wadsworth, and I. Simpson. Final report for LCM2007 - the new UK land cover map. countryside survey technical report. (11/07), 2011.

E. S. Mosher, J. A. Silander Jr, and A. M. Latimer. The role of land-use history in major invasions by woody plant species in the northeastern North American landscape. *Biol. Invasions*, 11(10):2317–2328, 2009.

J. Müller. Floristic and structural pattern and current distribution of tiger bush vegetation in Burkina Faso (west africa), assessed by means of belt transects and spatial analysis. *Appl. Ecol. Environ. Res.*, 11(2):153–171, 2013.

J. D. Murray. *Mathematical Biology II: Spatial Models and Biomedical Applications*. Springer, 3rd edition, 2003.

K. A. Murray, L. D. Verde Arregoitia, A. Davidson, M. Di Marco, and M. M. Di Fonzo. Threat to the point: improving the value of comparative extinction risk analysis for conservation action. *Glob. Chang. Biol.*, 20(2):483–494, 2014.

J. Musgrave and F. Lutscher. Integrodifference equations in patchy landscapes. *J. Math. Biol.*, 69(3):617–658, 2014.

J. Musgrave, A. Girard, and F. Lutscher. Population spread in patchy landscapes under a strong allee effect. *Theor. Ecol.*, 8(3):313–326, 2015.

R. Nathan. Long-distance dispersal of plants. *Science*, 313(5788):786–788, 2006.

R. Naylor. Invasions in agriculture: assessing the cost of the golden apple snail in Asia. *Ambio*, pages 443–448, 1996.

M. G. Neubert and H. Caswell. Demography and dispersal: calculation and sensitivity analysis of invasion speed for structured populations. *Ecology*, 81(6):1613–1628, 2000.

M. G. Neubert and I. M. Parker. Projecting rates of spread for invasive species. *Risk. Anal.*, 24(4):817–831, 2004.

M. G. Neubert, M. Kot, and M. A. Lewis. Dispersal and pattern formation in a discrete-time predator-prey model. *Theor. Popul. Biol.*, 48(1):7–43, 1995.

M. G. Neubert, M. Kot, and M. A. Lewis. Invasion speeds in fluctuating environments. *Proc. R. Soc. London, Ser. B*, 267(1453):1603–1610, 2000.

M. G. Neubert, H. Caswell, and J. Murray. Transient dynamics and pattern formation: reactivity is necessary for turing instabilities. *Math. Biosci.*, 175(1):1–11, 2002.

R. C. Neupane and J. A. Powell. Invasion speeds with active dispersers in highly variable landscapes: Multiple scales, homogenization, and the migration of trees. *J. Theor. Biol.*, 387:111–119, 2015.

E. Nicholson and O. Ovaskainen. Conservation prioritization using metapopulation models. In A. Moilanen, K. A. Wilson, and H. Possingham, editors, *Spatial Conservation Prioritisation: Quantitative Methods and Computational Tools*. Oxford University Press, 2009.

M. A. Nuñez and K. A. Medley. Pine invasions: climate predicts invasion success; something else predicts failure. *Divers. Distrib.*, 17(4):703–713, 2011.

C. Oliveira, A. Auad, S. Mendes, and M. Frizzas. Economic impact of exotic insect pests in Brazilian agriculture. *J. Appl. Entomol.*, 137(1-2):1–15, 2013.

J. G. B. Oostermeijer, M. L. Brugman, E. R. De Boer, and H. C. Den Nijs. Temporal and spatial variation in the demography of *gentiana pneumonanthe*, a rare perennial herb. *J. Ecol.*, 84(2):153–166, 1996.

M. P. Oreska and D. C. Aldridge. Estimating the financial costs of freshwater invasive species in Great Britain: a standardized approach to invasive species costing. *Biol. Invasions*, 13(2):305–319, 2011.

J. Pagel and F. M. Schurr. Forecasting species ranges by statistical estimation of ecological niches and spatial population dynamics. *Global Ecol. Biogeogr.*, 21(2): 293–304, 2012.

S. Pan and G. Lin. Propagation of second order integrodifference equations with local monotonicity. *Nonlinear Anal. Real World Appl.*, 12(1):535–544, 2011.

S. Pan and G. Lin. Coinvasion–coexistence travelling wave solutions of an integro-difference competition system. *J. Differ. Equ. Appl.*, 20(4):511–525, 2014.

S. Pan and P.-A. Zhang. Bistable wave fronts in integrodifference equations. In *Abstract and Applied Analysis*, volume 2011. Hindawi Publishing Corporation, 2011.

R. Pardini, A. de Arruda Bueno, T. A. Gardner, P. I. Prado, and J. P. Metzger. Beyond the fragmentation threshold hypothesis: regime shifts in biodiversity across fragmented landscapes. *PLoS One*, 5(10):e13666, 2010.

S. Parnell, F. Van Den Bosch, and C. Gilligan. Large-scale fungicide spray heterogeneity and the regional spread of resistant pathogen strains. *Phytopathology*, 96 (5):549–555, 2006.

A. Pauchard, N. Fuentes, A. Jiménez, R. Bustamante, and A. Marticorena. Alien plants homogenise protected areas: Evidence from the landscape and regional scales

in south central Chile. In L. C. Foxcroft, P. Pyek, D. M. Richardson, and P. Genovesi, editors, *Plant Invasions in Protected Areas*, pages 191–208. Springer, 2013.

L. Pejchar and H. A. Mooney. Invasive species, ecosystem services and human well-being. *Trends Ecol. Evol.*, 24(9):497–504, 2009.

C. Penz, P. DeVries, J. Tufto, and R. Lande. Butterfly dispersal across Amazonia and its implication for biogeography. *Ecography*, 38(4):410–418, 2015.

J. Pergl, J. Müllerová, I. Perglová, T. Herben, and P. Pyšek. The role of long-distance seed dispersal in the local population dynamics of an invasive plant species. *Divers. Distrib.*, 17(4):725–738, 2011.

C. Perrings, H. Mooney, and M. Williamson. *Bioinvasions and Globalization*. Oxford University Press, Oxford, 2010.

A. T. Peterson. Predicting the geography of species invasions via ecological niche modeling. *Q. Rev. Biol.*, 78(4):419–433, 2003.

A. Phillips and M. Kot. Persistence in a two-dimensional moving-habitat model. *Bull. Math. Biol.*, 77(11):2125–2159, 2015.

S. T. Pickett and P. S. White. *The Ecology of Natural Disturbance and Patch Dynamics*. Elsevier, 1985.

D. Pimentel. *Biological Invasions: Economic and Environmental Costs of Alien Plant, Animal, and Microbe Species*. CRC Press, 2011.

S. E. Pittman, R. Muthukrishnan, N. M. West, A. S. Davis, N. R. Jordan, and J. D. Forester. Mitigating the potential for invasive spread of the exotic biofuel crop, *Miscanthus* × *giganteus*. *Biol. Invasions*, 17(11):3247–3261, 2015.

J. R. Poulsen, C. W. Osenberg, C. J. Clark, D. J. Levey, and B. M. Bolker. Plants as reef fish: fitting the functional form of seedling recruitment. *Am. Nat.*, 170(2): 167–183, 2007.

J. A. Powell, P. White, and T. McMillen. Connecting a chemotactic model for mass attack to a rapid integro-difference emulation strategy. *SIAM J. Appl. Math.*, 59 (2):547–572, 1998.

L. R. Prugh, K. E. Hodges, A. R. E. Sinclair, and J. S. Brashares. Effect of habitat area and isolation on fragmented animal populations. *Proc. Natl. Acad. Sci. U.S.A.*, 105(52):20770–20775, 2008.

H. R. Pulliam. On the relationship between niche and distribution. *Ecol. Lett.*, 3(4): 349–361, 2000.

M. Puri, A. Srivathsa, K. K. Karanth, N. Kumar, and K. U. Karanth. Multiscale distribution models for conserving widespread species: the case of sloth bear *Melursus ursinus* in India. *Divers. Distrib.*, 21(9):1087–1100, 2015.

P. Pyšek, V. Jarošík, P. E. Hulme, J. Pergl, M. Hejda, U. Schaffner, and M. Vilà. A global assessment of invasive plant impacts on resident species, communities and ecosystems: the interaction of impact measures, invading species' traits and environment. *Glob. Chang. Biol.*, 18(5):1725–1737, 2012.

P. Pyšek and D. M. Richardson. Invasive species, environmental change and management, and health. *Annu. Rev. Env. Resour.*, 35(1):25–55, 2010.

M. Rees, D. Z. Childs, and S. P. Ellner. Building integral projection models: a user's guide. *J. Anim. Ecol.*, 83(3):528–545, 2014.

J. R. Reimer, M. B. Bonsall, and P. K. Maini. Approximating the critical domain size of integrodifference equations. *Bull. Math. Biol.*, 78(1):72–109, 2016.

M. Renton, N. Shackelford, and R. J. Standish. Habitat restoration will help some functional plant types persist under climate change in fragmented landscapes. *Glob. Chang. Biol.*, 18(6):2057–2070, 2012.

A. N. Reshetnikov and G. F. Ficetola. Potential range of the invasive fish rotan (*Perccottus glenii*) in the holarctic. *Biol. Invasions*, 13(12):2967–2980, 2011.

D. M. Richardson, P. A. Williams, and R. J. Hobbs. Pine invasions in the southern hemisphere: determinants of spread and invadability. *J. Biogeogr.*, pages 511–527, 1994.

C. Robinet, H. Kehlenbeck, D. J. Kriticos, R. H. Baker, A. Battisti, S. Brunel, M. Dupin, D. Eyre, M. Faccoli, Z. Ilieva, et al. A suite of models to support the quantitative assessment of spread in pest risk analysis. *PLoS One*, 7(10):e43366, 2012.

M. Robinson, M. Flegg, and R. Erban. Adaptive two-regime method: application to front propagation. *J. Chem. Phys.*, 140(12):124109, 2014.

M. A. Rodriguez-Cabal, K. L. Stuble, B. Guénard, R. R. Dunn, and N. J. Sanders. Disruption of ant-seed dispersal mutualisms by the invasive asian needle ant (*Pachycondyla chinensis*). *Biol. Invasions*, 14(3):557–565, 2012.

M. Rouget, D. M. Richardson, J. L. Nel, D. C. Le Maitre, B. Egoh, and T. Mgidi. Mapping the potential ranges of major plant invaders in South Africa, Lesotho and Swaziland using climatic suitability. *Divers. Distrib.*, 10(5-6):475–484, 2004.

N. Roura-Pascual, A. V. Suarez, C. Gómez, P. Pons, Y. Touyama, A. L. Wild, and A. T. Peterson. Geographical potential of Argentine ants (*Linepithema humile* Mayr) in the face of global climate change. *P. Roy. Soc. Lond. B Bio.*, 271(1557): 2527–2535, 2004.

H. E. Roy, J. Peyton, D. C. Aldridge, T. Bantock, T. M. Blackburn, R. Britton, P. Clark, E. Cook, K. Dehnen-Schmutz, T. Dines, et al. Horizon scanning for invasive alien species with the potential to threaten biodiversity in Great Britain. *Glob. Chang. Biol.*, 20(12):3859–3871, 2014.

K. L. Ryall and L. Fahrig. Response of predators to loss and fragmentation of prey habitat: a review of theory. *Ecology*, 87(5):1086–1093, 2006.

E. J. Rykiel. Towards a definition of ecological disturbance. *Aust. J. Ecol.*, 10(3): 361–365, 1985.

R. Salguero-Gómez, O. R. Jones, C. R. Archer, Y. M. Buckley, J. Che-Castaldo, H. Caswell, D. Hodgson, A. Scheuerlein, D. A. Conde, E. Brinks, et al. The COMPADRE Plant Matrix Database: an open online repository for plant demography. *J. Ecol.*, 103(1):202–218, 2015.

Y. Samia and F. Lutscher. Coexistence and spread of competitors in heterogeneous landscapes. *Bull. Math. Biol.*, 72(8):2089–2112, 2010.

L. Santini, T. Cornulier, J. M. Bullock, S. C. F. Palmer, S. M. White, J. A. Hodgson, G. Bocedi, and J. M. J. Travis. A trait-based approach for predicting species responses to environmental change from sparse data: how well might terrestrial mammals track climate change? *Glob. Chang. Biol.*, 22, 2016.

D. F. Sax and S. D. Gaines. Species invasions and extinction: the future of native biodiversity on islands. *Proc. Natl. Acad. Sci. USA*, 105(1):11490–11497, 2008.

K. Scerri, M. Dewar, and V. Kadirkamanathan. Estimation and model selection for an IDE-based spatio-temporal model. *IEEE Trans. Signal Process.*, 57(2):482–492, 2009.

M. Scheffer, J. Baveco, D. DeAngelis, K. Rose, and E. Van Nes. Super-individuals a simple solution for modelling large populations on an individual basis. *Ecol. Model.*, 80(2):161–170, 1995.

J. K. Schnell, G. M. Harris, S. L. Pimm, and G. J. Russell. Estimating extinction risk with metapopulation models of large-scale fragmentation. *Conserv. Biol.*, 27 (3):520–530, 2013.

P. Schofield. Spatially explicit models of turelli-hoffmann wolbachia invasive wave fronts. *J. Theor. Biol.*, 215(1):121–131, 2002.

S. J. Schreiber and J. O. Lloyd-Smith. Invasion dynamics in spatially heterogeneous environments. *Am. Nat.*, 174(4):490–505, 2009.

S. J. Schreiber and M. E. Ryan. Invasion speeds for structured populations in fluctuating environments. *Theor. Ecol.*, 4(4):423–434, 2011.

F. M. Schurr, J. Pagel, J. S. Cabral, J. Groeneveld, O. Bykova, R. B. OHara, F. Hartig, W. D. Kissling, H. P. Linder, G. F. Midgley, et al. How to understand species niches and range dynamics: a demographic research agenda for biogeography. *J. Biogeogr.*, 39(12):2146–2162, 2012.

D. H. Secor, L. A. Kerr, and S. X. Cadrin. Connectivity effects on productivity, stability, and persistence in a herring metapopulation model. *ICES J. Mar. Sci.*, 66(8):1726–1732, 2009.

J. A. Sherratt, B. T. Eagan, and M. A. Lewis. Oscillations and chaos behind predator–prey invasion: mathematical artifact or ecological reality? *Phil. Trans. R. Soc. B*, 352(1349):21–38, 1997.

Z. Shi, R. Sherry, X. Xu, O. Hararuk, L. Souza, L. Jiang, J. Xia, J. Liang, and Y. Luo. Evidence for long-term shift in plant community composition under decadal experimental warming. *J. Ecol.*, 103(5):1131–1140, 2015.

N. Shigesada and K. Kawasaki. *Biological Invasions: Theory and Practice*. Oxford Series in Ecology and Evolution. Oxford University Press, 1st edition, 1997.

N. Shigesada, K. Kawasaki, and E. Teramoto. Traveling periodic waves in heterogeneous environments. *Theor. Popul. Biol.*, 30(1):143–160, 1986.

O. Skarpaas and K. Shea. Dispersal patterns, dispersal mechanisms, and invasion wave speeds for invasive thistles. *Am. Nat.*, 170(3):421–430, 2007.

J. Skellam. Random dispersal in theoretical populations. *Biometrika*, 38(1/2):196–218, 1951.

P. Skelsey, W. Rossing, G. Kessel, J. Powell, and W. Van der Werf. Influence of host diversity on development of epidemics: an evaluation and elaboration of mixture theory. *Phytopathology*, 95(4):328–338, 2005.

P. Skelsey, W. A. Rossing, G. J. Kessel, and W. van der Werf. Invasion of *Phytophthora infestans* at the landscape level: how do spatial scale and weather modulate the consequences of spatial heterogeneity in host resistance? *Phytopathology*, 100(11): 1146–1161, 2010.

P. Skelsey, K. With, and K. A. Garrett. Why dispersal should be maximized at intermediate scales of heterogeneity. *Theor. Ecol.*, 6(2):203–211, 2013.

D. A. Smale and T. Wernberg. Extreme climatic event drives range contraction of a habitat-forming species. *P. Roy. Soc. Lond. B Bio.*, 280(1754):20122829, 2013.

C. A. Smith, I. Giladi, and Y.-S. Lee. A reanalysis of competing hypotheses for the spread of the California sea otter. *Ecology*, 90(9):2503–2512, 2009.

M. Smolik, S. Dullinger, F. Essl, I. Kleinbauer, M. Leitner, J. Peterseil, L.-M. Stadler, and G. Vogl. Integrating species distribution models and interacting particle systems to predict the spread of an invasive alien plant. *J. Biogeogr.*, 37(3):411–422, 2010.

R. E. Snyder. How demographic stochasticity can slow biological invasions. *Ecology*, 84(5):1333–1339, 2003.

V. Solodovnikov. Upper bounds on the complexity of solving systems of linear equations. *J. Sov. Math.*, 29(4):1482–1501, 1985.

M. B. Soons and G. W. Heil. Reduced colonization capacity in fragmented populations of wind-dispersed grassland forbs. *J. Ecol.*, 90(6):1033–1043, 2002.

K. V. Spellman, L. C. Schneller, C. P. Mulder, and M. L. Carlson. Effects of non-native *Melilotus albus* on pollination and reproduction in two boreal shrubs. *Oecologia*, 179(2):495–507, 2015.

A. Stein, K. Gerstner, and H. Kreft. Environmental heterogeneity as a universal driver of species richness across taxa, biomes and spatial scales. *Ecol. Lett.*, 17(7): 866–880, 2014.

K. E. Stokes, Y. M. Buckley, and A. W. Sheppard. A modelling approach to estimate the effect of exotic pollinators on exotic weed population dynamics: bumblebees and broom in Australia. *Divers. Distrib.*, 12(5):593–600, 2006.

J.-C. Svenning and F. Skov. Limited filling of the potential range in European tree species. *Ecol. Lett.*, 7(7):565–573, 2004.

J.-C. Svenning, D. Gravel, R. D. Holt, F. M. Schurr, W. Thuiller, T. Münkemüller, K. H. Schiffers, S. Dullinger, T. C. Edwards, T. Hickler, et al. The influence of interspecific interactions on species range expansion rates. *Ecography*, 37(12):1198–1209, 2014.

N. W. Synes, C. Brown, K. Watts, S. M. White, M. A. Gilbert, and J. M. Travis. Emerging opportunities for landscape ecological modelling. *Curr. Landsc. Ecol. Rep.*, 1(4):146–167, 2016.

N. Tamburello and I. Côté. Movement ecology of Indo-Pacific lionfish on Caribbean coral reefs and its implications for invasion dynamics. *Biol. Invasions*, 17(6):1639–1653, 2015.

B. Tenhumberg. Ignoring population structure can lead to erroneous predictions of future population size. *Nat. Educ. Knowl.*, 3(10):2, 2010.

B. Tenhumberg, A. J. Tyre, and R. Rebarber. Model complexity affects transient population dynamics following a dispersal event: a case study with pea aphids. *Ecology*, 90(7):1878–1890, 2009.

M. T. Tinker, D. F. Doak, and J. A. Estes. Using demography and movement behavior to predict range expansion of the southern sea otter. *Ecol. Appl.*, 18(7):1781–1794, 2008.

S. Tisue and U. Wilensky. Netlogo: A simple environment for modeling complexity. In *International Conference on Complex Systems*, pages 16–21. Boston, MA, 2004.

J. M. Travis, C. M. Harris, K. J. Park, and J. M. Bullock. Improving prediction and management of range expansions by combining analytical and individual-based modelling approaches. *Methods Ecol. Evol.*, 2(5):477–488, 2011.

J. M. Travis, M. Delgado, G. Bocedi, M. Baguette, K. Bartoń, D. Bonte, I. Boulangeat, J. A. Hodgson, A. Kubisch, V. Penteriani, et al. Dispersal and species responses to climate change. *Oikos*, 122(11):1532–1540, 2013.

J. M. J. Travis and C. Dytham. The evolution of dispersal in a metapopulation: a spatially explicit, individual-based model. *Proc. R. Soc. London, Ser. B*, 265(1390): 17–23, 1998.

M. G. Turner. Landscape ecology: what is the state of the science? *Annu. Rev. Ecol. Evol. Syst.*, 36:319–344, 2005.

M. Urban, G. Bocedi, A. Hendry, J.-B. Mihoub, G. Peer, A. Singer, J. Bridle, L. Crozier, L. De Meester, W. Godsoe, et al. Improving the forecast for biodiversity under climate change. *Science*, 353(6304), 2016. doi: 10.1126/science.aad8466.

M. C. Urban, B. L. Phillips, D. K. Skelly, and R. Shine. A toad more traveled: the heterogeneous invasion dynamics of cane toads in Australia. *Am. Nat.*, 171(3): E134–E148, 2008.

M. B. Usher. A matrix approach to the management of renewable resources, with special reference to selection forests. *J. Appl. Ecol.*, 3(2):355–367, 1966.

F. van den Bosch, J. A. J. Metz, and O. Diekmann. The velocity of spatial population expansion. *J. Math. Biol.*, 28(5):529–565, 1990.

R. W. Van Kirk and M. A. Lewis. Integrodifference models for persistence in fragmented habitats. *Bull. Math. Biol.*, 59(1):107–137, 1997.

M. Van Kleunen, E. Weber, and M. Fischer. A meta-analysis of trait differences between invasive and non-invasive plant species. *Ecol. Lett.*, 13(2):235–245, 2010.

R. van Klink, F. van der Plas, C. van Noordwijk, M. F. Wallis DeVries, and H. Olff. Effects of large herbivores on grassland arthropod diversity. *Biol. Rev.*, 90(2):347–366, 2015.

T. Vargas, W. Cheng, et al. Rhizosphere-mediated effects of the invasive grass *Bromus tectorum L.* and native *Elymus elymoides* on nitrogen cycling in Great Basin Desert soils. *Plant Soil*, 393(1-2):245–257, 2015.

R. R. Veit and M. A. Lewis. Dispersal, population growth, and the allee effect: dynamics of the house finch invasion of eastern North America. *Am. Nat.*, 8(2): 255–274, 1996.

M. Vilà, J. L. Espinar, M. Hejda, P. E. Hulme, V. Jarošík, J. L. Maron, J. Pergl, U. Schaffner, Y. Sun, and P. Pyšek. Ecological impacts of invasive alien plants: a meta-analysis of their effects on species, communities and ecosystems. *Ecol. Lett.*, 14(7):702–708, 2011.

M.-A. Villard and J. P. Metzger. Review: Beyond the fragmentation debate: a conceptual model to predict when habitat configuration really matters. *J. Appl. Ecol.*, 51(2):309–318, 2014.

R. Virkkala and A. Lehikoinen. Patterns of climate-induced density shifts of species: poleward shifts faster in northern boreal birds than in southern birds. *Glob. Chang. Biol.*, 20(10):2995–3003, 2014.

P. M. Vitousek, C. M. D'Antonio, L. L. Loope, R. Westbrooks, et al. Biological invasions as global environmental change. *Am. Sci.*, 84(5):468–478, 1996.

V. Volterra. Leçons sur la théorie mathématique de la lutte pour la vie. *Bull. Amer. Math. Soc.*, (42):304–305, 1936.

C. C. Vos, P. Berry, P. Opdam, H. Baveco, B. Nijhof, J. OHanley, C. Bell, and H. Kuipers. Adapting landscapes to climate change: examples of climate-proof ecosystem networks and priority adaptation zones. *J. Appl. Ecol.*, 45(6):1722–1731, 2008.

G. Vranckx, H. Jacquemyn, B. Muys, and O. Honnay. Meta-analysis of susceptibility of woody plants to loss of genetic diversity through habitat fragmentation. *Conserv. Biol.*, 26(2):228–237, 2012.

D. L. Wagner and R. G. Van Driesche. Threats posed to rare or endangered insects by invasions of nonnative species. *Annu. Rev. Entomol.*, 55:547–568, 2010.

L. R. Walker, D. J. Zarin, N. Fetcher, R. W. Myster, and A. H. Johnson. Ecosystem development and plant succession on landslides in the Caribbean. *Biotropica*, 28 (4):566–576, 1996.

J. R. Walsh, S. R. Carpenter, and M. J. Vander Zanden. Invasive species triggers a massive loss of ecosystem services through a trophic cascade. *Proc. Natl. Acad. Sci. USA*, 113(15):4081–4085, 2016.

G.-R. Walther. Community and ecosystem responses to recent climate change. *Phil. Trans. R. Soc. B*, 365(1549):2019–2024, 2010.

H. Wang and C. Castillo-Chavez. Spreading speeds and traveling waves for non-cooperative integro-difference systems. *Discrete Cont. Dyn. B*, 17(6):2243, 2012.

J. Q. Wang, L. Tang, X. D. Zhang, C. H. Wang, Y. Gao, L. F. Jiang, J. K. Chen, and B. Li. Fine-scale environmental heterogeneities of tidal creeks affect distribution of crab burrows in a Chinese salt marsh. *Ecol. Eng.*, 35(12):1685–1692, 2009.

M.-H. Wang, M. Kot, and M. G. Neubert. Integrodifference equations, allee effects, and invasions. *J. Math. Biol.*, 44(2):150–168, 2002.

J. V. Ward, K. Tockner, and F. Schiemer. Biodiversity of floodplain river ecosystems: ecotones and connectivity. *Regul. River*, 15(1):125–139, 1999.

H. F. Weinberger. Long-time behavior of a class of biological models. *SIAM J. Math. Anal.*, 13(3):353–396, 1982.

H. F. Weinberger. On spreading speeds and traveling waves for growth and migration models in a periodic habitat. *J. Math. Biol.*, 45(6):511–548, 2002.

H. F. Weinberger and X.-Q. Zhao. An extension of the formula for spreading speeds. *Math Biosci Eng*, 7:187–194, 2010.

H. F. Weinberger, M. A. Lewis, and B. Li. Analysis of linear determinacy for spread in cooperative models. *J. Math. Biol.*, 45(3):183–218, 2002.

H. F. Weinberger, K. Kawasaki, and N. Shigesada. Spreading speeds of spatially periodic integro-difference models for populations with nonmonotone recruitment functions. *J. Math. Biol.*, 57(3):387–411, 2008.

J. F. Weishampel, J. B. Drake, A. Cooper, J. B. Blair, and M. Hofton. Forest canopy recovery from the 1938 hurricane and subsequent salvage damage measured with airborne lidar. *Remote Sens. Environ.*, 109(2):142–153, 2007.

C. K. Wikle. A kernel-based spectral model for non-gaussian spatio-temporal processes. *Stat. Modelling*, 2(4):299–314, 2002.

C. K. Wikle and M. B. Hooten. A general science-based framework for dynamical spatio-temporal models. *Test*, 19(3):417–451, 2010.

D. S. Wilcove, D. Rothstein, J. Dubow, A. Phillips, and E. Losos. Quantifying threats to imperiled species in the United States. *BioScience*, 48(8):607–615, 1998.

M. Williamson. Invasions. *Ecography*, 22(1):5–12, 1999.

E. O. Wilson. *The Diversity of Life*. WW Norton & Company, 1999.

M. S. Wisz, J. Pottier, W. D. Kissling, L. Pellissier, J. Lenoir, C. F. Damgaard, C. F. Dormann, M. C. Forchhammer, J.-A. Grytnes, A. Guisan, et al. The role

of biotic interactions in shaping distributions and realised assemblages of species: implications for species distribution modelling. *Biol. Rev.*, 88(1):15–30, 2013.

M. O. Woodburne. The great American biotic interchange: dispersals, tectonics, climate, sea level and holding pens. *J. Mamm. Evol.*, 17(4):245–264, 2010.

R. Wright and A. Hastings. Spontaneous patchiness in a host-parasitoid integrodifference model. *Bull. Math. Biol.*, 69(8):2693–2709, 2007.

H. Yamano, K. Sugihara, and K. Nomura. Rapid poleward range expansion of tropical reef corals in response to rising sea surface temperatures. *Geophys. Res. Lett.*, 38 (4), 2011.

Z.-X. Yu and R. Yuan. Properties of traveling waves for integrodifference equations with nonmonotone growth functions. *Z. Angew. Math. Pgys.*, 63(2):249–259, 2012.

Y. Zhou and M. Kot. Discrete-time growth-dispersal models with shifting species ranges. *Theor. Ecol.*, 4(1):13–25, 2011.

Y. Zhou and M. Kot. Life on the move: Modeling the effects of climate-driven range shifts with integrodifference equations. In M. A. Lewis, P. K. Maini, and S. V. Petrovskii, editors, *Dispersal, Individual Movement and Spatial Ecology*, pages 263–292. Springer, 2013.

K. Zhu, C. W. Woodall, and J. S. Clark. Failure to migrate: lack of tree range expansion in response to climate change. *Glob. Chang. Biol.*, 18(3):1042–1052, 2012.